University of Alberta

SUBGLACIAL CONDITIONS ASSOCIATED WITH THE LAURENTIDE, LAC LA BICHE ICE STREAM

by

Paul James Wilson ©

A thesis submitted to the Faculty of Graduate Studies and Research in partial fulfillment of the requirements for the degree of Master of Science

in

Department of Earth and Atmospheric Sciences

Edmonton, Alberta

Spring 1998

Abstract

Basal till preconsolidation values represent a proxy for past subglacial stress and hydrologic conditions. Preconsolidation results obtained from the path of the Laurentide, Lac La Biche ice stream were low, ranging from 137 kPa to 268 kPa with a mean of 201 kPa. Postglacial pedogenic processes have not significantly altered the effective pressure signal imparted on the till by the overriding Lac La Biche ice stream. The observed low variation in preconsolidation values suggests that vertical groundwater drainage was not the dominant control in the maintenance of local effective basal pressures.

Geologic interpretation indicates the dominant basal flow process was sliding with associated heterogeneous ductile sediment deformation. Pervasive sediment deformation was a transitory process restricted to localized areas of the bed. Evidence of a widespread network of narrow, high pressure canals at the ice/bed interface suggests that the till bed acted to restrict basal meltwater drainage to underlying aquifers.

Acknowledgments

I would like to thank the many people who have assisted me along the way in the production of this thesis. I would very much like to thank Dr. Nat Rutter for his financial support through the Climate System History Dynamics Project and for his great faith in my abilities. This thesis could not have been possible without the kind support and commitment of the Albertan landowners who allowed me to dig up their backyards and planted fields with a backhoe. Dr. Dave Sego, Gerry Cyre, and Steve Gamble of the Civil Engineering Department helped me immensely with consolidation testing and access to the resources of their great Department. Kate Witte was a fantastic field assistant, she kept me organized and was responsible for the warm reception we received from many of the landowners in the field area. "Soon to be Doctors" Dean, Loren, Ted and Arlene provided a stimulating environment in which I was privileged to have found myself immersed. Their editing achievements were legendary. Special thanks to Ted and Loren for the many great marathon sessions, and Julie for the cool ruler used in all of my figure formatting. Dr. Garry Clarke and Dr. Shawn Marshall of the Geophysics Department at UBC kept me going by their keen interest in my thesis topic and results. Many thanks go to Shanna, my parents and my Grandmother for their unending encouragement, patience and support over the years. I could not have finished this thesis without them.

Table of Contents

Page

Chapter 1 INTRODUCTION

1.1 Introduction 1
1.2 Thesis Objectives 4
1.3 Thesis Outline 6

Chapter 2 STUDY AREA

2.1 Location 8
2.1.1 Present Climate 13
2.1.2 Soils 13
2.1.3 Bedrock 14
2.1.4 Quaternary Stratigraphy 16
2.2 Lac La Biche Flute Field and Ice Stream 21
2.2.1 Alternate Hypothesis for the Formation of the Lac La Biche Flute Field 27
2.3 Deglacial History 28
2.4 Post-glacial Climate 29

Chapter 3 METHODS

3.1 Field Methods 31
3.1.1 Sample Collection 32
3.1.2 Section Description 33
3.1.3 Clast Fabric Measurements 33
3.2 Laboratory Methods 35
3.2.1 Consolidation Testing 35
3.2.2 Grain Size Analysis 36
3.2.3 Coarse Sand Petrology 36
3.2.4 Coefficient of Permeability 37

Chapter 4 CONSOLIDATION THEORY

4.1 Introduction 39
4.2 Consolidation Theory 39
4.3 Consolidation Tests 44
4.4 Previous work 45

Table of Contents cont.

4.5 Application of Consolidation Theory to Glacial Sediments 50
4.5.1 Disturbance Effects 51
4.5.2 Effect of Temperature 53
4.5.3 Effect of Time 53

Chapter 5 POSTGLACIAL PROCESSES

5.1 Introduction 56
5.2 Sediment Structure 57
5.3 Desiccation and Rehydration 58
5.4 Expanding Clay 61
5.5 Freezing and Thawing 62
5.6 Carbonate and Sulfate Leaching/Deposition 64
5.7 Clay Translocation 65
5.8 Discussion 66

Chapter 6 ICE STREAM BASAL PROCESSES

6.1 Introduction 68
6.2 Ice Stream Motion 68
6.2.1 Internal Ice Deformation 69
6.2.2 Coupled Basal Sliding 69
6.2.3 Sediment Deformation 70
6.2.3.1 Factors Controlling Sediment Deformation 74
6.2.3.2 Deformation Layer Thickness 76
6.2.4 Hydraulic Jacking and Decoupled Basal Sliding 77
6.3 Subglacial Hydrology 79
6.3.1 Darcian Flow 80
6.3.2 Subglacial Channels 82

Chapter 7 SITE GEOLOGY INTERPRETATION

7.1 Introduction 84
7.2 Till Forming Processes 84
7.3 Section Descriptions/Interpretations 85
DS01 85
DS02 94
DS03 95
DS04 97
DS05 100

Table of Contents cont.

DS07 103
DS08 106
DS09 109
DS10 113
DS11 114
DS12 117
DS13 118
DS14 121
DS16 123
DS18 124

7.4 Discussion 126
7.4.1 Sand Lenses 130

Chapter 8 PRECONSOLIDATION TEST RESULTS

8.1 Introduction 133
8.2 Unsuccessful Consolidation Tests 133
8.3 Preconsolidation Results 135

Chapter 9 DISCUSSION OF PRECONSOLIDATION DATA

9.1 Discussion 141

Chapter 10 CONCLUSION

10.1 Conclusion 151

REFERENCES 154

APPENDICES

Appendix I: Raw Consolidation Data 166
Appendix II: Void Ratio Calculations 180
Appendix III: Casagrande Method / Consolidation Curves 194
Appendix IV: Grain Size Data 208
Appendix V: Control Well Logs 224

List of Tables

Table 1: Proposed regional correlations and ages of lithostratigraphic units..... 22

Table 2: Geological applications of consolidation testing, previous work..... 48

Table 3: End member till depositional processes..... 86

Table 4: Summary of clast fabric data statistics..... 88

Table 5: Coarse sand grain petrology summary..... 89

Table 6: Site investigation summary..... 127

Table 7: Preconsolidation test summary data..... 134

Table 8: Till coefficient of permeability summary..... 145

List of Figures

Figure 1: Study area 2

Figure 2: Location of excavated sites 9

Figure 3: Location of profile transects 10

Figure 4: Topographic profile A 11

Figure 5: Topographic profiles B, C and D 12

Figure 6: Map of bedrock geology, east-central Alberta 15

Figure 7: Map of preglacial valley thalwegs, east-central Alberta 17

Figure 8: Map of surficial geology, east-central Alberta 18

Figure 9: Distribution of Mougeot's (1991) Diamicton Unit E 20

Figure 10: Representation of sediment consolidation 40

Figure 11: Casagrande (1936) method 41

Figure 12: Stages of sediment consolidation with Taylor (1948) method 43

Figure 13: Theoretical consolidation curve (load, unload, reload cycle) 46

Figure 14: Consolidation process with meltwater flux 52

Figure 15: Time / Unit consolidation profiles 55

Figure 16: Drying and wetting hysteresis curve 60

Figure 17: Theorized thaw consolidation pathway 63

Figure 18: Styles of deformation 71

Figure 19: Subglacial process relationship model (Boulton and Dobbie, 1993) 75

Figure 20: Modality-isotropy diagram 87

List of Figures cont.

Figure 21: Section exposed at DS01 site 91

Figure 22: Clast fabric projections for DS01, DS02 and DS03 92

Figure 23: View of DS03 / DS14 sample site location 96

Figure 24: Clast fabric projections for DS04, DS05 and DS07 99

Figure 25: Section exposed at DS05 site 101

Figure 26: Photo of sand lens at DS07 section 105

Figure 27: View of DS08 / DS09 sample site location 108

Figure 28: Clast fabric projections for DS08, DS09 and DS10 110

Figure 29: Clast fabric projections for DS11, DS12 and DS13 116

Figure 30: Section exposed at DS13 site 120

Figure 31: Clast fabric projections for DS14, DS16 and DS18 122

Figure 32: Intra-site and inter-site preconsolidation range with histogram 136

Figure 33: Distribution of site preconsolidation values 138

Figure 34: Depositional process and sand lenses correlation with consolidation value 140

Figure 35: Plot of till thickness versus site preconsolidation value 147

Chapter One

Introduction

1.1 Introduction

The glacial sediments associated with the Laurentide, Lac La Biche ice stream (Figure 1) provides an excellent opportunity to study the characteristics of ice stream basal hydrology and flow mechanics. An understanding of the basal processes associated with fast flowing ice remains incomplete, as direct observation of the beds of modern ice streams is difficult. Through the use of proxy data derived from basal tills, it is possible to determine at least some of the characteristics of the past subglacial environments. It appears that one of the most promising methods of collecting subglacial proxy data is through the application of geotechnical consolidation tests carried out on basally deposited tills (eg. Boulton and Dobbie, 1993; Jenson, 1993; Brown *et al.* 1987). The magnitudes and patterns of consolidation in fine grained sediments overrun by glacial ice reflect patterns of glacial loading, subglacial deformation and water flow, and therefore can be used as a guide to interpret subglacial drainage characteristics (Boulton and Dobbie, 1993).

The consolidation testing method was originally developed for use in foundation engineering and building settling analysis. Casagrande (1936) found that by applying a series of known stresses to a sample of natural clay and measuring the change in the rate of deformation, he was able to determine the preconsolidation value of the samples, which is the maximum stress applied to the sample previously, or in its geologic history. Since that time, numerous authors have used the Casagrande method in geologic applications, performing consolidation tests on glacially overrun lacusterine clays (Harrison, 1958; Kazi and Knill, 1969; Sauer and Christiansen, 1988), silts (Van Gelder *et al.* 1990), and basal tills (MacDonald and Sauer, 1970; Boulton and Dobbie, 1993).

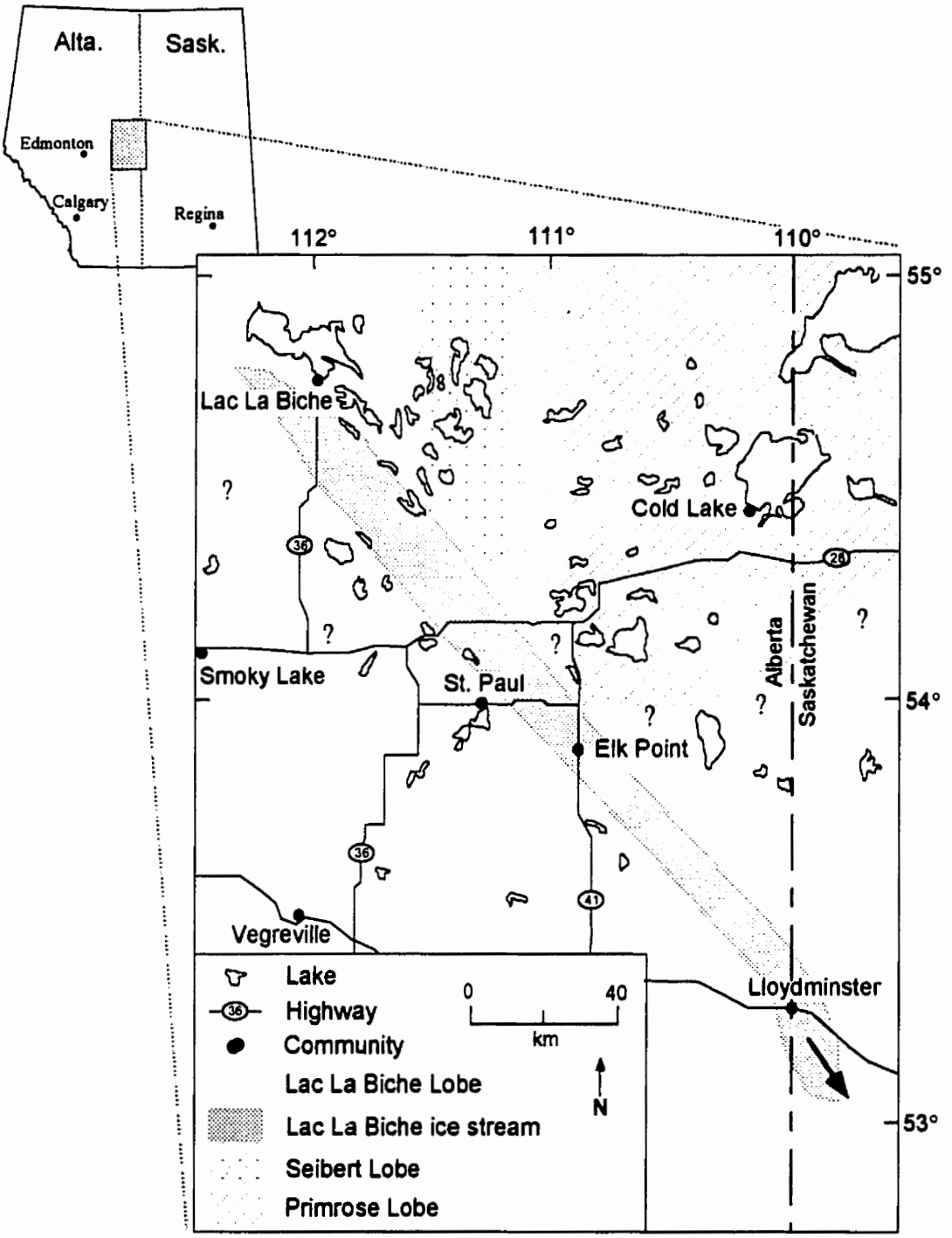

Figure 1. Location of the Lac La Biche Lobe and ice stream. The ice stream portion of the lobe flowed along a path 15-25 km in width southeastwards along the margin of the Seibert and possibly Primrose Lobes. The extent of coverage within Saskatchewan is uncertain, as is the southern margin of the Primrose Lobe and the extent of ice coverage west of the Lac La Biche Lobe.

Consolidation tests carried out on glacially overrun tills provide preconsolidation values which ideally represent a proxy for the subglacial maximum net effective basal pressure (Boulton and Dobbie, 1993). Effective basal pressure is defined as:

$$p' = p_i - p_w \quad (1)$$

where; p_i is the pressure induced by the weight of the overlying ice and p_w is the subglacial water pressure which acts to support a portion of the weight of the overlying ice.

Boulton *et al.* (1995) suggested that horizontal groundwater flow is a primary control on water pressures at the ice/bed interface. Thus, the effective pressure at the glacier sole is largely determined by the extent to which meltwater can drain away through the substratum. Thus, by noting changes in calculated preconsolidation values along different portions of the bed of the Lac La Biche ice stream, preconsolidation data can be used to infer past subglacial hydrological conditions (Brown *et al.* 1987; Boulton and Dobbie, 1993; Sauer and Christiansen, 1988; and Harrison, 1958). High basal till consolidation suggests low basal water pressures while low till consolidation suggests high basal water pressures. For example, Boulton and Paul (1976) note that zones of low sediment permeability beneath a glacier may lead to the local development of net buoyancy beneath a glacier.

Ice streams have been found to play an important role in determining the dynamics of an ice sheet (Marshall, 1996). Modern ice streams can be 30-80 km wide and up to 500 km long and move on the order of 800 m/yr, as opposed to bounding ice sheets which travel at approximately 10 m/yr (Bentley, 1987). For example, Antarctic ice streams cover 11% of the coast line but drain 90% of the inland ice accumulation (Goldstein *et al.* 1993). Jakobshavns Glacier alone is said to drain ~6% of Greenland's annual ice accumulation (36.6 km^3) at an average velocity of 8630 m/yr (Clarke, 1987). It may be assumed that Laurentide ice streams played a similar role in determining the

distribution of mass within the Laurentide Ice Sheet. For Laurentide ice sheet modelers, this realization has enormous implications. With the inclusion of basal process components into recent ice dynamics models (eg. Marshall, 1996; Tully, 1995; Jenson, 1993), it is now possible to determine the importance of ice streams on the dynamics and mass balance of ice sheets.

Ice dynamics models are based primarily on simplified theoretical relationships which have been developed through limited observations of modern glacial processes (Alley, 1991; 1992; MacAyeal, 1989). In order to test properly the accuracy of ice dynamics model predictions, direct comparisons must be made with glaciological data derived from modern or paleo-glacial environments. By determining the preconsolidation values of basal sediments along the path of the Lac La Biche ice stream, insight into the processes responsible for ice stream flow, and the general character of the subglacial hydrologic system may be revealed.

The results obtained in this thesis will aid in testing and constraining the basal process components and subglacial hydrologic input parameters of the Climate System History Dynamics project (CSHD) North American ice dynamics model. Proxy data will be compared with ice model predictions to determine the accuracy of model parameters.

1.2 Thesis Objectives

The use of preconsolidation values as a proxy data tool requires that all factors which could have produced and/or influenced preconsolidation results be relatively well understood. These factors include subglacial processes associated with till deposition and basal hydrology as well as postglacial pedogenic processes. The mode of till sample collection may have also affected individual preconsolidation results. The first part of

this thesis is a qualitative investigation of the limitations in interpreting the preconsolidation value derived from samples of oxidized till. The primary question addressed is:

1) *How did postglacial pedogenic processes affect the calculated preconsolidation value of sampled sediments?*

This question will be addressed through a review of relevant geotechnical, and geologic literature. Understanding how the sediment structure may have been altered will allow for the proxy data signal represented by preconsolidation values to be evaluated properly, assisting in the interpretation of results.

Also, as samples for preconsolidation testing were obtained by two different sampling methods (Methodology Chapter 3) it must be determined whether the sampling method had any effect on calculated preconsolidation values.

The second part of this thesis involves the interpretation of preconsolidation values derived from basal tills deposited by the Laurentide, Lac La Biche ice stream. Preconsolidation results will, in effect, provide quantitative proxy data regarding the maximum effective basal pressure and characteristics of the subglacial drainage system associated with the late Pleistocene ice stream.

Objectives include addressing the following questions:

2) *What does the geology of the now exposed bed of the Lac La Biche ice stream indicate about the characteristics of the subglacial drainage system and the mode of ice stream flow?*

3) *What was the likely maximum effective basal pressure for the Lac La Biche ice stream, and how did it change along the path of the glacier within Alberta?*

4) *Did the presence of buried preglacial valleys containing thick sequences of sand and gravel (as well as sequences of glacial diamicton) act to preferentially drain portions of the Lac La Biche ice stream?*

These questions will be addressed through the interpretation of preconsolidation results, till genesis and the environment of deposition at each site.

1.3 Thesis Outline

The following chapters will introduce relevant concepts regarding the use of consolidation testing to gain insight and provide a proxy for the subglacial conditions of the Laurentide, Lac La Biche ice stream. Preconsolidation results will be evaluated to derive a proxy signal regarding maximum effective basal pressure and changes in subglacial hydrology. Chapter 2 provides information regarding the study area including, Quaternary stratigraphy, climate and the current understanding of the morphology of the Lac La Biche ice stream as it has been interpreted by previous authors (eg. Ellwood, 1961; Jones, 1981; Andriashek, 1985; and Mougeot, 1991).

The methods employed to achieve the thesis objectives are presented in Chapter 3. Chapter 4 outlines consolidation theory, of which an understanding is fundamental to the interpretation of preconsolidation results. A review of previous work in which consolidation testing has been applied to geologic applications is also included within this chapter.

The use of consolidation data as a proxy for subglacial hydrologic and stress conditions requires that all processes which could affect preconsolidation results be reasonably understood and accounted for in the interpretation of results. Therefore, Chapter 5 will provide a qualitative assessment of the effect that postglacial pedogenic processes may have had on the preservation of till preconsolidation values imposed by the overriding Lac La Biche ice stream. A review of the basal and hydrologic processes thought to be responsible for the rapid flow associated with streaming glaciers will be presented in Chapter 6 so that the processes of till deposition and mode of ice stream flow can be evaluated for each site from geologic evidence. The geologic descriptions and interpretations of the exposed sections will be presented in Chapter 7. Calculated preconsolidation results will be presented in Chapter 8. Discussions concerning the interpretation of preconsolidation results will be undertaken in Chapter 9. As a conclusion and summary, the questions raised within the thesis objectives will be addressed in Chapter 10.

Chapter Two

Study Area

2.1 Location

The study area is located in the western half of NTS 73L (Sand River Map Sheet) and in the central and eastern portions of NTS 73E (Vermilion Map Sheet) (Figure 2). The sample sites are distributed along the Alberta portion of the Lac La Biche flute field which has been interpreted to have been formed by the late Wisconsin, Laurentide Lac La Biche ice stream (Andriashek, 1985; Mougeot, 1991). The Lac La Biche flute field has a total length of approximately 390 km and extends from the town of Lac La Biche, Alberta, south eastwards to North Battleford, Saskatchewan. The flute field is dominated by southeast oriented, streamlined terrain, (characterized by flutes and drumlinoids of varying dimensions) as well as generally flat to undulating topography representing a wide variety of glacial and post-glacial surficial deposits and erosional features. The northwest-southeast orientation of the flute field is transverse to the regional Laurentide ice flow direction in this area (Andriashek, 1985).

Topographic profiles constructed along and across the path of the Lac La Biche ice stream are presented in Figures 4 and 5. The long profile (A-A') along the path of the ice stream is approximately 240 km in length (Figure 4, A). The highest present day elevation (685 m) is located in the Moose Hills, southeast of DS08 and DS09, while the lowest present day elevation (outside of the post-glacially eroded river valleys) is 568 m, located near the northern end of the transect at Missawawi Lake. It can be seen in Figure 4 (B), that the Lac La Biche ice stream ascended average surface gradients of 0.77 m/km and 1.30 m/km for almost its entire length within Alberta. Variable local steeper ascending and descending gradients are also evident. The three cross topographic

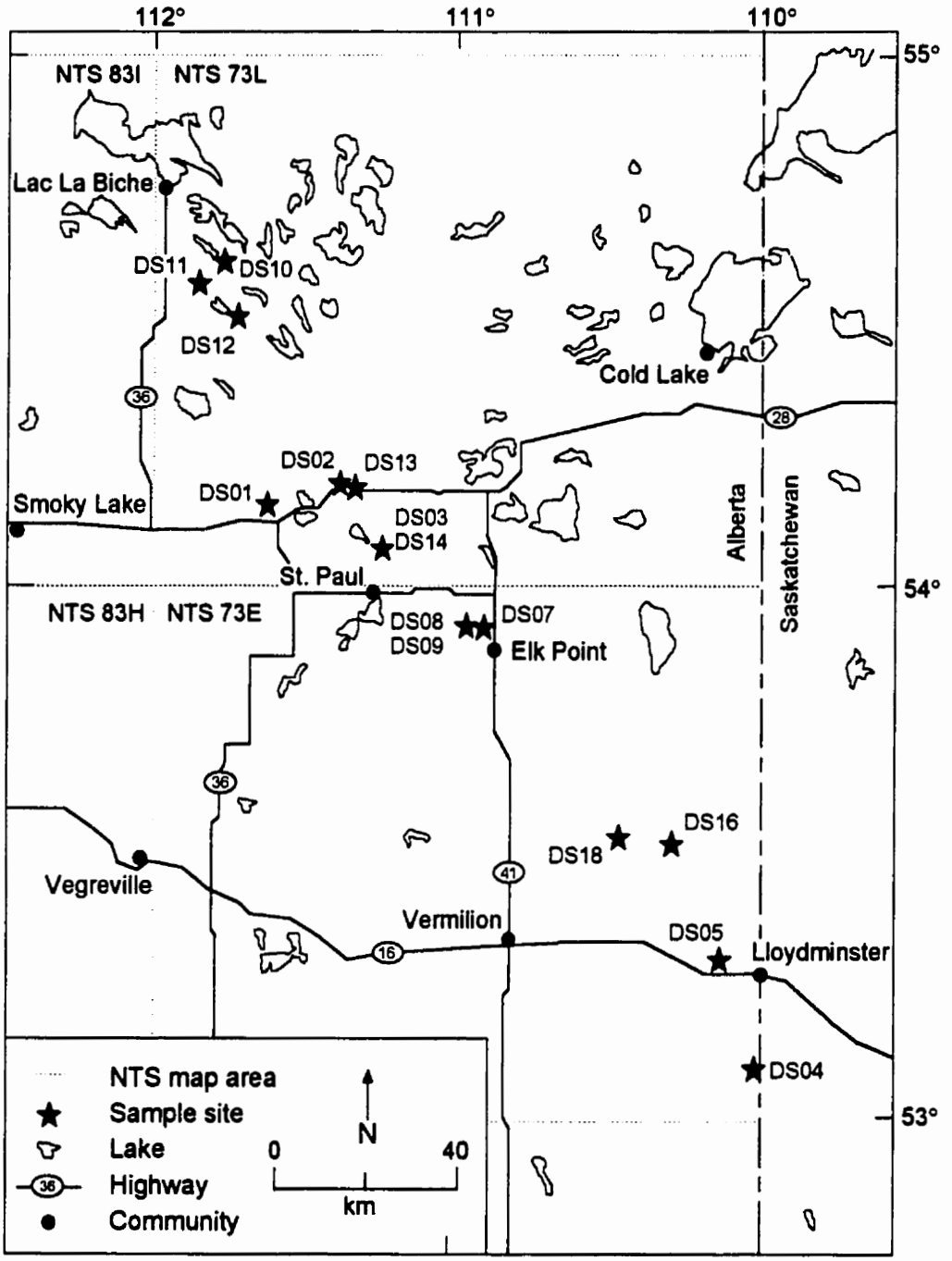

Figure 2. Location of excavated sites along the path of Lac La Biche ice stream. Detailed location descriptions are included in Chapter 7.

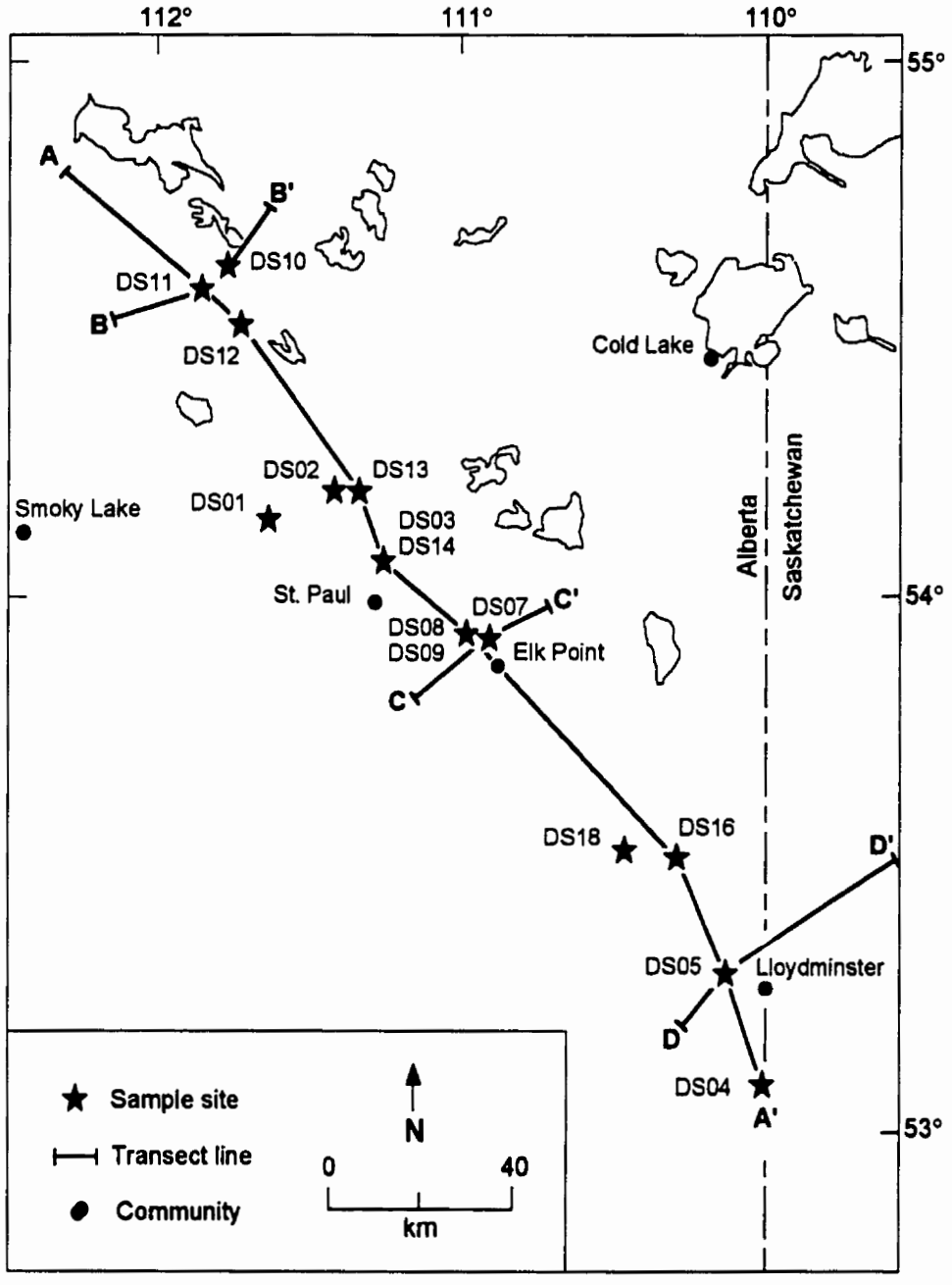

Figure 3. Location of profile transects and sample sites along and across the path of the Lac La Biche ice stream.

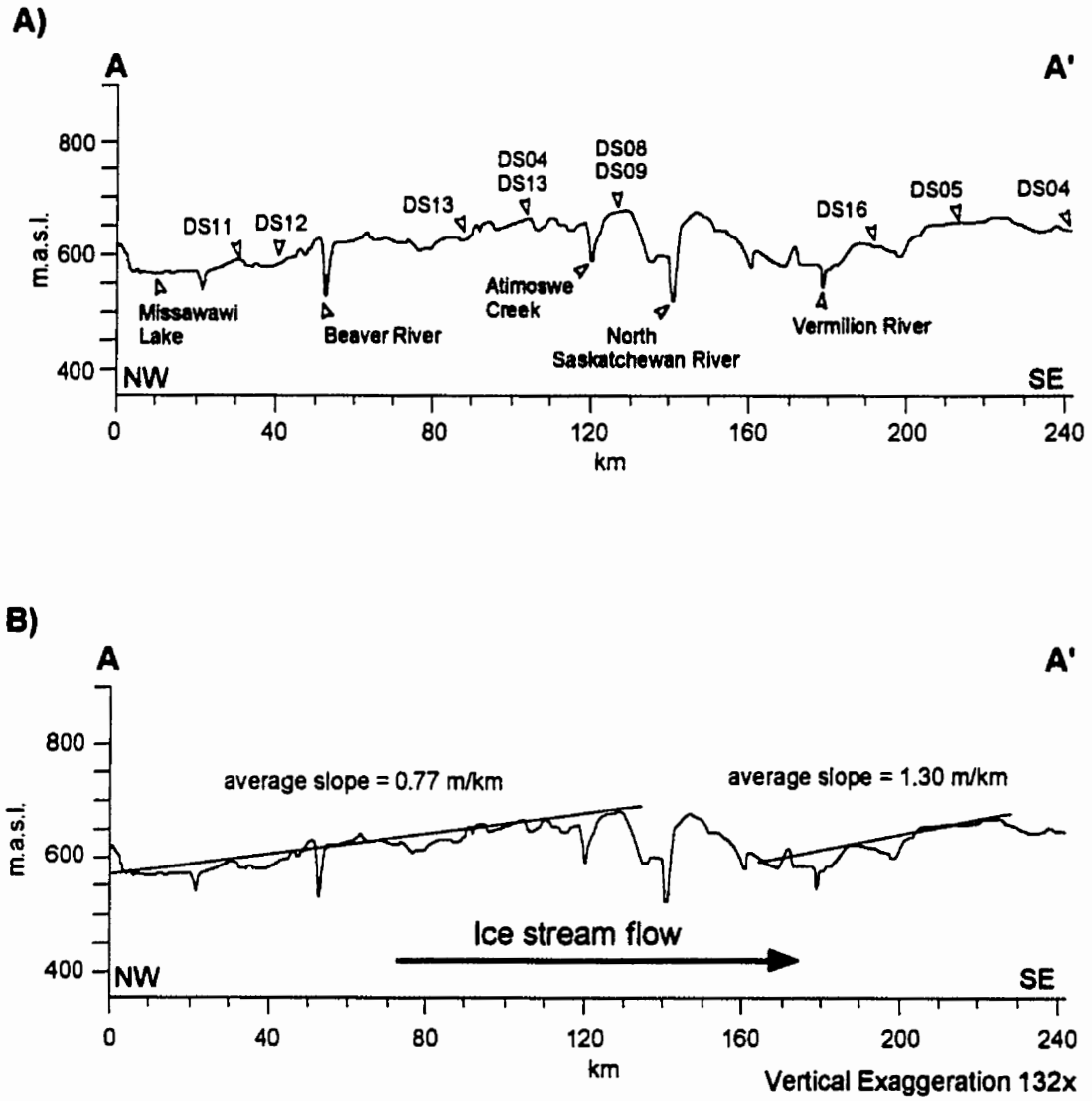

Figure 4. A) Long topographic profile showing sample site locations along the path of the Lac La Biche ice stream. B) Variation in average slope along ice stream path. It can be seen that on average, the ice stream flowed up slope from Missawawi Lake to south of Lloydminster.

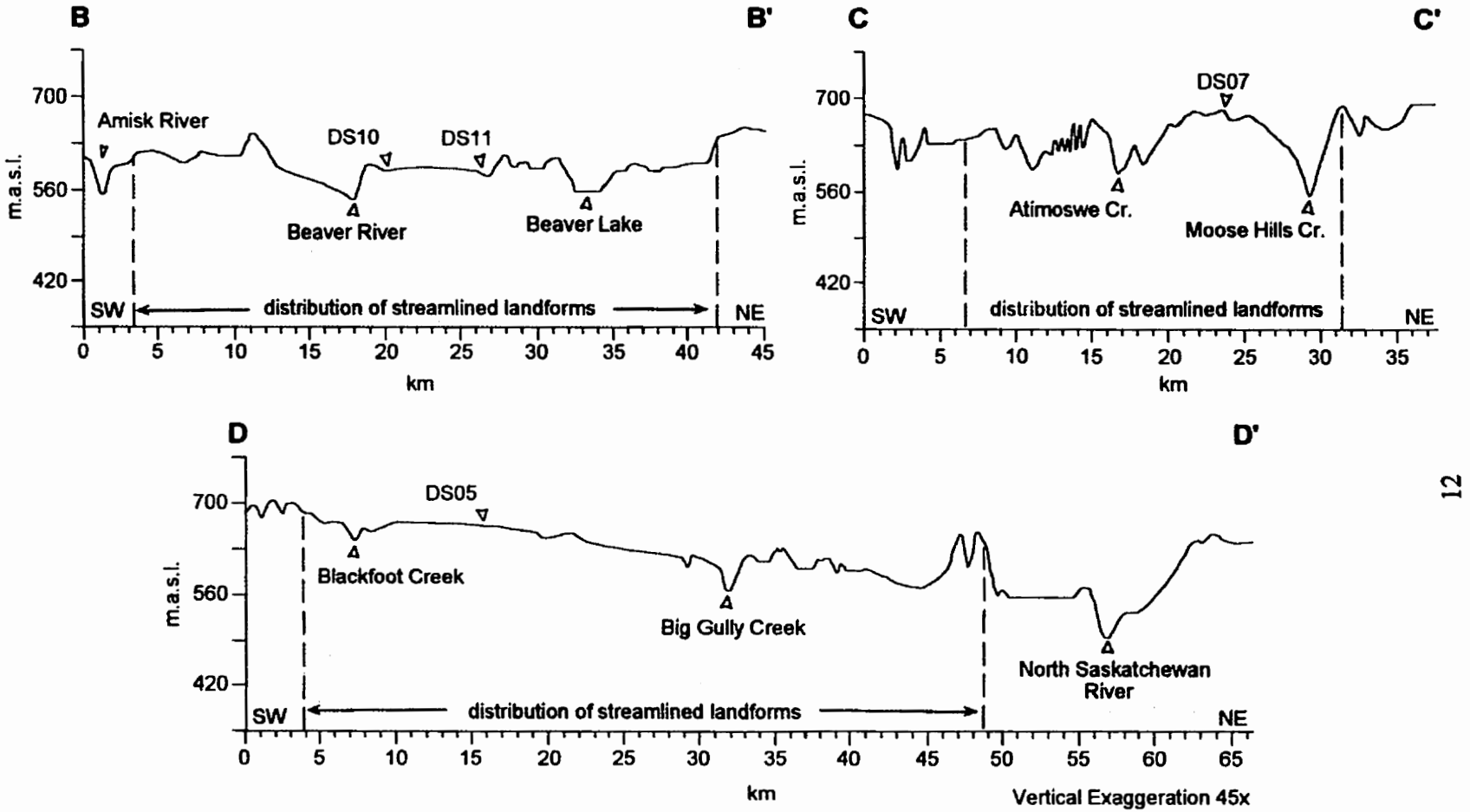

Figure 5. Topographic profiles B-B', C-C' and D-D' showing distribution of southeast oriented streamlined landforms and sampled sites. The profiles show a distict lack of lateral topographic control for the Lac La Biche Lobe suggesting the presence of bounding ice at the margins of the ice stream. See Figure 3 for the location of the transects.

profiles (B-B', C-C' and D-D') are presented in Figure 5. Here, the width of the path of the ice stream is interpreted from the distribution of southeast oriented streamlined landforms. Based on this evidence, the ice stream portion of the Lac La Biche Lobe is interpreted to have varied from approximately 24 km to 45 km in width.

2.1.1 Present Climate

The northern study sites are located in the Boreal Transition ecoregion while the southern stations lie within the Aspen Parkland ecoregion. The Boreal Transition ecoregion is characterized by a continental climate with a mean annual temperature of 1°C and mean annual precipitation of approximately 450 mm. Aspen Parkland is characterized by a continental climate with a mean annual temperature of 1.5°C and a mean annual precipitation of approximately 400 mm.

The annual average depth of ground freezing in the study area is highly variable. Ground freezing depth will be the deepest in areas where the surface has been compacted and disturbed by human activity, exposed grassland sites, areas of high soil moisture and north facing slopes. For undisturbed, treeless sites located on generally flat to undulating topography (typical of the consolidation sample sites) the annual freezing depth ranges from 0.75 m to no more than 1.5 m (Kenton Miller, Environmental Consultant, pers. comm., 1997).

2.1.2 Soils

Shields and Lindsay (1986) mapped the soils of Alberta at a scale of 1:1,000,000. Their map indicates that the soils of the study area are generally divided into three soil zones. The northern half of the area is dominated by Gray Luvisols.

Both Dark Gray Luvisols and Dark Gray Chernozems are found along a narrow belt from St. Paul to Elk Point and east to the Alberta-Saskatchewan border. The remainder of the southern portion of the field area is dominated by Black Chernozems. Regosols are found at the bottom of the major river valley systems.

2.1.3 Bedrock

Green (1972) mapped the bedrock in the province of Alberta at a scale of 1:1,276,000. The bedrock underlying the Sand River and Vermilion map sheets consists of late Cretaceous Belly River and Lea Park Formations (Figure 6). The bedrock is generally covered by variable thicknesses of Quaternary surficial deposits except in exposed sections along major river valleys and at the surface where glacially tectonized fragments of bedrock are present. The Belly River Group consists of nonmarine, gray to greenish gray, thick bedded feldspathic sandstone; gray clayey siltstone, gray and green mudstone and concretionary ironstone beds (Green, 1972). Many of the sandstone formations which make up the Belly River Group are considered excellent aquifers (Ozoray *et al.* 1990). Conformably underlying the Belly River Group, the Lea Park Formation is made up of marine dark gray shale, and pale gray glauconitic silty shale with ironstone concretions (Green, 1972). The Lea Park Formation is generally considered to represent an impermeable aquitard to the flow of groundwater in the area (Ozoray *et al.* 1990).

Tertiary erosion caused by uplift during the Laramide orogeny resulted in the development of an extensive network of eastward draining valley systems into the Cretaceous bedrock surface (Andriashek, 1985). However, these preglacial valley systems lie buried beneath a variable thickness of Tertiary and Quaternary sediments. Between valley systems, the thickness of Quaternary sediments is generally thinner, the

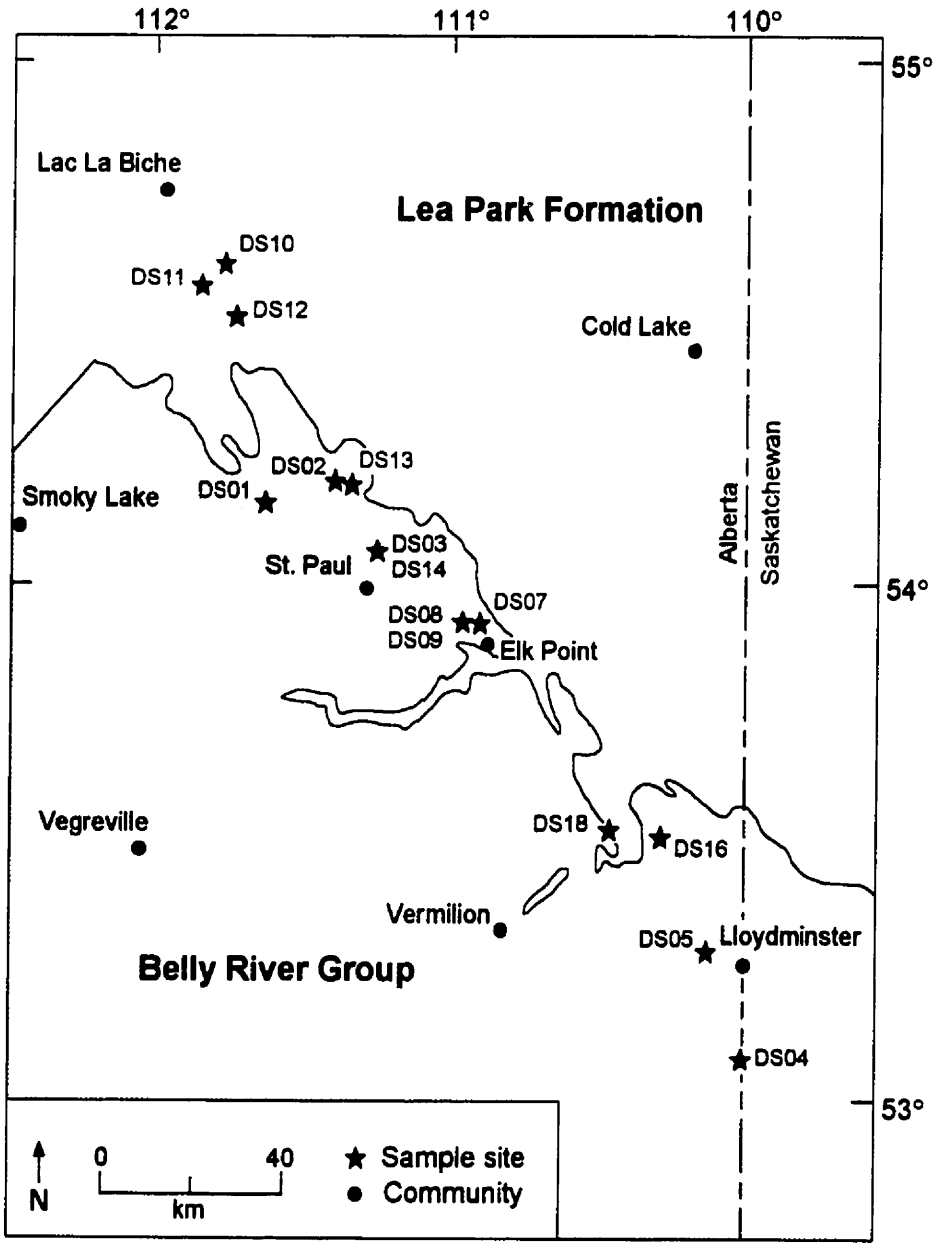

Figure 6. Map of bedrock outcrops below Quaternary sediments. The non-marine sandstones and siltstones of the Belly River Group conformably overly the marine shales of the Lea Park Formation. Adapted from Green (1972).

result of erosion by overriding glaciers (Carlson and Currie, 1975). Figure 7 shows the distribution of preglacial valley thalwegs in the Sand River and East-Vermilion map areas. Almost certainly, valleys not yet identified lie buried beneath portions of Alberta and Saskatchewan (Lawrence Andriashek, pers. comm., 1996).

2.1.4 Quaternary Stratigraphy

The Quaternary sediments of central Alberta and bordering Saskatchewan consist of variable stratigraphies which have been investigated and interpreted on a regional basis. For regions along the path of the Lac La Biche flute field in Alberta, Ellwood (1961) mapped the surface deposits of the Vermilion map area. Gold (1978) mapped the subsurface topography of bedrock and four distinct till units within the Sand River map area using an interpretive computer model and subsurface borehole data. Andriashek (1985) and Fenton and Andriashek (1983) mapped the lithostratigraphy and surficial geology of the Sand River area. Shetsen (1990) mapped the surficial geology of central Alberta at a scale of 1:500,000 while Mougeot (1991) investigated Quaternary lithostratigraphy and mapped the surficial geology of the eastern half of the Vermilion map sheet at a scale of 1:250,000. A surficial geology map of the field area is presented in Figure 8.

Andriashek (1985) recognized eight Quaternary formations within the Sand River map area. These include four glacial deposits (tills) which are separated by interglacial fluvial deposits and periods of erosion and weathering representing nonglacial periods. Of these major Quaternary formations, the youngest is the Vilna Member of the Grand Centre Formation which was deposited by the Lac La Biche Lobe moving from the northwest (Andriashek, 1985). The Vilna Member is described as consisting of massive clayey diamicton containing few pebbles or granules. In places the diamicton

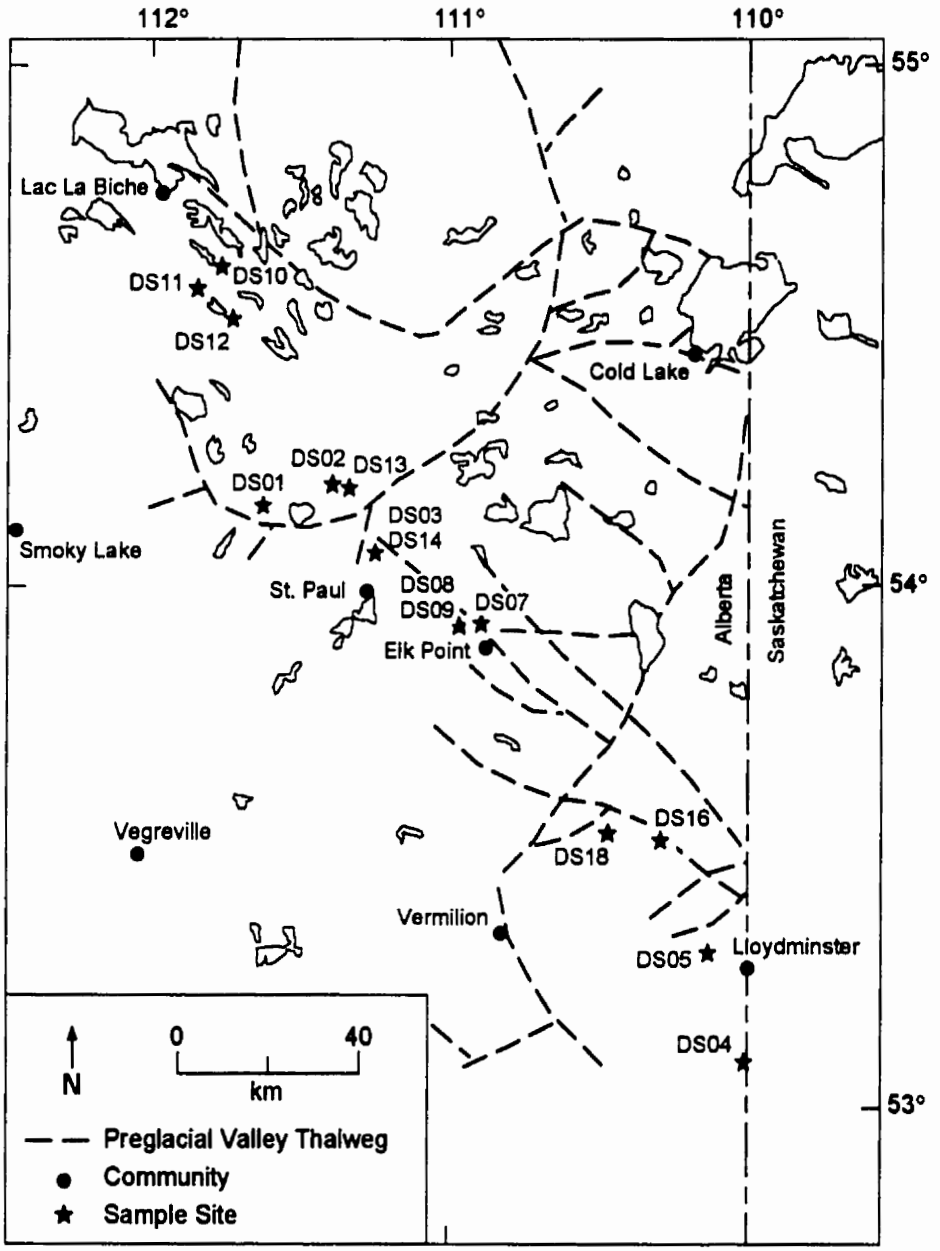

Figure 7. Map showing the location of known preglacial valleys within the Sand River and East-Vermilion map areas. Modified from Andriashek (1985) and Mougeot (1991).

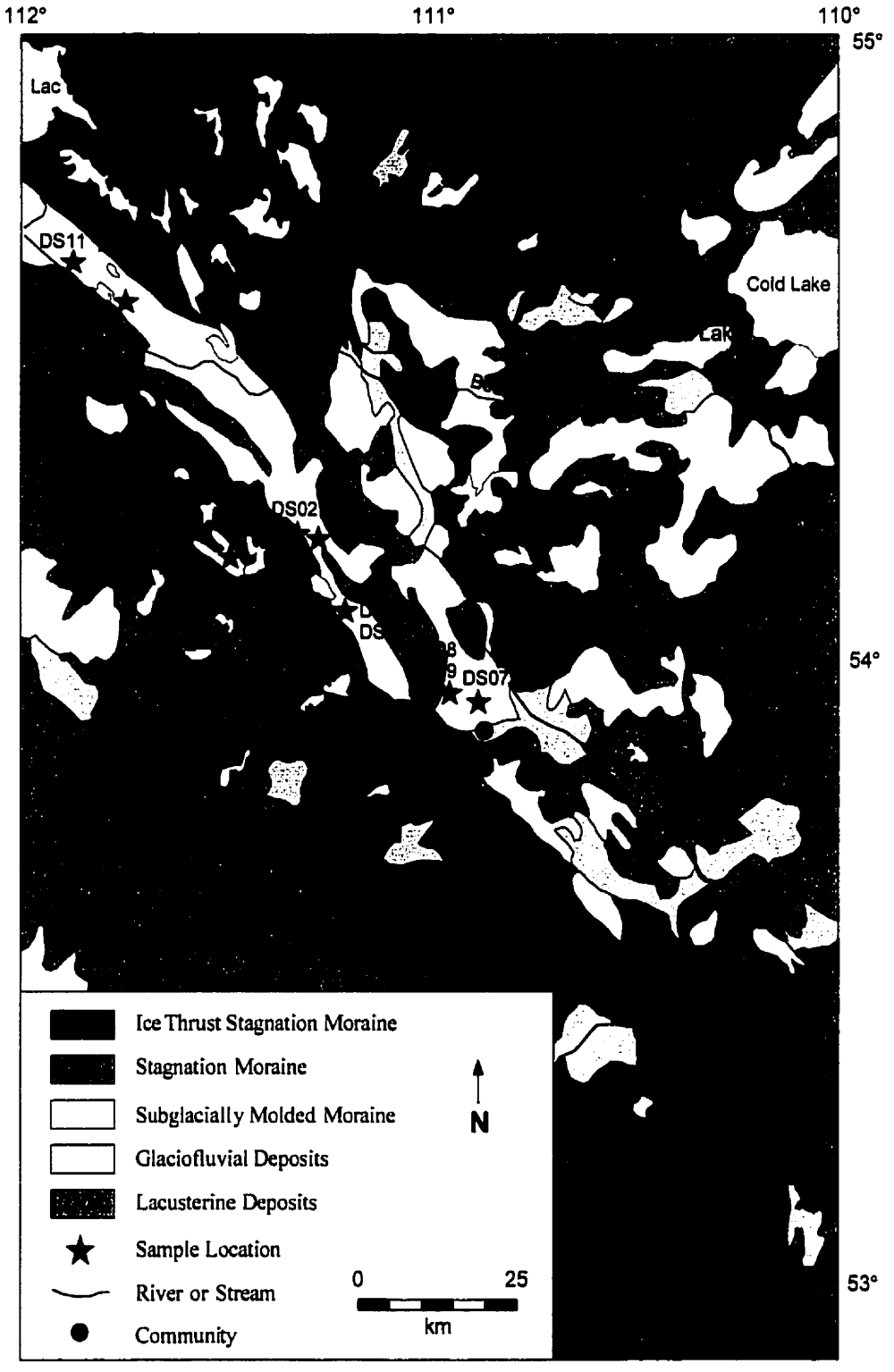

Figure 8. Surficial geology of east-central Alberta. Modified from Shetsen (1990) and Fenton and Andriashek (1983).

has a pseudostratified appearance. Strata generally consist of older sediment which has been glacially displaced and attenuated in the form of layers or beds within the diamicton (Andriashek, 1985). The Vilna Member has an average matrix texture consisting of about 32% sand, 32% silt and 36% clay. Textural variations range between 20-40% sand, 30-40% silt and 25-50% clay (Andriashek, 1985).

South of the Sand River map area, Mougeot (1991) identified a lithostratigraphic framework for the east half of the Vermilion map sheet. The Quaternary geology of this region is composed of six diamicton units associated with four major glacial events, and three stratified units related to the corresponding interglacial intervals (Mougeot, 1991). Diamicton Unit E is interpreted to have been deposited by a late glacial ice stream advance which correlates to the Lac La Biche Lobe of Andriashek (1985).

The distribution of Diamicton Unit E is well known (Figure 9). Its thickness is variable, ranging from 3 m to 24 m. The upper 2 m is generally oxidized and is described as a grayish brown to dark grayish brown diamicton with a low percentage of coarse fragments and occasionally a high content of pebbles (Mougeot, 1991). The diamicton matrix consists of clayey sand to sandy silt (average 31% clay, 28% silt and 41% sand). The surface morphology of Diamicton Unit E is predominantly fluted in a southeast orientation.

Mougeot (1991) notes that Diamicton Unit E, as a stratigraphic unit, is composed of several distinct facies. The dominant facies contained within Diamicton Unit E is Mougeot's (1991) "Dss" facies, diamicton with sand stringers. This facies exhibits discontinuous bands of diamicton interfingered with thin, discontinuous lenticular bands of moderately well-sorted massive sands. The diamicton bands are 2-10 cm thick, have a well-developed fissility and are subparallel to the topography. The sand stringers are elongated, stringy bodies that seem to have been stretched, smudged or

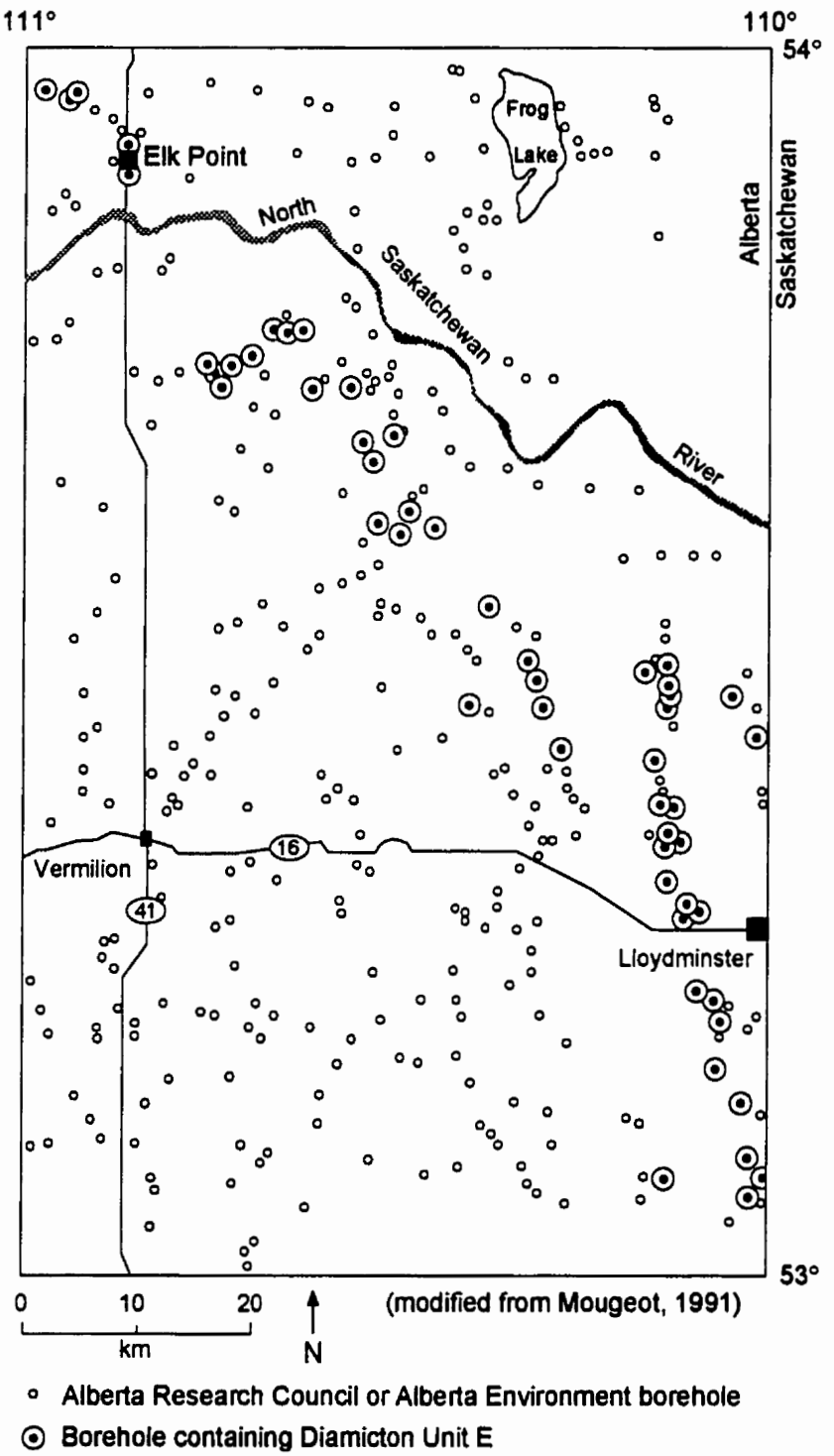

Figure 9. Distribution of Mougeot's (1991) Diamicton Unit E. Distribution of this till lithology provides evidence defining the pathway of the streaming Lac La Biche Lobe.

squeezed. Their thickness varies between 0.5 and 3 cm and their length between 10-45 cm (Mougeot, 1991). Mougeot (1991) interprets this facies as a lodgement till.

Table 1 correlates the stratigraphy of Andriashek (1985) for the Sand River map area with Mougeot (1991) for the east half of the Vermilion map area with stratigraphic units recognized in neighbouring Saskatchewan.

2.2 Lac La Biche Flute Field and Ice Stream

The dominant surface morphology within the study area are the fluted landforms which make up the Lac La Biche flute field. The field originates south and west of Lac La Biche, Alberta and extends southeastwards almost to North Battleford, Saskatchewan, a distance of approximately 390 km (Jones, 1981). However, Gravenor and Meneley (1958) noted that the Lac La Biche flute field is more extensive, having been identified through airphoto investigation to a location 48 km southeast of North Battleford Saskatchewan. Within Saskatchewan, the flutes located at the southern extent of this field are termed the North Battleford flute field (Grant, 1996). Geological investigations contrasting the diamictons contained within the flutes of Alberta and Saskatchewan have never been carried out. However, Grant (1996) suggests that the similarity in flute morphology and orientation leads to the conclusion that the Lac La Biche and North Battleford flute fields were formed by the same mechanism.

Various flute and drumlin morphologies are present; however, similar morphologies tend to be grouped together along the length of the flute field. The flutings can be roughly divided into relatively short (<5 km) and high (~5 m) fluted forms, and more elongated (15-20 km) lower (1-2 m) forms (Jones, 1981). Drumlins and drumlinoid features up to 10 m in height and 1-2 km long are also present within the field.

Table 1. Proposed regional correlations and ages of lithostratigraphic units (adapted from Andriashek, 1997).

Stratigraphic Units in east-central Alberta		Stratigraphic Units in Saskatchewan		Possible Age
Andirashek (1985)	Mougeot (1991)			
Grand Centre Formation		Battleford Formation	Upper Till ?	Late Wisconsin
Vilna Member	Diamicton Unit E		Lower Till ?	
Kehiwin Lake Member	Diamicton Unit E ?			
Reita Lake Member	Diamicton Unit D ?			
Hilda Lake Member	Diamicton Unit D ?			
Sand River Formation	Stratified Unit D			Mid-Wisconsin
Marie Creek Formation	Diamicton Unit C	Floral Formation	Upper Till	Early Wisconsin
Unit 2			Riddell Member	
Unit 1				
Ethel Lake Formation	Stratified Unit C		Lower Till	Sangamon
Bonnyville Formation	Diamicton Unit B	Sutherland Group	Warman Formation	Pre-Wisconsin
Unit 2				
Unit 1				
Muriel Lake Formation	Stratified Unit B		Dundurn Formation	Pre-Wisconsin
Bronson Lake Formation	Diamicton Unit A		Mennon Formation	Pre-Wisconsin
Empress Formation	Stratified Unit A	Empress Group		Pre-glacial
Unit 3				
Unit 2				
Unit 1				

Flint (1971) suggests that only two conclusions can be made about a region where streamlined landforms exist:

1) the presence of streamlined landforms establishes the existence of an actively flowing glacier at the time of formation.

2) the long axes of streamlined forms are a reliable indicator of the general ice movement direction.

On this basis, several authors including Gravenor and Meneley (1958), Ellwood (1961), Jones (1981), Andriashek (1985), and Mougeot (1991) have proposed the existence of the so-called "Lac La Biche ice stream" to explain the formation of the Lac La Biche fluted landforms. Perhaps more importantly, geological evidence obtained by all of the above authors has provided further support to the interpretation of a narrow, fast-flowing late Wisconsin ice stream which flowed along the path of the Lac La Biche flute field.

Interpretations of the morphology and theories for the origin of the Lac La Biche ice stream have varied through time. Lac La Biche ice stream was first proposed by Gravenor and Meneley (1958), who mapped the distribution of fluted landforms within central and northern Alberta from airphoto investigations. Microfabric studies carried out by Gravenor and Meneley (1958) on till located in the upper 3 m beneath the crests of flutes in the North Battleford area showed trends parallel to the flute crest (NW-SE) with plunges of up to 20° to the northwest. Till sampled below 3 m had microfabrics trending a few degrees east of north, although there was no apparent change in the mechanical composition of the till or no evidence to suggest that more than a single till was present. Gravenor and Meneley (1958) state this fabric data indicates that the upper 3 m of till within the flutes was eroded and transported from the grooves between flutings and deposited to form the fluting ridges by ice flowing parallel to the trend of the flutings. Gravenor and Meneley (1958) suggest that the Lac La Biche flutings were

probably developed during deglaciation, the result of remolding of existing till by a local readvancing ice lobe.

Jones (1981) investigated the Lac La Biche flute field in the region of St. Paul, Alberta. Sand wedges in till just north of the Lac La Biche flute field were identified by Jones (1981). The sand wedges contained well-sorted, fine yellowish brown aeolian sand exhibiting vertical layering and sharp contacts with the surrounding till. Based on the presence of the sand wedges, Jones (1981) interpreted that an arid periglacial period existed for several hundred years after the retreat of the main late Wisconsin ice which was maintained during the Lac La Biche resurgence. Thus, Jones (1981) proposes that the Lac La Biche Lobe advanced over permafrost, thereby restricting subglacial drainage which assisted in the development of a streaming lobe and the associated glacio-tectonic thrusting. However, it is shown by Mougeot (1991) and in this thesis that sand wedges were also developed within till deposited by the Lac La Biche ice stream. Therefore, the timing of permafrost and its relation to the development of the ice stream is uncertain.

An area of ice convergence located between Cold Lake and Lac La Biche was also discovered by Jones (1981), who suggested that ice flowing in a southwest direction west of Cold Lake was contemporaneous with Lac La Biche ice flowing in a southeasterly direction. Ice convergence was interpreted by observing the orientation of streamlined landforms within this area. Areas of ice convergence are typically present at the head of ice streams as increased ice velocity is required to provide mass balance for the glacier (Marshall, 1996).

Clast fabrics for the diamicton contained within the fluted landforms investigated by Jones (1981) consisted of unimodal, bimodal and girdle (multimodal) distributions. "Herring bone" clast fabric patterns were observed in flute cross-sections, suggesting fluting formation by till migration due to subglacial pressure variation (Jones, 1981). Since lithologic analysis revealed that most till samples showed little variation in coarse

sand mineralogy percentages across the study area, Jones (1981) suggested that the same till is present throughout all of the fluted landforms. This also may imply that the material making up the flutings was derived from the same source area, and formation occurred during only one ice advance (Jones, 1981).

Through investigations of the Quaternary stratigraphy of the Sand River map area Andriashek (1985) and Andriashek and Fenton (1989) suggest that the Lac La Biche flute field was formed by the Lac La Biche Lobe during a readvance of the retreating margin of the Seibert Lobe. The Lac La Biche lobe flowed southeast, essentially parallel to the margin of the Seibert Lobe to the north (Andriashek, 1985). These lobes are believed to have formed by the differentiation of the Late Wisconsin Laurentide ice subsequent to the commencement of its retreat from the glacial maximum in southern Alberta. The Lac La Biche Lobe may have originated in southwestern Saskatchewan, where the terminus of the lobe is recognized, with the ice flow gradually extending up-glacier from that area into the Sand River area. (Andriashek and Fenton, 1989). This interpretation of the morphology of the Lac La Biche ice stream is similar to the morphologies of contemporary Antarctic ice streams. This suggests that the previous authors interpretations that the Lac La Biche ice stream resulted from the readvance of a streaming ice lobe into an otherwise ice free area may be incorrect.

Andriashek and Fenton (1983) note that the ice stream which was erosive along the northeast facing flank of the regional topographic uplands located in the southwest corner of the Sand River map area. This erosion occurred in the form of extensive glacial ice-thrusting which displaced large, intact blocks of the underlying units (eg. Figure 8, ice thrust stagnation moraine northwest and southeast of St. Paul)(Fenton and Andriashek, 1983). Moran *et al.* (1980) suggest that glacier thrusting is associated with frozen bed conditions, while the presence of flutes and drumlins indicates a wet glacial bed. The distribution of thrust moraine and fluted landforms in the study area may therefore

reflect the variable bed conditions of the Lac La Biche Lobe and partially explain the dynamics of the Lac La Biche ice stream.

Working in the region of North Battleford, Saskatchewan, Stauffer *et al.* (1990) note that the flutes of the southeast oriented North Battleford flute field were eroded into the upper surface of the underlying Floral Formation and are now mantled by a thin Battleford Formation till. A boulder pavement located at the base of the Battleford till, showed striations with an average trend of 111°, matching that of the surface morphology of the flutes (Stauffer *et al.* 1990). The flutes were therefore interpreted to have been formed by the late Wisconsin Battleford Lobe during glacial advance and retreat.

Further geologic evidence supporting the existence of the Lac La Biche ice stream is provided by "ice crevasse fill" ridges in the Lloydminster region which are interpreted to have been deposited by the stagnating Lac La Biche ice stream (Ellwood, 1961; Mougeot, 1991). The ridges consist predominantly of till; however, ridges containing deformed bedrock have also been identified. Most of the ridges are 1 m to 12 m high, 3-300 m wide and up to 6 km long. They are concave in plan view towards the northwest which is normal to the direction of ice advance as evidenced by the direction of the flutings. The arcuate ridges are connected by a radiating array of generally straight ridges forming a polygonal or netted pattern with a variable spacing averaging 100-300 meters (Mougeot, 1991).

Both Ellwood (1961) and Mougeot (1991) have interpreted the ice crevasse fill ridges as being deposited within remnant stress fractures in the stagnating ice of the Lac La Biche ice stream as it advanced up the topographic slope toward Lloydminster. As the ice stagnated and melted, entrained material filled the melting fractures producing the observed crevasse fill deposits (Ellwood, 1961).

2.2.1 Alternative Hypothesis for the Formation of the Lac La Biche Flute Field

An alternative hypothesis proposes that flute formation resulted from subglacial megaflood erosion of basal sediments and the underside of the Laurentide ice sheet (Shaw, 1983; 1989; 1994; Shaw and Sharpe, 1987; Shaw, Kvill and Rains, 1989). According to this hypothesis, flutes result from the erosion of existing subglacial material through the development of helical horseshoe vortices within subglacial sheet flows (Shaw, 1994). On the basis of form analogy only, Rains *et al.* (1993) and Shaw *et. al.* (1996) use the Lac La Biche flutings as regional scale evidence defining the path of a subglacial megaflood within Alberta.

Further to the south, a geomorphic and geologic investigation of the North Battleford flutings was carried out by Grant (1996). Grant concluded that the North Battleford flutings were erosional forms and that the most likely agent of erosion was subglacial megaflood. The fluted forms would have had to have been eroded some time near the late Wisconsin glacial maximum (Rains *et al.* 1993).

Although the formation of flutes and drumlins through erosion by subglacial megaflood may be valid in some areas, this hypothesis is rejected for the formation of the Lac La Biche flute field. Abundant geologic evidence supports the interpretation of the Lac La Biche ice stream while there is a general lack of physical geologic evidence to support the flood hypothesis for this same area. Grant's (1996) interpretation of an erosional form to some of the Battleford flutes is justified, however there is no convincing geologic evidence to suggest that the erosional mechanism was subglacial sheet flow.

Several lines of geologic evidence support the ice stream hypothesis for the formation of the Lac La Biche flutes and drumlins. These include: 1) the corresponding narrow distribution, fluted surface morphology and stratigraphic position of both

Mougeot's (1991) Diamicton Unit E (Figure 9) and Andriashek's (1985) Vilna Member in the Vermilion-east and Sand River map sheets. 2) Clast fabric data (Gravenor and Meneley, 1958; Jones, 1981; and this thesis) and boulder pavement striation data (Stauffer *et al.* 1990) obtained from diamicton making up the flutes suggests a corresponding ice flow direction towards the southeast. This agreement between the internal sedimentology of the flutes and external flute morphology suggests a formative relationship between the two which is not explained by Shaw's theory. 3) The presence and plan view pattern of "ice crevasse ridges" (Ellwood, 1961; Mougeot, 1991) in the region of Lloydminster. The pattern and distribution of the ridges suggests deposition by a narrow stagnating ice mass which flowed from the northwest.

2.3 Deglacial History

Christiansen (1979) proposed a late Wisconsin deglacial sequence for southern Saskatchewan and the adjacent portions of eastern Alberta and western Manitoba. A down-melting model of deglaciation was used as a guide in reconstructing ice-marginal positions (Christiansen, 1979). Nine phases of deglaciation are recognized, with the deglaciation of the Sand River and Vermilion map sheets occurring between 12,500 and 11,000 ^{14}C yrs BP. More recently, the lowermost ^{14}C dates obtained from core sampled at both Moore Lake (54° 30' N, 110° 30' W) and Lofty Lake (54° 44' N, 112° 29' W) suggest that these regions in the Sand River and Tawatinaw map sheets were ice free by approximately 11, 300 ^{14}C yrs BP (Schweger and Hickman, 1989; Lichti-Federovich, 1970).

Geological evidence from the path of the Lac La Biche ice stream in the region of Lloydminster suggests glacial retreat through ice stagnation and downmelting. However, the presence of streamlined landforms to the northwest, suggests either active retreat or

the stagnant melting of relatively debris free Lac La Biche ice. Stagnant downmelting of debris laden basal ice would have likely obscured these basally molded deposits. Regions of flow extension in surging glaciers and ice streams typically have a thin layer of debris laden basal ice which is unlikely to release sufficient debris to veneer the subglacially molded surface (Martin Sharpe, pers. comm. 1998). The absence of ice stagnation features and significant meltwater erosion in the fluted terrain also indicate that meltwaters were probably restricted to meltwater channels which flank the flute field (Jones, 1981). However, minor ponding might have occurred locally at the surface of the melting ice, as indicated by small and thin deposits of fine-grained sediments overlying the flutes and crevasse fills (Mougeot, 1991).

2.4 Post-Glacial Climate

Patterned ground created by permafrost conditions (i.e., sand wedges) is recognized in various locations around the Vermilion map area by Ellwood (1961), Jones (1981), and Mougeot (1991). The presence of sand wedges with widths of up to 1 m and depths penetrating to 2.5 m below the surface led Ellwood (1961) to suggest that a 500 year period of permafrost conditions existed after deglaciation. The well-preserved nature of the wedges combined with the degree of sorting and sand grain size suggest the sand was deposited by aeolian processes associated with arid conditions (Ellwood, 1961; Jones, 1981).

Using pollen analysis as a proxy for paleoclimate, Schweger and Hickman (1989) describe changes in the Holocene climate of central Alberta. The pollen record obtained from a 9 m core from Moore Lake is dominated by spruce pollen from 11,300 ± 170 ^{14}C yrs BP until 9250 ± 80 ^{14}C yrs BP, when a transition occurred to grassland and saline tolerant species dominating until 5850 ± 80 C^{14} years. After that time, spruce pollen is

seen to dominate until the present day. This pollen record, combined with other evidence seen in the core, suggests the presence of an arid climate in the early to mid Holocene. Schweger and Hickman (1989) also suggested the arid climate may have resulted in a possible 15 m drop in the level of Moore lake during this interval.

Chapter Three

Methods

3.1 Field Methods

Field methods involved the selection of sites suitable for collection of undisturbed diamicton samples for geotechnical consolidation tests, and bulk samples for grain size analysis and coarse sand grain mineralogical analysis. A wheeled backhoe was used to excavate pits from which all samples were collected, section descriptions were recorded and diamicton clast fabrics measured.

Sample sites were selected according to the following criteria:

1) Close proximity to a preexisting borehole or water well location where lithologic information is recorded for the subsurface. Subsurface lithologic information is required to allow for comparison with calculated preconsolidation values at each site, between sites and to indicate the potential for subglacial drainage through groundwater flow. Borehole and water well records containing lithologic information were obtained from Alberta Environmental Protection Water Well Drillers Report Forms obtained from Alberta Environment and Alberta Environment scientific borehole records obtained from Mougeot (1991) and Andriashek (1985).

2) Likelihood that the samples recovered would represent basally deposited material which was overrun by the Lac La Biche ice stream. Sampling was restricted to areas where flutes or fluted landforms were present on the surface, and/or to areas mapped as fluted moraine, draped moraine with southeast-oriented fluted landform symbols and discontinuous stagnation moraine with southeast-oriented fluted landform symbols on the surficial maps published by Shetsen (1990), Mougeot (1991), and

Fenton and Andriashek (1983). Andriashek (1985) and Mougeot (1991) contain regional cross-sections which indicate the thickness and distribution of sediments interpreted to have been deposited by the Lac La Biche ice steam.

3) Value of the site in terms of providing data from regionally diverse areas as well as areas which could provide potentially useful information. Sample sites were chosen at both the northern and southern extent of the ice stream path within Alberta, as well as locations interpreted to be near the ice stream margin.

4) Land owners' permission and the availability of non-productive or "out of the way" locations.

3.1.1 Sample Collection

Samples of diamicton for all laboratory tests were collected from sites in east-central Alberta meeting the above criteria (Figure 2, Figure 8). All samples were collected from the base of ~2.0 m - 3.0 m deep pits excavated by wheeled backhoe from below the level of major pedogenic influence and annual freezing.

At three locations (DS01, DS02 and DS03), 75 mm tapered end Shelby tubes were used to obtain samples for consolidation testing. The tubes were pushed into the diamicton at the base of the sample pit using the backhoe bucket. It was originally planned that all samples for consolidation testing would be collected using Shelby tubes; however, the hardness of the diamicton combined with the presence of clasts limited the effectiveness of this sampling technique. It was suspected that the samples collected may have been significantly disturbed. Four tube samples were taken at each of the three excavation sites in the hope of obtaining at least one with minimal disturbance. Immediately after sampling, the ends of the tubes were sealed with melted paraffin to prevent moisture loss.

The primary method used to obtain undisturbed samples for consolidation testing was the block sampling technique. One 25 cm cubic block sample was collected from each of twelve sample locations (DS04, DS05, DS07, DS08, DS09, DS10, DS11, DS12, DS13, DS14, DS16, DS18). Samples were cut using saw and shovel from a 75-100 cm high, 50 cm wide diamicton "wall" left in place along the centre of the base of the sample pits. Block samples were wrapped in plastic before being placed inside plywood boxes for transport back to the laboratory the same day.

All samples were brought to the University within 8 hours of sampling and stored overnight in the Civil Engineering Department moisture room. The next day, the samples were wrapped in plastic wrap, cheese cloth and coated with melted wax to prevent moisture loss. Samples were then stored in the Civil Engineering laboratory moisture room at a temperature of 4°C until tested.

3.1.2 Section Description

Diamicton clast shape, lithologic contacts and sedimentary structures were described and measured in each excavated section. Colours were described using a Munsell colour chart. Clasts larger than 1 cm were discarded from bulk samples and their percentage visually estimated.

3.1.3 Clast Fabric Measurements

A single set of clast fabric data were obtained from the diamictons exposed within each sample pit for the purpose of assisting in the interpretation of the processes responsible for till deposition and subglacial modification. It is clearly understood that multiple criteria, including *assemblages* of clast fabric data are required to properly

characterize and interpret the processes responsible for the emplacement of any diamicton. However, the use of a backhoe (hired by the hour) to excavate a temporary exposure resulted in a limitation in the amount of data which could be reasonably collected at each site.

The orientation of clasts with a:b axes of at least 3:2 were measured from as small an area as possible (in most cases within 1 m^2). The trend and plunge of a minimum of 25 stones larger than 1 cm (measured along the a axis) were measured at each location. Fabric data were entered into a computer program (Rockworks STEREO) and projected onto lower hemisphere equal area Schmidt net for interpretation. Density plots of clast fabric data were also plotted using a 2% contour interval.

Eigenvalues are related to fabric shape which is largely determined by the mode of sediment formation (Mark, 1974; Dowdeswell and Sharp, 1986; Hart, 1994; Benn, 1994a; Hicock *et al.* 1996). Therefore, as a means of assisting in the interpretation of multimodal clast fabrics and the mode of deposition of exposed tills, isotropy data (S_3/S_1) derived from clast fabric measurements at each site was plotted against qualitatively derived modality categories on a modality-isotropy diagram as presented by Hicock *et al.* (1996). The modality categories presented in Hicock *et al.* (1996) include:

Unimodal cluster (un) - tightly grouped single concentration of long axis points as plotted and contoured on a Schmidt equal-area net.

Spread unimodal (su) - loosely grouped but still a single concentration; no breaks or deep indents in the central parts of contour envelopes.

Bimodal clusters (bi) - Distinctly grouped concentrations and envelopes are separated at about 90°.

Spread bimodal (sb) - loosely grouped concentrations separated by about 90°, contour envelopes are separated or are deeply indented in their central parts.

Multimodal (mm) - three or more distinct concentrations to random distribution of points, contour envelopes are either broken up into several envelopes, are continuous around the perimeter, are continuous around a great circle, or are a combination of these patterns.

3.2 Laboratory Methods

3.2.1 Consolidation Testing

Consolidation testing was carried out using floating-ring type oedometers following the procedure of Bowles (1992). Consolidation tests were carried out on three 63 mm diameter consolidation ring samples cut by hand from each undisturbed field sample. Preconsolidation values were determined for each sub-sample by applying the graphical Casagrande (1936) method to consolidation test results. The Casagrande method is suitable for use in this study as the majority of derived consolidation curves show a distinct break in slope above the virgin compression line. Also, calculated preconsolidation values are generally low, allowing for relatively concise evaluation of graphical results. The mean of the three preconsolidation values derived from individual consolidation test results is assumed to represent the site preconsolidation value.

Consolidation tests involved the application of eight consecutively doubling load increments (37 kPa, 74 kPa, 148 kPa, 296 kPa, 592 kPa, 1184 kPa, 2368 kPa then 3500 or 4736 kPa) to each 63 mm ring sample. It was noted for some samples that sediment was extruded out of the consolidation ring with the application of the 4736 kPa load increment. Sediment extrusion can result in significant error in the calculated void ratio

for that load increment. Therefore, the final load increment for later tests was changed to 3500 kPa in an attempt to avoid this problem. Dial readings were recorded to the nearest thousandth of a millimeter. Time versus dial readings for each load increment were plotted using the square root-time methodology of Taylor (1948). Both the Taylor method square root-time plots and the Casagrande method void ratio versus log of normal stress plots were constructed using KaleidaGraph version 3.0.5 software for Macintosh.

The sample in situ overburden pressure was calculated using an estimated value of 15 kPa per meter depth below the surface. Ice overburden pressure (p_i, Equation 1) was calculated by assuming a meter-square column of glacial ice imposes a load of 8.9 kPa per meter height (Jenson, 1993).

3.2.2 Grain Size Analysis

Grain size was calculated to characterize the till at each site and so that the permeability of the bed can be compared between sites. Grain size analysis was carried out using the A.S.T.M (1964) hydrometer and sieving methods. Grain size classification is based on the Wentworth (1922) classification scale with a sand-silt boundary at 0.0625 mm (+4 ϕ) and the silt-clay boundary at 0.0039 mm (+8 ϕ). Sediment specific gravity was assumed to be 2.65.

3.2.3 Coarse Sand Petrology

Characterization of the diamicton sampled at each site includes lithologic analysis of the coarse sand fraction (1-2 mm). Petrographic identification was carried out following the procedures and criteria of Andriashek (1985). A minimum of 300

grains were identified from each sample and sorted by lithology. Lithologic categories include; igneous and metamorphic, quartz, quartzite and quartz sandstone, local (siltstone, shale, ironstone, sandstone), dolostone, limestone and other. Dolostone and limestone were differentiated by staining with alizarin dye following the procedure of Friedman (1959).

3.2.4 Coefficient of Permeability

A coefficient of permeability was calculated for the diamicton at each sample site for the purpose of estimating the potential for sub-glacial drainage through the glacier bed at each location. The coefficient of permeability of clay rich sediments can be calculated from the consolidation parameters m_v and C_v derived from standard consolidation tests (Head, 1994) where:

$$k_t = 0.31 \times 10^{-9} C_v m_v \qquad (2)$$

k_t = coefficient of permeability (m/s), at the test temperature of $T°$, during a stated load increment. C_v = coefficient of consolidation (m^2/year). m_v = coefficient of volume compressibility (m^2/kPa). k_t was calculated for a confining pressure of 148 kPa at the laboratory temperature of approximately 23°C. Coefficient of consolidation is calculated from

$$C_v = \frac{0.197 H_{50}^2}{t_{50}} \qquad (3)$$

where H_{50} = one half of the height of the sample at 50% consolidation , and t_{50} = time for 50% consolidation as determined from consolidation test data. Coefficient of volume compressibility is calculated from

$$m_v = \frac{\Delta e}{\Delta p} \div (1 + e_0) \qquad (4)$$

where $\Delta e/\Delta p$ is the slope of the consolidation curve and e_0 is the initial void ratio. Results were not corrected to reflect sub-glacial temperature conditions. Corrections for temperature are normally made more for the standardization of results that for the apparent increase in accuracy of C_v and k_f values, which are little more than an indication of an order of magnitude (Head, 1994:368).

Chapter Four

Consolidation Theory

4.1 Introduction

This chapter includes a review of consolidation theory, including its application to laboratory consolidation testing and problems associated with the application of consolidation theory to glacial sediments. A review of previous work where consolidation testing was applied to geologic applications is also contained within this chapter. An understanding of consolidation theory and its application to glacial sediments is fundamental to the interpretation of preconsolidation results derived from basal tills deposited by the Lac La Biche ice stream.

Consolidation occurs where particles are packed under the application of a load (Figure 10). Sediments which are consolidated only by the weight of overlying material including water are considered to be normally consolidated. Sediments consolidated beyond their vertical confining stress are termed overconsolidated. The maximum stress experienced by an overconsolidated sediment is termed the preconsolidation value which represents a record of stress history, independent of lithology (Sauer and Christiansen, 1991). Casagrande (1936) found that the preconsolidation value of an overconsolidated sediment could be determined with the application of a simple graphical technique to a void ratio versus log of pressure plot (herein called the consolidation curve) derived from consolidation test data (Figure 11).

4.2 Consolidation Theory

When an external load is applied to a saturated fine-grained sediment, the entire

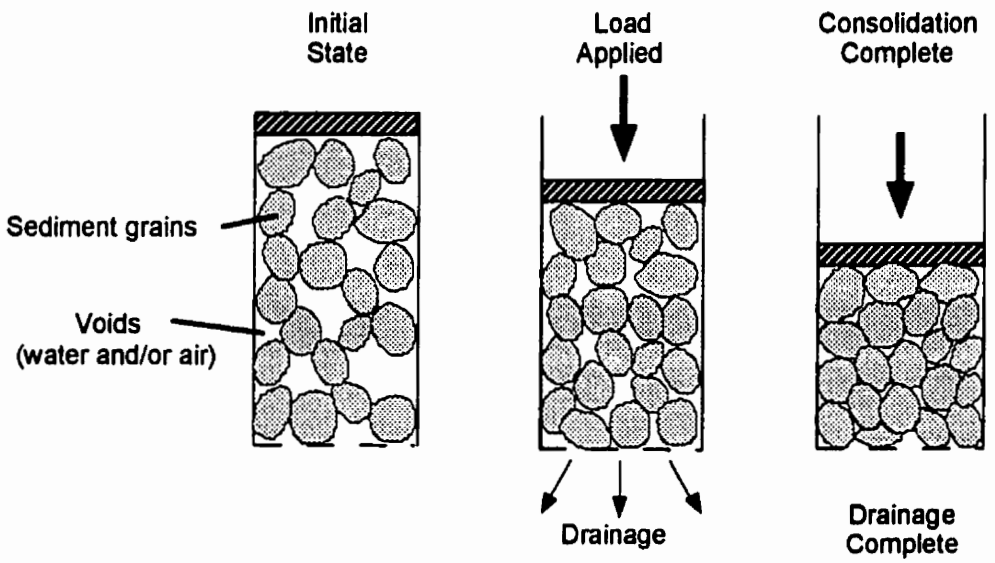

Figure 10. Representation of sediment consolidation. Compression results in consolidation due to a reduction of void space through drainage. Consolidation is complete when intergranular contact supports the applied load. Drainage ceases due to the dissipation of internal pore water pressure. Adapted from Boulton and Dobbie (1993).

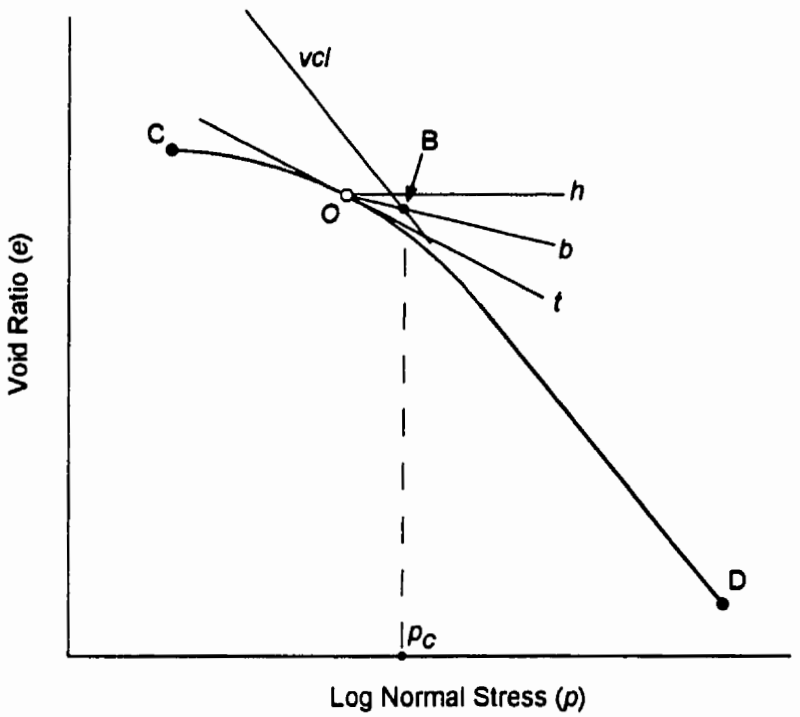

Figure 11. Consolidation curve CD of an overconsolidated fine grained sediment. Preconsolidation value (p_c) at B is found by applying the Casagrande (1936) method. *O* is point of maximum curvature determined by eye, *h* is horizontal, *t* is tangent to *O*, *b* is the bisector of the angle *hOt*, *vcl* is the virgin compression line extension, B is the preconsolidation value.

load is first carried by the pore water. This external stress induces pore water pressure equal to the applied load (Head, 1994). The resulting hydraulic pressure gradient gradually dissipates if pore water is permitted to drain into the surrounding medium. During drainage, the excess load is transferred from the pore water to the sediment grains, resulting in plastic deformation and a corresponding reduction in sediment void space. The difference in the total applied load (p) and the pore water pressure (p_w) is termed effective pressure (p'):

$$p' = p - p_w \tag{5}$$

Primary consolidation is considered complete when interstitial pore water pressure is reduced to zero, drainage ceases and the load is carried by the sediment skeleton. The length of time for consolidation to occur depends on how fast excess pore pressure dissipates by Darcian flow. The coefficient of permeability, the viscosity of the escaping liquid and the distance the pore fluid must travel to dissipate the excess pressure are the primary controls that determine how fast consolidation takes place.

The volume change during consolidation takes place only in the voids as the sediment particles are assumed to be incompressible. The change in void space is described in terms of a void ratio, defined as the ratio of the volume of void space within a sediment to the volume of the solid particles (Head, 1994). During a consolidation test, the change in sample height (ΔH) from an initial height (H_0) corresponds to a change in voids ratio (Δe) from an initial void ratio (e_0).

The compression of fine-grained sediment is divided into three possibly overlapping phases: initial compression, primary consolidation and secondary compression (Figure 12). Initial compression occurs after the application of a load and

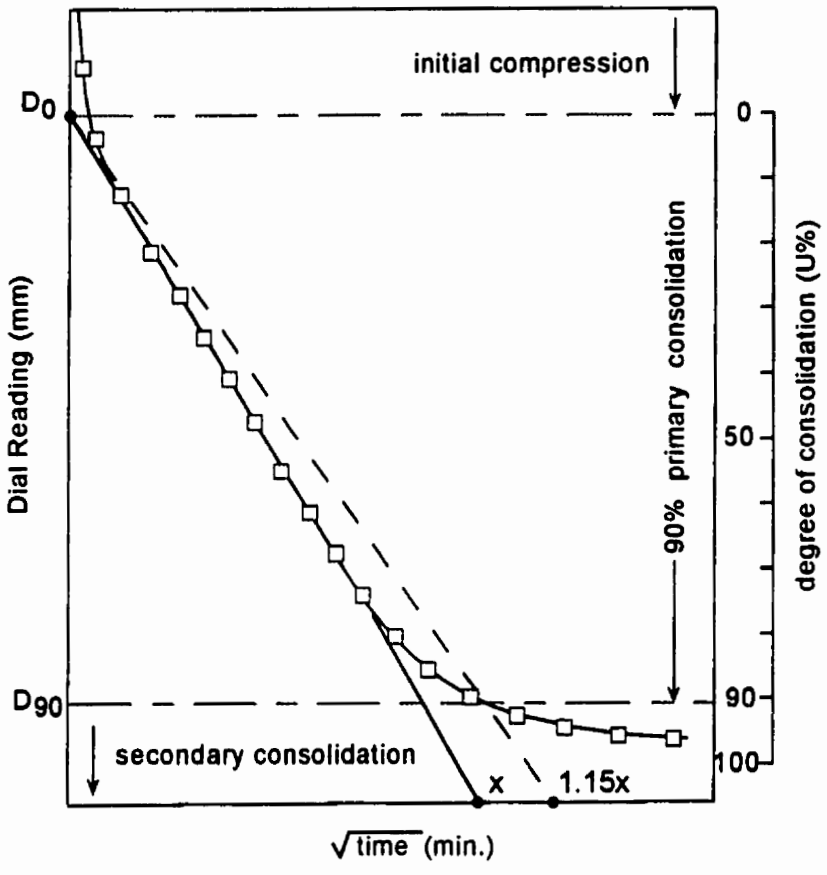

Figure 12. Taylor (1948) method for determining time and dial reading at 100% primary consolidation. D_0 is the dial reading at the beginning of primary consolidation, D_{100} is calculated by $D_{100} = D_0 + 10/9 (D_{90} - D_0)$. Boxes represent individual dial readings taken as consolidation proceeds. The shape of the curve denotes when initial, primary and secondary consolidation occurs within the sample.

before the commencement of drainage. It is due to compression of small pockets of gas within the pore spaces and to the compression of contact surfaces in the consolidation cell and in the load frame (Bowles, 1992). Primary consolidation represents the transfer of the applied stress from the pore water to the sediment skeleton. Secondary compression continues after the excess pore pressure of the primary phase has dissipated. Secondary compression may represent the continued movement of particles as the sediment structure adjusts to the increasing effective stress (Head, 1994).

During the process of primary consolidation, the extent or degree of consolidation (U), is determined from the change in height of the sample (ΔH), at time (t) divided by the total change in height (ΔH_f):

$$U = \frac{\Delta H}{\Delta H_f} \times 100\% \qquad (6)$$

Taylor (1948) notes that the rate of consolidation proceeds along an approximate exponential curve so that low degrees of consolidation occur very rapidly after the onset of normal stress. Beyond 95% consolidation, the curve becomes asymptotic so that theoretically, the time required to achieve 100% consolidation is infinite (Figure 12). However, the time to achieve U=100% under a static load can be determined by employing the Taylor (1948) method (Figure 12). This time value is required to calculate a void ratio for U=100% during each load increment.

4.3 Consolidation Tests

Consolidation tests are carried out on an oedometer which measures the change in a sample's height with the application of consecutively doubling loads. This progressive consolidation of a sample is recorded by calculating the void ratio at U=100% for each load increment. The void ratios from consecutive load increments are

plotted on a graph of e versus log p forming a consolidation curve (Figure 13, see Appendix 3). So long as drainage from the system is uninhibited, consolidation proceeds at a logarithmically decaying rate that is a function of the effective confining pressure (Jenson, 1993):

$$e = e_0 - C_c \log \frac{p}{p_0} \tag{7}$$

where e is the void ratio, p is the applied vertical stress, e_0 is the void ratio at the designated pressure p_0, and C_c is the compression index which is equal to the change in void ratio for one log cycle of pressure change along the straight line portion of the consolidation curve. The straight line portion of this curve is termed the virgin compression line (Figure 13, line AB and BD).

A release of all or a portion of the confining stress from fine grained surficial sediment will result in a slight increase in void ratio due to the semi-plastic nature of the sediment. This expansion is visualized by line BC (Figure 13). With the re-application of normal stress the void ratio will only decrease slightly until the preconsolidation value is exceeded, when the consolidation curve will once again approximate the virgin compression line (line CD, Figure 13). Consolidation data derived from tests carried out on overconsolidated sediments (eg. glacially overrun tills) represents a recompression curve (eg. Figure 11) from which the previous maximum stress experienced by the sample can be determined.

4.4 Previous Work

With the earliest work in preconsolidation testing, Casagrande (1936) noted the potential of this technique as a tool to assist in geological investigation and interpretation. Casagrande (1936) suggests:

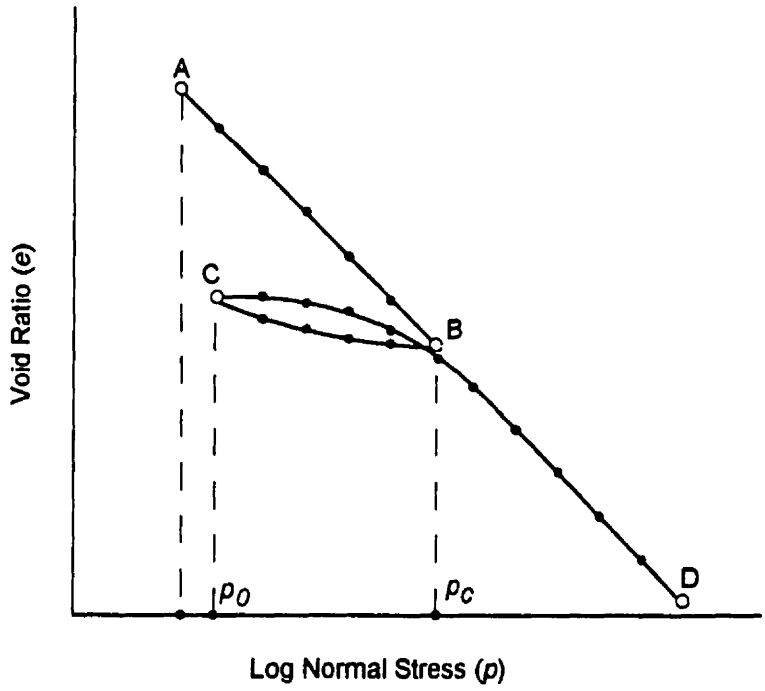

Figure 13. Theoretical consolidation curve for a single fine-grained sediment undergoing a load-unload-reload consolidation cycle. Dots represent *e* calculated at U=100% for individual load increments during consolidation test. Line AB follows the virgin consolidation curve to the preconsolidation pressure (p_c) at B. Unloading produces curve BC to C which represents the *in situ* effective overburden pressure (p_0). The reloading curve CD approaches the virgin consolidation line past p_c.

> "Most fine grained, compressible soils, particularly all clays, seem to have their geologic history recorded like a photograph in an undeveloped negative."

The real key to developing this geologic "photograph" lies in increasing our understanding of the subglacial processes which have acted to imprint their signature upon overrun sediments. Consolidation theory is well understood, it is our interpretation of preconsolidation results which leads us to gain insight into quantifying subglacial processes, and to allow preconsolidation data to act as a proxy record of past glacial events.

Since the promising statement of Casagrande (1936) was published, the use of preconsolidation testing in geological interpretation has evolved as its limitations, and new potential are realized. A compilation of published works employing consolidation testing in applications of geologic interpretation is summarized on Table 2.

In the earliest work (Harrison, 1958; Kazi and Knill, 1969) assumed that consolidation testing of glacially overrun sediments simply provided estimates of local Pleistocene ice thickness. Advances were made by Aario (1971) and Boulton, Dent and Morris (1974) who included the effects of subglacial hydrology in their interpretation of sediment preconsolidation values. The first comprehensive use of consolidation testing in determining subglacial conditions of a Pleistocene glacier was published by Brown *et al.* (1987). Sauer and Christiansen (1988; 1991) and Sauer, Egeland and Christiansen (1993) interpreted the mode of deposition of glacial sediments and aspects of Laurentide basal hydrology in Saskatchewan in part, from consolidation test results.

The most far-reaching utilization of consolidation results was presented by Boulton and Dobbie (1993). They inferred basal melting rates, subglacial ground water flow patterns, ice overburden thicknesses, basal shear stress and the amount of sediment removed by erosion from sites in England and the Netherlands by noting changes in till

Table 2. Summary of previous work

Author	Application	Findings
Casagrande (1936)	Noted potential of the consolidation test as a tool to assist in geological investigation.	Stress history recorded in sediments like a "photographic negative".
Rominger and Rutledge (1952)	Used consolidation testing to investigate Lake Agassiz water level fluctuations. Sediments exposed by Lake Agassiz retreat were consolidated by desiccation.	Recorded periods of sediment desiccation.
Harrison (1958)	Constructed Laurentide ice profiles from consolidation results obtained from glacially overrun silts. Assumed no pore water effect.	Preconsolidation values of 627-4540 kPa suggested ice thicknesses of 71-516 m in central Saskatchewan.
Kazi and Knill (1969)	Determined thickness of glacial ice which deposited the Cromer, Norfolk Till. Assumed no pore water effect.	Preconsolidation values of 620-1150 kPa along a 12 mile transect.
MacDonald and Sauer (1970)	Used consolidation testing to distinguish till units in central Saskatchewan. Speculated that differing preconsolidation values resulted from differing geological history.	Preconsolidation value of Battleford Formation till 352 kPa. Floral Formation till 861 kPa.
Aario (1971)	Comprehensive work to determine the presence of glacially consolidated glaciomarine sediments in Finland. Does not attempt estimate at ice thickness due to presumed basal pore water pressure.	Recorded distribution of glacially overrun marine sediments.
Boulton, Dent and Morris (1974)	Used consolidation tests to determine relationship between ice thickness, subglacial hydrology and shear deformation for the till deposited by the Breidamerkurjokull glacier, Iceland.	Effective basal pressure is more influenced by the geology and hydrology of the subglacial bed than by ice thickness.
Boulton and Paul (1976)	Investigate consolidation characteristics of supra and subglacial tills. Investigated the effect of postglacial processes on sediments preconsolidation value.	Consolidation models developed for supra and subglacial tills. Determined that postglacial processes can affect preconsolidation values.
Mickelson, Acomb and Edil (1979)	Consolidation testing of tills deposited by the Lake Michigan Lobe.	Preconsolidation values of 1600-2000 kPa. Interpret temperate glaciation during late Wisconsin with basal pore water pressure 69-76% of ice thickness.
Brown *et al.* (1987)	Multicriterial investigation of subglacial conditions of the Cordilleran, Puget Lobe.	Preconsolidation values 1000-3000 kPa indicate basal pore water pressures exceeding 90% of ice overburden pressure.

Table 2. continued

Author	Application	Findings
Sauer and Christiansen (1988)	Consolidation tests on Floral Formation silts in central Saskatchewan.	Preconsolidation values of 1430 kPa indicate presence of basal pore water pressures of 80% ice thickness.
Van Gelder *et al.* (1990)	Reconstructed Pleistocene valley glacier profiles with consolidation testing of overrun sediments in Vorarlberg Valley, Austria.	Preconsolidation values of 3800-5250 kPa were less than expected from geomorphic evidence of ice thickness. Suggested pore water effect.
Sauer and Christiansen (1991)	Consolidation testing of 134 samples of Floral and Battleford Formation tills.	Floral Fm. preconsolidation values 1500-2200 kPa while Battleford Fm. values 350-750 kPa. Suggest Battleford Fm deposited from stagnant and supraglacial ice.
Sauer, Egeland and Christiansen (1993)	Consolidation testing of 119 samples of pre-Battleford tills and intertill clays.	Preconsolidation values of 1600-2000 kPa. Interpret temperate glaciation during late Wisconsin with basal pore water pressure 69-76% of ice thickness.
Boulton and Dobbie (1993)	Use consolidation test results to assist in calculation of basal melting rates, subglacial ground water flow patterns, ice overburden thickness, basal shear stress and amount of sediment removed by erosion.	Determined that consolidation characteristics of glacial sediments can help us understand general attributes of subglacial hydrology. Not possible to infer ice thickness from single horizon consolidation tests.
Jenson (1993)	Use consolidation test results from clays overrun by Lake Michigan Lobe as proxy data for ice dynamics model.	Basal effective pressure of Lake Michigan Lobe was 1500 kPa.

and clay overconsolidation with depth. Where overconsolidation of basal tills is low, high basal water pressures are assumed. Where overconsolidation is high, basal water pressures are assumed to have been low. Boulton and Dobbie (1993) also model four effective pressure end member states for subglacial shearing and consolidation. These geologic scenarios include both high and low permeability tills underlain by thick aquifers or impervious lower substrates. Boulton and Dobbie (1993) summarize: 1) In general, it is not possible to calculate former ice thicknesses directly from single horizon measurements of the state of preconsolidation of fine-grained sediments. 2) Consolidation characteristics of glacial sediments can help us to understand general attributes of subglacial hydrology. 3) Subglacial hydrologic conditions conducive to subglacial sediment deformation were widespread beneath late Wisconsin continental ice sheets.

Significant progress has been made in the interpretation of preconsolidation results derived from glacially overrun sediments. It is clear that preconsolidation values are more sensitive to variation in subglacial hydrologic characteristics than to the thickness of the overlying glacier. However, where the affect of post-depositional conditions are understood, it appears that preconsolidation results obtained from basally deposited glacial sediments provide a proxy for the maximum effective basal pressure for the overlying glacier.

4.5 Application of Consolidation Theory to Glacial Sediments

The application of consolidation theory to sediments overrun by glacial ice requires several considerations. The generic pressure term (p) in Equation 5, must be replaced with p_i, (the pressure induced by the weight of the overlying ice) as in Equation 1. However, the most significant change involves the presence and flow of

basal meltwater through subglacial sediments. A load on sediment in a consolidation cell sets up a potential pressure in the interstitial water. This causes water to flow out of the cell and allows the reduction of void space in the sediment until the additional load is supported by granular contact and the pore water pressure is reduced to zero. Beneath a melting glacier, and in areas where there are no channels at the ice-bed interface, the equilibrium consolidated state must still permit basal meltwater to drain through sediment at a rate fast enough to discharge the basal meltwater. Discharge of this water requires a permanent potential pressure gradient, adding an additional pore water pressure component to the subglacial system. Thus, the effective pressure (load pressure minus basal pore water pressure) will be less than in the case of non-glacial consolidation beneath a similar load (Boulton and Dobbie, 1993) (Figure 14). However as a subglacial proxy, preconsolidation values derived from subglacial sediments will accurately represent the maximum effective basal pressure which includes any basal water discharge pressure gradient (Boulton and Dobbie, 1993).

4.5.1 Disturbance Effects

Sampling and preparation of individual "undisturbed" till specimens can result in the test sample becoming slightly disturbed. An increase in sample disturbance results in a slight decrease in the slope of the virgin compression line (Head, 1994). The break in slope evident on the consolidation curve of an overconsolidated sediment can also be significantly muted with sample disturbance resulting in an increased uncertainty associated with the application of the Casagrande Method.

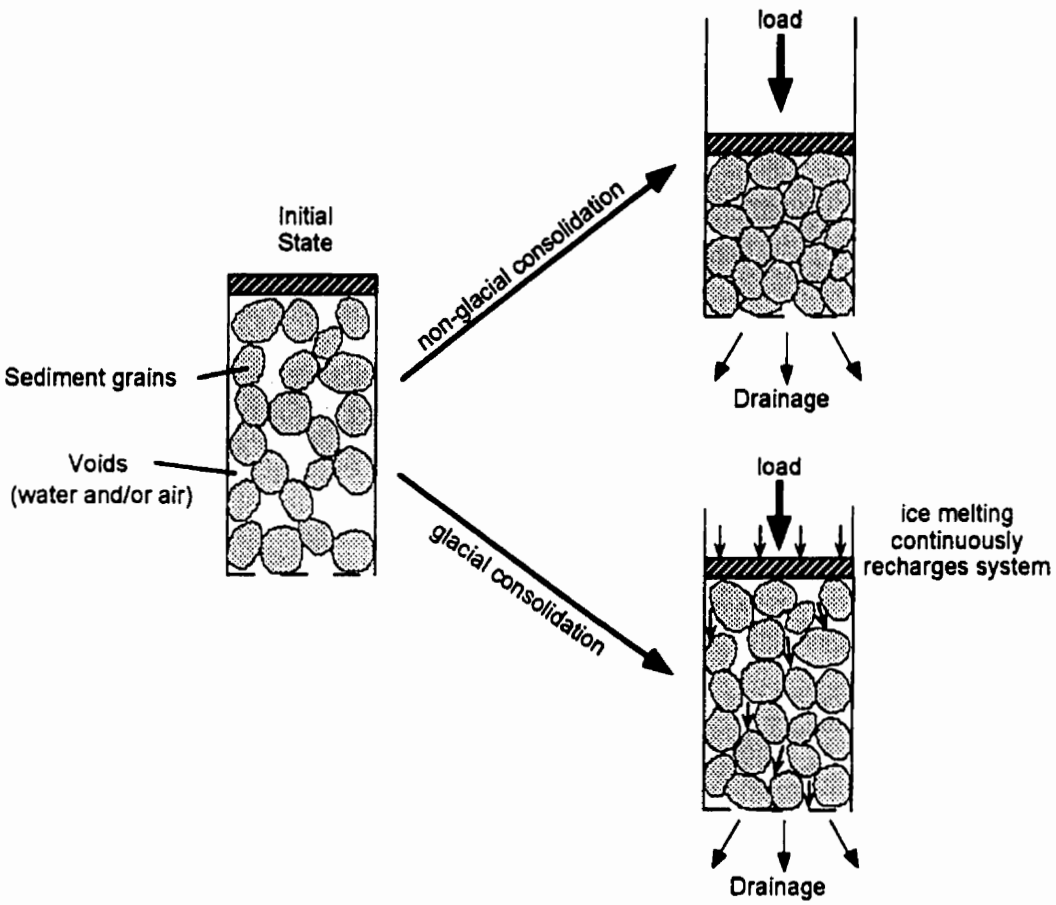

Figure 14. Consolidation process of subglacial sediments in the presence of basal meltwater discharge. The static consolidated state will be less than in a nonglacial system under the same load due to the presence of a meltwater flux. Modified from Boulton and Dobbie (1993).

4.5.2 Effect of Temperature

As mentioned previously, the viscosity of the draining liquid affects the rate of consolidation. Temperature is one of the main controls on the viscosity of water and thus affects the slope of the virgin compression line. Although an increase in temperature (eg. subglacial consolidation versus lab consolidation) increases the rate of consolidation, it does not affect the *amount* of consolidation during the primary stage (Head, 1994). Hence, temperature should not have an affect in altering the calculated preconsolidation pressure of sediment consolidated at one temperature and tested at another.

4.5.3 Effect of Time

Prolonged secondary compression under a static load will result in an overestimation of the sample's true preconsolidation value (Crawford, 1986). Prolonged particle readjustment under a static load (secondary compression) results in a "reserve resistance" and a decrease in sediment void ratio which delays the recompression portion of the consolidation curve from joining the virgin compression line during the reloading phase of a consolidation curve (Head, 1994). This prolonged particle readjustment results in an overestimation of past preconsolidation pressure which may be a problem for glacially overrun sediments exposed to subglacial effective pressures for periods measured in 1000's of years. Therefore, barring any other effect, preconsolidation values would likely represent maximum values where prolonged secondary compression resulted in a reduction in void ratio beyond that achieved during primary consolidation.

Pore water pressures in tills of low permeability can take significant time to equilibrate to external changes in water discharge rate or pressure (Boulton and Dobbie, 1993). However, as all consolidation samples were obtained from depths of less than 3.0 m below the present surface (assumed ice-till contact) it is presumed that all samples achieved near 100% consolidation resulting from the maximum effective basal pressure associated with the Lac La Biche ice stream. This assumption is based on the percent consolidation/depth ratio time factor graph published by Taylor (1948) (Figure 15) which shows rapid, near complete primary consolidation at the surfaces of units undergoing compressive stress.

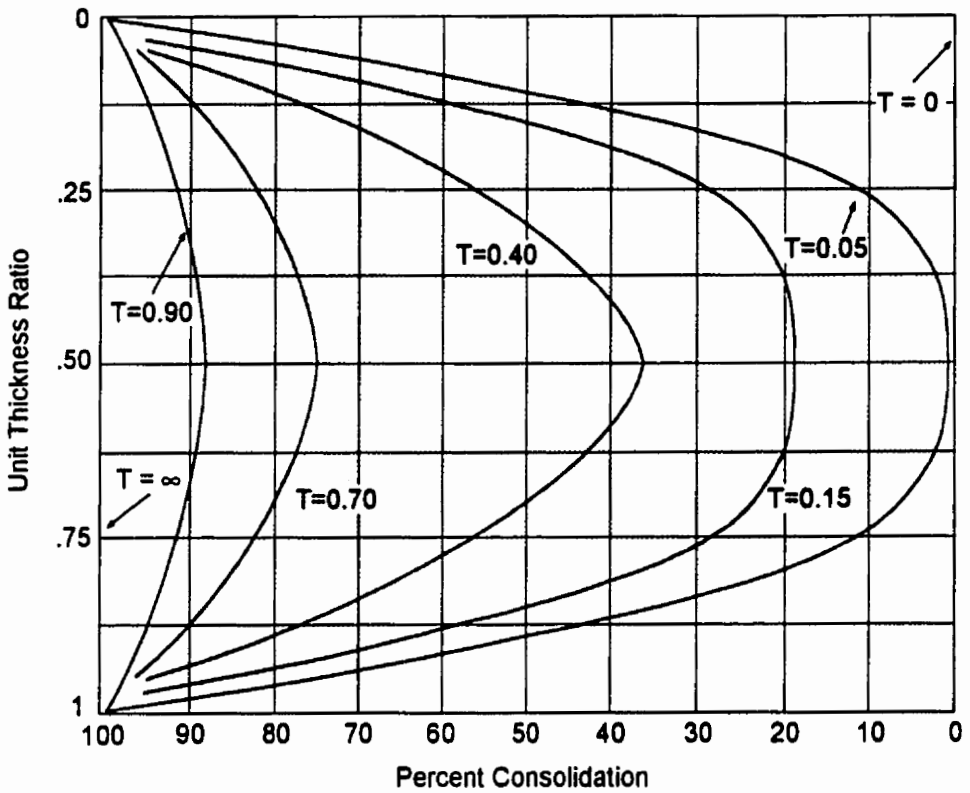

Figure 15. Simplification of Taylor's (1948) plot showing the relationship between unit thickness and the rate and degree of consolidation with depth. After the initiation of stress, consolidation profiles change from T=0.05 toward T=0.9 as the percentage of consolidation at every point increases. After an infinite time, consolidation is 100% throughout the unit. It can be seen that throughout the consolidation process, degrees of consolidation approaching 100% are noted at both unit edges. This model assumes free drainage from both the upper and lower surfaces and does not take into account any external water flux.

Chapter Five

Postglacial Processes

5.1 Introduction

This chapter will provide a qualitative evaluation of the effects of postglacial pedogenic processes on the sedimentary structure of overconsolidated glacial till. The use of preconsolidation data as a proxy indicator of subglacial conditions requires that the effect that these processes had on the original till structure be understood and evaluated.

For this thesis, tills are assumed to have been deposited in an initial saturated and overconsolidated state (eg. Boulton and Hindmarsh, 1987). It is also recognized that basally deposited sediments may have experienced varying degrees of pervasive shear deformation induced by overriding ice. Shear deformation of overconsolidated sediment tends to push the sediment particles apart at points of contact, permitting water to enter into the growing void spaces (Lambe, 1960). This process would act to effectively "erase" any preconsolidation signal imparted earlier. The processes controlling till deposition are outlined in Chapter 6.

Immediately after ice retreat, till is exposed to processes (temperature changes, drying and wetting cycles, freeze-thaw and pedogenic processes) which may act to alter initial conditions. Calculated preconsolidation values obtained from the samples collected for this thesis may therefore represent initial consolidation by overriding ice and the subsequent effects of postglacial pedogenic processes.

All samples for preconsolidation testing were collected from lower oxidized pedogenic C horizons averaging 2.0-2.5 m below the surface. Several physical and

pedogenic processes are thought to have occurred at this depth. For example, the average sample depth is below the present average annual freezing depth for this area (Kenton Miller, Environmental Consultant, pers. comm., 1997). However, the presence of well-developed sand wedges within the sediments of the Vermilion map area (Ellwood, 1961; Jones, 1981; Mougeot, 1991; and this thesis) indicate that permafrost was at one time a feature of the landscape. The presence of rare gypsum rosettes and more commonly soft diffuse carbonate nodules within the sampled sediments indicates secondary deposition of these minerals within the till structure and the process of clay illuviation has been noted within the C horizons of Luvisolic soils in the Peace River area (Pawluk and Dudas, 1978). Therefore, the processes which will be assumed to have acted on the sampled sediment include; freeze-thaw, desiccation-re-hydration, clay illuviation, and the addition of carbonates and gypsum to the solum.

5.2 Sediment Structure

In order to qualitatively evaluate the effect of various processes on the structure of clay-rich sediments, the relevant defining characteristics of sediment structure must first be understood. Sediment structure is both the geometric, skeletal arrangement of particles (including void space) and the inter-particle forces which may act on them (Bowles, 1984). Consolidation theory includes the assumption that the individual sediment particles and water are incompressible. During compression, inter-particle bonds may form in response to contact forces generated by either applied stresses, physio-chemical forces of interaction or both (Mitchell *et al.* 1969). For normally consolidated clays, the number of bonds developed is directly proportional to the effective consolidation pressure. The reduction of the consolidation pressure is not accompanied by a disappearance of all the bonds formed during consolidation, thus

accounting for higher strengths and lower void ratios in overconsolidated clays (Mitchell *et al.* 1969). Therefore, sediment consolidation results from the reduction of both micro and macro pore space within the sediment structure.

This change in void space also affects the role of water in a sediments structure. Water retention is due to capillary forces arising from curved air-water interfaces in the sediment voids, or due to surface forces bonding water molecules. The capillary forces depend upon the size of voids within the sediment and the surface forces upon the amount and nature of the surfaces of the sediment grains (Yong and Warkentin, 1975). The following sections will review the physical and chemical processes which may have affected the sediment structure associated with the overconsolidated till deposited by the Lac La Biche ice stream.

5.3 Sediment Desiccation and Rehydration

Sediment desiccation has been cited as a process responsible for overconsolidating glacial sediments (Harrison, 1958; Soderman and Kim, 1970; Aario, 1971; Van Gelder *et al.* 1990). Its effect on the sediments deposited by the Lac La Biche ice stream must be understood as it may represent a source of error regarding the interpretation of derived preconsolidation values.

The process of drying consolidation of fine-grained sediments takes place by the loss of interstitial water which results in the formation of water pore meniscus and water tension stresses. As water loss continues, the surface tension stresses increase as the radius of the interstitial pore water globules decrease. This tension brings the sediment grains closer together, thus consolidating the sediment. The limiting case occurs when interparticle contacts prevent further consolidation of the soil matrix and the volume will reduce no further from the water tension stresses. A sediments

shrinkage limit is defined as the water content below which no further volume change occurs with further drying (Bowles, 1984). After the shrinkage limit has been exceeded, the water simply evaporates with no further soil structure change (Bowles, 1984). This consolidation effect commonly produces preconsolidation values as large as 200-800 kPa in many areas of the United States (Bowles, 1984).

Sediment desiccation and re-hydration has a component of hysteresis where the wetting and drying cycles operate at slightly different energy levels. (Yong and Warkentin, 1975). In clay sediments, part of the hysteresis is due to movement of fabric elements and particles into different arrangements which accompanies the volume changes (Yong and Warkentin, 1975). This fabric distortion represents a plastic readjustment where interparticle contacts and forces at the points of contact differ on wetting and drying.

Figure 16 shows idealized water potential (suction) - water content characteristics for a clay sediment undergoing multiple wetting-drying cycles. The shape and magnitude of the first drying curve (increasing water potential) can be quite different from the first rewetting curve. It is seen that the original water content is not regained at the first resaturation. These are not reversible changes as they are due to changes in the structure of the clay sediment (Yong and Warkentin, 1975). The second drying and wetting can however result in a closed loop and hence show hysteresis. A soil that is wet or dried from an intermediate position (not fully saturated or dried) will follow some intermediate path within the envelope produced by volume changes associated with complete wetting and drying.

Identical consolidation processes take place with the drying of a saturated, previously overconsolidated fine-grained sediment (Fleureau *et al.* 1993). Drying from

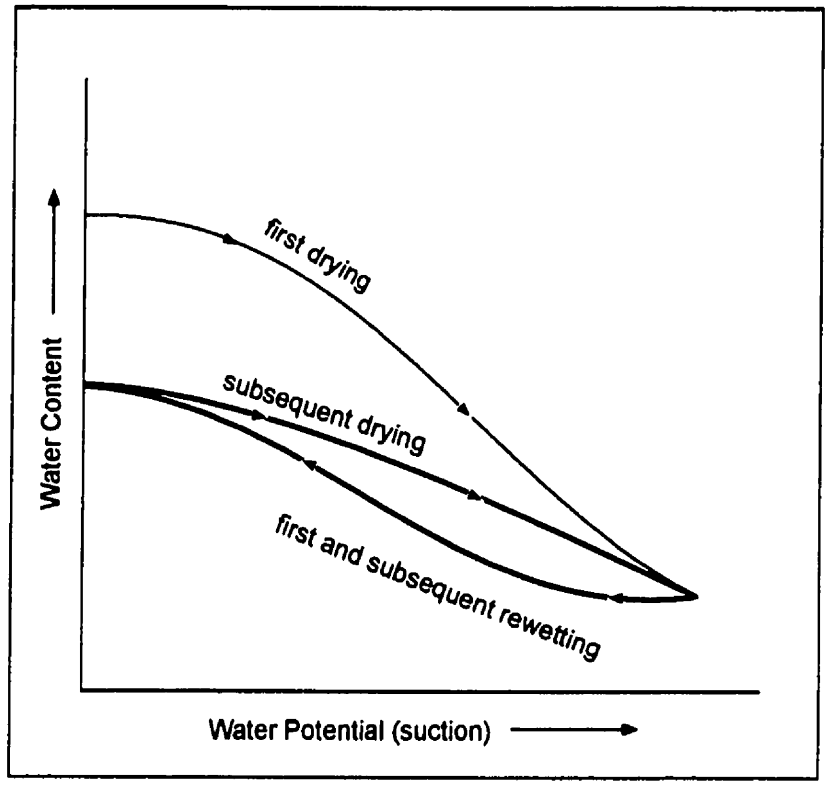

Figure 16. Drying and wetting curve for an initially saturated clay-rich fine-grained sediment. A sediments water potential is a factor of water content, sediment grainsize and sediment structure. Cyclic wetting and drying will not alter sediment structure (void ratio) more than which occurs during the initial drying. Drying acts to further consolidate, overconsolidated fine grained sediments. Modified from Yong and Warkentin (1975).

an initial saturated condition would further consolidate an overconsolidated sediment resulting in an increase in that sediments preconsolidation value. It is generally accepted however, that the degree of swelling associated with wetting of the sediment (void ratio increase) is generally less than the void ratio reduction associated with the previous drying (Fleureau *et al.* 1993). Chang and Warkentin (1968) found that total volume changes decreased with increasing compaction level for fine grained aggregates experiencing a wetting and drying cycle. Therefore highly overconsolidated sediments will show minimal void ratio changes with desiccation and rehydration. They suggested this observation is due to a lessened potential for particle rearrangement within the previously overconsolidated sediments.

5.4 Expanding Clay

Sediment desiccation and rehydration also has an effect on the structure and bonding relationships of different clay minerals. The presence of expanding clay within overconsolidated tills deposited by the Lac La Biche ice stream may therefore have acted to alter the original sediment structure (defined by the state of consolidation) with changes in sediment water content. Samples of Vilna Member till collected by Andriashek and Fenton (1989) contained 53% illite, 19% kaolinite, 18% smectite, and 10% chlorite. As no other data are available from the study area, these percentages will be taken as representative of the clay mineralogy of unweathered till deposited by the Lac La Biche ice stream.

The effect of approximately 20% smectite (an expanding clay) within the matrix of an overconsolidated basal till containing 20-50% total clay content is unknown. Grim (1962) notes that the magnitude of swelling of expanding clay varies widely depending upon the presence and type of exchangeable ions, electrolyte content, particle size

distribution, void size and distribution, internal structure, water content, superimposed load and possibly other factors. The large number of variables involved in the process of clay expansion limits the potential for an accurate evaluation of the effect of this process on the state of till consolidation.

5.5 Freezing and Thawing

Evidence of postglacial permafrost in east-central Alberta (eg. Mougeot, 1991; Jones, 1981; this thesis) requires that the affect of freeze-thaw on the sediment structure of overconsolidated sediments be understood and considered in the interpretation of preconsolidation results derived from till deposited by the Lac La Biche ice stream. In the only published work concerning the affect of freeze-thaw on the structure of a previously overconsolidated clay sediment, Konrad (1989a) found that for overconsolidated clayey silt (26% clay), the void ratio should be expected to increase only slightly after the first freeze-thaw cycle but show negligible structural changes in subsequent freeze-thaw events.

The effects of freeze-thaw on an overconsolidated fine-grained sediment are primarily controlled by the characteristics and size of the water filled pore spaces within the sediment (Konrad, 1989a). The void ratio changes associated with an initial freeze-thaw cycle in an overconsolidated fine-grained sediment are visualized in Figure 17. Point *c* represents an *in situ* overconsolidated fine-grained sediment which had previously experienced a maximum preconsolidation pressure at *b*. From point *c*, freezing of the sediment will result in an increased effective stress value due to the pressure gradient induced by the phase change of sediment pore water. However, the subsequent structural disruption caused by the delayed freezing of small diameter pore water behind the freezing front acts to counteract any consolidation effect resulting from

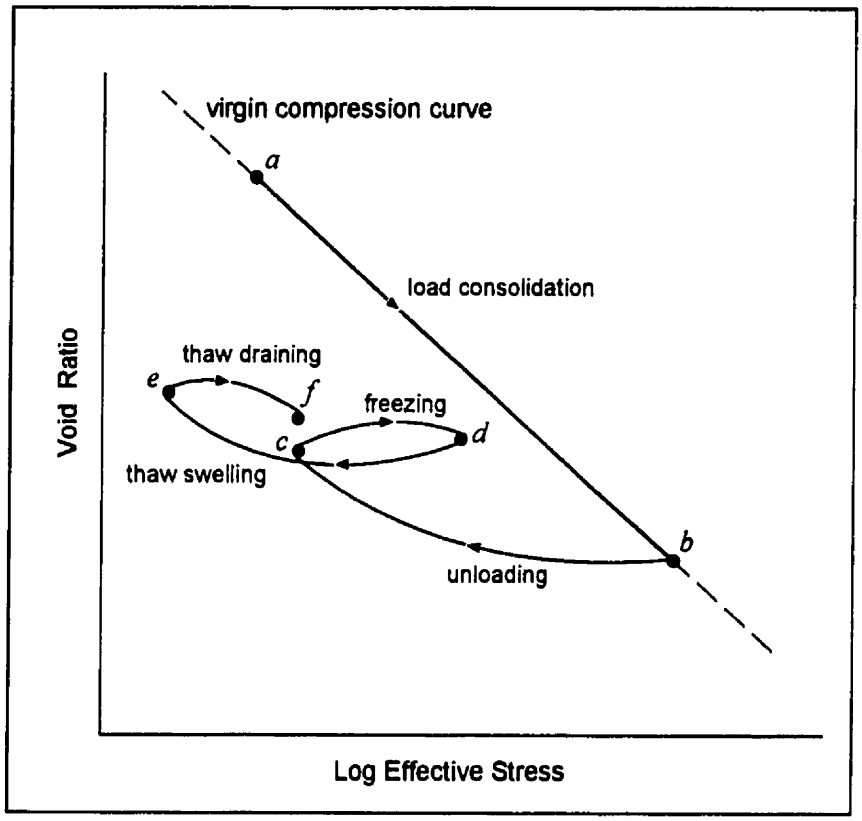

Figure 17. Hypothetical thaw consolidation pathway for an overconsolidated fine-grained sediment. In this scenario, freeze-thaw results in a slight increase in sediment void ratio from *c* to *f*. A normally consolidated sediment at *a* is consolidated to *b* then unloaded to *c*. Freezing of the overconsolidated sediment from *c* to *d* results in an increased void ratio at *d*. With thawing to point *e*, the void ratio is increased just as the release of stress at *b* results in an unloading increase to *c*. Final draining of excess water slightly reduces the void ratio to *f*. Modified from Konrad (1989a).

increased effective pressures at the freezing front (point *d*) (Konrad, 1989b). With thawing and the release of free water from the melting of segregated ice, the soil will swell almost instantaneously to absorb the excess water into its marcopore structure (point *e*). If the soil swells to a low effective stress condition and free water is still available, drainage of that water will result in a final thaw consolidation to point *f* where the void ratio is only marginally above its previous overconsolidated condition (point *c*).

Konrad (1989a) also determined that the degree to which an overconsolidated sediment's void ratio increases with freeze-thaw, is proportional to the sediments' original overconsolidation ratio. Overconsolidation ratio (OCR) is defined as the ratio of maximum preconsolidation pressure to the present *in situ* effective overburden pressure of a sediment (Head, 1994). Sediments with an OCR of 1 (normally consolidated) to 2 (low overconsolidation), showed void ratio decreases representing additional overconsolidation. However, for sediments with OCR's of 4 and 8 (low to moderate overconsolidation), Konrad (1989a) noted average relative void ratio increases of 2% and 8% respectively for the first freeze-thaw cycle. After the third freeze-thaw cycle, additional cycles had no effect on the structure of overconsolidated sediments (Konrad, 1989a; Konrad, 1989b). This structural change would result in an under estimation of the sediments original preconsolidation value.

5.6 Carbonate and Sulfate Leaching/Deposition

The presence of secondary carbonates and gypsum crystals within the upper ~1.5 m of all excavated sample pits is obvious evidence of postglacial alteration of till sediment structure within the study area. Secondary carbonates consist mostly of calcite in fine silt and clay size crystals (St. Arnaud, 1976; Acton and Fehrenbacher, 1976; McKeague and St. Arnaud, 1969). The deposition of these fine-grained carbonate

crystals within the void spaces of a lower C horizon would act to lower the sediment void ratio, resulting in a further consolidation of the sediment. The growth of generally rare, large (~1cm) diffuse carbonate and gypsum ($CaSO_4 \cdot 2H_2O$) nodules present within some sample pits certainly resulted in significant structural changes to the surrounding till matrix. However, the growth of the crystals and displacement of the adjacent sediment matrix may have resulted in additional compressional forces which acted to further consolidate the sediment beyond its original state of overconsolidation.

5.7 Clay Translocation

Clay particles are predominately elluviated from the A horizons of Chernozemic and Luvisolic soils subjected to drying and leaching after soluble salts and carbonates have been removed (McKeague and St. Arnaud, 1969). Illuviated clay minerals (argillans) occur predominantly as coatings in voids, on soil peds and individual grains within the B soil horizon. However, argillans may occur in any horizon. (Brewer and Sleeman, 1969). In general, illuviation of clay in the C horizons of Chernozemic and Luvisolic soils is not a major process responsible for the reduction of sediment void space (McKeague and St. Arnaud, 1969). However, the presence of fractures and remnant root casts which penetrate the C horizon sediments may allow for the rapid transport of colloidal clays into deeper horizons. The deposition of these clays within sediment pore spaces will result in a natural decrease in the sediment void ratio, thus acting to consolidate the sediment without the application of normal forces.

5.8 Discussion

It has been shown that the physical and chemical processes which have acted on the samples collected for consolidation testing may have resulted in changes to the original structure of the sediment. Sediment desiccation, carbonate translocation and clay illuviation have been found to further consolidate previously overconsolidated fine-grained sediments. Sediment rehydration is thought to have had little or no effect on altering the preconsolidation value of the overconsolidated sediments while freeze-thaw has been proven to only marginally increase the void ratios of moderately overconsolidated sediments by 2-8% (Konrad, 1989a). It is unknown how this void ratio increase would affect the calculated preconsolidation value for a given sediment, although it will be assumed that it would result in a general lowering of preconsolidation value.

The combined and overall effect that these processes had on the original structure of the basal sediments deposited by the Lac La Biche ice stream is unknown. However, if the order in which these processes occurred is taken into consideration, it may be suggested that the overall effect would have been a general reduction in void ratio through time. The first significant process to have acted on the newly exposed basal sediments would be freezing and thawing. Assuming an initial moderate overconsolidation for these sediments, freeze-thaw process would act to marginally increase the sediments void ratio (by 2-8%), resulting in the lowering of the calculated preconsolidation value. If however, the sediments are assumed to have been deposited in a weakly overconsolidated state, the freeze-thaw may have had little effect on sediment void ratios (Konrad, 1989b). After the first three freeze-thaw events, this process would not alter the sediment structure further. Theoretically, the later processes to occur (desiccation, rehydration, and the translocation of carbonates and

clays), would have acted generally to reduce the void ratios of the sediments, resulting in an increase in the calculated preconsolidation value.

It can therefore be suggested that the initial overconsolidation ratio of the tills (after deposition and before any processes had acted on them) would have determined how the later postglacial process affected the sediment structure and preconsolidation value. If the initial overconsolidation ratio was high, the magnitude of the expansion effect of freeze-thaw may have been greater than the general consolidating effect of the later processes, thus resulting in an underestimation of the basal preconsolidating pressure. With a low initial overconsolidation ratio, the freeze-thaw effect would be minimal and the later processes would have resulted in a general increased consolidation.

Measurements of basal effective pressures from modern ice streams indicate a general trend of low to moderate overconsolidation potential with effective basal pressures ranging from 10-160 kPa (Blankenship *et al.* 1986; 1987; Engelhardt *et al.* 1990). Based on this evidence, it is suggested that the postglacial sediment structure alteration which affected the samples tested would likely result in an overestimation of the subglacial effective pressures associated with the Lac La Biche ice stream.

It must also be realized that these postglacial processes have not occurred uniformly throughout the field area. Sample depth, sediment grain size, site aspect and drainage potential, have contributed to this heterogeneity and the varying intensity of each of the processes mentioned above. Obviously this factor limits the usefulness and comparability of preconsolidation data collected from samples which have been exposed to postglacial physical and chemical processes. It is also likely that postglacial alteration is responsible for some of the observed variation in the individual preconsolidation values obtained from consolidation tests carried out on samples obtained from each site.

Chapter Six

Ice Stream Basal Processes

6.1 Introduction

This chapter will present theories regarding enhanced glacier flow and subglacial hydrology. An increased understanding of ice stream basal processes will promote the development of informed interpretations of the glacial geology of the bed of the Lac La Biche ice stream.

There are several interpretations of what constitutes an "ice stream". Swithinbank (1954) defines an ice stream as "part of an inland ice sheet in which the ice flows more rapidly than, and not necessarily in the same direction as, the surrounding ice." Examples of this type include west Antarctic ice streams B, D and E. Bentley (1987) suggests there is a graduation between ice streams totally confined by slowly moving ice and outlet glaciers bounded by bedrock on one or both sides. The Jakobshavns Glacier of Greenland, the Rutford Ice Stream and Byrd Glaciers of Antarctica are included in this category. Interpretations for North American paleo-ice streams are proposed by Brown *et al.* (1987) for the Cordilleran Puget Lobe, and Patterson (1997), Jenson *et al.* (1995) and Hicock (1988) respectively for the Laurentide Des Moines, Lake Michigan and Superior Lobes.

6.2 Ice Stream Motion

The processes responsible for glacial ice flow include: 1) internal deformation of ice under the influence of gravity, 2) coupled basal sliding, 3) decoupled basal sliding and

4) basal sediment deformation. All of these processes have been suggested as mechanisms to explain the high flow rates associated with streaming glaciers (Alley *et al.* 1987b; Iverson *et al.* 1995; Marshall, 1996).

6.2.1 Internal Ice Deformation

The deformation of ice in response to stress is called creep and consists of the mutual displacement of ice crystals relative to each other (Sugden and John, 1984). The fast flow of Jacobshavn Isbrae in Greenland has been attributed to thermally enhanced creep deformation with little or no basal flow component (Iken *et al.* 1993). It is believed that similar Laurentide ice streams, which may have resulted from the same flow process would have left little or no geologic evidence due to the lack of a rapid basal flow component (Marshall *et al.* 1996).

6.2.2 Coupled Basal Sliding

Coupled basal sliding refers to the movement of basal ice over a ridged substrate through enhanced basal creep, pressure melting and slippage at the ice/bed interface (eg. Weertman, 1957; Kamb, 1970). Enhanced basal creep results from the increased strain associated with the presence of an immobile obstacle at the bed of a glacier. The higher levels of stress induced by the obstacle on the upstream side of the glacier results in increased strain in the ice. It is important to note that this mechanism does not necessitate sliding between ice and rock (Sugden and John, 1984).

Pressure melting can also result in the movement of ice along the bed (eg. Weertman, 1957). Stress induced melting can result in water flow along the bed in a

downstream direction and subsequent refreezing (regelation). In this way, the glaciers mass may be transferred around an obstacle.

Slippage at the ice/bed interface occurs where the shear stress at the contact is greater than frictional resistance. This process is moderated by basal water pressure which acts to reduce frictional resistance between basal ice and its bed. Where basal water pressure is equal to or greater than the pressure induced by the overlying ice, bed decoupling may occur. The processes of coupled basal sliding are responsible for at least a portion of the flow of most glaciers. However, it has been proposed that the majority of the flow associated with streaming glaciers is likely the result of decoupled basal sliding and pervasive sediment deformation processes (Alley, et al. 1987b; Iverson et al. 1995; Marshall, 1996).

6.2.3 Sediment Deformation

A subglacial layer of deforming sediment may be regarded as a shear zone, bounded below by the undeformed part of the substratum and above by the base of the ice (Benn and Evans, 1996). Two fundamental types of sediment deformation are recognized: 1) brittle deformation, in which movement is confined to clearly-defined failure surfaces or faults, and 2) ductile deformation in which strain is distributed throughout the entire mass. Ductile deformation can be either homogeneous or heterogeneous and includes squeeze deformation, and pure and simple shear (Figure 18). Deformation is usually heterogeneous; however, strain can approximate homogeneous deformation at certain spatial scales (Benn and Evans, 1996). Both ductile squeeze and simple shear processes result in soft deformable beds under enhanced glacier flow (Hicock *et al.* 1989). A sediment deformation model for glacial movement was proposed

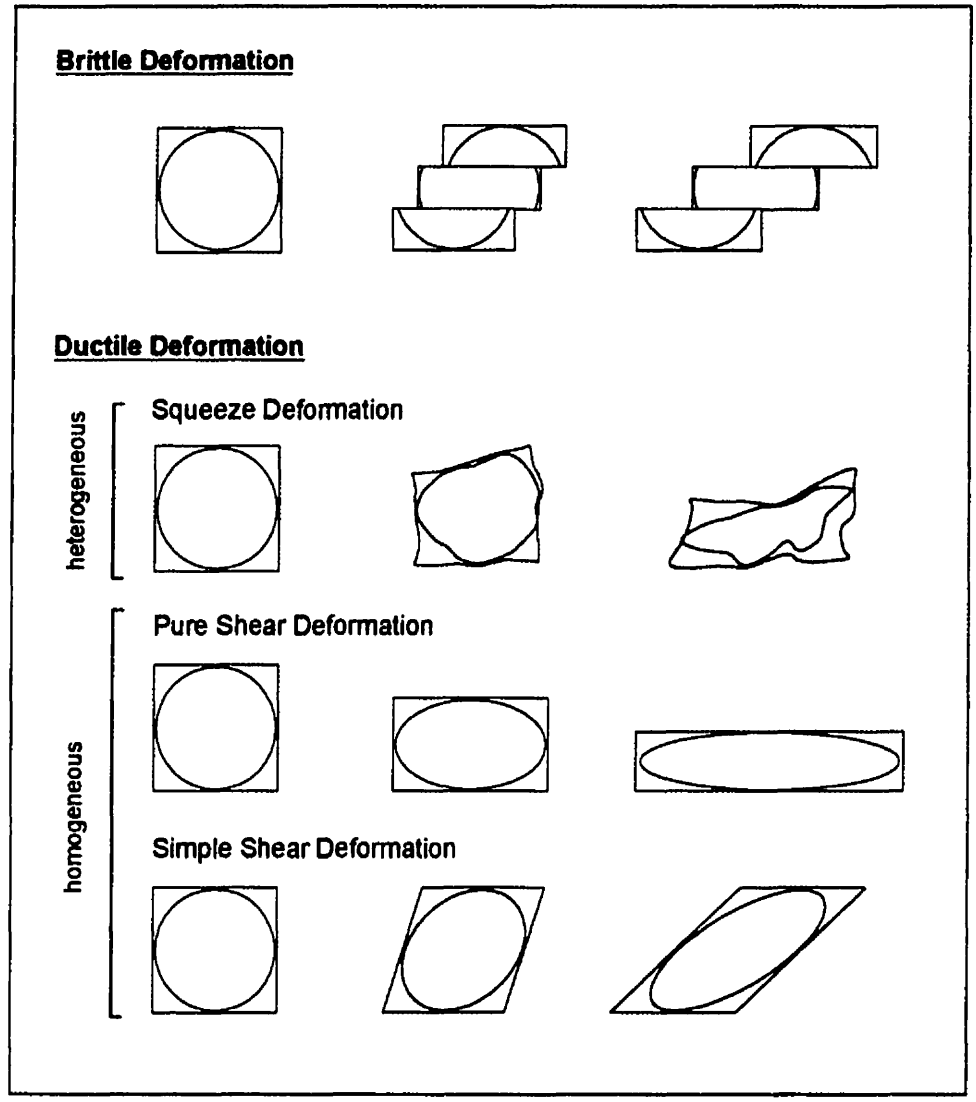

Figure 18. Idealized styles of deformation with deformation ellipsoids. Deforming till occurs through a combination of heterogeneous and homogeneous ductile deformation. Brittle deformation may occur within basal tills experiencing stress levels below yield strength. After Benn and Evans (1996).

by Boulton and Jones (1979). They revealed that the surface profile of a glacier is related to the hydraulic and strength properties of the underlying unconsolidated sediments. For glaciers resting on poorly-drained unconsolidated sediment, till deformation can account for the majority of glacial movement. Measurements of sediment deformation from beneath Breidamerkurjökull Glacier in Iceland revealed that sediment deformation accounts for 80-95% of the forward movement of the glacier (Boulton and Hindmarsh, 1987).

Inherent in the sediment deformation model of Boulton and Jones (1979), is the assumption that the total volume of sediment transported to the glacier terminus by this process must be some small proportion of the total ice volume moving through the glacier (Beget, 1986). This also suggests that erosion must be occurring beneath the glacier to resupply the basal sediment flux and keep the ice moving. However, most estimates of subglacial erosion and terminal moraine volumes are several orders of magnitude lower than ice flux (Beget, 1986). Beget (1986) also notes that this situation is especially true for contemporary ice streams where the ice flux is very high (eg. west Antarctic ice streams).

Boulton and Hindmarsh (1987) observed a widespread two layer deforming sediment structure in the basal till of the Breidamerkurjökull Glacier. The layers consisted of a 0.5-1.0 m thick dilated upper *A* horizon overlying a denser *B* horizon with platy structure. The layers have similar textures but are structurally distinct. The upper horizon is massive and shows a bubbly texture when dried, while the denser lower horizon shows sub-horizontal joints, some of which are slickensided and lacks a bubbly texture (Boulton, 1987). In the *A* horizon, large amounts of strain appear to occur by continuous ductile deformation, while the slickensided joints in the *B* horizon reflect low strain rates by discontinuous brittle movement along well defined planes.

Although Boulton and Hindmarsh (1987) did not observe decollement surfaces, they suggest that sliding could occur at the base of the *A* horizon or at the ice-sediment interface. A similar layered model of deforming till has been proposed by Menzies (1989). Hart (1994), and Hicock and Dreimanis (1992) support the multiple layer deformation model.

In order for basal shear stress to cause deformation in underlying sediments, a normal force is required at the glacier sediment interface (Boulton and Hindmarsh, 1987). This can only occur when the basal water pressure is less than the ice overburden pressure, resulting in a positive net effective pressure. Boulton and Hindmarsh (1987) state that where water pressures in subglacial till are less than ice overburden pressures, infiltration of ice into the sediment layer may occur. This process will cause the inclusion of basal debris into the ice, resulting in a mechanical coupling between the ice and substrate, thereby reducing the possibility of sliding (Shoemaker, 1986). This connection also acts to transfer shear stress to the underlying sediment. Where basal water pressures are at or near the ice overburden pressure, sliding will result (Boulton and Hindmarsh, 1987).

Research on the west Antarctic ice streams may not support multiple till layer models. The dynamics of rapidly flowing ice streams in the west Antarctic ice sheet have been related to the presence of a uniform subglacial deforming layer. Alley *et al.* (1987a) and Blankenship *et al.* (1986) provide evidence from seismic studies that the entire ~6.5 m thick till layer beneath ice stream B is deforming as a single unit. In opposition, Engelhardt *et al.* (1990) calculated a net effective basal pressure of 30 to 160 kPa for a similar location under ice stream B. Engelhardt *et al.* (1990) conclude from their results that in addition to subglacial sediment deformation, basal sliding due to high basal water pressure may be a factor in controlling ice stream mechanics.

6.2.3.1 Factors Controlling Sediment Deformation

Basal till deformation is primarily determined by pore water pressure, matrix grain size and clast content. In general, coarser, permeable, clast-rich till will be more resistant to deformation than finer, impermeable, clast-poor till (Boulton and Hindmarsh, 1987). Rising pore-water pressures cause a reduction in shear strength of granular materials because intergranular friction is directly proportional to the effective normal pressure (Boulton and Dobbie, 1993; Mathews and MacKay, 1960).

Boulton and Dobbie (1993) recognize four potential sediment deformation scenarios (Figure 19) which highlight the relationship between sediment deformation, permeability, substrate drainage potential and effective basal pressure. Where subglacial drainage is good, due to high till permeability and the presence of sub-bed aquifers, high effective basal pressures dominate resulting in reduced potential for sediment deformation (A and C, Figure 19). Poor drainage resulting from low till permeability will induce high subglacial water pressures and sediment deformation (B and D, Figure 19).

Theoretically, the initial yield stress of a granular sediment can be determined by the Coulomb equation;

$$T = c + p' \tan \phi \qquad (8)$$

where T is the stress at which the material begins deforming viscoplastically, c is cohesion, p' is effective pressure and ϕ is the angle of internal friction. The term p'tan ϕ represents the frictional strength of the granular material. Decreasing p' increases the

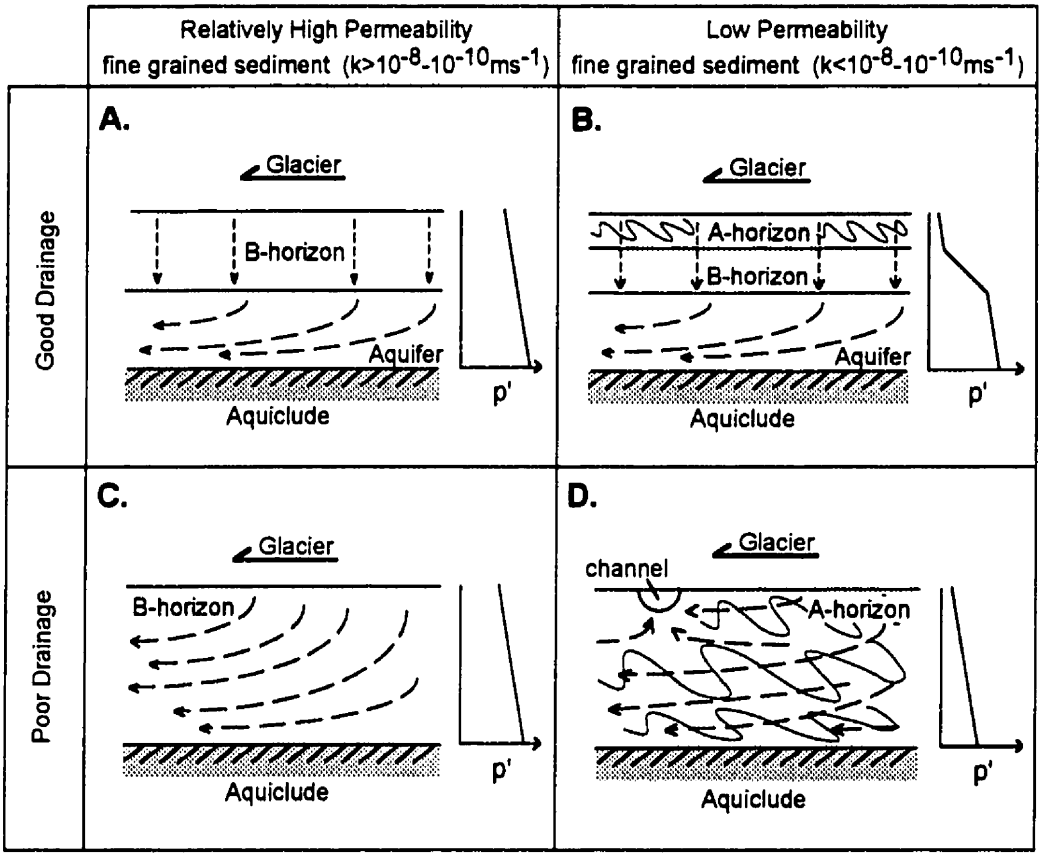

Adapted from Boulton and Dobbie (1993)

Figure 19. The effect of till permeability and sub-till drainage conditions on the occurrence of subglacial shear deformation and effective pressure gradients (p') in the till. Dashed lines represent water drainage pathways. Panels A-D show end-member states proposed by Boulton and Dobbie (1993): (A) High till permeability and good vertical drainage potential favours no sediment deformation and higher effective basal pressures. (B) A till of low permeability underlain by a thick aquifer favours steep effective pressure gradients and deformation in the upper part of the till. (C) High till permeability and poor vertical drainage potential will induce higher effective pressures which may fail to induce deformation in a small glacier if the till can transmit a sufficient water discharge. (D) Low till permeability and poor vertical drainage potential results in thick deforming layers, low effective basal pressures and channel formation. Deformation may occur throughout the till unit or in all but a basal horizon if the till is very thick (not shown).

likelihood of sediment failure resulting in strain deformation of the glacial substrata and a forward movement of the glacier.

The Coulomb equation assumes that natural sediments are perfectly plastic with no deformation up to the yield strength. The model also assumes that deforming sediments are capable of infinitely high strain rates at the yield strength with no additional stress increment (Boulton, 1987). However, experiments showing significant till elastic-plastic strains at stress levels below T have been conducted by Boulton (1987). Over long periods of time, stresses less than T produced significant strains which were clearly visible as sediment deformation structures.

By testing a till sample obtained from beneath west Antarctic ice stream B, Kamb (1991) improved on basal deformation theory by exploring the characteristics of residual strength of water saturated basal till and suggesting that the viscosity of deforming till is highly nonlinear which implies important consequences for the deforming bed mechanism. Nonlinearity can result in a positive feedback mechanism where frictional heat generated by shearing of basal till will result in increased melting of basal ice (Kamb, 1991). This increased water input could weaken the basal sediment further, allowing for increased deformation and the release of additional heat. Kamb (1991) concludes that the apparent lack of instability in the Antarctic ice streams indicates that their motion is not restrained by the bed deformation process but by some other mechanism.

6.2.3.2 Deformation Layer Thickness

The thickness of the deformed layer is dependent upon the degree of basal shear stress, effective basal pressure, sediment porosity and the subglacial hydrologic system (Boulton and Dobbie, 1993). Modeling the sediment flux associated with the advance of

the Lake Michigan lobe, Jenson *et al.* (1995) calculated that in a deforming sediment layer with low viscosity, sediment flux velocities (therefore ice flux velocities) are very large (300-600 m/yr) although the thickness of the shear zone is extremely thin, on the order of a few centimeters. Boulton and Caban (1995), and Jenson *et al.* (1995) note that active deformation tends to be shallow, but the sediments can be depositionally stacked to greater thickness. Jenson *et al.* (1995) also found that deforming layers with high viscosity exhibit very thick shear zones (several meters) but the associated maximum sediment velocities are on the order of tens of meters per year. The findings of Jenson *et al.* (1995) suggest that earlier interpretations of a thick basal sediment deforming layer beneath the Antarctic ice streams may be incorrect as a thick uniform deforming layer is incompatible with high ice velocities.

6.2.4 Hydraulic Jacking and Decoupled Basal Sliding

Jansson (1995), working on the Storglaciaren glacier in Sweden, determined that the glacier's velocity variations are caused by hydraulic jacking at the glacier's bed. Hydraulic jacking occurs where subglacial water pressures effectively act to support a large portion of the weight of the overlying ice, resulting in a weakening of the frictional strength of the ice-bed contact. Similarly, Iverson *et al.* (1995) concluded that Storglaciaren flows by a process of bed decoupling (sliding) associated with high basal water pressures rather than by bed deformation. It appears from Iverson *et al.* (1995) that the coupling of ice and basal till is reduced during periods of high water pressure and rapid flow, because glacial velocity peaks correlate with till strain rate minima, and subglacial water pressure never exceeded ice overburden pressure. Iverson *et al.* (1995) also suggests that till-bed decoupling may in fact be a misnomer for glaciers with a soft bed. It is likely that soft sediments may expand to fill the intervening space resulting

from hydraulic jacking of the glacier. In this instance, bed decoupling would refer to the resulting reduced transfer of stress to the glaciers bed. Hydraulic jacking has also been described for Findelengletscher Glacier in Switzerland (Iken and Bindschadler, 1986), and Variegated Glacier in Alaska (Kamb and Engelhardt, 1987).

The presence of remnant channel fills in deformation till has also been used to promote ice-bed separation as a process responsible for the rapid flow of streaming glaciers (eg. Clayton *et al.* 1989; Brown *et al.* 1987). Assuming that all of the basal motion associated with the Puget Lobe was due to substrate deformation, cumulative strain recorded in the till would be extremely high (Brown *et al.* 1987). However, the abundance of sorted sediment structures within the till that have not been attenuated into thin streaks by extensive shear strain implies that the magnitude of strain associated with basal deforming till may be generally less than expected (Brown *et al.* 1987). This evidence may indicate that large shear strains and pervasive shearing of the till did not contribute significantly to the basal motion of the glacier. However, shearing along discrete shear zones is evident and may amount to significant displacement. The low effective stress reconstructed for the Puget Lobe implies widespread ice-bed separation and basal sliding.

The studies by Iverson *et al.* (1995) and Jansson (1995) are important as they indicate that where basal water pressures are sufficiently close to the ice overburden pressure, the shear strength of the ice-sediment interface may be weakened more than that of the underlying sediment. This may indicate that sliding along the ice-sediment interface could make up most of the glacier's motion. Therefore, both sediment deformation and basal sliding may play a role in determining ice stream motion. In all of the above studies, it is apparent that high subglacial water pressures are associated with fast moving ice, even when the actual mechanism of ice stream motion is debated. For

this reason, the following section includes a review of several aspects of subglacial hydrology relating to rapid ice flow.

6.3 Subglacial Hydrology

One of the objectives of this thesis is to characterize the subglacial hydrologic system of the Lac La Biche ice stream, therefore an understanding of the current literature regarding the subglacial hydrologic systems is required. Subglacial hydrology is an important factor in determining ice sheet dynamics (Boulton *et al.* 1995). This statement can be backed up through the realization that when water is confined in an unconsolidated, porous substratum, part of the weight of the overlying ice is transferred from the basal sediment to the pore water (Equation 1) (Benn and Evans, 1996). The presence of high pressure basal pore water therefore results in a lowering of the effective basal pressure, which is positively correlated with fast glacial flow and the presence of ice streams (Hooke, 1998; Jansson, 1995; Marshall, 1996). High subglacial water pressures are achieved where the inputs of water from pressure melting and/or surface runoff are equal or greater than discharge outputs.

Two main sources of meltwater are recognized by Sugden and John (1984): 1) seasonal surface meltwater, and 2) basal and internal meltwater sources. Surface melting can represent a variable seasonal input source to the bed through transport by moulins while basally derived meltwaters fluctuate less markedly and commonly exist throughout the year (Sugden and John, 1984). The relative contribution of the sources to water found at the bed of thick continental scale ice sheets and glaciers is highly variable near ice sheet marginal areas. However, away from the marginal areas basally derived meltwater is by far the most significant source of water at the ice/bed interface (Boulton and Dobbie, 1993; Piotrowski, 1997; Marshall, 1996). Meltwater at the base

of a glacier can be generated by geothermal heating or frictional heating due to internal deformation of glacial ice, sediment deformation at the bed, or friction produced by the flow of meltwater itself (Sugden and John, 1984).

Drainage of subglacial water occurs through one of the following routes: 1) Both vertical and horizontal Darcian flow of meltwater through subglacial sediment. 2) Channel flow at the interface, and 3) Sheet flow at the glacier-sediment interface (Boulton and Dobbie, 1993). However, Boulton *et al.* (1995) suggest that horizontal groundwater flow may be a primary control of water pressures at the ice/bed interface. Thus, the effective pressure at the glacier sole may largely be determined by the extent to which meltwater can drain through the substratum.

6.3.1 Darcian Flow

The flow of water through a permeable sediment (either horizontal or vertical flow) is driven by pressure differences. As mentioned in Chapter 4 (Consolidation Theory) the water pressure immediately beneath a glacier consists of two components: 1) a gravitational component due to hydraulic head and 2) the potential pressure component resulting from the pressure required to discharge basal meltwater through the sediment at the rate of melting. The relative magnitude of these components are determined by the sediment permeability (Boulton and Dobbie, 1993). The gravitational component is normally equivalent to about 10 kPa/m. Where sediment permeability are less than 10^{-8} to 10^{-10} m/s, the potential gradient required to discharge meltwater is much greater. This results in a vertical effective pressure gradient well in excess of the gravitational gradient (Boulton and Dobbie, 1993). Beds of low permeability, therefore act as dams to water flow, inducing high pressure gradients that maintain discharge.

Similar discharge can be maintained with a low pressure gradient for beds of high permeability (Boulton, 1976b).

The discharge of water through till must increase towards the glacier margin due to the increased area of basal melting being drained by the sediment. If the permeability and thickness of the stratum remain constant, the potential gradient required to drive the flow will increase until the piezometric surface matches the glacier-surface slope (Boulton and Dobbie, 1993). At that point, effective pressure at the bed will be zero. Where sub-bed sediments have a constant or decreasing permeability with depth, the vertical groundwater flux will be small compared to the horizontal flux, and the vertical effective pressure gradient will be a gravitational one (Figure 19, C and D). Where a low permeability substratum overlies a higher permeability stratum, water will be driven by vertical Darcian flow through the upper stratum by relatively high potential gradients (Figure 19, B) resulting in very low or negative effective pressures at the ice/bed interface.

Both low and high permeability glacial substrates have been cited as promoting low effective basal pressures at the ice/bed interface (Shoemaker, 1986; Boulton *et al.* 1974). For example, Piotrowski (1997) calculated that fine-grained subglacial sediments with an average coefficient of permeability of 10^{-7} m/s were only able to discharge 25% of the annual basal meltwater production of the Scandinavian ice sheet. She determined that this may have resulted in a cyclic buildup of subglacial hydraulic pressure, increased storage and ultimately catastrophic release of water from the ice/bed interface. Similarly, Brown *et al.* (1987) calculated that a 100 m thick aquifer underlying the Puget Lobe was only able to drain half of the water produced by basal melting. Brown *et al.* (1987) state that an inefficient basal drainage system resulted in massive basal porewater pressure buildup and hydraulic jacking at the ice/bed interface.

Murray and Dowdeswell (1992) note that subglacial bed deformation results in sediment dilation and or particle alignment parallel or subparallel to the direction of principal strain. This particle realignment increases the hydraulic conductivity of the deforming bed by an order of magnitude resulting in an increase in the rate of water flow parallel to deformation. The increase in flow can result in the removal of fines from the deforming matrix, further increasing conductivity (Murray and Dowdeswell, 1992). This increase in bed hydraulic conductivity can result in horizontal Darcian flow becoming effectively trapped within the deformed regions where dilation has occurred.

6.3.2 Subglacial Channels

Channels will develop at the glacier-bed interface where the capacity for both vertical and horizontal intergranular drainage is exceeded by the melting rate. (Boulton and Dobbie, 1993). Channelized sub-ice stream drainage has not been directly observed, however theoretical predictions of drainage morphology have been proposed.

Kamb (1987) describes a glacier surge-sliding mechanism which is based on a linked cavity configuration. A linked cavity system can exist as a system of many interconnected conduits distributed across the glacier bed, in contrast to a tunnel system which must condense to one or at most a few main tunnels (Kamb, 1987). The linked cavity model allows for higher basal water pressures at basal water fluxes $>1 m^3/s$ over low relief beds. The linked conduit system may show unusual transient behaviour due to changes in linkages with sliding, sediment deformation, and basal melting (Kamb, 1987).

Walder and Fowler (1994) theoretically predict the existence of many wide, shallow, high pressure braided canals distributed along the ice-sediment interface in subglacial environments characterized by deforming sediment (Walder-Fowler canals).

Although not exclusively associated with high ice flux conditions, it appears that Walder-Fowler canals are present at the ice-sediment interface where low slopes and low effective pressures dominate. It also appears that these canals are retained to some degree in the geologic record, despite sediment deformation (Alley, 1992).

Walder-Fowler type canals have been described in the geologic record by Johnson and Hansel (1990), Eyles *et al.* (1982), and Brown *et al.* (1987). There are numerous sorted sediment bodies within the Vashon till, which was deposited by the fast flowing Cordilleran Puget Lobe (Brown *et al.* 1987). Sorted sediment structures were found in roughly 60% of the outcrops of Vashon till. Lenses range from predominantly clay to gravel and from well to poorly sorted. The lack of a channel form and the coarse grain sizes suggest that these sediments appear to record deposition from water flowing in broad sheet-like layers under the ice (Brown *et al.* 1987). Brown *et al.* (1987) interpreted the sorted sediments as having been deposited in subglacial conduits, and estimate the width of such conduits as ranging from 0.1 to 8 m. Evidence of only limited shear strain observed in much of the till implies that pervasive shearing did not contribute significantly to the motion of the streaming Puget Lobe.

Eyles *et al.* (1982) described "shoestring" deposits in Northumberland, England which they interpreted as channel fills that may have been deposited within a canal system. The deposits are elongated sub-parallel to the direction of ice flow. They have nearly flat upper surfaces and irregular, concave lower surfaces that are much wider than their vertical thickness. Eyles *et al.* (1982) proposed that these deposits represent cut and fill structures formed by subglacial drainage. Diapiric deformation at the channel bases indicates low effective pressure in the till at the time of channel formation.

Evidence of subglacial channelization associated with the Lac La Biche ice stream has been presented by Mougeot (1991). The implications of this evidence will be combined with other geological evidence and discussed in the following chapter.

Chapter Seven

Site Geology Interpretation

7.1 Introduction

This chapter includes discussion concerning the processes responsible for till deposition beneath the Lac La Biche ice stream. The primary objective of the geologic investigation at each site is to characterize the processes and environment of till deposition. The processes responsible for till deposition at each site will provide insight into the interpretation of preconsolidation results as well as suggest the primary mode of ice stream flow. Sample site locations were restricted to regions where till deposited by the Lac La Biche ice stream has been identified by Mougeot (1991), Andriashek (1985) and Fenton and Andriashek (1983). A summary of the physical characteristics associated with "end member" till genetic processes will be presented for comparison with observed till characteristics exposed along the path of the Lac La Biche ice stream. Control well stratigraphies are presented in Appendix 5.

7.2 Till Forming Processes

The subglacial environment is one of the most complex in nature, involving multiple events that include deposition, erosion and deformation (Hicock *et al.* 1996). This complexity results in the development of a variety of hybrid tills which have undergone a number of "end member" processes. The recognized "end member" processes responsible for the deposition and/or modification of till include; lodgement, melt-out, deformation and gravity flow (Dreimanis, 1976; 1989; Hicock *et al.* 1996).

However, Hicock (1990) suggest that most tills are formed through a combination of processes. Table 3 presents a summary of the end member processes responsible for till deposition/modification and the associated geologic evidence used in the interpretation of each process. Till clast fabrics have in part, also been used to infer end member glacial processes by numerous authors including Hicock *et al.* (1996), Dowdeswell and Sharp (1986), Hart (1994) and Mark (1974) however, clast fabrics are likely reoriented and modified with changing subglacial conditions (Hicock *et al.* 1996).

7.3 Section Descriptions / Interpretations

The following summaries include section locations, surface topography, till description and the surficial map unit designation. Map unit designations from each site were recorded from Mougeot (1991), Fenton and Andriashek (1983) and/or Shetsen (1990). Lithologic descriptions and clast fabric data are presented to facilitate interpretation of the processes responsible for sediment deposition. Figure 20 shows clast fabric data plotted on the Hicock *et al.* (1996) modality-isotropy diagram. Clast fabric statistics are summarized on Table 4. Coarse sand grain petrology is presented on Table 5. See Figures 2 and 8 for general sample site locations, specific location descriptions are provided.

DS01

Section Location: LSD 9, Sec 5, Tp 60, R 11, W 4 M; centre of cowfield ~ 20 m west of road and ~40 m south of main house.

Distance from Control Well: Section is ~400 m south of control well.

Consolidation Sample Type: Shelby tube samples taken at 3.0 m depth.

Table 3. End Member Till Depositional Processes

Name	Process	Geologic Evidence	References
Lodgement	The frictional retardation of basally transported debris against a ridged bed (Benn and Evans, 1996), or a plastering of subglacial debris from the base of a moving glacier by pressure melting and/or other mechanical processes (Dreimanis, 1989).	Aligned unimodal clast fabrics. May have bimodal clast fabric with weak transverse component. Boulder pavements, bullet shaped clasts with stria parallel to ice flow direction. Aligned clasts dip up glacier. Massive till structure. Plowing structures.	Boulton and Paul (1976), Dreimanis (1989), Hicock *et al.* (1996), Benn (1995), Hicock (1991), Dowdeswell and Sharp (1986).
Melt-out	Slow release of glacial debris from ice that is not sliding or deforming internally (Dreimanis, 1989). Can be either subglacial or supraglacially deposited.	Supraglacial melt-out: Often redeposited as a flow till (see below). Low degree of consolidation, presence of draped sediments over clasts. Clast fabric orientation can be unimodal to multimodal.	Dreimanis (1989), Hicock *et al.* (1996), Shaw (1982).
		Subglacial melt-out: Clast fabrics similar to those formed by lodgement or deformation. Draped lenses of sorted sediment. Concave up channel fill deposits. May have experienced winnowing of fines by water. May be moderately overconsolidated.	Dreimanis (1989), Shaw (1982), Boulton (1976b), Sugden and John (1984).
Deformation	Till formed by subglacial squeeze flow or simple shear (Dreimanis, 1989).	Clast stoss-lee orientations reversed and/or at high angles to ice flow direction. Multimodal clast fabrics. Irregular stone pavements. Soft sediment clasts, attenuated or isoclinally folded lenses or boudins. Extreme strain can produce homogenization.	Dreimanis (1989), Hart (1994), Hicock *et al.* (1996), Hicock and Dreimanis (1992), Hart *et al.* (1990), Benn and Evans (1996).
Flow	A secondary or resedimented deposit from glacial ice or from freshly deposited till in direct association with glacier ice. Flows under the influence of gravity usually in direct association with water (Dreimanis, 1989).	Random, parallel or transverse clast fabrics. Facies association with water sorted sediments. May have a stratified or semi-stratified appearance. Sedimentary structures variable over short distance.	Dreimanis (1989), Dowdeswell and Sharp (1986).

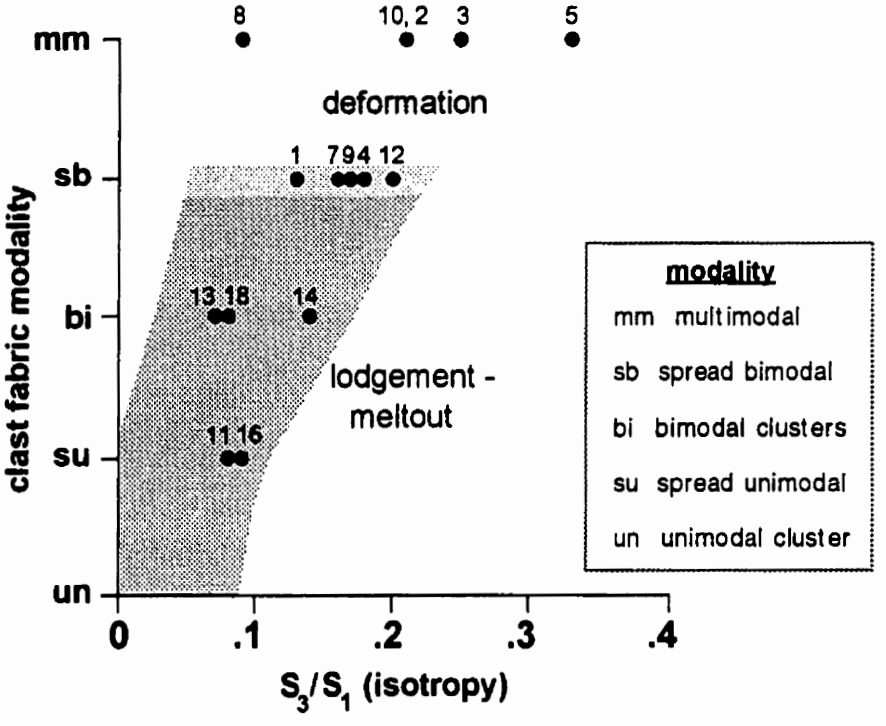

Figure 20. Modality-isotropy diagram with measured clast fabric data from all sampled sites. Numbered points correspond to "DS" site numbers. The Deformation and Lodgement-Meltout process fields correspond to those given in Hicock *et al.* (1996). Process fields overlap for the spread bimodal modality category. Process fields are only valid for tills deposited subglacially.

Table 4. Summary of Clast Fabric Data Statistics

Sample Site	n	S_1	S_2	S_3	S_3/S_1	S_1/S_3	k-value	Modality Hicock *et al.* (1996)	Mean Lineation Vector (trend, plunge)
DS01	25	0.536	0.392	0.072	0.13	7.44	0.18	spread bimodal	308,02
DS02	25	0.485	0.414	0.101	0.21	4.80	0.11	multimodal	175,10
DS03	25	0.539	0.325	0.135	0.25	3.99	0.58	multimodal	320,01
DS04	25	0.555	0.345	0.101	0.18	5.50	0.39	spread bimodal	127,03
DS05	25	0.497	0.341	0.162	0.33	3.07	0.51	multimodal	026,18
DS07	25	0.571	0.336	0.093	0.16	6.14	0.41	spread bimodal	337,13
DS08	25	0.548	0.403	0.049	0.09	11.18	0.15	multimodal	004,07
DS09	25	0.619	0.275	0.105	0.17	5.90	0.84	spread bimodal	034,11
DS10	25	0.520	0.371	0.108	0.21	4.81	0.27	multimodal	088,04
DS11	26	0.715	0.231	0.054	0.08	13.24	0.78	spread unimodal	086,07
DS12	26	0.621	0.254	0.126	0.20	4.93	1.27	spread bimodal	176,01
DS13	25	0.608	0.347	0.045	0.07	13.51	0.27	bimodal cluster	144,01
DS14	25	0.667	0.239	0.094	0.14	7.10	1.11	bimodal cluster	145,07
DS16	25	0.772	0.115	0.073	0.09	10.58	2.12	spread unimodal	328,08
DS18	25	0.679	0.271	0.051	0.08	13.31	0.55	bimodal cluster	202,02

Table 5. 1-2 mm Coarse Sand Petrology Summary

Sample	Igneous & Metamorphic %	Quartz %	Quartzite & Quartz sandstone %	Local %	Dolostone %	Limestone %	Other %	Total Grains
DS01	61	30	3	2	1	3	-	557
DS02	65	27	2	1	2	3	0	378
DS03	69	22	2	0	3	4	-	537
DS04	66	22	2	2	3	4	1	465
DS05	60	27	5	1	3	4	-	547
DS07	61	30	2	1	3	3	0	462
DS08	61	30	4	2	1	2	-	469
DS09	62	27	2	2	4	3	-	507
DS10	61	25	6	2	1	5	-	380
DS11	57	33	2	2	2	3	1	476
DS12	52	31	6	1	3	6	1	348
DS13	59	27	4	2	2	5	1	411
DS14	60	26	6	2	3	3	-	378
DS16	64	26	3	2	2	3	-	304
DS18	57	31	3	2	3	4	-	456
Average All Sites	**61.0**	**27.6**	**3.5**	**1.6**	**2.4**	**3.7**	-	
SD	4.1	3.2	1.6	0.6	0.9	1.0		

DS01 is located within generally flat to undulating topography on 1-2° dipping north-facing slope. Approximately 40 m south is an irregular low hummock with a generally streamlined shape oriented northwest-southeast. DS01 is mapped by Fenton and Andriashek (1983) as MFhm1 (fluted moraine with hummocks of mixed lithology, local relief of less than 3 m).

The exposure consists of 3.0 m of massive, oxidized, silty clay diamicton (sand 37.8%, silt 27.7%, clay 34.5%) with a colour of 10YR 3/3 moist (dark brown) (Figure 21). The diamicton consists of ~2% clasts, sub-rounded to rounded with an average diameter of 2-5 cm and a maximum size of 35 cm. Soft angular sandstone clasts 2-3 cm in diameter are also present. From 0-0.95 m depth the diamicton is structureless and unfractured. From 0.95-3.0 m an angular, blocky structure is evident with a horizontal joint spacing of 1-2 cm. The structural transition is sharp, dipping slightly towards the northeast.

Clast fabric shows a spread bimodal distribution with both parallel and transverse components (Figure 22). The dominant mode is aligned nearly parallel to ice flow direction trending approximately west northwest-east southeast, dipping towards the west northwest. The transverse component trends northeast-southwest dipping towards the northeast.

DS01 Interpretation

The abrupt change in till jointing at 0.95 m could be the result of three possible processes: 1) The similarity of the observed structural characteristics at DS01 are comparable to Boulton's (1982) two layer till deformation model. The upper meter of

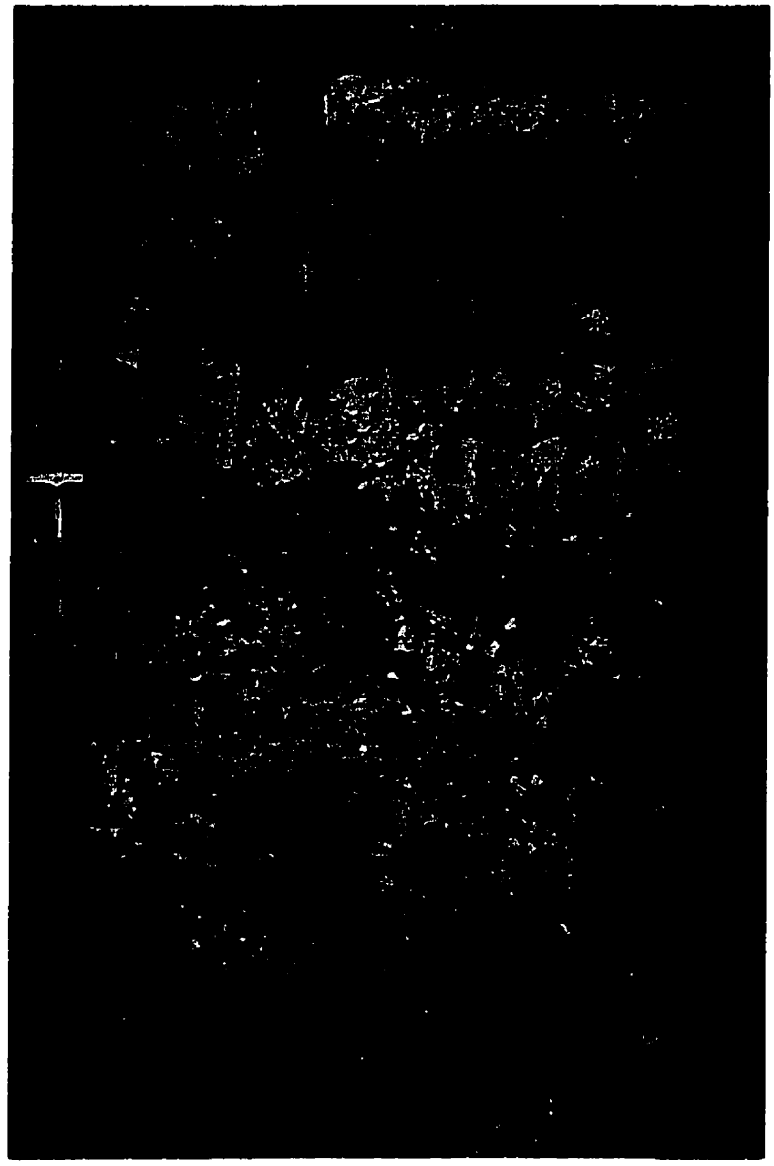

Figure 21. Diamicton section exposed at DS01. The abrupt change in till jointing is evident at 95 cm depth. The structural change is interpreted as evidence of a two layer sediment deformation process similar to Boulton's (1982) model. Hammer is 28 cm in length.

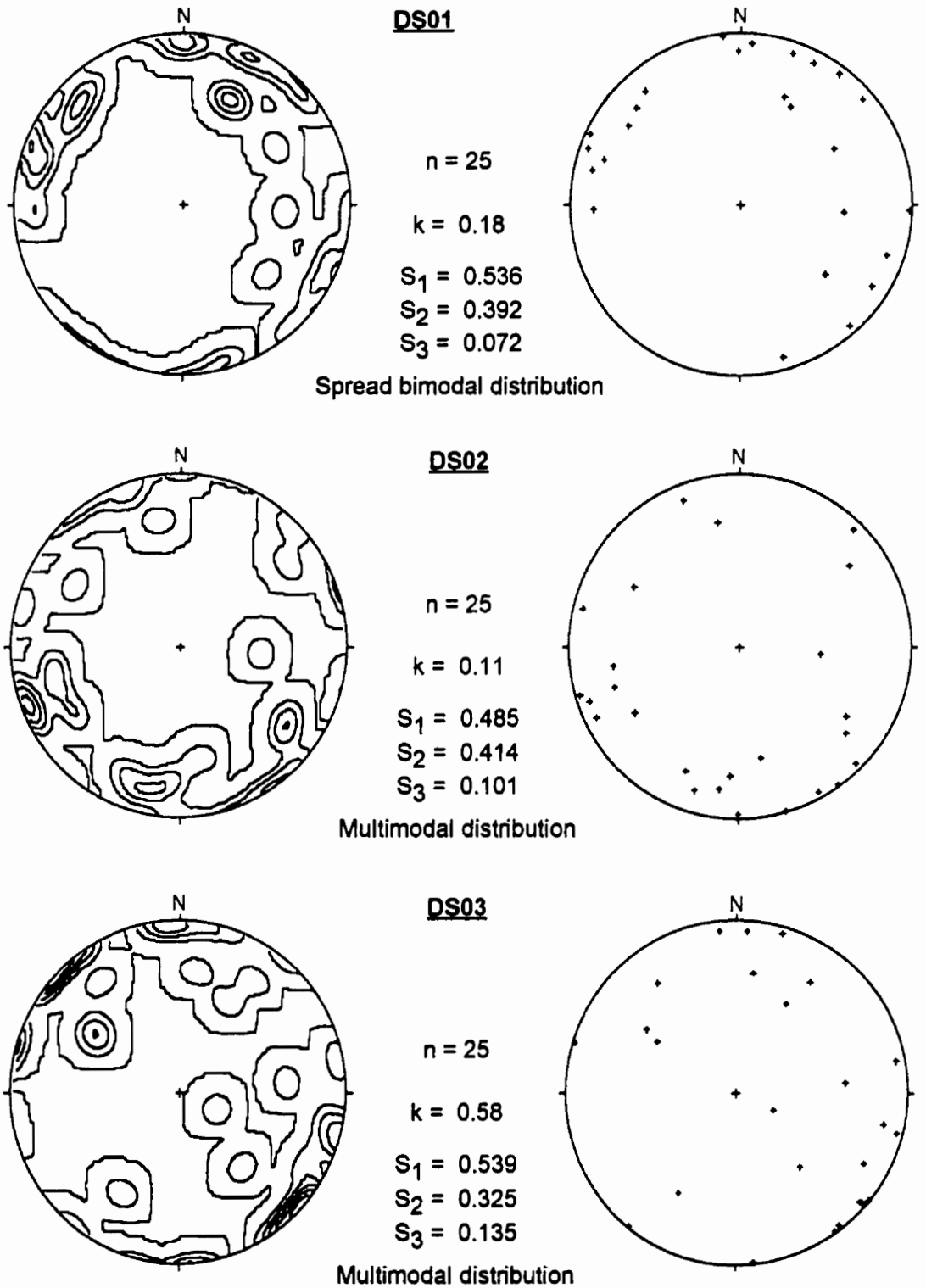

Figure 22. Schmidt equal-area lower hemisphere projections of measured clast fabric data for sites DS01, DS02 and DS03. Contour diagrams use a 2% contour interval.

till may represent the once dilatent A horizon sediments which overly the lower, heavily jointed B horizon. The thickness of the upper till and the presence of joints in the lower unit are both similar to sediments described by Boulton (1987). 2) The abrupt change in jointing pattern could be explained by the presence of two distinct till units. 3) Cryoturbation associated with annual ground freezing may have acted to homogenize the structural characteristics of the upper portion of the exposed till. The depth of the upper till is similar to the annual average freezing depth for this portion of Alberta (Kenton Miller, Environmental Consultant, pers. comm. 1997). However, it is suspected that gradual changes in till jointing would be observed if annual cryoturbation had acted to alter the till sediment structural characteristics. The lack of defining structural characteristics within the exposed section and the absence of clast fabric data from the upper till unit precludes a definitive answer to the process involved.

The spread bimodal clast fabric distribution measured in the lower portion of the section (Figure 22) falls within the overlap area of the deformation and lodgement-melt-out fields of the Hicock *et al.* (1996) modality-isotropy diagram (Figure 20). The dominant fabric mode is generally aligned to regional ice flow direction with clasts dipping in both the "up ice" and "down ice" directions. This fabric component could have been produced by either lodgement or melt-out processes or within a till undergoing shear deformation. The transverse fabric component could also be interpreted as produced by lodgement or melt-out processes perhaps associated with a compressive stress regime. However, a transverse component would be expected in shear deformation till only where the thickness of the deforming layer is similar to the clast size (Hicock *et al.* 1996). The spread bimodal nature of the measured clast fabric data supports a more complex depositional process, influenced by melt-out processes or shear deformation.

The presence of angular soft sandstone clasts within the till suggests a short transport distance within deforming till accompanied by low effective basal stress, or deposition by melt-out processes from stagnating ice. It is likely that lodgement processes would have destroyed the soft sandstone clasts.

There may be no single interpretation for the genesis of the till exposed at DS01. The interpretation of a two layer deforming structure similar to that described by Boulton and Hindmarsh (1987) cannot be discounted, nor can the interpretation of deposition by passive basal melt-out processes.

DS02

Section Location: LSD 15, Sec 14, Tp 60, R 10, W 4 M; section located 15 m northeast of Ranger Oil well, at edge of hayfield.

Distance from Control Well: Section is ~750 m east southeast of control well.

Consolidation Sample Type: Shelby tube samples at 2.50 m depth.

DS02 is mapped by Fenton and Andriashek (1983) as MFrm2 (fluted moraine with ridged surface elements of mixed lithologies; local relief of 3 to 10 m). The sample section is on a ~4° north facing slope of a hill with a relief of ~5 m. The hill is teardrop shaped ~100 m long and ~80 m wide with its long axis trending north-northwest south-southeast.

The exposure consists of 2.50 m of massive, oxidized, silty clay diamicton (sand 34.0%, silt 27.8%, clay 38.2%) with a colour of 10YR 4/4 moist (dark yellowish brown). The clast content is ~1%, subrounded to rounded with an average size of 1-5 cm and a maximum size of 10 cm. Clast fabric for DS02 shows a multimodal distribution (Figure 22).

DS02 Interpretation

The massive nature of the till limits the interpretation of subglacial conditions (with respect to consolidation history) at the site to landform morphology and measured clast fabric. The generally streamlined nature of the surrounding topography, along with the Fenton and Andriashek (1983) interpretation of the area as MFrm2 suggests that the till was deposited subglacially beneath actively flowing ice.

The multimodal clast fabric measured at the site falls within the deformation process field on Hicock *et al.* (1996) modality-isotropy diagram (Figure 22). The multimodal fabric suggests a complex and variable basal deformation history. According to Hart (1994) the calculated S_1/S_3 ratio of 4.80 for DS02 (Table 4) suggests a thick deforming layer.

DS03

Section Location: LSD 2, Sec 33, Tp 58, R 9 W 4 M; section is ~100 m west-northwest of the main house. DS03 is ~4 m north of DS14.

Distance from Control Well: Section is 125 m west of the control well.

Consolidation Sample Type: Shelby tube samples at 2.05 m depth.

DS03 is mapped by Fenton and Andriashek (1983) as MFrm2 (fluted moraine with ridged surface elements of mixed lithologies; local relief of 3 to 10 m). The section is located on the crest of a ~10 m high, south-southeast oriented drumlinoid form (~100 m wide, ~1 km long). The crest of the drumlinoid feature is slightly undulatory to hummocky with hummock crests oriented toward the southeast (Figure 23). The

Figure 23. View looking south at the DS03 / DS14 sample site (3 m west of truck in distance). Site is located on the crest of a ~10 m high drumlinoid landform. The landform's long axis is oriented northwest-southeast. The surface morphology of the streamlined landform is undulatory to hummocky. The diamicton exposed at DS03 / DS14 is interpreted to have been deposited by sediment deformation processes.

section consists of 2.50 m of massive, oxidized, silty clay diamicton (sand 32.6%, silt 28.6%, clay 38.8%) with a colour of 10YR 3/2 moist (dark greyish brown). The clast content is 1-2%, consisting of subrounded to rounded clasts with an average size of 1-3 cm, and a maximum size of 4 cm. Clast fabric shows a multimodal distribution, however 11 of the 25 clasts plotted in the southeast quadrant (Figure 22).

Interpretation DS03

The till characteristics at DS03 are very similar to those described at DS02. The southeast oriented drumlinoid form is indicative of molding by active glacial ice flowing in a southeast direction (Flint, 1971). The multimodal fabric measured at DS03 plots within the deformation field of the Hicock *et al.* (1996) modality-isotropy diagram (Figure 20). Therefore, the multimodal distribution suggests a complex depositional processes involving deformation resulting from variable local stress fields. According to Hart (1994), the S_1/S_3 ratio of 3.99 for DS03 (Table 4) suggests a thick deforming layer.

DS04

Section Location: LSD 12, Sec 36, Tp 47, R 1 W 4 M; section is located ~80 m south of southernmost building of the Fleming homestead on a generally flat spot near the top of a regional high area.

Distance from Control Well: Section is located 175 m south of the control well.

Consolidation Sample Type: Block sample was taken at 2.45 m depth.

The area surrounding DS04 is mapped as stagnation moraine by Shetsen (1990), (moderately to weakly developed hummocky topography with irregularly shaped, poorly defined knobs and kettles with a local relief of 3-10 m). Mougeot (1991)

mapped the site as MSChm1 (rolling crevasse filling moraine with hummocky ridges; local relief of less than 3 m).

The section is subdivided into upper and lower units. The upper 1.55 m consists of silty, fine-grained, massive sand. The contact with the underlying unit is sharp and undulating to irregular. The lower unit consists of 0.90 m of massive, oxidized, silty clay diamicton (sand 34.2%, silt 30.2%, clay 35.6%) with a colour of 10YR 3/3 moist (dark brown). Clast content consists of 1-2%, subrounded to rounded clasts with an average size of 1-3 cm and a maximum size of 60 cm. A discontinuous concentration of 10-60 cm diameter granitic and quartzite boulders are present at the contact between the two units. The upper sand unit in-fills the space between boulders.

A spread bimodal clast fabric is present at the base of the exposure (Figure 24). The dominant fabric mode is oriented north-northwest, which is parallel to the regional ice flow direction as indicated by Ellwood (1961) and Mougeot (1991).

DS04 Interpretation

The stratigraphic position, and erosional lower contact of the upper massive sand unit suggests the sand was deposited by deglacial fluvial or postglacial aeolian processes. The boulder concentration at the till/sand contact represents a lag deposit, indicating a period of fluvial erosion. Stria were not visible on the boulders.

The till fabric plots within both the sediment deformation and lodgement-melt-out process fields of the Hicock *et al.* (1996) modality-isotropy diagram (Figure 20). However, the interpretation of the till as being deposited by both englacial and supraglacial melt-out processes is strengthened by the presence of crevasse fillings, hummocky terrain and general lack of streamlined landforms near the section. Therefore, due to the presence of stagnant ice topography in the area and nondistinctive clast

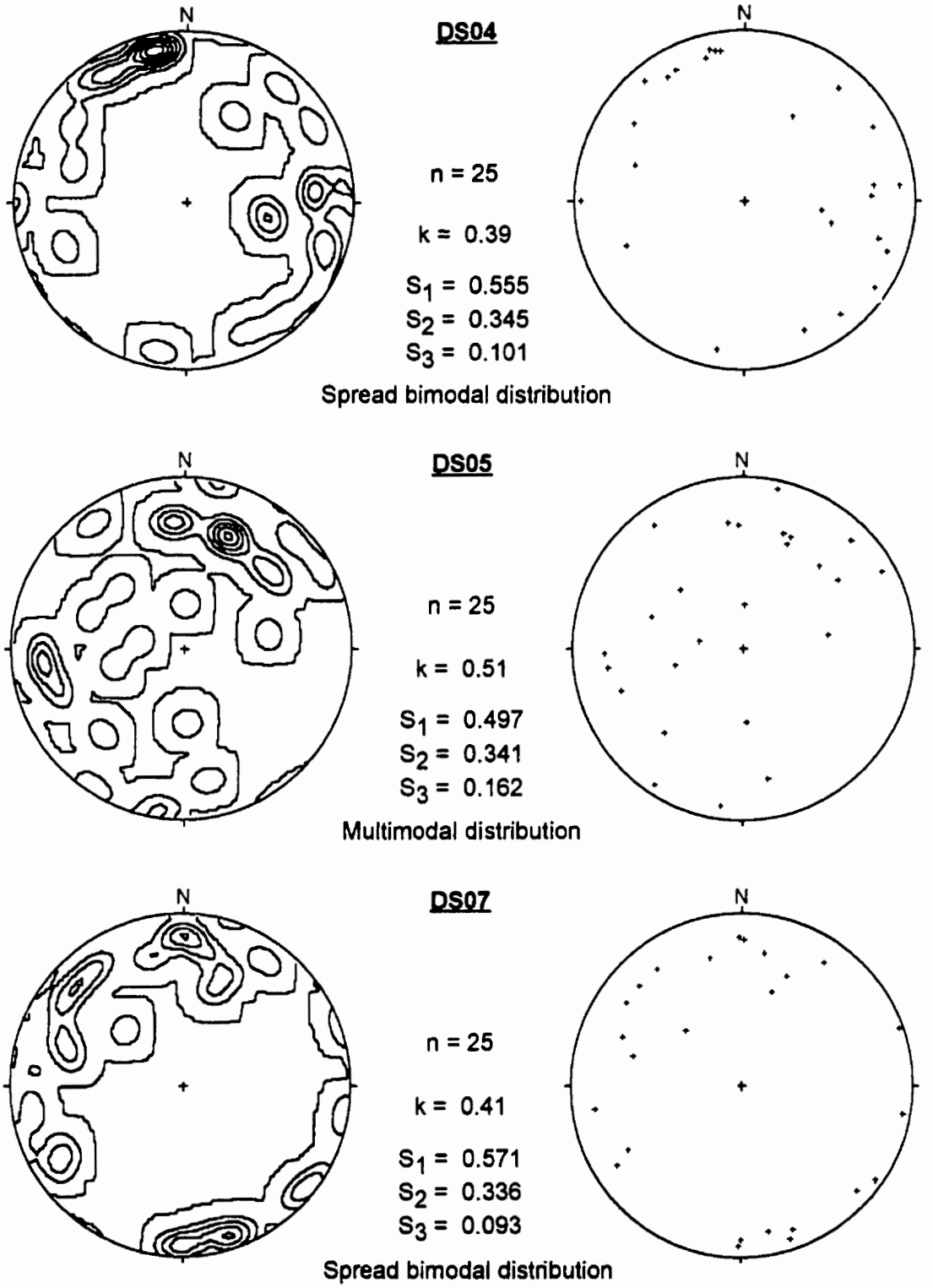

Figure 24. Schmidt equal-area lower hemisphere projections of measured clast fabric data for sites DS04, DS05 and DS07.

fabric, the till is interpreted as deposited by melt-out processes associated with a stagnating ice mass.

DS05

Section Location: LSD 4, Sec 9, Tp 50, R 1, W 4 M; section is located at edge of a field ~20 m north of the westernmost small building north of the main driveway.

Distance from Control Well: Section is 250 m east-northeast of control well.

Consolidation Sample Type: Block sample was taken at 2.20 m depth.

DS05 is mapped by Shetsen (1990) as Stagnation moraine (undulating topography with local relief generally less than 3 m). Mougeot (1991) mapped the site as MSCh1 (crevasse filling moraine with hummocky ridges; local relief of less than 3 m). However, the specific section is located within a flat field. Regional reconnaissance suggests that flat topography surrounds the site for several kilometers in each direction. Isolated, distinct 1-2 m high crevasse fill deposits (Ellwood, 1961; Mougeot, 1991) are evident throughout the area with a spacing of about several hundred meters to a kilometer. Approximately 100 m north of the section a slight northeast-southwest trending ridge with no more than 1 m in relief is visible. The ridge is several hundred meters in length, its crest curves forming a slight concave arc towards the northwest.

The section consists of two lithologic units (Figure 25). The upper unit consists of massive, silty fine-grained sand ~1 m thick. On the northern face of the excavated pit, the fine sand continues to a depth of at least 2.40 m, forming a slightly irregular wedge shape 1.90 m long, 35 cm wide at the top and thinning to 7 cm wide at the bottom of the exposure. A faint vertical lamination is visible within the sand wedge due to a slight colour change between lamina. No grain size or mineralogical change is evident between

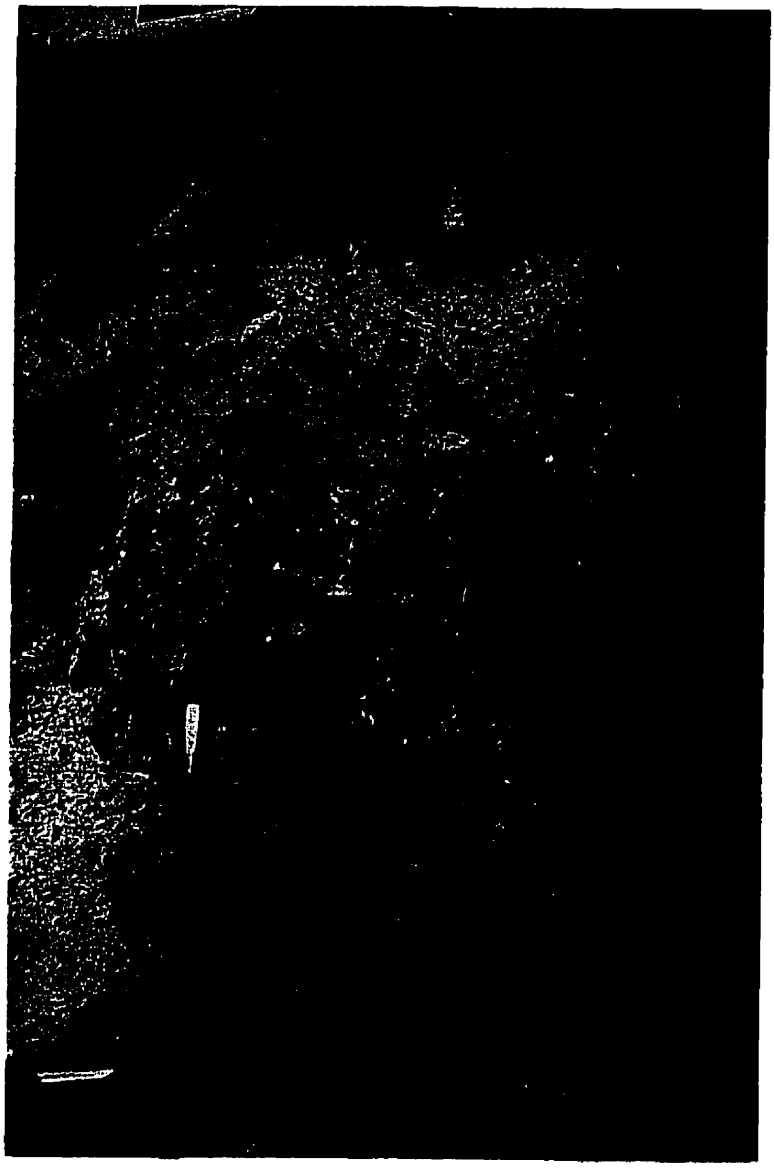

Figure 25. Section exposed at the DS05 site. The upper 1 m of the exposure consists of massive, silty, fine grained sand. This sand unit is continuous into a sand wedge 1.90 m deep, 35 cm wide at the top and 7 cm wide at the bottom of the exposure. A faint vertical lamination is evident within the sand making up the wedge. Clast poor diamiction flanks the sand wedge from 1 m depth to the base of the pit. The presence of the sand wedge is evidence of postglacial permafrost. The diamicton at DS05 is interpreted as deposited by basal melt-out processes.

the vertical lamina. The sand wedge is not visible on any other wall of the excavated pit. On either side of the sand wedge and below 1 m depth in the remainder of the pit, there is a heavily jointed, oxidized, sandy clay diamicton (sand 41.4%, silt 28.9%, clay 29.7%) with a colour of 10YR 4/3 moist (brown). The dominant joint planes strike at 250° and dip 25° towards the southeast. Diamicton clast content is ~5%, subrounded to rounded clasts with an average size of 2-3 cm and a maximum size of 30 cm.

The clast fabric has a multimodal distribution with a large percentage of the clasts dipping at a high angle (Figure 24). Only two clasts plot within the southeast quadrant.

DS05 Interpretation

Sand wedges are associated with aeolian deposition of sand within thermal contraction wedges in permanently frozen ground (Ritter, 1986). The uniform, fine grained nature of the upper sand unit and the continuation of the sand into the vertically laminated wedge shape suggests that the sand was deposited by aeolian processes after the retreat of the Lac La Biche ice stream. Thus, a cold and arid environment is interpreted for this region following the retreat of Laurentide ice.

The extreme flatness of the terrain suggests a basal till plain (within the local Stagnation map unit of Mougeot (1991) and Shetsen (1990)). The general lack of ice stagnation features locally other than the clearly defined low ice "crevasse fillings" suggests that the overlying ice may have been either: 1) relatively clean, lacking significant entrained debris, or 2) uniformly laden with entrained debris which was deposited with little or no reorganization or slumping.

The heavily jointed nature of the till may indicate the release of confining stress by the melting of overlying ice (Boulton, 1976a). However, the presence of joints

within till is not sufficient evidence to suggest the till was basally deposited, as joints are also found in supraglacial and englacial tills (Boulton and Paul, 1976).

The multimodal clast distribution falls within the deformation field of the Hicock *et al.* (1996) modality-isotropy diagram (Figure 20). The lack of significant parallel fabric and the presence of clasts dipping at a high angle suggests sediment deformation may have occurred by squeeze flow (Hicock *et al.* 1996), or may indicate a compressive basal stress regime (Dreimanis, 1989). However, postglacial till disturbance resulting from the development of permafrost and the sand wedge may have altered the original clast fabric. Frost action could have resulted in the development of vertical and near vertical oriented clasts (Ritter, 1986). The geology of the till exposed at DS05 lacks suitable defining characteristics indicative of any till "end member" process. Therefore, the interpretation of the mode of till deposition by melt-out seems justified due to the terrain classification of Shetsen (1990) and Mougeot (1991).

DS07

Section Location: LSD 13, Sec 23, Tp 57, R 7, W 4 M; the section is located in the centre of a narrow area clear of trees, approximately 40 m north of the road. The section is located ~50 m east of the crest of a low (<1 m) large scale streamlined hill oriented in a northwest-southeast direction.

Distance from Control Well: Section is ~200 m west of control well.

Consolidation Sample Type: Block sample taken at 1.95 m depth.

DS07 is mapped by Shetsen (1990) as draped moraine (an undifferentiated, subglacially molded deposit with streamlined features with a flat to undulating surface). Mougeot (1991) mapped the site as MFu1 (fluted moraine, undulating local relief of less than 3 m).

The section consists of 2.10 m of oxidized, sandy diamicton (sand 56.4%, silt 23.4%, clay 20.2%) with a colour of 10YR 4/3 moist (brown). Uniformly distributed within the diamicton are elongated, stringy to highly sinusoidal and irregular-shaped lenses of coarse to medium-sized, well-sorted massive quartz sand (Figure 26). The sand lenses are subparallel to the surface, 3 to 25 cm thick and at least 1 m wide. Lenses make up ~ 5% of the exposed section. At least one of the sorted lenses has the appearance of boudinage. Structurally, the upper 40 cm of the diamicton is massive. Below 40 cm the diamicton increasingly shows a jointed to blocky structure with depth. Clast content is ~3%, subrounded to rounded, with an average clast size of 1-3 cm and a maximum size of 45 cm.

DS07 clast fabric shows a spread bimodal distribution with the majority of clasts plotting in the northwest and southeast quadrants (Figure 24).

DS07 Interpretation

The streamlined nature of the site suggest the till was molded by active ice flowing towards the southeast. The till is therefore interpreted as subglacially deposited. The *in situ* sand lenses are interpreted to represent subglacial channel deposits similar to those observed by Brown *et al.* (1987) and identical to the "sand stringers" of Mougeot (1991). The well-sorted nature of the sand suggests uniform flow associated with the channels. The presence of the deformed sand lenses likely indicates that till deformation was limited (nonpervasive) and did not result in complete homogenization. It is also possible however, that the presence of the deformed channels may indicate that the rate of channel creation simply exceeded the rate of channel destruction within a pervasively deforming bed. It is suspected however, that if this were the case, a graduation in the degree of individual lens deformation would have been

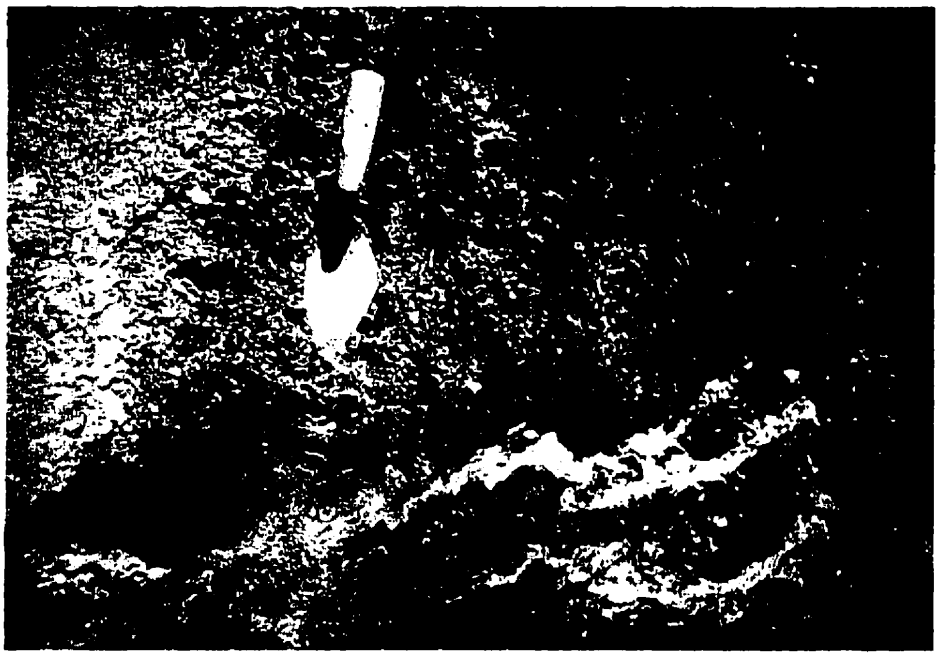

Figure 26. Photograph of typical deformed sand lenses within the exposure at DS07. The lenses shown above are similar in shape and contain sand which appears to be lithologically identical to the lenses described at DS08, DS09, DS10, DS11 and DS14. Trowel is 20 cm in length.

observed.

The sandy till matrix may be the result of processes which added sand and/or removed clay-size particles during till deposition. The low clay content may be associated with horizontal Darcian flow resulting in a winnowing of fines (Murray and Dowdeswell, 1992; Boulton *et al.* 1995). The sandy nature of the till may also represent the reworking of subglacial channel deposits into the till during earlier phases of pervasive deformation.

Fabric data for DS07 plot within the deformation and lodgement-melt-out fields of the Hicock *et al.* (1996) modality-isotropy diagram. The spread out nature and "up ice" dip of the clast fabric as well as the presence of deformed sand lenses suggests a complex stress history likely dominated by some degree of non-pervasive sediment deformation.

DS08

Section Location: LSD 2, Sec 28, Tp 57, R 7 W 4 M; the section is located near the centre of an open field, on the highest crest of a southeast oriented flute, approximately 250 m north of the road. The section is 35 m west of DS09.

Distance from Control Well: Section is located between two control wells where lithologies have been profiled and correlated by Mougeot (1991). The wells are located 2.7 km east and 3.5 km northwest of DS08.

Consolidation Sample Type: Block sample was collected at 2.05 m depth.

DS08 is mapped by Shetsen (1990) as draped moraine (an undifferentiated subglacially molded deposit with streamlined features, with a flat to undulating surface). Mougeot (1991) mapped the site as MFu1 (fluted moraine, undulating local relief of less than 3 m). The section is located in a large hay field on the crest of a >1 km long flute

with an amplitude of 2 m and wavelength of ~70 m (Figure 28). The flute trends at 142° and is rounded and symmetrical in profile. A series of similar flutes with a slightly lower amplitude are clearly visible for several hundred metres on either side of the site.

The exposure consists of 2.20 m of oxidized, sandy diamicton (sand 54.2%, silt 26.2%, clay 19.6%) with a colour of 10YR 4/3 moist (brown). Small, irregular to elongate sinusoidal sand lenses are present below 1 m depth. The lenses are 1-5 cm in thickness and up to 50 cm long and oriented subparallel to the surface. The sand is quartz-rich, consistently massive, medium-grained, well-sorted and well-rounded. The sand lenses increase in number with depth, making up 20% of the pit wall near the base of the pit. The upper 80 cm of the diamicton is massive with 1%, subrounded to rounded clasts averaging 3-5 cm in diameter. The largest visible clast is 30 cm in diameter.

An abrupt, wavy boundary occurs at 80 cm depth. The diamicton below this level shows near horizontal jointing with a spacing of 3-4 mm. The joint fracture spacing increases with depth in the pit so that the diamicton at 2.20 m is nearly massive and unfractured. The clast fabric at DS08 has a multimodal distribution and is dominated by clasts dipping at low angles (Figure 28).

DS08 Interpretation

The interpretation of the structural characteristics (high sand content, deformed sand lenses) observed within the till at DS08 is similar to the interpretations provided for the till at DS07. However, there are no joints within the upper 80 cm, which may represent the dilatent A horizon of a two layer deforming bed process similar to that described by Boulton (1982). The thickness of the upper massive till is similar to the thickness of the upper deforming layer observed at Breidamerkurjökull glacier by

Figure 27. View looking north at the DS08 / DS09 sample site locations. DS08 is located on the crest of the flute in distance, while DS09 is located in the flute trough located south of the person in the photo. The surface morphology of the area is dominated by long (> 1 km), rounded, symmetrical flutes with an amplitude of ~2-3 m and a wavelength of ~70 m. The long axis of the flutes trend 142°. The diamicton exposed at DS08 / DS09 is interpreted to have been deposited by a two layer sediment deformation process.

Boulton and Hindmarsh (1987). The lack of sand lenses within the upper portion of the till also supports the interpretation of pervasive sediment deformation within the upper 80 cm of the exposed till.

The sinusoidal to highly deformed sand lenses below 80 cm depth are identical in shape and sand lithology to the those described at DS07 and by Mougeot (1991). Mougeot (1991) states, "the presence of sand stringers within this facies may suggest the presence of a dense drainage network of small subglacial fluvial channels located at the ice-bed interface." As the lenses are only visible below 80 cm depth, the channel deposits could not have been deposited as pipe flow associated with horizontal flow of basal meltwater through the deforming till as suggested by Murray and Dowdeswell (1992). A change in basal conditions seems likely where active bed deformation resulted in the homogenization of till which previously contained sorted sand lenses. A period of accelerated till accretion at the bed may have also resulted in the burial of older channel deposits.

The fabric data plots within the deformation field of the Hicock *et al.* (1996) modality-isotropy diagram (Figure 20). There is no significant fabric mode aligned to the flute orientation as might be expected with the location of the pit on the crest of a flute (Jones, 1981). The clast fabric, and the presence of a two layer deforming till structure indicates that the overlying ice flowed by a process of pervasive bed deformation.

DS09

Section Location: LSD 2, Sec 28, Tp 57, R 7 W 4 M; the section is located in the centre of an open field in a trough between crests of southeast oriented flutes, approximately 250 m north of the road. The section is 35 m east of DS08.

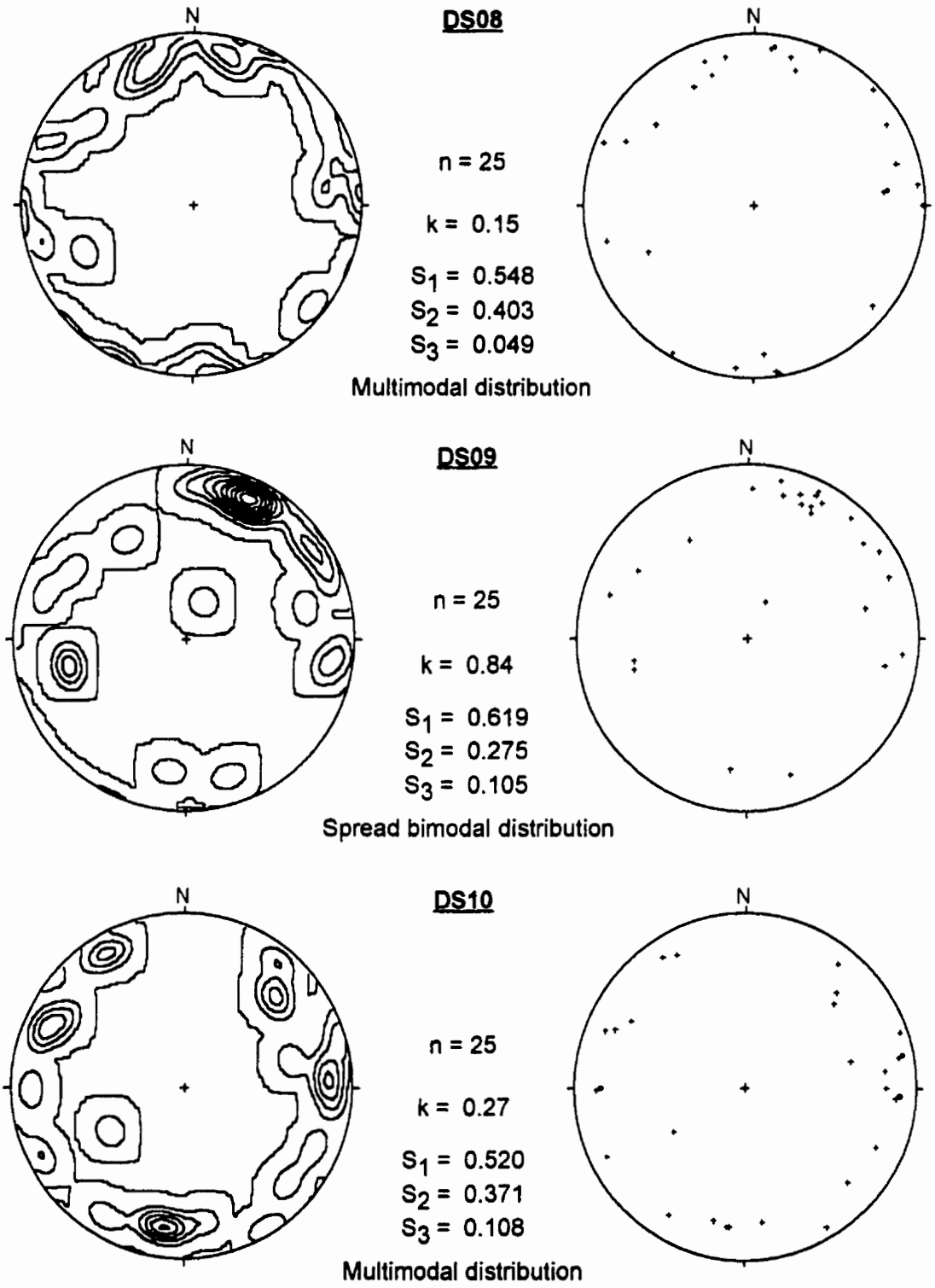

Figure 28. Schmidt equal-area lower hemisphere projections of measured clast fabric data for sites DS08, DS09 and DS10.

Distance from Control Well: The section is located between two control wells where lithologies have been profiled and correlated by Mougeot (1991). The wells are located 2.7 km east and 3.5 km northwest of DS09.

Consolidation Sample Type: Block sample was collected at 2.50 m depth.

DS09 is located in the trough between two southeast oriented flutes. The flutes are >1 km long, linear and have an amplitude of 2 m and a wavelength of ~70 m (Figure 27). The flutes trend 142° and are rounded and symmetrical in profile. A series of similar flutes with a slightly lower amplitude are clearly visible for several hundred metres on either side of the excavated section.

The site is mapped by Shetsen (1990) as draped moraine (an undifferentiated subglacially molded deposit with streamlined features with a flat to undulating surface). Mougeot (1991) mapped the site as MFu1 (fluted moraine; undulating local relief of less than 3 m).

Two units of sandy oxidized diamicton are evident within this exposure. The upper 1.50 cm of the exposure is soft, massive and has a colour of 10YR 4/6 moist (dark yellowish brown). The upper diamicton appears to be very clay-rich (no sample taken) within the upper 30 cm. Rare, subrounded to rounded clasts averaging 3-5 cm diameter make up about 1% of the upper diamicton. Several large subrounded granitic boulders (maximum size 80 cm) form a discontinuous pavement at 1.50 m depth. Striations were not evident on the boulders.

Below 1.50 m the diamicton is sandy (sand 41.2%, silt 27.5%, clay 31.3%) with a colour of 10YR 4/3 moist (brown). The diamicton is highly jointed with 3-6 mm spacing between joint planes. The joint spacing increases to 1 to 2 cm at base of pit. Dark manganese stains are evident along fracture planes. Also present below 1.5 m depth are small irregular sinusoidal to elongate stringy sand lenses. The lenses are subparallel to the surface, 1-5 cm in thickness and up to 50 cm long. The sand within

the lenses is quartz-rich, consistently massive, medium-grained, well-sorted and well-rounded.

Clast fabric at DS09 shows a spread bimodal distribution (Figure 28). The dominant mode is centered on 020° with a much less significant east-west oriented transverse mode.

DS09 Interpretation

The topographic position and clearly defined lower contact of the upper 1.5 m of diamicton suggests this unit may represent an upper "A horizon" deforming till layer similar to that observed at DS08 and DS01. This interpretation is supported by the lack of sand lenses, loose concentration of boulders at the lower contact and the jointed till structure below 1.5 m depth. Deformation pavements are interpreted to form within pervasively deforming till by alteration of previously lodged pavements and/or by clast-settling upon release from basal ice (Hicock, 1991). Clay within the upper 30 cm may have been deposited within standing water during deglaciation or may have been redeposited by slope wash from the adjacent flute crests.

The DS09 clast fabric plot falls within both the deformation and lodgement-melt-out fields of the Hicock *et al.* (1996) modality-isotropy diagram (Figure 20). The orientation of the dominant fabric mode suggests flow from the north-northeast. This is contrary to the southeasterly ice flow direction as indicated by the flute orientation. Hence the orientation of the till fabric may result from strains within the deforming till layer. Jones (1981) measured similar clast fabric orientations from the troughs between southeast oriented flutes and drumlins near St. Paul, Alberta. The fabrics formed a "herring bone" pattern which has most recently been attributed to till deformation and the formation of flutes by Benn (1994b). These data, along with the irregular shape of

the sand lenses, suggest that a two layer sediment deformation process occurred at this location beneath the Lac La Biche ice stream.

DS10

Section Location: LSD 9, Sec 18, Tp 65, R 12 W 4 M; the section is located in a cow pasture, 150 m south of the main house.

Distance to Control Well: The section is 200 m south of the control well.

Consolidation Sample Type: Block sample at 1.85 m depth.

The site is mapped by Fenton and Andriashek (1983) as MFm12/MTh2 (fluted moraine with rolling morphology of low to moderate relief, overlying thrust moraine with hummocks of moderate relief).

DS10 is located on a 5-7° south facing slope of a southeast oriented irregular ridge. The ridge crest is 2 m above the surrounding flat pasture. The ridge is ~150 m in length and 30-50 m in width. Approximately 400 m north of DS10 is a ~30 m high system of southeast oriented hummocks and ridges.

The section consists of 1.97 m of weakly-jointed, silty clay diamicton (sand 26.2%, silt 29.2%, clay 44.4%) with a colour of 10YR 3/3 moist (dark brown). Clast content consists of 1%, subrounded to rounded clasts with an average size of 1-2 cm and a maximum size of 25 cm. The diamicton is weakly-jointed, forming a blocky structure to the base of the pit. A few highly contorted to sinusoidal, 1-2 cm thick quartz rich sand lenses are evident from 30 to 60 cm depth. The sand lenses make up 30% of surface area from 30 to 60 cm depth, while sand lenses below this depth are rare. The sand within the lenses is massive, medium-grained, well-rounded and well-sorted. The clast fabric has a multimodal distribution (Figure 28).

DS10 Interpretation

The southeast oriented streamlined landform suggests molding by active ice. The lens shape, grain size, sorting and lithology of the sand lenses are similar to those observed at DS07, DS08 and DS09. The highly distorted nature of the lenses within a narrow band may represent subglacial conduit channels which have experienced a high degree of heterogeneous squeeze (ductile) deformation similar to those described by Mougeot (1991). The uniform sand grain size within the lenses suggests relatively uniform flow.

The multimodal clast fabric orientation for DS10 falls within the deformation field of the Hicock *et al.* (1996) modality-isotropy diagram (Figure 20). The deformed appearance of the sand lenses and the clast fabric suggest a complex subglacial non-pervasive sediment deformation process for this location beneath the Lac La Biche ice stream.

DS11

Section Location: LSD 10, Sec 34, Tp 64, R 13, W 4 M; the section is located 15 m east of Highway 55 and 3 m southwest of the southwest corner of a silage pit.

Distance to Control Well: The section is 250 m south of the control well.

Consolidation Sample Type: Block sample was collected from 1.90 m depth.

The site is mapped by Fenton and Andriashek (1983) as MFm12 (fluted moraine with rolling morphology of low to moderate relief). The surrounding terrain is generally flat to undulating with a slight northeast aspect of 1-2°. A series of ~3-4 m

high, 300 m wide and > 1 km long southeast oriented flutes are visible ~600 m towards the southwest.

The exposed section consists of 2.1 m of oxidized, sandy diamicton (sand 40.0%, silt 27.1%, clay 32.9%) with a colour of 10YR 4/2 (dark greyish brown). The upper 70 cm is massive with a clast content of less than 1%. Clasts are subrounded to rounded with an average size of 1-2 cm and a maximum size of 20 cm. From 70-140 cm depth there is weak to moderately developed, blocky jointed structure with 1-2 cm horizontal joint spacing. Below 140 cm the diamicton is generally massive. Several sinusoidal-shaped sand lenses with a wavelength of 3-4 cm are evident at 145 cm depth. Lenses are 1-2 cm thick and 30 cm long. Sand within the lenses is quartz rich, medium-grained, well-sorted and well-rounded.

Clast fabric for DS11 has a spread unimodal distribution (Figure 29). The majority of clasts have a shallow plunge, plotting near the eastern edge of the stereo net.

DS11 Interpretation

The generally flat to undulating, southeast oriented, streamlined terrain suggests the till exposed at DS11 was subglacially deposited and overrun by active ice flowing in a southeast direction. The lens shape and sand texture of sand lenses is nearly identical to the lenses at DS07, DS08, DS09 and DS10 and is therefore interpreted as formed by similar subglacial fluvial channelization. The lenses at DS11 however, show a lesser degree of deformation.

The spread unimodal clast fabric falls within the lodgement-melt-out field of the Hicock *et al.* (1996) modality-isotropy diagram (Figure 20). The strong fabric measured at DS11 suggests ice flow from the east. However, the fabric orientation does not correspond to the local southeasterly ice flow direction, as suggested by the orientation

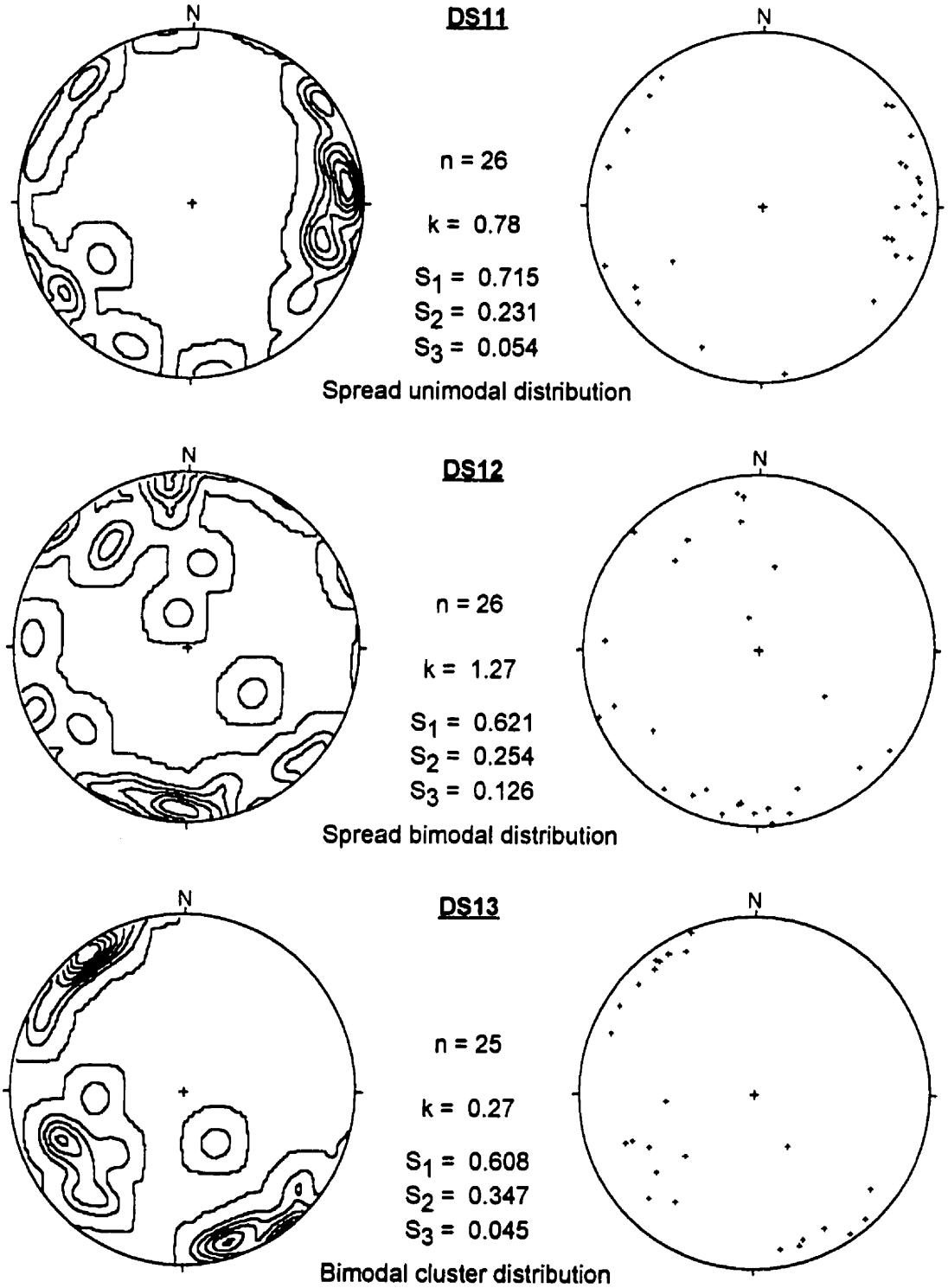

Figure 29. Schmidt equal-area lower hemisphere projections of measured clast fabric data for sites DS11, DS12 and DS13.

of streamlined landforms, nor is the fabric orientation transverse to it. Contrary to the interpretation of Hicock *et al.* (1996), the clast fabric may have resulted from localized sediment shear deformation associated with the processes responsible for the formation of the fluted landforms. Similar clast fabrics were measured by Jones (1981) within till on slopes of several flutes in the area of St. Paul.

DS12

Section Location: LSD 16, Sec 9, Tp 64, R 12, W 4 M; the section is 10 m south of a east-west oriented road allowance, 80 m west of a north-south oriented road and 2 m into the edge of farmers field.

Distance to Control Well: The section is 550 m south of the control well.

Consolidation Sample Type: Block sample taken at 1.75 m depth.

DS12 is mapped by Fenton and Andriashek (1983) as MFm1 (fluted moraine with rolling morphology of low relief). The local topography is generally flat with a southwestern aspect of approximately 2°. Approximately 600 m to the north and northeast of the section is a ~30 m high southeast oriented ridge. A southeast oriented regional low area is located 500 m to the southwest.

The exposed section consists of 2.0 m of massive to jointed, oxidized, silty clay diamicton (sand 31.8%, silt 29.9%, clay 38.3%) with a colour of 10YR 3/3 moist (dark brown). The diamicton has 1-2% subrounded to rounded clasts with an average size of 0.5-2 cm and a maximum size of 10 cm. The diamicton is heavily jointed from 70 cm depth to the bottom of the pit with a 0.5-2 cm spacing between the horizontally oriented joints.

Clast fabric at DS12 has a spread bimodal distribution (Figure 29). The dominant mode is oriented approximately north-south to northwest-southeast. A weak transverse component trends west-southwest. Several of the stones dip at high angles.

DS12 Interpretation

The generally flat to sloping nature of the site topography and the regional southeast orientation of the local streamlined landforms suggests the observed till was deposited within a subglacial environment by active ice flowing in a southeast direction. The generally massive nature of the exposed till, the presence of horizontal jointing within the till and the weak transverse fabric componenet suggests deposition by lodgement processes (Dreimanis, 1989). However, the fabric data plots within both the deformation and lodgement-melt-out fields of the Hicock *et al.* (1996) modality isotropy diagram (Figure 20). The dominant fabric mode is generally aligned to the regional ice flow direction; however, as the fabric is weak (S_1=.621), the till may have been exposed to local deformational processes.

DS13

Section Location: LSD 1, Sec 13, Tp 60, R 10, W 4 M; the section is located 30 m west of Secondary Highway 881 and 50 m north of Highway 28

Distance to Control Well: The section is 400 m NW of the control well.

Consolidation Sample Type: Block sample taken at 2.20 m depth.

DS13 is mapped as MSDdh1 / MFm1 by Fenton and Andriashek (1983) (discontinuous doughnut moraine which forms low relief hummocky topography overlying rolling fluted moraine).

The region around the site consists of low relief undulations to hummocks which is adjacent to an apparent northwest-southeast trending meltwater channel ~200 m to the east. The section is located near the centre of a slight rise approximately 80 cm high, 25 m in diameter and nearly circular in plan view.

The section consists of 2.70 m of oxidized, silty clay diamicton (sand 32.0%, silt 35.1%, clay 32.9%) with a colour of 10YR 4/4 moist (dark yellowish brown) (Figure 30). The upper 1.20 m is massive. A weak jointed structure is present from 1.20 m to the base of the pit. Clasts make up approximately 1-2% of the diamicton, with an average size of 2-3 cm and a maximum size of 25 cm. The clasts are predominantly subrounded to rounded.

Clast fabric at DS13 has a strong bimodal cluster distribution (Figure 29). The dominant fabric mode trends northwest to southeast which is parallel to the regional ice flow direction. The transverse fabric component has a slightly greater dip than the parallel mode and plots in the southwest quadrant of the stereo net.

DS13 Interpretation

Doughnut moraine is deposited from stagnant ice conditions (Fenton and Andriashek, 1983). The clast fabric plots within the lodgement-melt-out field of the Hicock *et al.* (1996) modality-isotropy diagram (Figure 20). Therefore, the strong parallel fabric and presence of the stagnant ice topography suggests the till exposed at DS13 was deposited by melt-out processes from stagnant basal ice.

Figure 30. Section exposed at the DS13 site. The section consists of massive, jointed clast poor diamicton. The unimodal clast fabric and presence of intermittant doughnut moraine at the surface suggests this diamicton was deposited from stagnant basal ice.

DS14

Section Location: LSD 2, Sec 33, Tp 58, R 9 W 4 M; the section is located on the edge of a cultivated field at the crest of a 10 m high drumlinoid. The section is ~100 m west-northwest of the main house. DS14 is 4 m south of DS03.

Distance from Control Well: The section is 125 m west of the control well.

Consolidation Sample Type: Block sample taken at 1.95 m depth.

The site is mapped by Fenton and Andriashek (1983) as MFrm2 (fluted moraine with ridged surface elements of mixed lithologies; local relief is 3 to 10 m).

DS14 is located on the crest of a high relief south-southeast oriented drumlinoid (~100 m wide, ~1 km long). The ridge crest is undulatory to hummocky with individual hummock crests oriented northwest-southeast

The section at DS14 consists of 2.30 m of massive, oxidized, silty clay diamicton (sand 27.4%, silt 29.0%, clay 43.6%) with a colour of 10YR 3/3 moist (dark brown). Clast content is approximately 1-2% with predominantly subrounded to rounded clasts. Average clast size is 0.5-3 cm, with a maximum size of 30 cm. Small elongate to irregular sinusoidal sand lenses 1-5 cm in length, 0.5-2 cm thick comprise ~5% of the surface area of the exposure. Sand within the lenses is quartz-rich, medium-grained, well-sorted and well-rounded.

Clast fabric at DS14 shows a bimodal cluster distribution (Figure 31). The primary mode is aligned parallel to the ice flow direction and the orientation of the south-southeast oriented ridge crest. The transverse mode plots in the southwest quadrant of the stereo net.

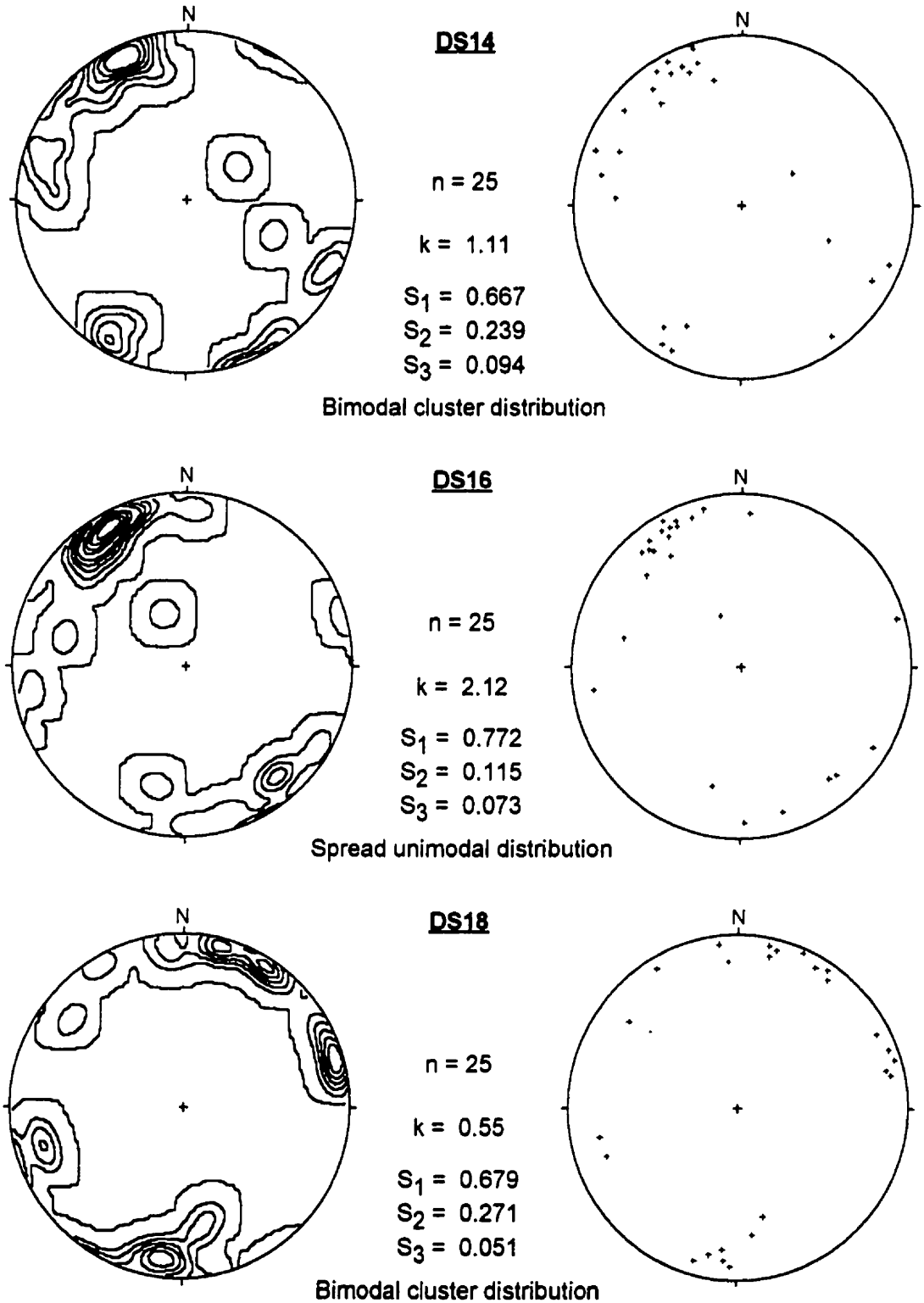

Figure 31. Schmidt equal-area lower hemisphere projections of measured clast fabric data for sites DS14, DS16 and DS18.

DS14 Interpretation

The southeast oriented drumlinoid form is indicative of molding by glacial ice flowing in the same direction. Fabric data plots within the lodgement-melt-out field of the Hicock *et al.* (1996) modality-isotropy diagram (Figure 20). The strong parallel "up ice" dipping fabric component of the bimodal cluster distribution suggests the till was deposited in a subglacial position by lodgement and/or basal melt-out processes. The sand lenses observed at DS14 are nearly identical to those observed at DS07, DS08, DS09, DS10, and DS11 and are therefore interpreted as being formed by the same process of subglacial channelization and associated non-pervasive sediment deformation.

DS16

Section Location: LSD 9, Sec 25, Tp 52, R 3, W 4 M; the section is 80 m north-northeast of the main house and 30 m west of the road in a horsefield.

Distance from Control Well: The section is 50 m north of the control well.

Consolidation Sample Type: Block sample was taken at 1.95 m depth.

The area around DS16 is mapped by Shetsen (1990) as stagnation moraine (undulating topography with local relief generally less than 3 m) with fluted landforms. Mougeot (1991) mapped the site as sFGu1 / MFE (undulating glaciofluvial sand of low local relief overlying eroded fluted moraine). The section is located on a south facing 2-3° slope. The surrounding region is generally flat. The head of a southwest draining coulee is located 10-15 m southwest of the section.

The section consists of 2.30 m of oxidized, silty clay diamicton (sand 30.4%, silt 30.3%, clay 39.3%) with a colour of 10YR 4/3 moist (brown). Clast content is

approximately 1% with subrounded to rounded clasts averaging 1-2 cm in diameter and a maximum clast size of 25 cm. The upper 80 cm of the pit is heavily bioturbated by rodent burrows, while from 80-130 cm depth the diamicton is massive. The diamicton becomes increasingly jointed with depth from approximately 1.3 m to the base of the pit. At 1.5 m depth there is a 15 cm diameter oval-shaped lens of poorly-sorted, clast-supported pebbly gravel. The gravel consists of rounded clasts with an average size of 3-4 mm and maximum size of 1 cm within a poorly sorted sand matrix.

The clast fabric at DS16 shows a relatively strong spread unimodal distribution (Figure 31) which is parallel to the ice flow direction (as indicated by Mougeot, 1991).

DS16 Interpretation

The clast fabric at DS16 plots within the lodgement-melt-out field of the Hicock *et al.* (1996) modality-isotropy diagram (Figure 20). The strong parallel "up ice" dipping fabric suggests the till was deposited in a subglacial position by lodgement and/or basal melt-out processes (Dreimanis, 1989). The undeformed nature of the oval gravel lens indicates there has been a lack of subglacial sediment deformation at this site. This favours a passive basal melt-out interpretation since deposition beneath active ice would have resulted in some degree of sediment (lens) deformation.

DS18

Section Location: LSD 13, Sec 36, Tp 52, R 4, W 4 M; the section is 20 m south of the 14th Baseline road and 80 m west of the main house.

Distance from Control Well: The section is 80 m west of the control well.

Consolidation Sample Type: Block sample taken at 2.05 m depth.

Mougeot (1991) mapped the site as bFLGu1 / MFE (undulating glaciofluvial sand and silt of low local relief overlying eroded fluted moraine). The regional topography is generally flat to slightly rolling. A 1.5 m high, elongated, southeast oriented sinuous ridge ~200 m long crosscuts the baseline road about 350 m east of the DS18 section.

The section consists of 2.60 m of oxidized, massive, sandy diamicton (sand 40.0%, silt 32.9%, clay 27.1%) with a colour of 10YR 4/4 (dark yellowish brown). The clast content is 2-3% subrounded to rounded clasts with an average size of approximately 1 cm and a maximum size of 20 cm. The diamicton has a weak blocky jointed structure from 2.0 m depth to the base of the pit. The horizontal joint spacing is approximately 3-4 mm and increases with depth.

Clast fabric consists of a bimodal cluster distribution (Figure 31) where the modes are separated by approximately 60°. Both fabric modes are transverse to the regional southeasterly ice flow direction.

DS18 Interpretation

The clast fabric plots within the lodgement-melt-out field of the Hicock *et al.* (1996) modality-isotropy diagram (Figure 20). However, the lack of ice stagnation topography, the massive nature of the till and the presence of horizontal jointing suggests deposition by lodgement processes (Dreimanis, 1989). The transverse fabric components may be associated with subglacial compressive flow stresses (Hicock *et al.* 1996; Dreimanis, 1989) resulting from the ascending nature of this portion of the ice stream pathway.

7.4 Discussion

Diamicton is present in all pits, although aeolian and possibly fluvial sand units were encountered at DS05 and DS04, respectively. The diamicton at each section is confirmed as till due to the presence of striated clasts, and igneous and metamorphic erratics derived from the Canadian Shield (Mougeot, 1991; Andriashek, 1985) (Table 5). The depositional environments, sedimentary structures, clast fabric distribution and sand, silt and clay percentages at each site are summarized in Table 6.

Although there was an attempt to restrict sampling to till overrun by active ice, the till at DS04, DS05, DS13 and DS16 is interpreted as deposited by melt-out processes from stagnant ice. Melt-out till was interpreted from the presence of stagnation topography (e.g. doughnut moraine of Fenton and Andriashek, 1983; ice crevasse fills of Mougeot, 1991), strong clast fabrics aligned to the local ice flow direction (Dreimanis, 1989) and the presence of an undeformed (oval) gravely lens within the till exposed at DS16. The fact that the oval gravel lens was undeformed, indicates there was a general lack of subglacial sediment deformation associated with this site. This observation favours the passive basal melt-out interpretation as deposition beneath active ice would likely have resulted in some degree of sediment deformation.

The interpretation of both lodgement and deformation till at the majority of exposed sections indicates that both basal sliding and pervasive sediment deformation were responsible for the forward motion of the Lac La Biche ice stream. Lodgement till was interpreted from a combination of strong to moderate clast fabric aligned or transverse to the direction of ice flow (e.g. Hicock *et al.* 1996; Dreimanis, 1989) and a generally massive to jointed till structure (e.g. Boulton and Paul, 1976). Deformation till was interpreted from a combination of: 1) multimodal clast fabrics indicating moderate degrees of heterogeneous deformation (e.g. Benn and Evans, 1996; Hicock *et al.* 1996);

Table 6. Site investigation summary.

Site	Interpreted Process	Sediment Structures	Fabric Modal Distribution	Till Sand %	Till Silt %	Till Clay %
DS01	two layer deformation	massive/jointed	spread bimodal	37.8	27.7	34.5
DS02	deformation	massive	multimodal	34.0	27.8	38.2
DS03	deformation	massive	multimodal	32.6	28.6	38.8
DS04	melt-out	boulder pavement/massive	spread bimodal	34.2	30.2	35.6
DS05	basal melt-out	jointed	multimodal	41.4	28.9	29.7
DS07	deformation	deformed/sinusoidal sand lenses	spread bimodal	56.4	23.4	20.2
DS08	two layer deformation	deformed/sinusoidal sand lenses	multimodal	54.2	26.2	19.6
DS09	two layer deformation	deformed/sinusoidal sand lenses	spread bimodal	41.2	27.5	31.3
DS10	deformation	deformed/sinusoidal sand lenses	multimodal	26.2	29.2	44.6
DS11	deformation	deformed/sinusoidal sand lenses	spread unimodal	40.0	27.1	32.9
DS12	lodgement/deformation	massive/jointed	spread bimodal	31.8	29.9	38.3
DS13	basal melt-out	massive/jointed	bimodal cluster	32.0	35.1	32.9
DS14	lodgement/deformation	deformed/sinusoidal sand lenses	bimodal cluster	27.4	29.0	43.6
DS16	basal melt-out	undeformed oval gravel lens	spread unimodal	30.4	30.3	39.3
DS18	lodgement	massive	bimodal cluster	40.0	32.9	27.1

2) two layer deformation structure (e.g. Boulton and Hindmarsh, 1987; Menzies, 1989); 3) the presence of significantly attenuated or highly deformed sand bodies within the till (e.g. Hart, 1994; Benn and Evans, 1996), and 4) the presence of preserved soft sediment clasts (e.g. Dreimanis, 1989).

The presence of both lodgement and deformation till within the bed of the Lac La Biche ice stream is not unique. Benn (1994b) describes fluted till in Norway formed by a combination of lodgement and subsole deformation. Lodgement processes (dragging and plowing) were found to be dominant for the larger than >1 cm diameter clasts while the smaller material was more susceptible to heterogeneous ductile deformation (Benn, 1994b). Hart (1994) suggests that both sediment deforming and lodgement processes will probably both have occurred in any sequence of basal till.

The relative contribution of sediment deformation (represented by deformation till) and basal sliding (represented by lodgement till) to the total amount of ice stream movement is unknown. The lack of strong parallel clast fabrics in the majority of sections suggests that lodgement processes may have only played a minor role in the deposition of the basal tills observed along the path of the Lac La Biche ice stream. A two layer deforming sediment structure has been identified at three of the eleven sites interpreted to have been overrun by active ice. Significant heterogeneous till deformation was interpreted at five sites, while three are interpreted to have been deposited predominantly by lodgement processes beneath sliding ice.

The widespread distribution and abundance of deformed sand lenses within the basal till suggests that glacial flow by pervasive sediment deformation may have been the exception and not the rule. Although showing signs of heterogeneous ductile deformation, the majority of the sand lenses have not been attenuated into thin streaks by extensive shear strain. This implies that the magnitude of strain associated with deforming till may be generally less than expected if it was assumed that sediment

deformation was responsible for the majority of ice stream movement. It is more likely that pervasive sediment deformation similar to that observed by Boulton and Hindmarsh (1987) was a transitory process restricted to localized areas of the bed. The dominant basal flow process is therefore assumed to be sliding which was associated with a limited degree of heterogeneous ductile sediment deformation similar to that proposed by Iverson *et al.* (1995).

The tills uncovered along the path of the Lac La Biche ice stream showed a great tendency to be fractured or jointed with a generally blocky structure to the base of the exposure. Joints are commonly found in overconsolidated sediment (Terzaghi, 1936; Boulton and Paul, 1976). Joints in tills originate as a result of unloading, or shrinkage due to drying out, of contraction due to freezing, and of failure during shear (Boulton, 1976a; Boulton and Paul, 1976). The horizontal fractures may also represent shear fractures as a result of advancing glacial ice, but the lack of slickenslides or displacement in other than obvious thrust zones in tills makes this questionable (Grisak *et al.* 1976). Vertical fracture sets may be accounted for by several mechanisms, including; 1) regional extension of the earth's crust due to isostatic rebound, 2) shearing in response to over-riding ice, or 3) tension fracturing as a result of vertical stress release from the unloading of glacial ice. The fracturing may have been assisted by volume changes due to desiccation during dry postglacial periods or by geochemical processes such as ion exchange or osmosis occurring during groundwater circulation (Grisak *et al.* 1976).

The till at all sections is clast poor (estimated 1-5% clasts larger than 1 cm), however matrix grainsize distributions are seen to vary significantly between some sections (Table 6). Variation in till matrix grainsize distribution is likely the result of changes in subglacial hydrologic characteristics and variations in sub-bed lithology along the path of the ice stream. Horizontal Darcian flow through deforming sediment beds can result in the removal of clay particles from the deforming matrix (Murray and

Dowdeswell, 1992). However, the observed changes in till clay content between sites does not appear to correlate well where pervasive sediment deformation has been interpreted. Although, in all cases, samples for grainsize analysis were collected from below units interpreted to have been pervasively deformed ("A" horizons at DS01, DS08 and DS09).

Boulder-size clasts are rare, although when observed, are usually present as lags or cluster bedforms at the contact between lithologic units (e.g. DS04, DS09). Stone clusters are also formed within pervasively deforming till by alteration of previously lodged pavements and by clast settling upon release from basal ice according to the specific gravity of individual stones (Hicock, 1991). Boulton and Paul (1976) suggest that during basal transport by sliding, large boulders may plough so deeply into the till that ice must flow around it and the boulder becomes a nucleation point for other stones that collect behind it as a stone cluster.

The lack of stria on the boulders observed at DS09 and DS04 limits the interpretation of the processes responsible for their deposition. However, the stone pavement observed at DS09 may have been the product of deformation settling as it is found at the base of what is interpreted as a deforming "A" horizon. The stone accumulation observed at the upper till contact at DS04 is interpreted to have been formed as an erosional lag due to the boulders prominent position on the buried till surface.

7.4.1 Sand lenses

Mougeot (1991) describes "sand stringers" within the till making up the flutes along the path of the Lac La Biche ice stream as:

"consisting of very fine-grained to medium-grained, moderately to well-sorted massive sands. The stringers are found in elongate, stringy bodies and seem to have been stretched, smudged and squeezed. Their thickness varies between 0.5 and 3 cm and their length between 10 and 45 cm. Boudinage and mixing at the contact of the diamicton are common and very common at the ends of the sand bodies" (Mougeot, 1991).

This description is very similar to the lenses of sorted sand observed at DS07, DS08, DS09, DS10, DS11 and DS14 (Figure 26). Mougeot (1991) interprets the sand stringers as the product of fluvial channelization at the ice/bed interface.

The presence of deformed sand lenses at the six location mentioned above is the primary evidence for widespread nonpervasive sediment deformation beneath the Lac La Biche ice stream. It is possible however, that the presence of the deformed channels may indicate that the rate of channel creation simply exceeded the rate of channel destruction within a pervasively deforming bed. It is suspected however, that if this were the case, a greater graduation in the degree of individual lens deformation would have been observed.

Similar sand bodies were described within lodgement till by Eyles *et al.* (1982) and Brown *et al.* (1987). In each case the sand lenses were interpreted to have been deposited by high pressure sub-glacial cut and fill fluvial channelization similar to the basal drainage morphology described as Walder-Fowler canals by Walder and Fowler (1994). Hence, the meltwater drainage pathways along the ice/bed interface must have occurred as a distributed network of interconnected water layers covering a significant portion of the bed under the Lac La Biche ice stream.

The widespread distribution and remarkable consistency in lens shape, size, texture, degree of sorting and maturity of the sand implies that the physical conditions responsible for their deposition and irregular deformation were also widespread at the

base of the streaming glacier. Boulton and Dobbie (1993) note that channels will develop at the glacier-bed interface where the capacity for horizontal and vertical intergranular drainage is exceeded by the basal melting rate (Figure 19, D). Therefore, the presence of sorted sediment bodies within the basal till indicate that the bed acted to restrict the vertical and horizontal intergranular meltwater drainage pathways. Considering the extensive coverage of the ice stream, restricted vertical and horizontal drainage through the bed must have produced significantly high basal pore water pressures resulting in low effective basal pressures.

Sorted sand lenses were observed within the DS14 exposure where as no lenses were apparent at DS03 (4 m away). As the presence of sorted sediments is seen to vary over short distances within the till, other exposures which showed no sorted sediments may not typify the general character of the till in the area. The uneven distribution of sorted sand lenses within the exposed till relates to the heterogeneous character of the sub-ice stream drainage system and/or any local sediment deformation processes which may have acted to preferentially remold or homogenize portions of the basal till.

Chapter Eight

Preconsolidation Test Results

8.1 Introduction

This chapter will present the calculated preconsolidation values obtained from consolidation tests carried out on block and Shelby tube samples. Raw consolidation test data are presented in Appendix 1, and 2. Plots showing the application of the Casagrande method (1936) to consolidation curves are presented in Appendix 3. A summary of all calculated preconsolidation values is provided on Table 7.

8.2 Unsuccessful Consolidation Tests

Unsuccessful consolidation tests resulted from several factors. The consolidation curves for DS01 (Appendix 3) failed to show a distinct separation between the upper curved portion and the lower straight virgin compression line, as is required for the application of the Casagrande Method. Bowles (1992) suggests that sample disturbance can result in the "flattening" of consolidation curves. It is likely that the consolidation curves for DS01 resulted from unacceptable levels of sample disturbance associated with the Shelby tube sampling method. Laboratory core extraction and cutting of the individual subsamples from the core likely added to the sample disturbance. However, consolidation testing of the other samples collected by the Shelby tube method (DS02 and DS03) produced adequate consolidation curves typical of undisturbed samples.

Consolidation tests could not be completed for subsamples DS16 #9 and DS18

Table 7. Preconsolidation test summary data

Sample Site	Preconsolidation Value (kPa)				Mean Site Value	Intra-site Standard Deviation
	Sub-Sample				(kPa)	(kPa)
	#7	#8	#9	Re-test		
DS01	-	-	-		-	-
DS02	211	248	244		234	20.3
DS03	129	150	135		138	10.8
DS04	267	267	247		260	11.5
DS05	163	147	154		155	8.0
DS07	200	222	234		219	17.2
DS08	samples not obtained				n/a	n/a
DS09	-	-	260		260	-
DS10	222	253	190		222	31.5
DS11	samples not obtained				n/a	n/a
DS12	682*	150	119	143	137	16.3
DS13	195	163	176		178	16.1
DS14	180	205	150		178	27.5
DS16	228	176	-		202	36.8
DS18	-	308	228		268	56.6

Min. site value	137 kPa
Max. site value	268 kPa
Mean of all site values	204 kPa
Mean of actively deposited sites	201 kPa
Standard Deviation (site values)	47.16 kPa

* this preconsolidation value is not used in the calculation of the site preconsolidation value for DS12.

#7 because relatively large clasts (~1 cm diameter) hidden within the samples prevented consolidation early in the load increment sequence. Subsamples for consolidation testing could not be cut from the DS08 or DS11 block samples as both were brittle and highly fractured. Only one suitable subsample was able to be cut from the DS09 block sample.

8.3 Preconsolidation Results

It was proposed in Chapter 5 that postglacial sediment disturbance resulted in an increase in the preconsolidation pressure value determined from the sampled sediments. Therefore, as a proxy for the subglacial effective basal pressure of the Lac La Biche ice stream, preconsolidation values presented in Table 7 represent maximum values. Additionally, postglacial affects such as freeze-thaw, desiccation and carbonate translocation were surely not uniform throughout the field area, resulting in reduced potential for intersite comparison.

Mean site preconsolidation values were calculated from successful individual sub-sample results. The general low variability in intrasite subsample preconsolidation values suggests that the calculated mean preconsolidation value for each site represents a true physical characteristic of the till (Table 7, Figure 32, A). The variation in intersite preconsolidation values indicates differential site consolidation and/or postglacial alteration histories.

Of the 15 sites excavated and described, preconsolidation values were obtained from only 12 sites. Of the 12 site preconsolidation values, eight came from sites interpreted as basally deposited by active Lac La Biche ice (DS02, DS03, DS07, DS09, DS10, DS12, DS14, and DS18), and four from sites interpreted as deposited from stagnant Lac La Biche ice (DS04, DS05, DS13, DS16). The mean of all site

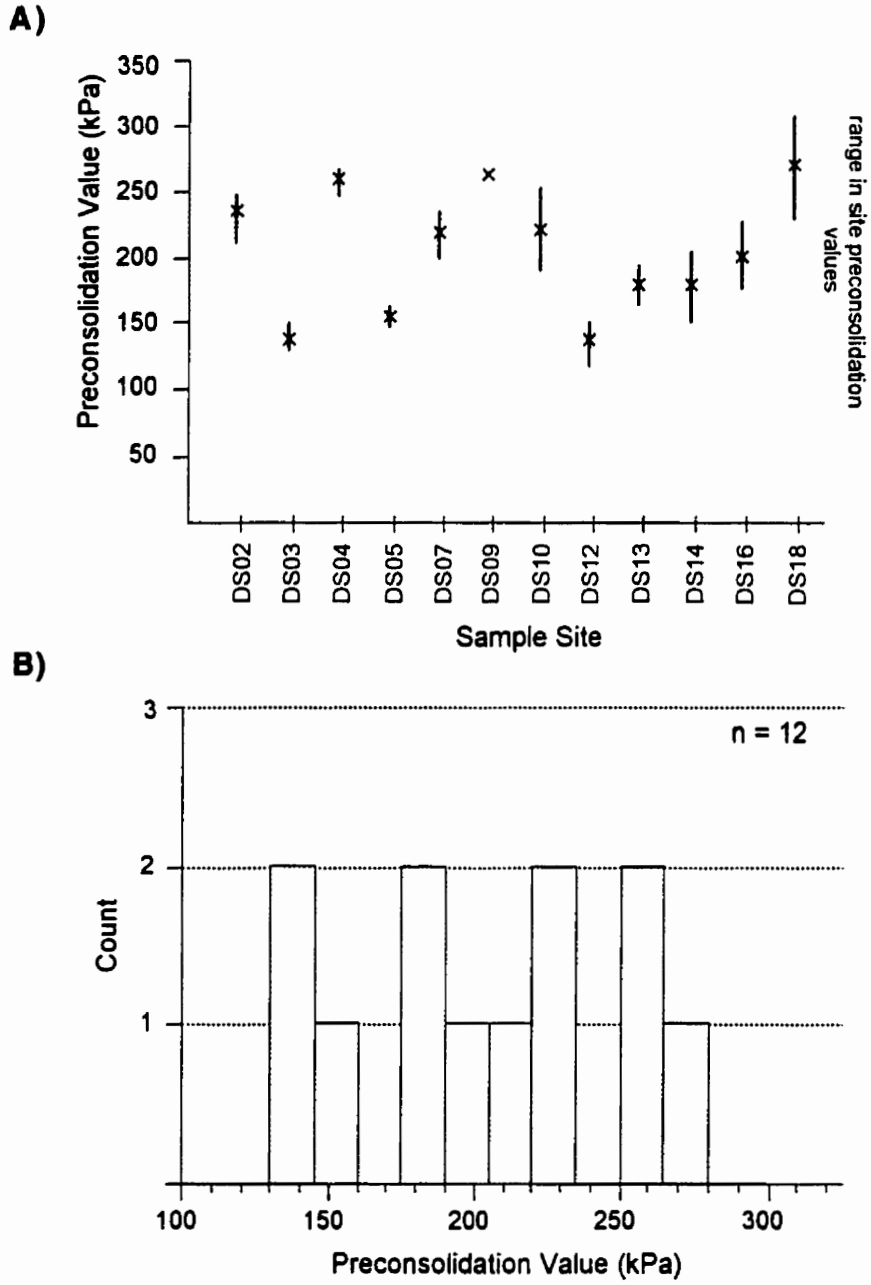

Figure 32. A) Mean site preconsolidation values and range of values obtained from sub-sample consolidation tests for each sample site. X marks mean value within range of preconsolidation values calculated for that site (line). Clear differences in intersite preconsolidation values can be easily recognized. Shaded area covers 131 kPa range in site preconsolidation values. B) Histogram showing the even frequency of occurrence of site preconsolidation values.

preconsolidation values is 204 kPa, while the mean preconsolidation value from actively deposited till is 201 kPa.

Preconsolidation values from all 12 sites ranged from a maximum of 268 kPa at DS18 to a minimum of 137 kPa at DS12. The total range in calculated site average preconsolidation values is 131 kPa (shaded region Figure 32, A) which is equivalent to the pressure caused by a column of ice 14.7 m high. The preconsolidation values along the path of the Lac La Biche ice stream are remarkably consistent, especially considering the distance between sample sites, and the variation in stratigraphy, depositional environment, deformation and postglacial histories. Figure 32 (B) shows the uniform frequency of occurrence of site preconsolidation values between 137 and 268 kPa. Figure 33 shows the distribution of site preconsolidation values along the path of the Lac La Biche ice stream within Alberta.

Samples DS03 and DS14 were collected from pits located 4 m apart on the crest of a high relief drumlinoid landform. The samples were collected using two different sampling techniques (Shelby tube at DS03 and block sampling at DS14) from similar depths (2.05 and 1.95 m respectively). These samples were collected to test the consistency of preconsolidation values within a small area.

The subsample preconsolidation values for DS03 and DS14 are consistent (Figure 32, A; and Table 7), with intra-site standard deviations of 10.8 and 27.5 kPa respectively. Their consolidation curves show distinct "breaks" above the virgin compression line (Appendix III) suggesting sample disturbance did not occur during sample collection. These findings suggest that the sampling methods each provide consistent, accurate results and therefore the preconsolidation data from different methods are directly comparable. DS03 had a site preconsolidation value of 138 kPa, while 4 m away, the DS14 site preconsolidation value was 178 kPa. This unexpected

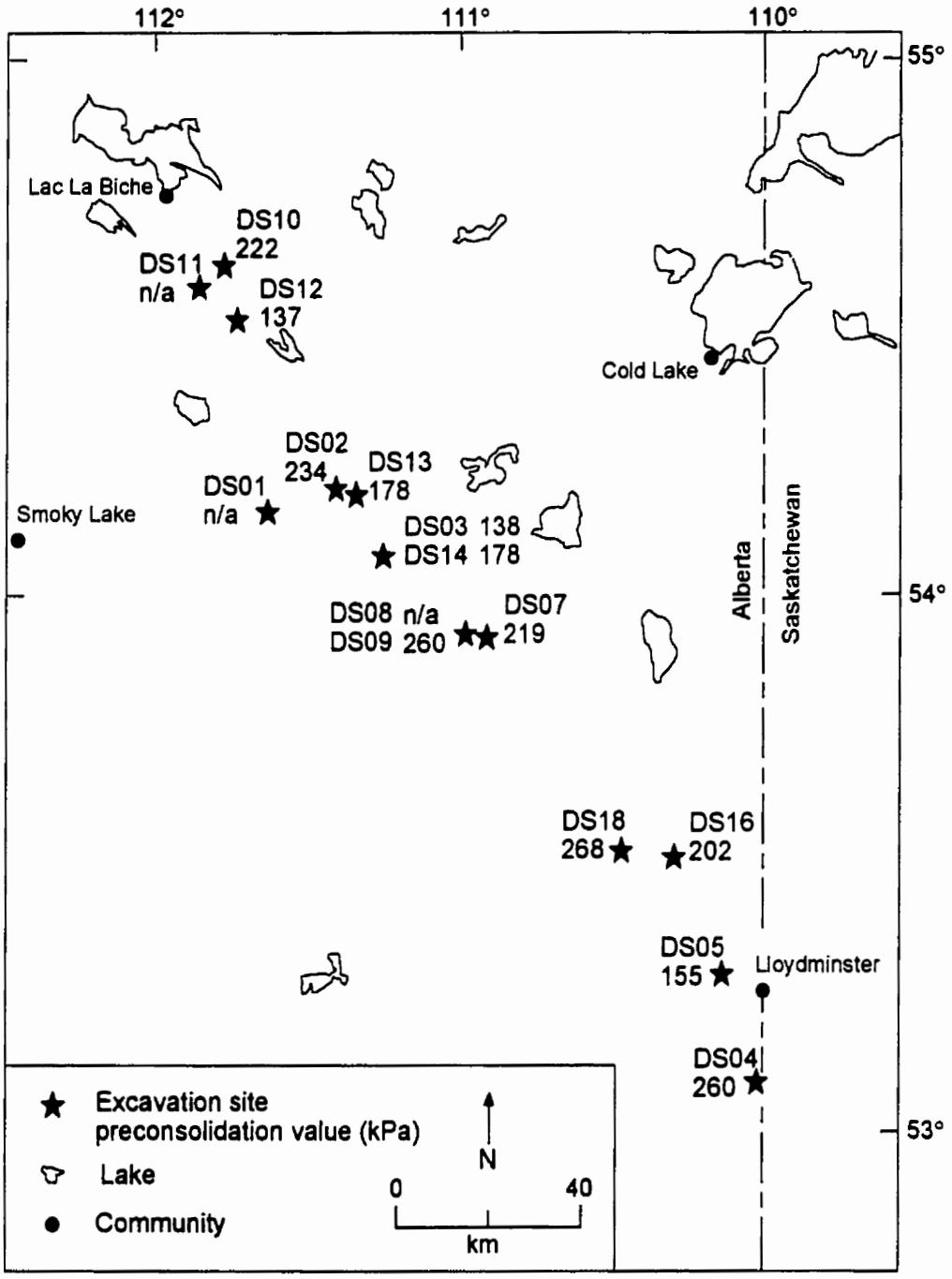

Figure 33. Distribution of site preconsolidation values. The lack of a visible trend in the preconsolidation values suggests the presence of moderating subglacial pore water pressure during till consolidation. Site preconsolidation values may have also been influenced by heterogeneous postglacial sediment alteration. Data unavailable for DS01, DS08 and DS11.

result suggests a natural variation in the till preconsolidation values over distances of at least 4 meters.

Figure 34 compares site preconsolidation values with the mode of till deposition and the presence of sand lenses (indicating subglacial fluvial channelization). There is no relationship between the mode of till deposition and the preconsolidation values for each site as the melt-out, lodgement and deformation process preconsolidation values strongly overlap (Figure 34; A). The preconsolidation values suggest that all till depositional processes took place in a low effective pressure environment. Preconsolidation values also overlap between sites grouped according to the presence of sand lenses within actively deposited till (Figure 34; B). This suggests that there is no detectable correlative relationship between the presence or absence of subglacial fluvial channelization and subglacial effective basal pressure.

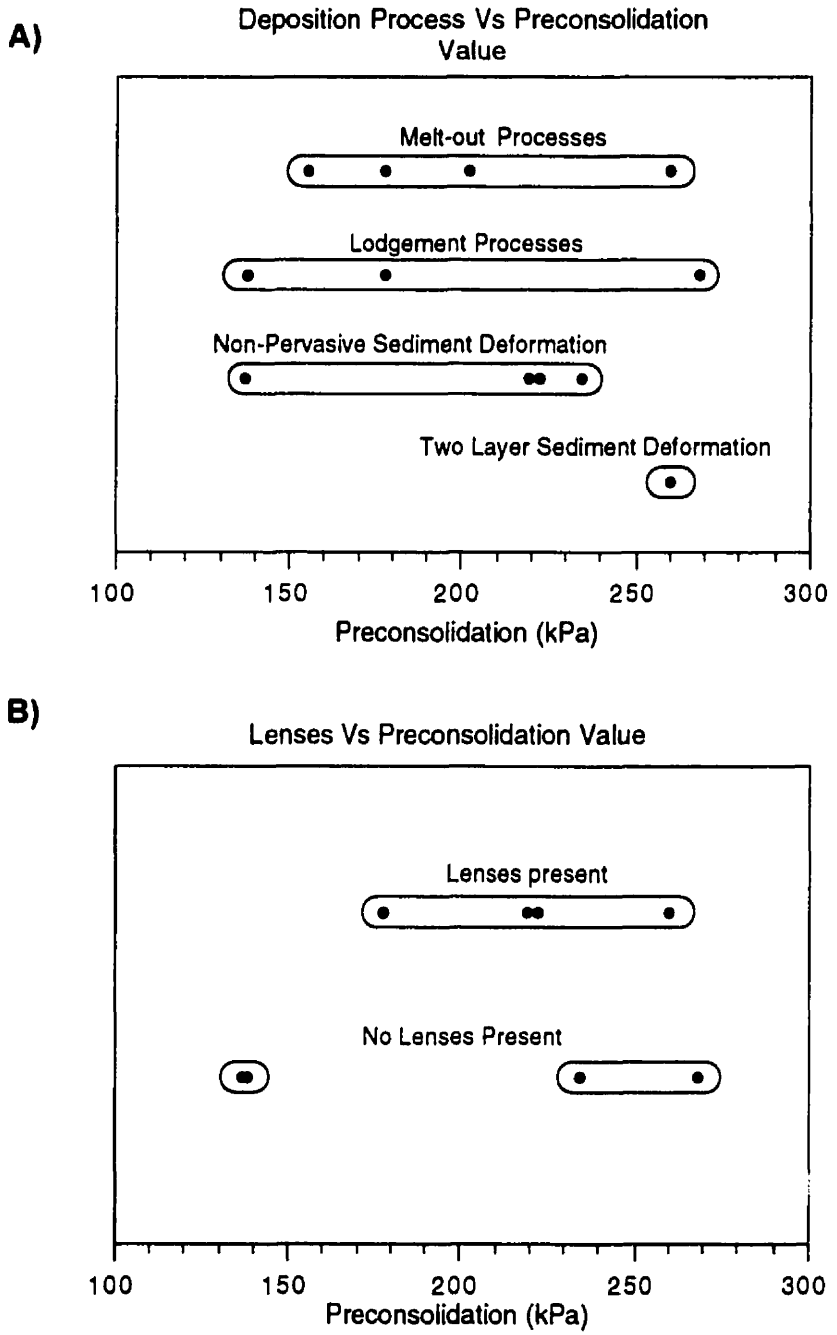

Figure 34. Range of preconsolidation values associated with: (A) interpreted till depositional processes, and (B) the presence or absence of sand lenses within till deposited by active ice. It is noted that neither the interpreted till depositional process nor the presence of subglacial channelization are associated with characteristic till preconsolidation values.

Chapter Nine

Discussion of Preconsolidation Data

9.1 Discussion

Ideally, preconsolidation values derived from glacially overridden fine-grained sediments represent the maximum effective basal pressure (Boulton and Dobbie, 1993; Sauer and Christiansen, 1991; Brown *et al.* 1987). On their own, the preconsolidation values represent proxy effective pressure data for the Lac La Biche ice stream. However, as both p_i and p_w are unknown for the Lac La Biche ice stream, only through investigation of the possible causes of variation in effective pressure (p') along the bed, are the preconsolidation values able to be adequately interpreted to infer subglacial hydrologic conditions. Variation in site preconsolidation values may relate to the physical characteristics of the site, including: 1) sub-bed stratigraphy, 2) till coefficient of permeability and/or 3) presence of basal channels.

The possibility also exists that postglacial pedogenic processes were responsible for the observed variation in calculated preconsolidation values along the bed of the Lac La Biche ice stream. The qualitative observations discussed in Chapter 5 proposed that the sedimentary structure of the till had been altered by pedogenic processes although the effective basal pressure signals imposed by the Lac La Biche ice stream were generally intact. The overall effect was interpreted to have been an increased overconsolidation of the till beyond the stress imposed by the overriding ice. This implies that the effective basal pressure for the Lac La Biche ice stream was somewhat less than the preconsolidation pressures measured in the samples of basal till.

Therefore, it is clear that the measured preconsolidation values indicate that low effective basal pressures dominated the Lac La Biche ice stream.

The degree of postglacial alteration is unknown and it is likely that its effect was nonuniform throughout the field area. This realization limits the potential for intersite comparison of preconsolidation values. However, as no other method of inferring subglacial hydrological characteristics is applicable considering the available data, the effect of postglacial pedogenic alteration will be assumed to have been negligible.

Several options must be considered as a means of exploring the validity of the site preconsolidation values as representing a proxy of subglacial hydrologic conditions. The simplest case would involve the interpretation of preconsolidation values as the result of consolidation by ice without the effects of basal water pressure. This would imply a perfectly drained basal water system where effective basal pressure equals the weight of the overlying ice. If this were the case, a gradual increase in preconsolidation values along the path of the glacier towards the northwest would have occurred as the ice thickened towards its source area. This is surely not the case as can be seen in the distribution of site preconsolidation values (Figure 33). Also, the measured preconsolidation values of 137 kPa to 268 kPa would represent ice thicknesses of only 15 m to 30 m, which are well below the ice thickness required for a glacier to flow when driven by the gravitational driving stresses associated with low-relief terrain[1]. Therefore water pressure must have played a role in maintaining low effective basal pressures under the Lac La Biche ice stream. This observation supports the interpretation made in Chapter 7 that high basal pore water pressures at the ice/bed interface resulted in hydraulic jacking supported basal sliding as the dominant mode of ice stream movement.

---

[1]Calculated from shear stress equation ($\tau=\rho g h \sin\alpha$) and Glen's flow law ($e=A\tau^n$) where: τ is shear stress, ρ is the density of ice, g is acceleration due to gravity, h is the thickness of the glacier, α is the slope of the upper surface of the glacier, e is strain rate, A is a constant related to the temperature of the ice, and n is an exponent with a mean value of 3 (Sugden and John, 1991).

The next issue is to determine if the dominant basal meltwater pathway was through channelized flow at the ice/bed interface, horizontally within the till by Darcian flow, or was draining vertically through the till into underlying aquifers.

A simple test proposed by Boulton and Dobbie (1993) predicts higher basal effective pressures overlying regions where a significant proportion of the basal meltwater flux drains vertically into underlying aquifers (Figure 19, A), or horizontally through the bed to be discharged at the margin (Figure 19, C). For a given basal melting rate, effective basal pressure at the glacier's sole is related to the coefficient of permeability of the basal till, till thickness and the hydraulic pressure in the underlying aquifer (Boulton and Dobbie, 1993). Each of these factors must be considered so that the site preconsolidation values can be directly compared to the underlying stratigraphy for the purpose of understanding the dominant meltwater drainage pathway.

Typical values for basal ice melting due to geothermal heating average 6 mm/yr (Paterson, 1994), while heat produced by glacial movement at the bed can melt from 6-60 mm of basal ice annually depending on the rate of glacial flow (Sugden and John, 1984). For the purposes of this investigation, basal meltwater production is assumed to have been nearly uniform over the length of the Lac La Biche ice stream. This assumption is almost certainly not correct for the short term due to local variation in the process and rate of ice stream flow and changes in the basal topography along the bed. However, due to the apparent transient nature of the basal processes interpreted in Chapter 7, this assumption is likely valid over a longer term and will therefore be used.

The coefficient of permeability was calculated for the till at each sample site from consolidation test results at a confining pressure of 148 kPa (similar to the estimated maximum effective basal pressure for the Lac La Biche ice stream). Coefficient of permeability values range from a low of 5.41×10^{-10} m/s at DS02 to a high

of 3.87 x 10^{-9} m/s at DS14 with an average for all sites of 1.67 x 10^{-9} m/s (Table 8). Thus, for all sites the coefficient of till permeability varies over one order of magnitude. Considering the inaccuracy of the method employed to derive coefficient of permeability values (Chapter 3), and the presumed natural variability in the permeability of till, it will be assumed that the coefficient of permeability is uniform for all tills underlying the Lac La Biche ice stream.

Boulton and Dobbie (1993) note that glacier beds with a coefficient of permeability of less than 10^{-8} to 10^{-10} m/s require potential hydraulic gradients in excess of 10 kPa/m (gravitational gradient) to discharge basal meltwater. The mean coefficient of permeability of the bed of the Lac La Biche ice stream falls within this range. Therefore, the pressure gradient required to discharge the basal meltwater is unknown for the Lac La Biche ice stream. The 10^{-9} m/s coefficient of permeability value for the bed of the Lac La Biche ice stream limits the interpretation of the bed as "relatively high permeability" or "low permeability" according to the Boulton and Dobbie (1993) model (Figure 19, A-D), as this coefficient of permeability falls within the unclassified range of 10^{-8} to 10^{-10} m/s. Therefore, it is assumed that none of the four Boulton and Dobbie (1993) process scenarios can be excluded as representing subglacial processes associated with the Lac La Biche ice stream.

The hydraulic pressure at the top of any underlying aquifer cannot be estimated with the data available, however two scenarios will be considered. The first scenario is that underlying aquifers existed at a lower hydraulic pressure than the bed of the glacier, allowing sub-bed aquifers to be utilized as a basal meltwater pathway. This implies that the aquifers are capable of discharging accumulated meltwater, either beyond the margin

Sample Site	Coefficient of Permeability (m/s)
DS01	-
DS02	5.41×10^{-10}
DS03	1.76×10^{-9}
DS04	9.99×10^{-10}
DS05	1.31×10^{-9}
DS07	6.28×10^{-10}
DS08	-
DS09	1.18×10^{-9}
DS10	1.66×10^{-9}
DS11	-
DS12	1.47×10^{-9}
DS13	1.67×10^{-9}
DS14	3.87×10^{-9}
DS16	2.16×10^{-9}
DS18	2.77×10^{-9}
Average value	1.67×10^{-9}

Table 8. Till coefficient of permeability for each sample site. Coefficient of permeability was calculated from consolidation data at 148 kPa confining pressure. The above data reveals the near uniform permeability of the bed of the Lac La Biche ice stream, thereby excluding this variable as a possible explanation for the variation in measured till preconsolidation values.

of the glacier, or deeper into underlying bedrock, or some other low potential aquifer. The second scenario assumes that aquifers are limited in extent or are bounded by aquitards and unable to discharge meltwater inputs. Aquifers in the second scenario would soon pressurize, further restricting vertical Darcian flow from the glaciers bed.

As a test of the above scenarios, a strong negative correlation between the measured basal till preconsolidation pressure and till thickness overlying an aquifer would indicate that the dominant basal meltwater flow pathway was vertical into underlying aquifers as proposed by Boulton *et al.* (1995). A plot of till thickness versus preconsolidation value (Figure 35) shows no such relationship. The apparent lack of any correlation between effective basal pressure and till thickness may indicate: 1) The bed of the ice stream acted as a barrier to vertical flow of basal meltwater into underlying aquifers which may have been at lower hydraulic pressure. This would have resulted in the development of extremely high vertical pressure gradients and low effective basal pressures at the ice-bed interface. 2) Flow through the till bed was limited by the pressurization of underlying aquifers. This would have resulted in the development of low, or even negative vertical pressure gradients, and low effective basal pressures at the ice-bed interface.

The consistent, low preconsolidation values obtained from the bed of the Lac La Biche ice stream are compatible with both of the above sub-basal hydrology scenarios. Therefore this test does not help to resolve the subglacial hydrology characteristics for the Lac La Biche ice stream. It is possible to state however, that vertical groundwater drainage into underlying aquifers was not the dominant control in the maintenance of local effective basal pressures for the Lac La Biche ice stream. This effectively excludes the "Relatively High Permeability" glacial bed models (Figure 19, A and C) as describing the bed of the Lac La Biche ice stream.

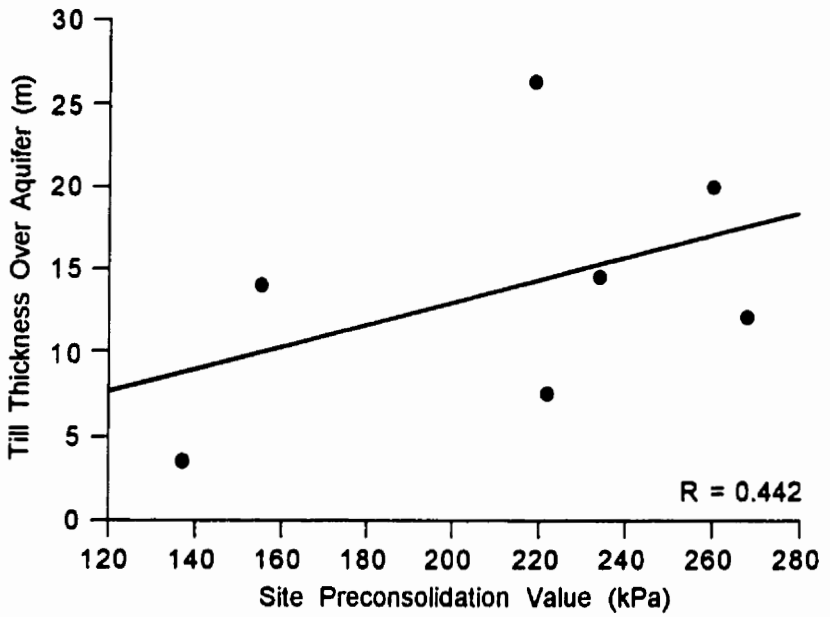

Figure 35. Plot of till thickness versus site preconsolidation value. Only sites interpreted to have been deposited by active ice have been included. Sites where aquifers do not exist below the ice stream bed have not been included in the above plot, these include DS03 (138 kPa) and DS14 (178 kPa) (Appendix 5). The poor correlation suggests that the vertical drainage pathway for basal meltwater was not significant in effecting local maximum effective basal pressures.

The geology and geologic history of the study area suggests pressurization of underlying sand and gravel aquifers was likely. As the ice stream is interpreted to have occurred as a late glacial resurgence during a time of general glacial retreat (Andriashek, 1985; Mougeot, 1991), the underlying aquifers may have been saturated and pressurized by basal meltwater derived from Laurentide ice earlier in the Late Wisconsin glaciation. The frequent occurrence of glaciotectonically displaced till and bedrock units along the path of the Lac La Biche ice stream (Andriashek, 1985; Mougeot, 1991) suggests that the disruption and segregation of previously continuous sand and gravel units was likely. This stratigraphic disruption could inhibit horizontal flow within the aquifers, allowing them to become more easily pressurized by basal meltwater.

The presence of a distributed channelized subglacial drainage network across the bed of the Lac La Biche ice stream was confirmed in Chapter 7. Boulton and Dobbie (1993) propose that the existence of channelized drainage at the ice/bed interface indicates that the ability of the substratum to transmit the basal meltwater flux has been exceeded. Hence, the presence of subglacial channels suggests that both the vertical and horizontal Darcian meltwater fluxes were inhibited by low till permeability at the glacier's bed.

Preconsolidation results, the presence of an extensive channelized basal drainage system, and the interpretation of sediment deformation at the bed suggest that Lac La Biche ice stream basal processes were the result of a low permeability bed and poor sub-bed drainage conditions similar to the model proposed by Boulton and Dobbie (1993) (Figure 19, D). However, the presence of two layer sediment deformation at several of the excavated sites (DS01, DS08, DS09) indicates that at these three locations, vertical drainage may have had more of an effect on effective basal pressure and the mode of sediment deformation (Figure 19, B).

This hypothesis cannot be tested directly because preconsolidation values were not obtained from the DS01 and DS08 sites. However, the presence of relatively shallow units of sand and gravel at DS01 (11 m below the surface, Appendix 5), and the lack of sand lenses in the DS01 exposure suggests that at this location, vertical sub-bed drainage may have had an effect on basal processes and therefore the mode of ice stream flow. Also supporting this hypothesis, the one preconsolidation value obtained from DS09 (260 kPa), is the second highest of all preconsolidation values. This value suggests that slightly lower than average basal pore water pressures may have existed at this site beneath the Lac La Biche ice stream. Evidence of channelized drainage within the "B horizons" at both DS08 and DS09 suggests a variable subglacial environment where excess basal meltwater was present for some time.

It seems likely that subglacial water pressures will fall near the ice margin as drainage paths become shorter. In this case, the observed uniform preconsolidation signature is likely to have been imposed during deglaciation, which may help to explain the high consistency of measured preconsolidation values along the bed of the ice stream. However, this scenario would still require low effective basal pressures away from the margin prior to glacial retreat. Therefore, the interpretation that the measured preconsolidation values represent a high end bounding value for maximum effective basal pressure for the Lac La Biche ice stream would still be valid.

The interpretation of the Lac La Biche Lobe as a streaming glacier is based on the interpretations of Gravenor and Meneley (1958), Ellwood (1961), Andriashek (1985) and Mougeot (1991). Although not part of the thesis objectives, the low measured preconsolidation values do support this interpretation.

The preconsolidation values in this thesis are comparable to effective basal pressures for the Antarctic Ice Stream B. Alley *et al.* (1986) determined the mean

effective pressure beneath ice stream B as 50 ± 40 kPa. Engelhardt *et al.* (1990) calculated a net effective basal pressure of 30 kPa to 160 kPa for a similar location under ice stream B. The mean preconsolidation value determined from till collected at the now exposed bed of the Lac La Biche ice stream is 201 kPa (Table 7). However, as a proxy for effective basal pressure, 201 kPa represents a maximum value due to the assumed net consolidating affect of pedogenic till disturbance since deglaciation (Chapter 5).

Sauer *et al.* (1991) published 119 preconsolidation values obtained from borehole samples of the Quaternary Sutherland and Saskatoon Groups from south and central Saskatchewan (see Table 1). They determined that subglacial consolidation by active, late Wisconsin Laurentide ice resulted in till preconsolidation values ranging from 1500 kPa to 2200 kPa to be imparted upon these buried sediments. Overlying these sediments, till deposited from stagnant Laurentide ice in the Battleford Formation was found to be only moderately overconsolidated with preconsolidation pressures of 370-480 kPa. Similarly, Jenson (1993) calculated a maximum effective basal pressure of 1200 kPa for the Lake Michigan Lobe from preconsolidation values measured in an overridden clay. Brown *et al.* (1987) estimated a maximum effective basal pressure of These data contrast significantly with the preconsolidation values presented in this thesis. This may reflect a difference in subglacial hydrologic characteristics between streaming and non-streaming Laurentide ice, and supports the interpretation of Gravenor and Meneley (1958), Ellwood (1961), Andriashek (1985) and Mougeot (1991).

Chapter Ten

Conclusion

The first objective of this thesis was to address the following question;

1) *How did postglacial pedogenic processes affect the calculated preconsolidation value of sampled sediments?*

Through qualitative evaluation of the structural effects of various postglacial processes on the sediment structure, it is proposed that the processes which acted on the samples collected resulted in only minor disturbances to the sediment structure. In general, these processes have not significantly altered the proxy effective pressure signal imparted on them by the overriding Lac La Biche ice stream. However, it has also been proposed that postglacial sediment disturbance resulted in a decreased sediment void ratio through time. This reduction in void ratio likely resulted in an apparent increase in the calculated preconsolidation pressure for the glacially overrun sediments. This implies that the preconsolidation values obtained represent maximum values. It is also noted that these effects were surely not uniform throughout the field area, resulting in a reduced potential for intersite comparison of calculated preconsolidation values.

The second objective of this thesis was to address the following question;

2) *What does the geology of the now exposed bed of the Lac La Biche ice stream indicate about the characteristics of the subglacial drainage system and the mode of ice stream flow?*

It has been shown that the dominant flow processes for the Lac La Biche ice stream was sliding at the ice/bed interface, which was associated with a limited degree of heterogeneous ductile sediment deformation similar to the observations of Iverson *et al.* (1995) and Jansson (1995). Pervasive sediment deformation associated with a two layer deformation process, similar to that observed by Boulton and Hindmarsh (1987), was responsible for at least part of the motion of the ice stream at some locations (DS01, DS08 and DS09). The limited number of sites where pervasive sediment deformation was recognized suggests that this was a transitory process restricted to localized areas of the bed.

The interpretation of a widespread, distributed, high pressure channel system at the ice/bed interface (Walder-Fowler canals) suggests that the Lac La Biche ice stream was wet-based and that the till bed acted to restrict basal meltwater drainage to underlying aquifers.

The third and fourth objectives were to address the following questions;

3) *What was the likely maximum effective basal pressure for the Lac La Biche ice stream, and how did it change along the path of the glacier within Alberta?*

4) *Did the presence of buried preglacial valleys containing thick sequences of sand and gravel (as well as sequences of glacial diamicton) act to preferentially drain portions of the Lac La Biche ice stream?*

The preconsolidation values suggest that all till depositional processes took place in a low effective pressure environment. It has been shown that the maximum effective basal pressure for the Lac La Biche ice stream ranged from 137 kPa to 268 kPa.

The mean preconsolidation value for all sites interpreted to have been deposited and/or overrun by active ice is 201 kPa. However, as these values represent maximum values, the actual average maximum effective basal pressures would have been less. The natural variation in till preconsolidation values is seen to vary over distances as short as 4 m. However, the low overall range in site preconsolidation values suggests that the subglacial effective pressures were similar for all portions of the bed of the ice stream.

There is no apparent correlation between the thickness of the till overlying sub-bed aquifers and the measured preconsolidation value. This implies that the vertical groundwater drainage pathway was not the dominant control in the maintenance of local effective basal pressures as has been suggested by Boulton *et al.* (1995) and Boulton and Dobbie (1993). The low coefficient of permeability of the bed of the Lac La Biche ice stream acted to restrict both vertical and horizontal sub-bed drainage. This result is in agreement with the geologic interpretation of an extensive subglacial fluvial drainage network at the ice bed interface. There is no detectable correlative relationship between the presence or absence of subglacial fluvial channelization and subglacial effective basal pressure.

References

Aario, R. 1971. Consolidation of Finnish Sediments by Loading Ice Sheets. Bulletin of the Geological Society of Finland, **43**, 55-65.

Acton, D.F., Fehrenbacher, J.B. 1976. Mineralogy and Topography of Glacial Tills and their Effect on Soil Formation in Saskatchewan. *In* Glacial Till an Inter-disciplinary Study. *Edited by* Legget, R.F. The Royal Society of Canada Special Publications No. 12. 170-185.

Alley, R.B. 1991. Deforming-bed origin for southern Laurentide till sheets? Journal of Glaciology, **37**, 67-76.

Alley, R.B. 1992. How can low-pressure channels and deforming tills coexist subglacially? Journal of Glaciology, **38**, 200-207.

Alley, R.B., Blankenship, D.D., Bentley, C.R., Rooney, S.T. 1986. Deformation till beneath ice stream B, West Antarctica. Nature, **322**, 57-59.

Alley, R.B., Blankenship, D.D., Bentley, C.R., Rooney, S.T 1987a. Till beneath Ice Stream B. 3. Till deformation: Evidence and Implications. Journal of Geophysical Research, **92**, 8921-8929.

Alley, R.B., Blankenship, D.D., Rooney, S.T., and Bentley, C.R. 1987b. Till beneath Ice Stream B: A coupled ice-till flow model. Journal of Geophysical Research, **92**, 8931-8940.

ASTM, 1964. Procedure for Testing Soils. American Society for Testing Materials, Philadelphia.

Andriashek, L.D. 1985. Quaternary Stratigraphy of the Sand River Area, NTS 73L. M.Sc. Thesis, University of Alberta.

Andriashek, L.D. 1997. Evidence of Pre Late-Wisconsinan Glaciation in the Edmonton Area, East Central Alberta. CSPG-SEPM Joint Convention, June 1-6, 1997. Program with Abstracts.

Andriashek, L.D., Fenton, M.M. 1989. Quaternary stratigraphy and surficial geology of the Sand River area 73L. Terrain Sciences Department and Alberta Geological Survey, Bulletin no. 57, Alberta Research Council.

Beget, J.E. 1986. Modeling the Influence of Till Rheology on the Flow and Profile of the Lake Michigan Lobe, Southern Laurentide Ice Sheet, U.S.A. Journal of Glaciology, **32**, 235-241.

Benn, D.I. 1994a. Fabric shape and the interpretation of sedimentary fabric data. Journal of Sedimentary Research, **A64**, 910-915.

Benn, D.I. 1994b. Fluted moraine formation and till genesis below a temperate glacier: Slettmarkbreen, Jotunheimen, Norway. Sedimentology, **41**, 279-292.

Benn, D.I. 1995. Fabric signature of subglacial till deformation, Breidamerkurjökull, Iceland. Sedimentology, **42**, 735-747.

Benn, D.I., Evans, D.J.A. 1996. The interpretation and classification of subglacially deformed materials. Quaternary Science Reviews, **15**, 23-52.

Bentley, C.R. 1987. Antarctic Ice Streams: A Review. Journal of Geophysical Research, **92**, 8843-8858.

Blankenship, D.D., Bentley, C.R., Rooney, S.T., Alley, R.B. 1986. Seismic measurements reveal a saturated porous layer beneath an active Antarctic ice stream. Nature, **322**, 54-57.

Blankenship, D.D., Bentley, C.R., Rooney, S.T., Alley, R.B. 1987. Till Beneath Ice Stream B 1. Properties derived from seismic travel times. Journal of Geophysical Research, **92**, 8903-8911.

Boulton, G.S. 1976a. The Development of Geotechnical Properties in Glacial Tills. *In*: Glacial Till an Inter-disciplinary Study. *Edited by* Legget, R.F. The Royal Society of Canada Special Publications No. 12, 292-303.

Boulton, G.S. 1976b. The Genesis of Glacial Tills-A framework for Geotechnical Interpretation. *In* The Engineering Behaviour of Glacial Materials. Proceedings of the Symposium held at the University of Birmingham 21-23rd April, 1975. The Midland Soil Mechanics Foundation Engineering Society. Birmingham. 52-59.

Boulton, G.S. 1982. Subglacial processes and the development of glacial bedforms. *In* Research in glacial, glacio-fluvial and glacio-lacusterine systems *Edited by* Davidson-Arnott, R. *et al.* Proceeding on the 6th Guelph Symposium on Geomorphology 1982. Norwich, Geo Books, p. 1-31.

Boulton, G.S. 1987. A theory of drumlin formation by subglacial sediment deformation. *In* Drumlin Symposium. *Edited by* Menzies, J., Rose J. A.A. Balkema, Rotterdam, p. 25-80.

Boulton, G.S., Caban, P. 1995. Groundwater flow beneath ice sheets: Part 2 - Its Impact on Glacier Tectonic Structures and Moraine Formation. Quaternary Science Review, **14**, 563-587.

Boulton, G.S., Dobbie, K.E. 1993. Consolidation of sediments by glaciers: relations between sediment geotechnics, soft-bed glacier dynamics and subglacial ground-water flow. Journal of Glaciology, **39**, 26-44.

Boulton, G.S., Hindmarsh, C.A. 1987. Sediment deformation beneath glaciers: rheology and geological consequences. Journal of Geophysical Research, **92**, 9059-9082.

Boulton, G.S., Jones, A.S. 1979. Stability of temperate ice sheets resting on beds of deformable sediment. Journal of Glaciology, **24**, 29-43.

Boulton, G.S., Paul, M.A. 1976. The influence of genetic processes on some geotechnical properties of glacial tills. Journal of Engineering Geology, **9**, 159-194.

Boulton, G.S., Caban, P.E., Van Gissel, K. 1995. Groundwater flow beneath ice sheets: Part 1- Large Scale Patterns. Quaternary Science Review, **14**, 545-562.

Boulton, G.S., Dent, D.L., Morris, E.M. 1974. Subglacial shearing and crushing, and the role of water pressures in tills from south-east Iceland. Geografiska Annaler, **56**, 135-145.

Bowles, J.E. 1984. Physical and Geotechnical Properties of Soils. McGraw-Hill Inc., Toronto.

Bowles, J.E. 1992. Engineering Properties of Soils and their measurement. McGraw-Hill Inc., Toronto.

Boyce, J.I. and Eyles, N. 1991. Drumlins carved by deforming till streams below the Laurentide ice sheet. Geology. **19**, 787-790.

Brewer, R., Sleeman, J.R. 1969. The Arrangement of Constituents in Quaternary Soils. Soil Science, **107**, 435-441.

Brown, N.E., Hallet, B., Booth, D.B. 1987. Rapid Soft Sliding of the Puget Glacial Lobe. Journal of Geophysical Research, **92**, 8985-8997.

Casagrande, A. 1936. The determination of the Pre-consolidation load and its practical significance. *In* First International Conference on Soil Mechanics and Foundation Engineering, 60-64.

Carlson, V.A., Currie, D.V., 1975. Bedrock Topography of the Vermilion Map Area, NTS 73E, Alberta. Alberta Research Council 1:250,000 scale map.

Chang, R.K., Warkentin, B.P. 1968. Volume Change of Compacted Clay Soil Aggregates. Soil Science, **2**, 106-111.

Christiansen, E.A. 1979. The Wisconsinan deglaciation of southern Saskatchewan and adjacent areas. Canadian Journal of Earth Science, **16**, 913-938.

Christiansen, E.A. 1992. Pleistocene stratigraphy of the Saskatoon area, Saskatchewan, Canada: an update. Canadian Journal of Earth Science, **29**, 1767-1778.

Clarke, G.K. 1987. Fast Glacier Flow: Ice Streams, Surging and Tidewater Glaciers. Journal of Geophysical Research, **92**, 8835-8841.

Clayton, L., Mickelson, D.M., Attig, J.W. 1989. Evidence against pervasively deformed bed material beneath rapidly moving lobes of the southern Laurentide Ice Sheet. Sedimentary Geology, **62**, 203-208.

Crawford, C.B. 1986. State of the Art: Evaluation and Interpretation of Soil Consolidation Tests. *In* Consolidation of Soils: Testing and Evaluation, ASTM STP 892, *Edited by* Yong, R.N., Townsend, F.C. American Society for Testing and Materials, Philadelphia, 71-103.

Dowdeswell, J.A., Sharp, M.J. 1986. Characterization of pebble fabrics in modern terrestrial glacigenic sediments. Sedimentology, **33**, 699-710.

Dreimanis, A. 1976. Tills: their origin and properties. *In* Glacial Till an Inter-disciplinary Study. *Edited by* Legget, R.F. The Royal Society of Canada Special Publications No. 12, 11-49.

Dreimanis, A. 1989. Tills: their genetic terminology and classification. *In* Genetic classification of glacigenic deposits. *Edited by* R.P. Goldthwait and C.L. Matsch. A.A. Balkema, Rotterdam, 17-83.

Ellwood, R.B. 1961. Surficial Geology of the Vermilion Area, Alberta, Canada. Unpublished PhD thesis, University of Illinois.

Englehardt, H., Humphrey, N., Kamb, B., Fahnestock, M. 1990. Physical Conditions at the Base of a Fast Moving Antarctic Ice Stream. Science, **248**, 57-59.

Eyles, N., Salden, J.A., Gilroy, S. 1982. A depositional model for stratigraphic complexes and facies superimposition in lodgement till. Boreas, **11**, 317-333.

Fenton, M.M., Andriashek, L.D. 1983. Surficial Geology Sand River Area, Alberta. NTS 73L. Alberta Research Council map. 1:250,000 scale.

Fleureau, J.M., Kheirbek-Saoud, S., Soemitro, R., Taibi, S. 1993. Behavior of clayey soils on drying-wetting paths. Canadian Geotechnical Journal, **30**, 287-296.

Flint, R.F. 1971. Glacial and Quaternary Geology. John Wiley and Sons Inc. New York.

Friedman, G.M. 1959. Identification of carbonate minerals by staining methods. Journal of Sedimentary Petrology, **29**, 87-97.

Gold, C.M. 1978. Quantitative Methods in the Evaluation of the Quaternary Geology of the Sand River (73L) Map Sheet, Alberta, Canada. Ph.D Thesis, University of Alberta.

Goldstein, R.M., Engelhardt, H., Kamb, B., Frolich, R.M. 1993. Satellite Radar Interferometry for Monitoring Ice Sheet Motion: Application to an Antarctic Ice Stream. Science, **262**, 1525-1529.

Grant, N. 1996. Genesis of the North Battleford Fluting Field, West-Central Saskatchewan. M.Sc. Thesis, University of Alberta.

Gravenor, C.P., Meneley, W.A. 1958. Glacial Flutings in Central and Northern Alberta. American Journal of Science, **256**, 715-728.

Green, R. 1972. Geological Map of Alberta. Alberta Geological Survey, Alberta Research Council 1:1,267,000 scale map.

Grim, R.E. 1962. Applied Clay Mineralogy. McGraw-Hill Book Company, Inc. Toronto.

Grisak, G.E., Cherry, J.A., Venhof, J.A., Blumele, J.P. 1976. Hydrogeologic and hydrochemical properties of fractured till in the Interior Plains region. *In* Glacial Till an Inter-disciplinary Study. *Edited by* Legget, R.F. The Royal Society of Canada Special Publications No. 12, 304-333.

Harrison, W. 1958. Marginal zones of vanished glaciers reconstructed from the preconsolidation values of overridden silts. Journal of Geology, **66**, 72-95.

Hart, J.K. 1994. Till Fabric Associated with Deformable Beds. Earth Surface Processes and Landforms, **19**, 15-32.

Hart, J.K., Hindmarsh, R.C.A., Boulton, G.S. 1990. Different styles of subglacial glaciotectonic deformation in the context of the Anglian ice sheet. Earth Surface Processes and Landforms, **15**, 227-241.

Head, K.H. 1994. Manual of Soil Laboratory Testing Volume 2: Permeability, Shear Strength and Compressibility Tests. Pentech Press. London.

Hicock, S.R. 1988. Calcareous Till Facies North of Lake Superior, Ontario: Implications for Laurentide Ice Streaming. Geographie Physique et Quaternaire, **42**, 120-135.

Hicock, S.R. 1990. Genetic till prism. Geology, **18**, 517-519.

Hicock, S.R. 1991. On subglacial stone pavements in till. Journal of Geology, **99**, 607-619.

Hicock, S.R., Dreimanis, A. 1992. Deformation till in the Great Lakes region: implications for rapid flow along the south-central margin of the Laurentide Ice Sheet. Canadian Journal of Earth Science, **29**, 1565-1579.

Hicock, S.R., Kristjansson, F.J., Sharpe, D.R. 1989. Carbonate till as a soft bed for Pleistocene ice streams on the Canadian Shield north of Lake Superior. Canadian Journal of Earth Science, **26**, 2249-2254.

Hicock, S.R., Goff, J.R., Lian, O.B., Little, E.C. 1996. On the interpretation of subglacial till fabric. Journal of Sedimentary Research, **66**, 928-934.

Hooke, R. 1998. Principles of Glacier Mechanics. Prentice Hall, New Jersey.

Iken, A., Bindschadler, R.A. 1986. Combined measurements of subglacial water pressure and surface velocity of Findelengletscher, Switzerland: conclusions about drainage system and sliding mechanism. Journal of Glaciology, **32**, 101-119.

Iken, A., Echelmeyer, K., Harrison, W., Funk, M. 1993. Mechanisms of fast flow in Jakobshavns Isbrae, West Greenland, Part 1, Measurements of temperature and water level in deep boreholes, Journal of Glaciology, **39**, 15-25.

Iverson, N.R., Hanson,B., Hooke, R., Jansson, P. 1995. Flow Mechanism of Glaciers on Soft Beds. Science, **267**, 80-81.

Jansson, P. 1995. Water pressure and basal sliding on Storglaciaren, northern Sweden. Journal of Glaciology, **41**, 232-240.

Jenson, J. 1993. A Nonlinear Model of the Lake Michigan Lobe, Laurentide Ice Sheet. PhD. Thesis, Oregon State University, Corvallis.

Jenson, J., Clark, P., MacAyeal, D., Ho, C.,Vela, J. 1995. Numerical modeling of advecting transport of saturated deforming sediment beneath the Lake Michigan Lobe, Laurentide Ice Sheet. Geomorphology, **14**, 157-166.

Johnson, W.H., Hansel, A.K. 1990. Multiple Wisconsinan Glacigenic Sequences at Wedron, Illinois. Journal of Sedimentary Petrology, **60**, 26-41.

Jones, N.K. 1981. Glacigenic Streamlined Landforms near St. Paul, Alberta. MSc. Thesis, University of Alberta, Edmonton.

Kamb, W.B. 1970. Sliding motion of glaciers: theory and observation. Review of Geophysics and Space Physics, **8**, 673-728.

Kamb, W.B. 1987. Glacier Surge Mechanism Based on Linked Cavity Configuration of the Basal Water Conduit System. Journal of Geophysical Research, **92**, 9083-9100.

Kamb, W.B. 1991. Rheological nonlinearity and flow instability in the deforming bed mechanism of ice stream motion. Journal of Geophysical Research, **96**, 16585-16595.

Kamb, W.B., Engelhart, H. 1987. Waves of accelerated motion in a glacier approaching surge: the mini-surges of Variegated Glacier, Alaska. USA. Journal of Glaciology, **33**, 27-46.

Kazi, A. Knill, J.L. 1969. The sedimentation and geotechnical properties of the Cromer Till between Happisburgh and Cromer, Norfolk. Quarterly Journal of Engineering Geology, **2**, 62-87.

Konrad, J.M. 1989a. Effect of freeze-thaw cycles on the freezing characteristics of a clayey silt at various overconsolidation ratios. Canadian Geotechnical Journal, **26**, 217-226.

Konrad, J.M. 1989b. Physical Processes During Freeze-Thaw Cycles in Clayey Silts. Cold Regions Science and Technology, **16**, 291-303.

Lambe, W.T. 1960. Compacted Clay: Structure. American Society of Civil Engineers, Transactions, **125**, 682-706.

Lichti-Federovich, S. 1970. The pollen stratigraphy of a dated section of Late Pleistocene lake sediment from central Alberta. Canadian Journal of Earth Sciences, 7, 938-945.

MacAyeal, D.R. 1989. Large scale ice flow over a viscous basal sediment: theory and applications to Ice Stream B, Antarctica. Journal of Geophysical Research, **94**, 4071-4087.

MacAyeal, D.R., Bindschadler, R.A., Scambos, T.A. 1995. Basal friction of Ice Stream E, West Antarctica. Journal of Glaciology, **41**, 247-262.

MacDonald, A.B., Sauer, E.K. 1970 The engineering significance of Pleistocene stratigraphy in the Saskatoon area, Saskatchewan, Canada. Canadian Geotechnical Journal, 7, 116-126.

Mark, D.M. 1974. On the Interpretation of Till Fabrics. Geology, **2**, 101-104.

Marshall, S.J. 1996. Modeling Laurentide Ice Stream Thermomechanics. PhD thesis. University of British Columbia, Vancouver.

Marshall, S.J., Clarke, G.K.C., Dyke, A.S., Fisher, D.A. 1996. Geologic and topographic controls on fast flow in the Laurentide and Cordilleran Ice Sheets. Journal of Geophysical Research, **101**, 17,827-17,839.

Mathews, W.H., MacKay, J.R. 1960. Deformation of soils by glacier ice and the influence of pore water pressure and permafrost. Transactions of the Royal Society of Canada, **54**, 27-36.

McKeague, J.A., St. Arnaud, R.J. 1969. Pedotranslocation: Eluviation-Illuviation in Soils During the Quaternary. Soil Science, **107**, 428-433.

Menzies, J. 1989. Subglacial hydraulic conditions and their possible impact upon subglacial bed formation. Sedimentary Geology, **62**, 481-493.

Mickelson, D.M., Acomb, L.J., Edil, T.B. 1979. The origin of preconsolidated and normally consolidated tills in Eastern Wisconsin, U.S.A.: *In* Moraines and Varves: Origin/Genesis/Classification. *Edited by* Schluchter, C. Proceedings of an INQUA Symposium on Genesis and Lithology of Quaternary Deposits, Zurich, 10-20 September 1978. Rotterdam: Balkema, 179-197.

Mitchell, J.K., Singh, A., Campanella, R.G. 1969. Bonding, Effective Stresses and Strength of Soils. Journal of the Soil Mechanics and Foundations Division, Proceedings of the American Society of Civil Engineers. SM5, **95**, 1219-1245.

Moran, S.R., Clayton, L., Hooke, R.LeB., Fenton, M.M., Andriashek, L.D. 1980. Glacier-bed landforms of the prairie region of North America. Journal of Glaciology, **25**, 457-476.

Mougeot, C. 1991. Quaternary Geology of the Vermilion-East area, Alberta. M.Sc. Thesis. University of Alberta, Edmonton.

Murray, T., Dowdeswell, J. 1992. Water Throughflow and the Physical Effects of Deformation on Sedimentary Glacier Beds. Journal of Geophysical Research, **97**, 8993-9002.

Ozoray, G., Dubord, M., Cowen, A. 1990. Groundwater Resources of the Vermilion 73E Map Area Alberta. Alberta Environmental Protection Water Resources Services, Hydrogeology Branch.

Paterson, W.S.B. 1994. The Physics of Glaciers. Pergamon Press, Oxford.

Patterson, C.J. 1997. Southern Laurentide ice lobes were created by ice streams: Des Moines Lobe in Minnesota, USA. Sedimentary Geology, **111**, 249-261.

Pawluk, S., Dudas, M. 1978. Reorganization of Soil Materials in the Genesis of an Acid Luvisolic Soil of the Peace River Region, Alberta. Canadian Journal of Earth Sciences, **58**, 209-220.

Piotrowski, J.A. 1997. Subglacial hydrology in north-western Germany during the last glaciation: Groundwater flow, tunnel valleys and hydrological cycles. Quaternary Science Reviews, **16**, 169-185.

Rains, B., Shaw, J., Skoye, R., Sjogren, D., Kvill, D. 1993. Late Wisconsin subglacial megaflood paths in Alberta. Geology, **21**, 323-326.

Ritter, D.F. 1986. Process Geomorphology. Wm. C. Brown Publishers. Dubuque.

Rominger, J.F., Rutledge, P.C. 1952. Use of soil mechanics data in correlation and interpretation of Lake Agassiz sediments. Journal of Geology, **60**, 160-180.

Sauer, E.K., Christiansen, E.A. 1988. Preconsolidation pressures in intertill glaciolacusterine clay near Blaine Lake, Saskatchewan. Canadian Geotechnical Journal, **25**, 831-839.

Sauer, E.K., Christiansen, E.A. 1991. Preconsolidation pressures in the Battleford Formation, southern Saskatchewan, Canada. Canadian Journal of Earth Science, **28**, 1613-1623.

Sauer, E.K, Egeland, A.K., Christiansen, E.A. 1993. Preconsolidation of tills and intertill clays by glacial loading in southern Saskatchewan, Canada. Canadian Journal of Earth Science, **30**, 420-433.

Schweger, C.E., Hickman, M. 1989. Holocene paleohydrology of central Alberta: testing the general-circulation-model climate simulations. Canadian Journal of Earth Science, **26**, 1826-1833.

Shaw, J. 1982. Melt-out till in the Edmonton area, Alberta, Canada. Canadian Journal of Earth Sciences, **19**, 1548-1569.

Shaw, J. 1983. Drumlin formation related to inverted melt-water erosional marks. Journal of Glaciology, **29**, 461-479.

Shaw, J. 1989. Drumlins, subglacial meltwater floods, and ocean responses. Geology, **17**, 853-856.

Shaw, J. 1994. A qualitative view of sub-ice-sheet landscape evolution. Progress in Physical Geography, **18**, 159-184.

Shaw, J., Sharpe, D.R. 1987. Drumlin formation by subglacial meltwater erosion. Canadian Journal of Earth Sciences, **24**, 2316-2322.

Shaw, J., Kvill, D., Rains, B. 1989. Drumlins and catastrophic subglacial floods. Sedimentary Geology, **62**, 177-202.

Shaw, J., Rains, B., Eyton, R., Weissling, L. 1996. Laurentide subglacial outburst floods: landform evidence from digital elevation models. Canadian Journal of Earth Sciences, **33**, 1154-1168.

Shetsen, I. 1990. Quaternary Geology, Central Alberta. Alberta Research Council map, 1:500,000 scale.

Shields, J.A., Lindsay, J.D. 1986. Soil Landscapes of Canada, Alberta. Agriculture Canada, 1:1,000,000 scale map.

Shoemaker, E.M. 1986. Subglacial hydrology for an ice sheet resting on a deformable aquifer. Journal of Glaciology, **32**, 20-30.

Soderman, L.G., Kim, L.D. 1970. Effect of groundwater levels on the stress history of the St. Clair clay till deposit. Canadian Geotechnical Journal, 7, 173-187.

St. Arnaud, R.J. 1976. Pedological Aspects of Glacial Till. *In* Glacial Till an Inter-disciplinary Study. *Edited by* Legget, R.F. The Royal Society of Canada Special Publications No. 12, 133-155.

Stauffer, M.R., Gendzwill, D.J., Sauer, E.K. 1990. Ice-thrust features and the Maymont landslide in the North Saskatchewan River Valley. Canadian Journal of Earth Science, **27**, 229-242.

Sugden, D.E., John, B.S. 1984. Glaciers and Landscape. Edward Arnold, London.

Swithinbank, C.M., 1954. Ice streams. Polar Record, 7, 185-186.

Taylor, D.W. 1948. Fundamentals of Soil Mechanics, John Wiley and Sons, New York.

Terzaghi, K. 1936. Stability of slopes of natural clay. Proceedings of the 1st. International Conference of Soil Mechanics, Harvard University, **1**, 161-165.

Tulley, M. 1995. Numerical Modeling of Erosion and Deposition Beneath Quaternary Ice Sheets. PhD. Thesis. Downing College, Cambridge.

Van Gelder, G., De Graff, L.S., Schurink, E. 1990. Subglacial consolidation of fine grained sediments: a neglected tool in reconstructing ice-thickness in Pleistocene valley glaciers. Arctic and Alpine Research, **22**, 329-340.

Walder, J.S., Fowler, A. 1994. Channelized subglacial drainage over a deformable bed. Journal of Glaciology, **40**, 3-15.

Weertman, J. 1957. On the sliding of glaciers. Journal of Glaciology, **3**, 33-38.

Wentworth, C. 1922. A scale of grade and class terms for clastic sediments. Journal of Geology, **30**, 377-392.

Whitaker, S.H., Christiansen, E.A. 1972. The Empress Group in Southern Saskatchewan. Canadian Jouranal of Earth Science, **9**, 353-360.

Yong, R.N., Warkentin, B.P. 1975. Soil Properties and Behaviour. Elsevier Scientific Publishing Company, New York.

Appendix I

Raw Consolidation Data

Sample Core: DS01

Test Sample #7 Dial Readings (mm)

Elapsed Time	Load Increment (kPa)							
(min)	37	74	148	296	592	1184	2368	4736
0.000	0.000	0.845	0.600	0.293	0.970	0.565	0.070	-
0.083	0.893	0.680	0.403	0.092	0.730	0.300	0.845	-
0.167	0.883	0.665	0.390	0.077	0.712	0.280	0.825	-
0.250	0.879	0.655	0.380	0.068	0.702	0.267	0.817	-
0.500	0.869	0.643	0.365	0.050	0.679	0.242	0.794	-
1.000	0.855	0.629	0.350	0.033	0.655	0.212	0.763	-
2.250	0.849	0.612	0.329	0.012	0.626	0.173	0.714	-
4.000	0.845	0.600	0.316	0.996	0.607	0.144	0.670	-
6.250			0.305	0.985	0.592	0.120	0.631	-
12.25			0.293	0.970	0.572	0.087	0.572	-
16.00					0.565	0.073	0.550	-
20.25							0.531	-
25.00							0.516	-
36.00								-

Test Sample #8 Dial Readings (mm)

Elapsed Time	Load Increment (kPa)							
(min)	37	74	148	296	592	1184	2368	4736
0.000	0.000	0.930	0.720	0.355	0.995	0.571	0.105	-
0.083	0.956	0.790	0.490	0.136	0.755	0.345	0.905	-
0.167	0.952	0.780	0.475	0.124	0.735	0.325	0.892	-
0.250	0.950	0.774	0.465	0.115	0.725	0.315	0.880	-
0.500	0.945	0.762	0.448	0.093	0.705	0.295	0.859	-
1.000	0.941	0.749	0.428	0.073	0.680	0.262	0.828	-
2.250	0.933	0.733	0.404	0.049	0.648	0.222	0.780	-
4.000	0.930	0.720	0.387	0.031	0.623	0.188	0.736	-
6.250			0.373	0.015	0.606	0.160	0.692	-
12.25			0.355	0.994	0.579	0.120	0.622	-
16.00					0.571	0.105	0.593	-
20.25							0.570	-
25.00							0.550	-
36.00								-

Test Sample #9 Dial Readings (mm)

Elapsed Time	Load Increment (kPa)							
(min)	37	74	148	296	592	1184	2368	4736
0.000	0.000	0.894	0.700	0.390	0.072	0.705	0.272	-
0.083	0.932	0.775	0.530	0.213	0.880	0.502	0.080	-
0.167	0.925	0.765	0.520	0.200	0.866	0.485	0.065	-
0.250	0.921	0.757	0.512	0.190	0.857	0.475	0.057	-
0.500	0.915	0.744	0.495	0.175	0.839	0.452	0.035	-
1.000	0.910	0.731	0.476	0.155	0.818	0.426	0.008	-
2.250	0.901	0.713	0.451	0.131	0.788	0.391	0.964	-
4.000	0.894	0.698	0.431	0.112	0.764	0.359	0.922	-
6.250			0.415	0.098	0.744	0.331	0.885	-
12.25			0.391	0.072	0.716	0.290	0.815	-
16.00					0.705	0.272	0.788	-
20.25							0.763	-
25.00							0.742	-
36.00								-

Sample Core: DS02

Test Sample #7 Dial Readings (mm)

Elapsed Time	Load Increment (KPa)							
(min)	37	74	148	296	592	1184	2368	4736
0.000	0.000	0.848	0.600	0.227	0.711	0.112	0.450	0.783
0.083	0.920	0.702	0.395	0.980	0.475	0.919	0.280	0.595
0.167	0.906	0.686	0.375	0.955	0.450	0.899	0.265	0.587
0.250	0.900	0.678	0.362	0.940	0.430	0.880	0.255	0.580
0.500	0.888	0.660	0.338	0.906	0.398	0.850	0.231	0.560
1.000	0.873	0.640	0.312	0.863	0.354	0.811	0.198	0.533
2.250	0.860	0.620	0.281	0.815	0.291	0.744	0.141	0.490
4.000	0.852	0.607	0.260	0.780	0.240	0.681	0.088	0.445
6.250	0.848	0.599	0.246	0.746	0.197	0.628	0.035	0.403
12.25			0.227	0.722	0.133	0.540	0.943	0.323
16.00				0.711	0.112	0.508	0.904	0.288
20.25						0.479	0.865	0.255
25.00						0.455	0.835	0.224
36.00							0.783	0.172

Test Sample #8 Dial Readings (mm)

Elapsed Time	Load Increment (KPa)							
(min)	37	74	148	296	592	1184	2368*	4736*
0.000	0.000	0.778	0.470	0.071	0.579	0.997	-	-
0.083	0.880	0.630	0.282	0.870	0.395	0.853	-	-
0.167	0.865	0.613	0.270	0.850	0.375	0.835	-	-
0.250	0.860	0.603	0.260	0.837	0.363	0.823	-	-
0.500	0.848	0.582	0.235	0.808	0.332	0.795	-	-
1.000	0.832	0.555	0.207	0.774	0.293	0.760	-	-
2.250	0.814	0.528	0.170	0.724	0.231	0.698	-	-
4.000	0.800	0.507	0.139	0.682	0.178	0.640	-	-
6.250	0.790	0.491	0.116	0.648	0.128	0.585	-	-
12.25	0.778	0.470	0.083	0.597	0.050	0.490	-	-
16.00			0.071	0.579	0.020	0.452	-	-
20.25					0.997	0.419	-	-
25.00						0.390	-	-
36.00							-	-

* Load increment not carried out due to sediment extrusion

Test Sample #9 Dial Readings (mm)

Elapsed Time	Load Increment (KPa)							
(min)	37	74	148	296	592	1184	2368*	4736*
0.000	0.000	0.842	0.568	0.145	0.510	0.139	-	-
0.083	0.923	0.702	0.375	0.955	0.495	0.985	-	-
0.167	0.915	0.690	0.360	0.935	0.482	0.970	-	-
0.250	0.910	0.682	0.350	0.925	0.456	0.958	-	-
0.500	0.902	0.671	0.321	0.900	0.421	0.930	-	-
1.000	0.891	0.654	0.287	0.871	0.367	0.896	-	-
2.250	0.877	0.629	0.240	0.828	0.315	0.833	-	-
4.000	0.865	0.608	0.211	0.788	0.269	0.778	-	-
6.250	0.856	0.591	0.188	0.755	0.193	0.724	-	-
12.25	0.842	0.568	0.157	0.703	0.164	0.628	-	-
16.00			0.145	0.684	0.139	0.590	-	-
20.25						0.558	-	-
25.00						0.528	-	-
36.00							-	-

* Load increment not carried out due to sediment extrusion

Sample Core: DS03

Test Sample #7 Dial Readings (mm)

Elapsed Time	Load Increment (KPa)							
(min)	37	74	148	296	592	1184	2368	4736*
0.000	0.000	0.910	0.670	0.316	0.949	0.489	0.000	-
0.083	0.935	0.742	0.435	0.080	0.640	0.220	0.761	-
0.167	0.930	0.730	0.420	0.065	0.625	0.205	0.750	-
0.250	0.927	0.725	0.410	0.055	0.613	0.195	0.740	-
0.500	0.924	0.712	0.393	0.039	0.594	0.172	0.722	-
1.000	0.920	0.701	0.378	0.020	0.575	0.148	0.700	-
2.250	0.914	0.688	0.358	0.998	0.555	0.118	0.665	-
4.000	0.910	0.679	0.343	0.983	0.534	0.093	0.632	-
6.250		0.671	0.332	0.972	0.521	0.071	0.602	-
12.25			0.316	0.954	0.499	0.035	0.546	-
16.00				0.949	0.489	0.018	0.520	-
20.25						0.003	0.496	-
25.00							0.472	-
36.00							0.429	-

* Load increment not carried out due to extrusion of sample

Test Sample #8 Dial Readings (mm)

Elapsed Time	Load Increment (KPa)							
(min)	37	74	148	296	592	1184	2368	4736*
0.000	0.000	0.930	0.760	0.423	0.978	0.397	0.834	-
0.083	0.950	0.820	0.530	0.150	0.580	0.050	0.580	-
0.167	0.947	0.810	0.518	0.130	0.560	0.035	0.560	-
0.250	0.945	0.805	0.509	0.115	0.548	0.025	0.550	-
0.500	0.942	0.795	0.494	0.090	0.524	0.004	0.534	-
1.000	0.939	0.785	0.477	0.065	0.501	0.981	0.512	-
2.250	0.934	0.774	0.460	0.380	0.472	0.952	0.480	-
4.000	0.930	0.767	0.448	0.020	0.451	0.929	0.448	-
6.250		0.760	0.438	0.006	0.435	0.907	0.419	-
12.25			0.423	0.983	0.408	0.868	0.360	-
16.00				0.978	0.397	0.851	0.330	-
20.25						0.834	0.301	-
25.00							0.278	-
36.00							0.229	-

* Load increment not carried out due to extrusion of sample

Test Sample #9 Dial Readings (mm)

Elapsed Time	Load Increment (KPa)							
(min)	37	74	148	296	592	1184	2368	4736*
0.000	0.000	0.925	0.780	0.480	0.079	0.633	0.120	-
0.083	0.950	0.835	0.600	0.210	0.790	0.330	0.860	-
0.167	0.945	0.827	0.585	0.195	0.775	0.310	0.845	-
0.250	0.943	0.822	0.578	0.185	0.765	0.300	0.835	-
0.500	0.939	0.812	0.562	0.170	0.744	0.279	0.818	-
1.000	0.935	0.802	0.547	0.155	0.724	0.257	0.793	-
2.250	0.929	0.792	0.527	0.132	0.700	0.227	0.756	-
4.000	0.925	0.785	0.508	0.118	0.683	0.200	0.719	-
6.250		0.780	0.496	0.105	0.668	0.179	0.683	-
12.25			0.479	0.086	0.643	0.139	0.618	-
16.00				0.079	0.633	0.121	0.588	-
20.25							0.562	-
25.00							0.535	-
36.00							0.485	-

* Load increment not carried out due to extrusion of sample

Sample Block: DS04

Test Sample #7 Dial Readings (mm)

Elapsed Time	Load Increment (KPa)							
(min)	37	74	148	296	592	1184	2368	3500
0.000	0.000	0.768	0.455	0.104	0.671	0.067	0.403	0.811
0.083	0.813	0.520	0.195	0.805	0.258	0.680	0.140	0.690
0.167	0.803	0.508	0.180	0.780	0.230	0.655	0.125	0.681
0.250	0.798	0.501	0.170	0.770	0.210	0.642	0.114	0.675
0.500	0.787	0.489	0.153	0.745	0.181	0.609	0.088	0.663
1.000	0.780	0.477	0.139	0.722	0.148	0.572	0.055	0.648
2.250	0.771	0.465	0.122	0.699	0.110	0.521	0.003	0.620
4.000	0.768	0.455	0.112	0.682	0.085	0.480	0.957	0.590
6.250			0.104	0.671	0.067	0.448	0.912	0.562
12.25						0.403	0.840	0.509
16.00							0.811	0.483
20.25								0.461
25.00								0.441
36.00								0.408

Test Sample #8 Dial Readings (mm)

Elapsed Time	Load Increment (KPa)							
(min)	37	74	148	296	592	1184	2368	3500
0.000	0.000	0.892	0.741	0.530	0.129	0.579	0.943	0.356
0.083	0.920	0.780	0.595	0.250	0.740	0.180	0.665	0.240
0.167	0.915	0.773	0.585	0.225	0.715	0.160	0.645	0.230
0.250	0.911	0.769	0.579	0.215	0.700	0.145	0.630	0.225
0.500	0.908	0.761	0.569	0.195	0.674	0.117	0.605	0.212
1.000	0.902	0.754	0.557	0.177	0.647	0.084	0.575	0.193
2.250	0.898	0.746	0.544	0.154	0.615	0.041	0.526	0.165
4.000	0.892	0.741	0.536	0.139	0.595	0.009	0.482	0.132
6.250			0.530	0.129	0.579	0.982	0.443	0.106
12.25						0.943	0.379	0.053
16.00							0.356	0.031
20.25								0.012
25.00								0.993
36.00								0.963

Test Sample #9 Dial Readings (mm)

Elapsed Time	Load Increment (KPa)							
(min)	37	74	148	296	592	1184	2368	3500
0.000	0.000	0.865	0.668	0.342	0.914	0.270	0.617	0.026
0.083	0.893	0.711	0.415	0.042	0.455	0.845	0.328	0.904
0.167	0.887	0.707	0.403	0.012	0.433	0.823	0.313	0.895
0.250	0.883	0.697	0.397	0.002	0.413	0.811	0.298	0.890
0.500	0.879	0.689	0.385	0.982	0.391	0.784	0.278	0.876
1.000	0.873	0.681	0.372	0.961	0.364	0.757	0.248	0.859
2.250	0.869	0.673	0.359	0.939	0.332	0.714	0.203	0.831
4.000	0.865	0.668	0.349	0.925	0.309	0.681	0.157	0.803
6.250			0.342	0.914	0.292	0.655	0.190	0.775
12.25					0.270	0.617	0.053	0.725
16.00							0.026	0.703
20.25								0.682
25.00								0.662
36.00								0.632

Sample Block: DS05

Test Sample #7 Dial Readings (mm)

Elapsed Time	Load Increment (KPa)							
(min)	37	74	148	296	592	1184	2368	3500
0.000	0.000	0.948	0.800	0.519	0.050	0.458	0.837	0.300
0.083	0.964	0.848	0.600	0.205	0.630	0.090	0.605	0.200
0.167	0.961	0.838	0.586	0.180	0.600	0.065	0.585	0.190
0.250	0.959	0.831	0.579	0.165	0.580	0.050	0.575	0.181
0.500	0.957	0.823	0.565	0.144	0.550	0.014	0.544	0.166
1.000	0.952	0.817	0.552	0.122	0.520	0.973	0.505	0.146
2.250	0.950	0.808	0.537	0.099	0.490	0.922	0.451	0.116
4.000	0.948	0.801	0.527	0.081	0.471	0.888	0.402	0.087
6.250			0.519	0.069	0.458	0.867	0.365	0.061
12.25				0.051		0.837	0.317	0.020
16.00							0.301	0.006
20.25								
25.00								
36.00								

Test Sample #8 Dial Readings (mm)

Elapsed Time	Load Increment (KPa)							
(min)	37	74	148	296	592	1184	2368	3500
0.000	0.000	0.839	0.627	0.279	0.811	0.290	0.710	0.169
0.083	0.876	0.683	0.375	0.960	0.460	0.975	0.485	1.070
0.167	0.869	0.672	0.357	0.935	0.430	0.950	0.465	1.060
0.250	0.864	0.666	0.348	0.920	0.415	0.930	0.450	1.054
0.500	0.858	0.655	0.332	0.898	0.388	0.896	0.423	1.039
1.000	0.850	0.646	0.316	0.875	0.358	0.855	0.386	1.021
2.250	0.843	0.633	0.298	0.852	0.326	0.803	0.327	0.991
4.000	0.839	0.627	0.288	0.838	0.305	0.768	0.275	0.961
6.250			0.279	0.828	0.290	0.743	0.237	0.937
12.25				0.811		0.710	0.183	0.892
16.00							0.169	0.877
20.25								
25.00								
36.00								

Test Sample #9 Dial Readings (mm)

Elapsed Time	Load Increment (KPa)							
(min)	37	74	148	296	592	1184	2368	3500
0.000	0.000	0.901	0.759	0.399	0.892	0.319	0.747	0.16
0.083	0.919	0.800	0.500	0.030	0.465	0.965	0.475	0.060
0.167	0.916	0.792	0.482	0.005	0.442	0.940	0.455	0.050
0.250	0.913	0.788	0.471	0.990	0.435	0.920	0.435	0.041
0.500	0.911	0.781	0.455	0.973	0.400	0.884	0.401	0.028
1.000	0.908	0.772	0.439	0.953	0.375	0.847	0.360	0.008
2.250	0.904	0.765	0.421	0.932	0.349	0.800	0.300	0.975
4.000	0.901	0.759	0.408	0.918	0.331	0.769	0.255	0.948
6.250			0.399	0.908	0.319	0.747	0.220	0.923
12.25				0.892			0.173	0.884
16.00							0.159	0.872
20.25								
25.00								
36.00								

Sample Block: DS07

Test Sample #7 Dial Readings (mm)

Elapsed Time	Load Increment (KPa)							
(min)	37	74	148	296	592	1184	2368	3500
0.000	0.000	0.643	0.352	0.998	0.555	0.051	0.526	0.027
0.083	0.702	0.435	0.090	0.665	0.185	0.072	0.270	0.890
0.167	0.692	0.420	0.070	0.645	0.160	0.698	0.242	0.878
0.250	0.688	0.412	0.062	0.635	0.148	0.670	0.225	0.870
0.500	0.677	0.400	0.045	0.615	0.120	0.640	0.182	0.850
1.000	0.663	0.389	0.028	0.598	0.098	0.609	0.144	0.825
2.250	0.651	0.367	0.009	0.578	0.073	0.573	0.094	0.792
4.000	0.643	0.358	0.998	0.564	0.060	0.553	0.065	0.770
6.250		0.352		0.555	0.051	0.541	0.048	0.753
12.25						0.526	0.027	0.732
16.00								
20.25								
25.00								
36.00								

Test Sample #8 Dial Readings (mm)

Elapsed Time	Load Increment (KPa)							
(min)	37	74	148	296	592	1184	2368	3500
0.000	0.000	0.873	0.613	0.294	0.899	0.433	0.892	0.372
0.083	0.914	0.685	0.370	0.000	0.555	0.070	0.590	0.260
0.167	0.907	0.672	0.360	0.983	0.535	0.045	0.565	0.240
0.250	0.902	0.665	0.350	0.973	0.520	0.030	0.545	0.228
0.500	0.897	0.656	0.339	0.956	0.498	0.999	0.510	0.213
1.000	0.889	0.645	0.325	0.938	0.478	0.970	0.474	0.190
2.250	0.881	0.632	0.311	0.920	0.458	0.938	0.431	0.158
4.000	0.873	0.622	0.301	0.908	0.444	0.920	0.408	0.137
6.250		0.613	0.294	0.899	0.433	0.909	0.392	0.121
12.25						0.892	0.372	0.098
16.00								
20.25								
25.00								
36.00								

Test Sample #9 Dial Readings (mm)

Elapsed Time	Load Increment (KPa)							
(min)	37	74	148	296	592	1184	2368	3500
0.000	0.000	0.845	0.684	0.443	0.121	0.723	0.238	0.749
0.083	0.870	0.720	0.505	0.200	0.830	0.430	0.995	0.655
0.167	0.865	0.713	0.495	0.189	0.810	0.400	0.970	0.645
0.250	0.862	0.710	0.487	0.180	0.800	0.380	0.951	0.635
0.500	0.858	0.702	0.477	0.168	0.780	0.352	0.915	0.615
1.000	0.853	0.697	0.465	0.153	0.763	0.320	0.872	0.592
2.250	0.848	0.689	0.452	0.140	0.744	0.287	0.822	0.558
4.000	0.845	0.684	0.443	0.129	0.732	0.268	0.791	0.532
6.250				0.121	0.723	0.253	0.772	0.513
12.25						0.238	0.749	0.490
16.00								
20.25								
25.00								
36.00								

Sample Block: DS09

Test Sample #7 Dial Readings (mm)

Elapsed Time	Load Increment (KPa)							
(min)	37	74	148	296	592	1184	2368	3500
0.000	0.000	0.814	0.551	0.220	0.829	0.397	0.917	0.398
0.083	0.865	0.625	0.320	0.950	0.523	0.085	0.660	0.300
0.167	0.855	0.611	0.305	0.930	0.502	0.070	0.640	0.291
0.250	0.850	0.602	0.292	0.918	0.490	0.055	0.625	0.285
0.500	0.839	0.590	0.272	0.896	0.469	0.025	0.599	0.270
1.000	0.830	0.574	0.257	0.877	0.446	0.993	0.564	0.248
2.250	0.821	0.559	0.240	0.854	0.422	0.958	0.512	0.212
4.000	0.814	0.551	0.229	0.840	0.408	0.933	0.472	0.181
6.250			0.220	0.829	0.397	0.917	0.441	0.154
12.25							0.398	0.112
16.00								0.096
20.25								
25.00								
36.00								

Test Sample #8 Dial Readings (mm)

Elapsed Time	Load Increment (KPa)							
(min)	37	74	148	296	592	1184*	2368*	3500*
0.000	0.000	0.810	0.579	0.432	0.272	-	-	-
0.083	0.835	0.642	0.535	0.321	0.270	-	-	-
0.167	0.830	0.630	0.520	0.315	0.270	-	-	-
0.250	0.827	0.625	0.510	0.298	0.270	-	-	-
0.500	0.824	0.612	0.493	0.282	0.270	-	-	-
1.000	0.820	0.601	0.478	0.277	0.270	-	-	-
2.250	0.814	0.588	0.458	0.275	-	-	-	-
4.000	0.810	0.579	0.443	0.274	-	-	-	-
6.250			0.432	0.272	-	-	-	-
12.25						-	-	-
16.00								
20.25								
25.00								
36.00								

* Load increment not carried out due to sample error

Test Sample #9 Dial Readings (mm)

Elapsed Time	Load Increment (KPa)							
(min)	37	74	148	296	592	1184	2368	3500
0.000	0.000	0.628	0.458	0.196	0.898	0.520	0.080	0.578
0.083	0.660	0.505	0.270	0.980	0.630	0.235	0.820	0.485
0.167	0.654	0.496	0.257	0.970	0.610	0.215	0.800	0.475
0.250	0.650	0.491	0.249	0.962	0.600	0.202	0.788	0.468
0.500	0.645	0.482	0.237	0.946	0.583	0.179	0.762	0.452
1.000	0.640	0.474	0.223	0.932	0.564	0.150	0.728	0.432
2.250	0.632	0.465	0.210	0.918	0.543	0.118	0.679	0.399
4.000	0.628	0.458	0.201	0.906	0.529	0.095	0.642	0.371
6.250			0.196	0.898	0.520	0.080	0.613	0.348
12.25							0.578	0.311
16.00								0.298
20.25								
25.00								
36.00								

Sample Block: DS10

Test Sample #7 Dial Readings (mm)

Elapsed Time	Load Increment (KPa)							
(min)	37	74	148	296	592	1184	2368	4736*
0.000	0.000	0.958	0.858	0.625	0.266	0.549	0.028	-
0.083	0.970	0.892	0.700	0.395	0.800	0.230	0.580	-
0.167	0.966	0.885	0.686	0.375	0.760	0.210	0.565	-
0.250	0.965	0.880	0.676	0.360	0.745	0.195	0.552	-
0.500	0.964	0.875	0.656	0.340	0.695	0.170	0.530	-
1.000	0.961	0.869	0.648	0.318	0.658	0.145	0.501	-
2.250	0.959	0.862	0.638	0.295	0.620	0.113	0.460	-
4.000	0.958	0.858	0.630	0.275	0.594	0.089	0.420	-
6.250			0.625	0.266	0.575	0.070	0.384	-
12.25					0.549	0.040	0.318	-
16.00						0.028	0.289	-
20.25							0.261	-
25.00								
36.00								

* Load increment not carried out due to sediment extrusion

Test Sample #8 Dial Readings (mm)

Elapsed Time	Load Increment (KPa)							
(min)	37	74	148	296	592	1184	2368	4736
0.000	0.000	0.953	0.796	0.560	0.650	0.389	0.669	0.079
0.083	0.975	0.825	0.611	0.325	0.610	0.950	0.380	0.840
0.167	0.970	0.819	0.605	0.305	0.585	0.920	0.360	0.825
0.250	0.967	0.815	0.599	0.295	0.546	0.907	0.350	0.815
0.500	0.962	0.809	0.589	0.270	0.507	0.880	0.330	0.799
1.000	0.959	0.806	0.580	0.249	0.465	0.849	0.305	0.773
2.250	0.957	0.800	0.570	0.226	0.437	0.805	0.266	0.731
4.000	0.953	0.796	0.564	0.209	0.416	0.768	0.229	0.693
6.250			0.560	0.196	0.389	0.735	0.193	0.653
12.25				0.175		0.689	0.129	0.578
16.00						0.669	0.100	0.541
20.25							0.079	0.507
25.00								0.473
36.00								0.411
64.00								0.318

Test Sample #9 Dial Readings (mm)

Elapsed Time	Load Increment (KPa)							
(min)	37	74	148	296	592	1184	2368	4736*
0.000	0.000	0.935	0.778	0.483	0.859	0.025	0.333	-
0.083	0.951	0.821	0.575	0.080	0.290	0.590	0.030	-
0.167	0.948	0.815	0.565	0.050	0.250	0.570	0.010	-
0.250	0.946	0.810	0.550	0.030	0.230	0.555	0.000	-
0.500	0.943	0.802	0.535	0.995	0.187	0.530	0.982	-
1.000	0.941	0.796	0.520	0.963	0.148	0.497	0.957	-
2.250	0.938	0.788	0.503	0.928	0.106	0.450	0.916	-
4.000	0.935	0.782	0.492	0.904	0.075	0.411	0.875	-
6.250		0.778	0.483	0.885	0.052	0.379	0.839	-
12.25				0.859	0.025	0.333	0.772	-
16.00							0.745	-
20.25							0.722	-
25.00								
36.00								

* Load increment not carried out due to sediment extrusion

Sample Block: DS12

Test Sample #7 Dial Readings (mm)

Elapsed Time	Load Increment (KPa)							
(min)	37	74	148	296	592	1184	2368	4736
0.000	0.000	0.849	0.570	0.230	0.829	0.365	0.820	0.269
0.083	0.895	0.650	0.340	0.980	0.540	0.070	0.595	0.075
0.167	0.885	0.635	0.322	0.960	0.510	0.050	0.580	0.065
0.250	0.880	0.625	0.312	0.945	0.495	0.035	0.570	0.055
0.500	0.871	0.610	0.293	0.923	0.472	0.013	0.552	
1.000	0.863	0.595	0.276	0.902	0.447	0.983	0.526	0.015
2.250	0.854	0.579	0.257	0.880	0.419	0.947	0.488	0.977
4.000	0.849	0.570	0.246	0.860	0.402	0.918	0.452	0.939
6.250			0.239	0.848	0.390	0.894	0.419	0.902
12.25			0.230	0.837	0.371	0.860	0.361	0.834
16.00				0.829	0.365	0.847	0.337	0.804
20.25						0.837	0.316	0.777
25.00						0.827	0.298	0.749
36.00							0.269	0.704
60.00								0.65

Test Sample #8 Dial Readings (mm)

Elapsed Time	Load Increment (KPa)							
(min)	37	74	148	296	592	1184	2368	4736
0.000	0.000	0.914	0.690	0.315	0.740	0.117	0.480	0.822
0.083	0.945	0.755	0.450	0.970	0.355	0.790	0.280	0.645
0.167	0.939	0.742	0.425	0.930	0.325	0.770	0.260	0.635
0.250	0.935	0.735	0.413	0.910	0.310	0.750	0.253	0.625
0.500	0.930	0.722	0.392	0.878	0.283	0.734	0.233	0.610
1.000	0.925	0.711	0.373	0.843	0.252	0.706	0.205	0.585
2.250	0.919	0.699	0.352	0.809	0.212	0.665	0.162	0.543
4.000	0.914	0.691	0.339	0.788	0.184	0.627	0.122	0.506
6.250			0.329	0.773	0.162	0.597	0.078	0.468
12.25			0.315	0.751	0.128	0.542	0.002	0.396
16.00				0.742	0.117	0.522	0.968	0.361
20.25						0.504	0.936	0.326
25.00						0.480	0.908	0.297
36.00							0.863	0.241
60.00								0.17

Test Sample #9 Dial Readings (mm)

Elapsed Time	Load Increment (KPa)							
(min)	37	74	148	296	592	1184	2368	4736
0.000	0.000	0.867	0.600	0.145	0.580	0.956	0.340	0.740
0.083	0.900	0.685	0.350	0.750	0.175	0.615	0.110	0.575
0.167	0.895	0.660	0.282	0.720	0.150	0.590	0.095	0.560
0.250	0.890	0.655	0.270	0.710	0.130	0.575	0.085	0.552
0.500	0.883	0.638	0.245	0.685	0.100	0.550	0.065	0.533
1.000	0.878	0.625	0.211	0.647	0.071	0.520	0.033	0.510
2.250	0.871	0.611	0.181	0.633	0.036	0.479	0.988	0.471
4.000	0.867	0.603	0.168	0.617	0.012	0.444	0.946	0.428
6.250			0.158	0.605	0.994	0.417	0.906	0.390
12.25			0.145	0.589	0.971	0.378	0.840	0.315
16.00				0.582	0.961	0.362	0.812	0.284
20.25					0.956	0.350	0.790	0.253
25.00						0.340	0.770	0.225
36.00							0.738	0.179
60.00								0.119

Sample Block: DS13

Test Sample #7 Dial Readings (mm)

Elapsed Time	Load Increment (KPa)							
(min)	37	74	148	296	592	1184	2368	4736
0.000	0.000	0.930	0.2*	0.893	0.364	0.705	0.044	0.430
0.083	0.950	0.862	0.020	0.540	0.940	0.360	0.805	0.225
0.167	0.950	0.859	0.000	0.515	0.910	0.340		0.210
0.250	0.950	0.855	0.990	0.495	0.890	0.325	0.770	0.195
0.500	0.950	0.850	0.975	0.470	0.862	0.290	0.740	0.174
1.000	0.930	0.835	0.958	0.445	0.825	0.251	0.702	0.135
2.250	0.930	0.830	0.939	0.417	0.787	0.197	0.635	0.072
4.000	0.930	0.828	0.927	0.400	0.760	0.155	0.582	0.013
6.250	0.930	0.823	0.916	0.388	0.740	0.121	0.536	0.960
12.25			0.899	0.370	0.713	0.072	0.462	0.871
16.00			0.893	0.364	0.708	0.057	0.437	0.835
20.25						0.044		0.807
25.00								0.783
36.00								0.751

Test Sample #8 Dial Readings (mm)

Elapsed Time	Load Increment (KPa)							
(min)	37	74	148	296	592	1184	2368	4736
0.000	0.000	0.940	.55*	0.121	0.697	0.040	0.380	0.755
0.083	0.951	0.875	0.260	0.869	0.255	0.685	0.140	0.540
0.167	0.950	0.870	0.240	0.852	0.230	0.670	0.120	0.520
0.250	0.949	0.865	0.220	0.830	0.215	0.650	0.108	0.510
0.500	0.947	0.861	0.200	0.804	0.190	0.618	0.078	0.480
1.000	0.944	0.859	0.184	0.781	0.158	0.580	0.039	0.444
2.250	0.941	0.854	0.164	0.755	0.121	0.528	0.975	0.385
4.000	0.940	0.850	0.150	0.739	0.095	0.486	0.920	0.328
6.250		0.849	0.140	0.725	0.073	0.451	0.870	0.277
12.25			0.127	0.697	0.048	0.409	0.798	0.192
16.00			0.121	0.697	0.040	0.393	0.775	0.158
20.25							0.755	0.130
25.00								0.109
36.00								0.079

Test Sample #9 Dial Readings (mm)

Elapsed Time	Load Increment (KPa)							
(min)	37	74	148	296	592	1184	2368	4736
0.000	0.000	0.890	0.735	0.414	0.890	0.195	0.533	0.918
0.083	0.910	0.790	0.515	0.070	0.415	0.840	0.310	0.745
0.167	0.904	0.780	0.500	0.050	0.385	0.815	0.290	0.725
0.250	0.902	0.770	0.490	0.035	0.370	0.790	0.275	0.715
0.500	0.900	0.765	0.478	0.010	0.338	0.763	0.245	0.690
1.000	0.896	0.760	0.464	0.986	0.304	0.722	0.200	0.652
2.250	0.893	0.751	0.450	0.959	0.267	0.665	0.133	0.588
4.000	0.890	0.746	0.440	0.941	0.244	0.626	0.070	0.530
6.250		0.742	0.432	0.933	0.228	0.595	0.025	0.472
12.25		0.735	0.419	0.910	0.205	0.555	0.958	0.387
16.00			0.414	0.898	0.198	0.542	0.935	0.356
20.25						0.533	0.918	0.332
25.00								0.312
36.00								0.287

Sample Block: DS14

Test Sample #7 Dial Readings (mm)

Elapsed Time	Load Increment (KPa)							
(min)	37	74	148	296	592	1184	2368	4736
0.000	0.000	0.863	0.650	0.330	0.865	0.250	0.623	0.030
0.083	0.920	0.725	0.440	0.040	0.475	0.870	0.340	0.860
0.167	0.910	0.710	0.430	0.020	0.445	0.845	0.330	0.850
0.250	0.906	0.705	0.420	0.000	0.430	0.830	0.325	0.840
0.500	0.900	0.698	0.398	0.980	0.398	0.805	0.300	0.830
1.000	0.895	0.687	0.382	0.950	0.370	0.780	0.275	0.808
2.250	0.880	0.678	0.365	0.925	0.334	0.744	0.240	0.775
4.000	0.883	0.669	0.356	0.909	0.310	0.716	0.210	0.742
6.250	0.880	0.662	0.349	0.895	0.293	0.694	0.179	0.710
12.25	0.874	0.656	0.338	0.878	0.271	0.660	0.124	0.651
16.00	0.863	0.652	0.331	0.870	0.262	0.645	0.102	0.621
20.25				0.865	0.255	0.633	0.083	0.598
25.00						0.623	0.064	0.571
36.00							0.030	0.523

Test Sample #8 Dial Readings (mm)

Elapsed Time	Load Increment (KPa)							
(min)	37	74	148	296	592	1184	2368	4736
0.000	0.000	0.860	0.580	0.230	0.782	0.100	0.380	0.740
0.083	0.940	0.660	0.340	0.930	0.340	0.650	0.080	0.570
0.167	0.935	0.645	0.320	0.910	0.305	0.620	0.060	0.550
0.250	0.930	0.640	0.310	0.900	0.280	0.600	0.050	0.540
0.500	0.925	0.630	0.297	0.875	0.255	0.575	0.025	0.520
1.000	0.915	0.620	0.283	0.855	0.224	0.548	0.000	0.497
2.250	0.876	0.599	0.268	0.832	0.190	0.508	0.960	0.455
4.000	0.869	0.592	0.258	0.819	0.169	0.480	0.924	0.419
6.250	0.866	0.589	0.250	0.807	0.152	0.459	0.892	0.381
12.25	0.861	0.581	0.238	0.788	0.129	0.422	0.838	0.314
16.00		0.579	0.230	0.782	0.120	0.410	0.813	0.282
20.25					0.111	0.398	0.793	0.254
25.00					0.105	0.388	0.775	0.227
36.00							0.745	0.180

Test Sample #9 Dial Readings (mm)

Elapsed Time	Load Increment (KPa)							
(min)	37	74	148	296	592	1184	2368	4736
0.000	0.000	0.878	0.620	0.180	0.570	0.820	0.120	0.465
0.083	0.910	0.710	0.320	0.770	0.080	0.410	0.830	0.265
0.167	0.905	0.700	0.300	0.735	0.035	0.390	0.810	0.255
0.250	0.902	0.690	0.290	0.720	0.020	0.370	0.800	0.230
0.500	0.900	0.680	0.270	0.690	0.985	0.340	0.780	0.213
1.000	0.899	0.670	0.252	0.665	0.955	0.307	0.742	0.185
2.250	0.894	0.656	0.230	0.636	0.918	0.265	0.698	0.137
4.000	0.890	0.645	0.219	0.617	0.895	0.232	0.658	0.095
6.250	0.888	0.638	0.208	0.605	0.876	0.207	0.622	0.053
12.25	0.883	0.628	0.194	0.586	0.851	0.170	0.562	0.977
16.00	0.881	0.624	0.188	0.578	0.842	0.155	0.539	0.941
20.25	0.878	0.620		0.572	0.835	0.142	0.517	0.910
25.00					0.828	0.132	0.498	0.881
36.00							0.468	0.830

Sample Block: DS16

Test Sample #7 Dial Readings (mm)

Elapsed Time	Load Increment (KPa)							
(min)	37	74	148	296	592	1184	2368	3500
0.000	0.000	0.851	0.630	0.315	0.823	0.205	0.570	0.960
0.083	0.895	0.702	0.415	0.988	0.395	0.830	0.310	0.865
0.167	0.885	0.690	0.400	0.960	0.356	0.805	0.290	0.855
0.250	0.879	0.682	0.390	0.945	0.345	0.785	0.277	0.848
0.500	0.871	0.671	0.372	0.921	0.315	0.752	0.249	0.832
1.000	0.864	0.659	0.355	0.899	0.286	0.711	0.210	0.814
2.250	0.858	0.647	0.335	0.872	0.254	0.661	0.146	0.780
4.000	0.851	0.639	0.322	0.856	0.235	0.627	0.093	0.748
6.250		0.632	0.315	0.842	0.221	0.602	0.049	0.717
12.25				0.823	0.205	0.570	0.985	0.664
16.00							0.962	0.642
20.25								0.622
25.00								0.607
36.00								0.592

Test Sample #8 Dial Readings (mm)

Elapsed Time	Load Increment (KPa)							
(min)	37	74	148	296	592	1184	2368	3500
0.000	0.000	0.840	0.600	0.260	0.740	0.113	0.463	0.858
0.083	0.875	0.650	0.350	0.898	0.300	0.715	0.195	0.760
0.167	0.865	0.640	0.333	0.870	0.265	0.685	0.175	0.753
0.250	0.860	0.634	0.323	0.856	0.256	0.670	0.157	0.745
0.500	0.856	0.624	0.309	0.829	0.219	0.632	0.132	0.732
1.000	0.851	0.617	0.294	0.807	0.189	0.592	0.090	0.712
2.250	0.845	0.607	0.278	0.782	0.161	0.545	0.030	0.681
4.000	0.841	0.600	0.267	0.767	0.143	0.512	0.979	0.650
6.250			0.259	0.757	0.130	0.491	0.937	0.621
12.25				0.740	0.113	0.463	0.878	0.570
16.00							0.858	0.549
20.25								0.532
25.00								0.516
36.00								0.492

Test Sample #9 Dial Readings (mm)

Elapsed Time	Load Increment (KPa)							
(min)	37	74	148	296	592	1184	2368	3500
0.000	0.000	0.852	0.647	0.489	-	-	-	-
0.083	0.892	0.732	0.523	0.480	-	-	-	-
0.167	0.887	0.720	0.515	0.478	-	-	-	-
0.250	0.876	0.712	0.510	0.478	-	-	-	-
0.500	0.871	0.701	0.502	0.478	-	-	-	-
1.000	0.864	0.690	0.498	0.478	-	-	-	-
2.250	0.858	0.669	0.492	*	-	-	-	-
4.000	0.852	0.652	0.491	-	-	-	-	-
6.250		0.647	0.490	-	-	-	-	-
12.25			0.489	-	-	-	-	-
16.00								
20.25								
25.00								
36.00								

* A clast in the sample prevented consolidation beyond 296 KPa.

Sample Block: DS18

Test Sample #7 Dial Readings (mm)

Elapsed Time	Load Increment (KPa)							
(min)	37	74	148	296	592	1184	2368	4736
0.000								
0.083								
0.167								
0.250								
0.500								
1.000								
2.250								
4.000								
6.250								
12.25								
16.00								
20.25								
25.00								
36.00								

Test Sample #7 was discarded as a large clast was embedded within the sample, prohibiting compression

Test Sample #8 Dial Readings (mm)

Elapsed Time	Load Increment (KPa)							
(min)	37	74	148	296	592	1184	2368	4736
0.000	0.000	0.850	0.640	0.355	0.980	0.470	0.870	0.180
0.083			0.540	0.110	0.650	0.100	0.550	0.960
0.167			0.460	0.090	0.620	0.080	0.520	0.940
0.250	0.880	0.700	0.430	0.080	0.600	0.060	0.495	0.920
0.500			0.415	0.065	0.590	0.030	0.450	0.890
1.000	0.870	0.680	0.400	0.050	0.570	0.995	0.515	0.850
2.250	0.860	0.670	0.390	0.030	0.540	0.960	0.340	0.790
4.000		0.660	0.380	0.020	0.525	0.940	0.300	0.740
6.250	0.860	0.655	0.375	0.010	0.512	0.920	0.275	0.702
12.25	0.850	0.650	0.365	0.000	0.495	0.900	0.242	0.655
16.00	0.850	0.640	0.360	0.990	0.490	0.890	0.230	0.645
20.25	0.850	0.640	0.358	0.988	0.480	0.880	0.220	0.630
25.00	0.850		0.355	0.980	0.480	0.877	0.215	0.619
36.00			0.350	0.980		0.870	0.202	0.605

Test Sample #9 Dial Readings (mm)

Elapsed Time	Load Increment (KPa)							
(min)	37	74	148	296	592	1184	2368	4736
0.000	0.000	0.850	0.565	0.190	0.740	0.150	0.470	0.800
0.083	-	-	0.450	0.890	0.340	0.740	0.150	0.560
0.167	-	-	0.330	0.860	0.310	0.690	0.110	0.530
0.250	0.880	0.610	0.310	0.850	0.300	0.670	0.090	0.510
0.500	-	-	0.280	0.840	0.275	0.640	0.050	0.480
1.000	0.870	0.600	0.260	0.820	0.250	0.600	0.000	0.440
2.250	0.865	0.590	0.245	0.795	0.230	0.570	0.940	0.380
4.000	-	0.580	0.235	0.780	0.212	0.540	0.905	0.325
6.250	0.860	0.580	0.230	0.775	0.200	0.520	0.880	0.285
12.25	0.850	0.575	0.215	0.760	0.185	0.500	0.850	0.242
16.00	0.850	0.570	0.210	0.760	0.180	0.495	0.840	0.228
20.25			0.205	0.755	0.170	0.490	0.830	0.215
25.00			0.202	0.750	0.170	0.480	0.823	0.208
36.00			0.195	0.740	0.160	0.470	0.810	0.190

Appendix II

Void Ratio Calculations

List of Abbreviations:

H_i = Height of sample (measured)

H_v = Height of voids (calculated)

H_s = Height of solids (calculated)

e_0 = Void ratio (initial) (measured)

e_f = Void ratio (final) (calculated)

D0 = deformation at 0% consolidation (measured)

D50 = deformation at 50% consolidation (calculated)

D90 = deformation at 90% consolidation (measured)

D100 = deformation at 100% consolidation (theoretical)

Dig Site:	DS01					Sample No.:	7
H_i:	1.822					e_o:	0.536
H_v:	0.636					e_f:	0.352
H_s:	1.186						

Load (kPa)		D0 (mm)	D90 (mm)	D100 (mm)	D50 (mm)	Equip. Deformation (mm)	Void Ratio
0							0.536
40		0.099	0.148	0.153	0.126	0.04	0.526
74		0.305	0.373	0.381	0.343	0.06	0.509
148		0.583	0.659	0.667	0.625	0.10	0.488
296		0.891	0.971	0.98	0.935	0.14	0.465
592		1.245	1.363	1.376	1.311	0.19	0.436
1184		1.671	1.831	1.849	1.76	0.24	0.400
2368		2.137	2.419	2.45	2.294	0.29	0.354

Dig Site:	DS01					Sample No.:	8
H_i:	1.870					e_o:	0.518
H_v:	0.638					e_f:	0.346
H_s:	1.232						

Load (kPa)		D0 (mm)	D90 (mm)	D100 (mm)	D50 (mm)	Equip. Deformation (mm)	Void Ratio
0							0.518
37		0.036	0.058	0.06	0.048	0.04	0.516
74		0.199	0.252	0.258	0.228	0.07	0.503
148		0.497	0.591	0.601	0.549	0.09	0.476
296		0.847	0.942	0.953	0.900	0.13	0.451
592		1.223	1.342	1.355	1.289	0.18	0.423
1184		1.632	1.816	1.836	1.734	0.23	0.388
2368		2.071	2.389	2.424	2.248	0.33	0.348

Dig Site:	DS01					Sample No.:	9
H_i:	1.923					e_o:	0.509
H_v:	0.649					e_f:	0.352
H_s:	1.274						

Load (kPa)		D0 (mm)	D90 (mm)	D100 (mm)	D50 (mm)	Equip. Deformation (mm)	Void Ratio
0							0.509
37		0.059	0.089	0.092	0.076	0.05	0.506
74		0.215	0.271	0.277	0.246	0.09	0.494
148		0.457	0.559	0.57	0.514	0.13	0.474
296		0.772	0.871	0.882	0.827	0.16	0.452
592		1.103	1.241	1.256	1.18	0.19	0.425
1184		1.478	1.640	1.658	1.568	0.23	0.397
2368		1.903	2.221	2.256	2.08	0.25	0.352

Dig Site: **DS02** Sample No.: **7**

H_i: 1.842 e_o: 0.640

H_v: 0.719 e_f: 0.331

H_s: 1.123

Load (kPa)		D0 (mm)	D90 (mm)	D100 (mm)	D50 (mm)	Equip. Deformation (mm)	Void Ratio
0							0.640
37		0.069	0.132	0.139	0.104	0.04	0.631
74		0.280	0.366	0.376	0.328	0.06	0.612
148		0.580	0.717	0.732	0.656	0.10	0.584
296		0.980	1.185	1.208	1.094	0.14	0.545
592		1.493	1.746	1.774	1.634	0.19	0.499
1184		2.049	2.398	2.437	2.243	0.24	0.444
2368		2.690	3.153	3.204	2.947	0.29	0.380
4736		3.383	3.829	3.879	3.631	0.36	0.327

Dig Site: **DS02** Sample No.: **8**

H_i: 1.900 e_o: 0.617

H_v: 0.725 e_f: 0.414

H_s: 1.175

Load (kPa)		D0 (mm)	D90 (mm)	D100 (mm)	D50 (mm)	Equip. Deformation (mm)	Void Ratio
0							0.617
37		0.105	0.172	0.179	0.142	0.04	0.605
74		0.351	0.468	0.481	0.416	0.07	0.582
148		0.696	0.839	0.855	0.775	0.09	0.552
296		1.110	1.309	1.331	1.221	0.13	0.515
592		1.575	1.905	1.942	1.758	0.18	0.467
1184		2.119	2.549	2.597	2.358	0.23	0.416

Dig Site: **DS02** Sample No.: **9**

H_i: 1.843 e_o: 0.558

H_v: 0.660 e_f: 0.368

H_s: 1.183

Load (KPa)		D0 (mm)	D90 (mm)	D100 (mm)	D50 (mm)	Equip. Deformation (mm)	Void Ratio
0							0.558
37		0.066	0.115	0.12	0.093	0.05	0.552
74		0.282	0.362	0.371	0.326	0.09	0.534
148		0.600	0.772	0.791	0.696	0.13	0.502
296		1.027	1.209	1.229	1.128	0.16	0.468
592		1.467	1.805	1.843	1.655	0.19	0.418
1184		1.992	2.467	2.52	2.256	0.23	0.364

Dig Site:	DS03					Sample No.:	7
H_i :	1.822					e_o :	0.615
H_v :	0.694					e_f :	0.413
H_s :	1.128						

Load (kPa)		D0 (mm)	D90 (mm)	D100 (mm)	D50 (mm)	Equip. Deformation (mm)	Void Ratio
0							0.615
37		0.059	0.081	0.083	0.071	0.04	0.611
74		0.244	0.289	0.294	0.269	0.06	0.594
148		0.543	0.624	0.633	0.588	0.10	0.568
296		0.899	0.992	1.002	0.951	0.14	0.539
592		1.338	1.429	1.439	1.389	0.19	0.504
1184		1.759	1.894	1.909	1.834	0.24	0.467
2368		2.217	2.458	2.485	2.351	0.29	0.420

Dig Site:	DS03					Sample No.:	8
H_i :	1.830					e_o :	0.623
H_v :	0.703					e_f :	0.407
H_s :	1.127						

Load (kPa)		D0 (mm)	D90 (mm)	D100 (mm)	D50 (mm)	Equip. Deformation (mm)	Void Ratio
0							0.623
37		0.046	0.062	0.064	0.055	0.04	0.621
74		0.175	0.220	0.225	0.200	0.07	0.609
148		0.454	0.532	0.541	0.497	0.09	0.583
296		0.831	0.951	0.964	0.898	0.13	0.549
592		1.399	1.521	1.535	1.467	0.18	0.503
1184		1.933	2.049	2.062	1.997	0.23	0.460
2368		2.404	2.710	2.744	2.574	0.33	0.409

Dig Site:	DS03					Sample No.:	9
H_i :	1.863					e_o :	0.652
H_v :	0.735					e_f :	0.450
H_s :	1.128						

Load (kPa)		D0 (mm)	D90 (mm)	D100 (mm)	D50 (mm)	Equip. Deformation (mm)	Void Ratio
0							0.652
37		0.046	0.065	0.067	0.057	0.05	0.650
74		0.154	0.202	0.207	0.181	0.09	0.642
148		0.382	0.456	0.464	0.423	0.13	0.622
296		0.778	0.874	0.885	0.831	0.16	0.588
592		1.191	1.302	1.314	1.253	0.19	0.552
1184		1.651	1.774	1.788	1.719	0.23	0.514
2368		2.121	2.377	2.405	2.263	0.25	0.461

Dig Site: **DS04** Sample No.: **7**

H_t: 1.872 e_o: 0.553

H_v: 0.667 e_f: 0.281

H_s: 1.205

Load (kPa)		D0 (mm)	D90 (mm)	D100 (mm)	D50 (mm)	Equip. Deformation (mm)	Void Ratio
0							0.553
37		0.183	0.225	0.23	0.206	0.04	0.537
74		0.472	0.532	0.539	0.505	0.06	0.513
148		0.791	0.868	0.877	0.834	0.10	0.489
296		1.183	1.29	1.302	1.242	0.14	0.457
592		1.721	1.872	1.889	1.805	0.19	0.412
1184		2.296	2.514	2.538	2.417	0.24	0.362
2368		2.835	3.157	3.193	3.014	0.29	0.312
3500		3.298	3.600	3.634	3.466	0.32	0.278

Dig Site: **DS04** Sample No.: **8**

H_t: 1.850 e_o: 0.680

H_v: 0.749 e_f: 0.440

H_s: 1.101

Load (kPa)		D0 (mm)	D90 (mm)	D100 (mm)	D50 (mm)	Equip. Deformation (mm)	Void Ratio
0							0.680
37		0.074	0.097	0.100	0.087	0.04	0.675
74		0.213	0.251	0.255	0.234	0.07	0.663
148		0.396	0.453	0.459	0.428	0.09	0.646
296		0.739	0.836	0.847	0.793	0.13	0.615
592		1.240	1.376	1.391	1.316	0.18	0.570
1184		1.793	1.970	1.990	1.891	0.23	0.520
2368		2.321	2.603	2.634	2.478	0.33	0.471
3500		2.747	3.014	3.044	2.895	0.39	0.439

Dig Site: **DS04** Sample No.: **9**

H_t: 1.873 e_o: 0.634

H_v: 0.727 e_f: 0.363

H_s: 1.146

Load (kPa)		D0 (mm)	D90 (mm)	D100 (mm)	D50 (mm)	Equip. Deformation (mm)	Void Ratio
0							0.634
37		0.104	0.129	0.132	0.118	0.05	0.627
74		0.282	0.325	0.330	0.306	0.09	0.613
148		0.577	0.637	0.644	0.610	0.13	0.589
296		0.952	1.052	1.063	1.008	0.16	0.555
592		1.522	1.663	1.679	1.600	0.19	0.504
1184		2.141	2.322	2.342	2.242	0.23	0.450
2368		2.650	2.948	2.981	2.816	0.25	0.396
3500		3.085	3.355	3.385	3.235	0.28	0.363

Dig Site: **DS05** Sample No.: **7**

H_t: 1.822 e_o: 0.506

H_v: 0.612 e_f: 0.284

H_s: 1.210

Load (kPa)		D0 (mm)	D90 (mm)	D100 (mm)	D50 (mm)	Equip. Deformation (mm)	Void Ratio
0							0.506
37		0.032	0.048	0.050	0.041	0.04	0.505
74		0.139	0.178	0.182	0.161	0.06	0.496
148		0.390	0.454	0.461	0.426	0.10	0.476
296		0.782	0.891	0.903	0.843	0.14	0.443
592		1.349	1.492	1.508	1.428	0.19	0.397
1184		1.886	2.084	2.106	1.996	0.24	0.352
2368		2.371	2.637	2.667	2.519	0.29	0.310
3500		2.791	2.968	2.988	2.889	0.31	0.285

Dig Site: **DS05** Sample No.: **8**

H_t: 1.830 e_o: 0.506

H_v: 0.615 e_f: 0.281

H_s: 1.215

Load (kPa)		D0 (mm)	D90 (mm)	D100 (mm)	D50 (mm)	Equip. Deformation (mm)	Void Ratio
0							0.506
37		0.120	0.154	0.158	0.139	0.04	0.496
74		0.313	0.361	0.366	0.340	0.07	0.482
148		0.616	0.690	0.698	0.657	0.09	0.456
296		1.025	1.132	1.144	1.084	0.13	0.423
592		1.526	1.658	1.673	1.599	0.18	0.383
1184		2.000	2.197	2.219	2.109	0.23	0.342
2368		2.488	2.757	2.787	2.637	0.33	0.304
3500		2.920	3.106	3.127	3.023	0.39	0.281

Dig Site: **DS05** Sample No.: **9**

H_t: 1.823 e_o: 0.535

H_v: 0.635 e_f: 0.294

H_s: 1.188

Load (kPa)		D0 (mm)	D90 (mm)	D100 (mm)	D50 (mm)	Equip. Deformation (mm)	Void Ratio
0							0.535
37		0.078	0.092	0.094	0.086	0.05	0.531
74		0.195	0.232	0.236	0.216	0.09	0.523
148		0.494	0.577	0.586	0.54	0.13	0.497
296		0.965	1.061	1.072	1.018	0.16	0.458
592		1.510	1.630	1.643	1.577	0.19	0.413
1184		2.016	2.191	2.21	2.113	0.23	0.368
2368		2.496	2.744	2.772	2.634	0.25	0.323
3500		2.929	3.088	3.106	3.017	0.27	0.296

Dig Site:	DS07					Sample No.:	7
H_t:	1.882					e_o:	0.503
H_v:	0.630					e_f:	0.267
H_s:	1.252						

Load (kPa)		D0 (mm)	D90 (mm)	D100 (mm)	D50 (mm)	Equip. Deformation (mm)	Void Ratio
0							0.503
37		0.291	0.353	0.36	0.325	0.04	0.477
74		0.563	0.641	0.65	0.606	0.06	0.456
148		0.906	0.993	1.003	0.954	0.10	0.431
296		1.119	1.330	1.353	1.236	0.14	0.406
592		1.805	1.922	1.935	1.870	0.19	0.364
1184		2.253	2.414	2.432	2.342	0.24	0.328
2368		2.707	2.910	2.933	2.820	0.29	0.292
3500		3.092	3.231	3.246	3.169	0.31	0.268

Dig Site:	DS07					Sample No.:	8
H_t:	1.850					e_o:	0.458
H_v:	0.581					e_f:	0.260
H_s:	1.269						

Load (kPa)		D0 (mm)	D90 (mm)	D100 (mm)	D50 (mm)	Equip. Deformation (mm)	Void Ratio
0							0.458
37		0.080	0.115	0.119	0.099	0.04	0.452
74		0.312	0.367	0.373	0.343	0.07	0.434
148		0.620	0.689	0.697	0.658	0.09	0.410
296		0.993	1.081	1.091	1.042	0.13	0.382
592		1.431	1.532	1.543	1.487	0.18	0.351
1184		1.941	2.063	2.077	2.009	0.23	0.312
2368		2.389	2.578	2.599	2.494	0.33	0.279
3500		2.714	2.841	2.855	2.785	0.39	0.261

Dig Site:	DS07					Sample No.:	9
H_t:	1.833					e_o:	0.440
H_v:	0.560					e_f:	0.264
H_s:	1.273						

Load (kPa)		D0 (mm)	D90 (mm)	D100 (mm)	D50 (mm)	Equip. Deformation (mm)	Void Ratio
0							0.440
37		0.127	0.150	0.153	0.140	0.05	0.432
74		0.276	0.308	0.312	0.294	0.09	0.423
148		0.488	0.548	0.555	0.521	0.13	0.407
296		0.790	0.864	0.872	0.831	0.16	0.384
592		1.155	1.249	1.259	1.207	0.19	0.356
1184		1.540	1.690	1.707	1.623	0.23	0.324
2368		1.977	2.186	2.209	2.093	0.25	0.286
3500		2.325	2.468	2.484	2.404	0.27	0.266

Dig Site: **DS09** Sample No.: **7**

H_t: 1.842 e_o: 0.514

H_v: 0.625 e_f: 0.301

H_s: 1.217

Load (kPa)		D0 (mm)	D90 (mm)	D100 (mm)	D50 (mm)	Equip. Deformation (mm)	Void Ratio
0							0.514
37		0.129	0.173	0.178	0.153	0.04	0.502
74		0.357	0.432	0.440	0.399	0.06	0.483
148		0.661	0.748	0.758	0.709	0.10	0.460
296		1.033	1.134	1.145	1.089	0.14	0.431
592		1.464	1.570	1.582	1.523	0.19	0.399
1184		1.888	2.042	2.059	1.974	0.24	0.364
2368		2.319	2.528	2.551	2.435	0.29	0.328
3500		2.682	2.883	2.905	2.794	0.31	0.300

Dig Site: **DS09** Sample No.: **8**

H_t: subsample not tested e_o:

H_v: e_f:

H_s:

Load (kPa)		D0 (mm)	D90 (mm)	D100 (mm)	D50 (mm)	Equip. Deformation (mm)	Void Ratio
0							
37		subsample not tested					
74							
148							
296							
592							
1184							
2368							
3500							

Dig Site: **DS09** Sample No.: **9**

H_t: 1.823 e_o: 0.504

H_v: 0.611 e_f: 0.304

H_s: 1.212

Load (kPa)		D0 (mm)	D90 (mm)	D100 (mm)	D50 (mm)	Equip. Deformation (mm)	Void Ratio
0							0.504
37		0.331	0.359	0.362	0.347	0.05	0.478
74		0.448	0.531	0.540	0.494	0.09	0.467
148		0.711	0.776	0.783	0.747	0.13	0.450
296		1.008	1.075	1.082	1.045	0.16	0.428
592		1.359	1.447	1.457	1.408	0.19	0.399
1184		1.753	1.887	1.902	1.827	0.23	0.366
2368		2.146	2.358	2.382	2.264	0.25	0.328
3500		2.500	2.658	2.676	2.588	0.27	0.306

Dig Site:	DS10					Sample No.:	7
H_i:	1.832					e_o:	0.596
H_v:	0.684					e_f:	0.382
H_s:	1.148						

Load (kPa)		D0 (mm)	D90 (mm)	D100 (mm)	D50 (mm)	Equip. Deformation (mm)	Void Ratio
0							0.596
37		0.026	0.039	0.04	0.033	0.04	0.596
74		0.101	0.131	0.134	0.376	0.06	0.590
148		0.282	0.352	0.36	0.321	0.10	0.573
296		0.583	0.692	0.704	0.644	0.14	0.547
592		1.168	1.345	1.365	1.266	0.19	0.496
1184		1.743	1 877	1.892	1.817	0.24	0.450
2368		2.402	2.698	2.731	2.566	0.29	0.383

Dig Site:	DS10					Sample No.:	8
H_i:	1.880					e_o:	0.622
H_v:	0.721					e_f:	0.344
H_s:	1.157						

Load (kPa)		D0 (mm)	D90 (mm)	D100 (mm)	D50 (mm)	Equip. Deformation (mm)	Void Ratio
0							0.622
37		0.018	0.041	0.044	0.031	0.04	0.622
74		0.171	0.194	0.197	0.184	0.07	0.611
148		0.38	0.427	0.432	0.406	0.09	0.592
296		0.639	0.763	0.777	0.708	0.13	0.565
592		1.328	1.524	1.546	1.437	0.18	0.504
1184		2.038	2.216	2.236	2.137	0.23	0.449
2368		2.615	2.919	2.953	2.784	0.33	0.395
4736		3.144	3.665	3.723	3.433	0.46	0.340

Dig Site:	DS10					Sample No.:	9
H_i:	1.843					e_o:	0.657
H_v:	0.731					e_f:	0.384
H_s:	1.112						

Load (kPa)		D0 (mm)	D90 (mm)	D100 (mm)	D50 (mm)	Equip. Deformation (mm)	Void Ratio
0							0.657
37		0.044	0.058	0.06	0.052	0.05	0.656
74		0.173	0.205	0.209	0.191	0.09	0.646
148		0.411	0.486	0.494	0.453	0.13	0.624
296		0.879	1.039	1.057	0.968	0.16	0.576
592		1.660	1.851	1.872	1.766	0.19	0.506
1184		2.383	2.583	2.605	2.494	0.23	0.443
2368		2.964	3.263	3.296	3.130	0.25	0.383

Dig Site:	DS12					Sample No.:	7
H_i:	1.867					e_o:	0.616
H_v:	0.712					e_f:	0.357
H_s:	1.155						

Load (kPa)		D0 (mm)	D90 (mm)	D100 (mm)	D50 (mm)	Equip. Deformation (mm)	Void Ratio
0							0.616
37		0.084	0.129	0.134	0.109	0.04	0.608
74		0.320	0.399	0.408	0.392	0.06	0.586
148		0.634	0.724	0.734	0.684	0.10	0.561
296		0.992	1.099	1.111	1.051	0.14	0.532
592		1.426	1.557	1.572	1.499	0.19	0.496
1184		1.904	2.057	2.074	1.989	0.24	0.457
2368		2.395	2.665	2.695	2.545	0.29	0.408
4736		2.907	3.295	3.338	3.123	0.36	0.358

Dig Site:	DS12					Sample No.:	8
H_i:	1.870					e_o:	0.590
H_v:	0.694					e_f:	0.304
H_s:	1.176						

Load (kPa)		D0 (mm)	D90 (mm)	D100 (mm)	D50 (mm)	Equip. Deformation (mm)	Void Ratio
0							0.590
37		0.045	0.073	0.076	0.061	0.04	0.587
74		0.227	0.289	0.296	0.261	0.07	0.571
148		0.522	0.629	0.641	0.581	0.09	0.543
296		1.003	1.161	1.179	1.091	0.13	0.501
592		1.619	1.786	1.805	1.712	0.18	0.452
1184		2.191	2.393	2.415	2.303	0.23	0.404
2368		2.706	3.121	3.167	2.937	0.33	0.349
4736		3.339	3.802	3.853	3.596	0.46	0.301

Dig Site:	DS12					Sample No.:	9
H_i:	1.863					e_o:	0.616
H_v:	0.710					e_f:	0.372
H_s:	1.153						

Load (kPa)		D0 (mm)	D90 (mm)	D100 (mm)	D50 (mm)	Equip. Deformation (mm)	Void Ratio
0							0.616
37		0.037	0.049	0.050	0.044	0.05	0.616
74		0.192	0.240	0.245	0.219	0.09	0.603
148		0.472	0.561	0.571	0.521	0.13	0.578
296		0.983	1.117	1.132	1.057	0.16	0.532
592		1.646	1.787	1.803	1.724	0.19	0.476
1184		2.250	2.399	2.416	2.333	0.23	0.426
2368		2.736	3.032	3.065	2.900	0.25	0.372

Dig Site: **DS13** Sample No.: **7**

H_t: 1.862 e_o: 0.612

H_v: 0.707 e_f: 0.329

H_s: 1.155

Load (kPa)		D0 (mm)	D90 (mm)	D100 (mm)	D50 (mm)	Equip. Deformation (mm)	Void Ratio
0							0.612
37		-	-	-	-	0.04	n/a
74		0.132	0.171	0.175	0.154	0.06	0.602
148		0.325	0.417	0.427	0.376	0.1	0.584
296		0.798	0.937	0.952	0.875	0.14	0.542
592		1.398	1.571	1.590	1.494	0.19	0.491
1184		1.978	2.204	2.229	2.104	0.24	0.440
2368		2.536	2.855	2.89	2.713	0.29	0.387
4736		3.128	3.558	3.606	3.367	0.36	0.331

Dig Site: **DS13** Sample No.: **8**

H_t: 1.910 e_o: 0.589

H_v: 0.710 e_f: 0.322

H_s: 1.205

Load (kPa)		D0 (mm)	D90 (mm)	D100 (mm)	D50 (mm)	Equip. Deformation (mm)	Void Ratio
0							0.589
37		0.046	0.059	0.060	0.053	0.04	0.588
74		0.112	0.139	0.142	0.127	0.07	0.583
148		0.411	0.505	0.515	0.463	0.09	0.554
296		0.794	0.928	0.943	0.868	0.13	0.522
592		1.422	1.584	1.602	1.512	0.18	0.471
1184		1.978	2.190	2.214	2.096	0.23	0.425
2368		2.530	2.891	2.931	2.731	0.33	0.373
4736		3.140	3.552	3.598	3.369	0.46	0.329

Dig Site: **DS13** Sample No.: **9**

H_t: 1.845 e_o: 0.641

H_v: 0.721 e_f: 0.336

H_s: 1.124

Load (kPa)		D0 (mm)	D90 (mm)	D100 (mm)	D50 (mm)	Equip. Deformation (mm)	Void Ratio
0							0.641
37		0.082	0.100	0.102	0.092	0.05	0.637
74		0.193	0.237	0.242	0.217	0.09	0.628
148		0.463	0.536	0.544	0.504	0.13	0.608
296		0.904	1.019	1.032	0.968	0.16	0.564
592		1.558	1.735	1.755	1.656	0.19	0.502
1184		2.117	2.336	2.36	2.239	0.23	0.452
2368		2.657	2.994	3.031	2.844	0.25	0.394
4736		3.225	3.652	3.699	3.462	0.28	0.337

Dig Site:	DS14					Sample No.:	7
H_i:	1.806					e_o:	0.669
H_v:	0.724					e_f:	0.381
H_s:	1.082						

Load (kPa)		D0 (mm)	D90 (mm)	D100 (mm)	D50 (mm)	Equip. Deformation (mm)	Void Ratio
0							0.669
37		0.069	0.103	0.107	0.088	0.04	0.663
74		0.256	0.308	0.314	0.285	0.06	0.646
148		0.539	0.623	0.632	0.586	0.10	0.620
296		0.931	1.071	1.087	1.009	0.14	0.582
592		1.486	1.646	1.664	1.575	0.19	0.533
1184		2.093	2.235	2.251	2.172	0.24	0.483
2368		2.634	2.814	2.834	2.734	0.29	0.434
4736		3.121	3.404	3.435	3.278	0.36	0.385

Dig Site:	DS14					Sample No.:	8
H_i:	1.836					e_o:	0.717
H_v:	0.767					e_f:	0.403
H_s:	1.069						

Load (kPa)		D0 (mm)	D90 (mm)	D100 (mm)	D50 (mm)	Equip. Deformation (mm)	Void Ratio
0							0.717
37		0.042	0.086	0.091	0.066	0.04	0.712
74		0.321	0.373	0.379	0.350	0.07	0.688
148		0.638	0.710	0.718	0.678	0.09	0.658
296		1.040	1.148	1.160	1.100	0.13	0.621
592		1.623	1.783	1.801	1.712	0.18	0.565
1184		2.313	2.472	2.490	2.401	0.23	0.506
2368		2.890	3.035	3.051	2.971	0.33	0.462
4736		3.404	3.687	3.718	3.561	0.46	0.412

Dig Site:	DS14					Sample No.:	9
H_i:	1.922					e_o:	0.818
H_v:	0.865					e_f:	0.449
H_s:	1.057						

Load (kPa)		D0 (mm)	D90 (mm)	D100 (mm)	D50 (mm)	Equip. Deformation (mm)	Void Ratio
0							0.818
37		0.074	0.100	0.103	0.088	0.05	0.813
74		0.269	0.325	0.331	0.300	0.09	0.795
148		0.649	0.751	0.762	0.706	0.13	0.758
296		1.194	1.335	1.351	1.272	0.16	0.705
592		1.860	2.031	2.050	1.955	0.19	0.642
1184		2.555	2.735	2.755	2.655	0.23	0.579
2368		3.142	3.325	3.345	3.244	0.25	0.525
4736		3.720	4.076	4.116	3.918	0.28	0.455

Dig Site: **DS16** Sample No.: **7**

H_t: 1.832 e_o: 0.656

H_v: 0.726 e_f: 0.376

H_s: 1.106

Load (kPa)		D0 (mm)	D90 (mm)	D100 (mm)	D50 (mm)	Equip. Deformation (mm)	Void Ratio
0							0.656
37		0.096	0.130	0.134	0.115	0.04	0.648
74		0.287	0.342	0.348	0.318	0.06	0.630
148		0.572	0.647	0.655	0.614	0.10	0.606
296		0.990	1.101	1.113	1.052	0.14	0.568
592		1.607	1.748	1.764	1.685	0.19	0.514
1184		2.138	2.343	2.366	2.252	0.24	0.464
2368		2.661	2.977	3.012	2.837	0.29	0.410
3500		3.120	3.382	3.411	3.266	0.31	0.376

Dig Site: **DS16** Sample No.: **8**

H_t: 1.860 e_o: 0.629

H_v: 0.718 e_f: 0.355

H_s: 1.142

Load (kPa)		D0 (mm)	D90 (mm)	D100 (mm)	D50 (mm)	Equip. Deformation (mm)	Void Ratio
0							0.629
37		0.116	0.144	0.147	0.132	0.04	0.620
74		0.343	0.382	0.386	0.365	0.07	0.601
148		0.632	0.708	0.716	0.674	0.09	0.574
296		1.087	1.202	1.215	1.151	0.13	0.534
592		1.670	1.823	1.840	1.755	0.18	0.484
1184		2.261	2.469	2.492	2.377	0.23	0.431
2368		2.739	3.081	3.119	2.929	0.33	0.385
3500		3.226	3.479	3.507	3.367	0.39	0.356

Dig Site: **DS16** Sample No.: **9**

H_t: e_o:

H_v: e_f:

H_s:

Load (kPa)		D0 (mm)	D90 (mm)	D100 (mm)	D50 (mm)	Equip. Deformation (mm)	Void Ratio
0							
37							
74							
148		no data					
296							
592							
1184							
2368							
3500							

Dig Site: **DS18** Sample No.: **7**

H_t : e_o :

H_v : e_f :

H_s :

Load (kPa)		D0 (mm)	D90 (mm)	D100 (mm)	D50 (mm)	Equip. Deformation (mm)	Void Ratio
0							
37							
74							
148		no data					
296							
592							
1184							
2368							
4736							

Dig Site: **DS18** Sample No.: **8**

H_t : 1.875 e_o : 0.561

H_v : 0.674 e_f : 0.317

H_s : 1.201

Load (kPa)		D0 (mm)	D90 (mm)	D100 (mm)	D50 (mm)	Equip. Deformation (mm)	Void Ratio
0							0.561
37		0.020	0.120	0.131	0.076	0.04	0.553
74		0.208	0.308	0.319	0.264	0.07	0.540
148		0.370	0.581	0.604	0.487	0.09	0.518
296		0.860	0.954	0.964	0.912	0.13	0.492
592		1.311	1.425	1.438	1.374	0.18	0.456
1184		1.863	2.033	2.052	1.957	0.23	0.409
2368		2.393	2.660	2.690	2.541	0.33	0.365
4736		3.000	3.303	3.337	3.168	0.46	0.321

Dig Site: **DS18** Sample No.: **9**

H_t : 1.902 e_o : 0.612

H_v : 0.722 e_f : 0.313

H_s : 1.180

Load (kPa)		D0 (mm)	D90 (mm)	D100 (mm)	D50 (mm)	Equip. Deformation (mm)	Void Ratio
0							0.612
37		0.025	0.121	0.132	0.078	0.05	0.605
74		0.340	0.390	0.396	0.368	0.09	0.586
148		0.530	0.727	0.749	0.639	0.13	0.560
296		1.080	1.205	1.219	1.149	0.16	0.522
592		1.618	1.751	1.766	1.692	0.19	0.478
1184		2.220	2.420	2.442	2.331	0.23	0.425
2368		2.787	3.060	3.090	2.939	0.25	0.371
4736		3.403	3.683	3.714	3.559	0.28	0.321

Appendix III

Casagrande Method / Consolidation Curves

List of Abbreviations:

Cc = Consolidation coefficient

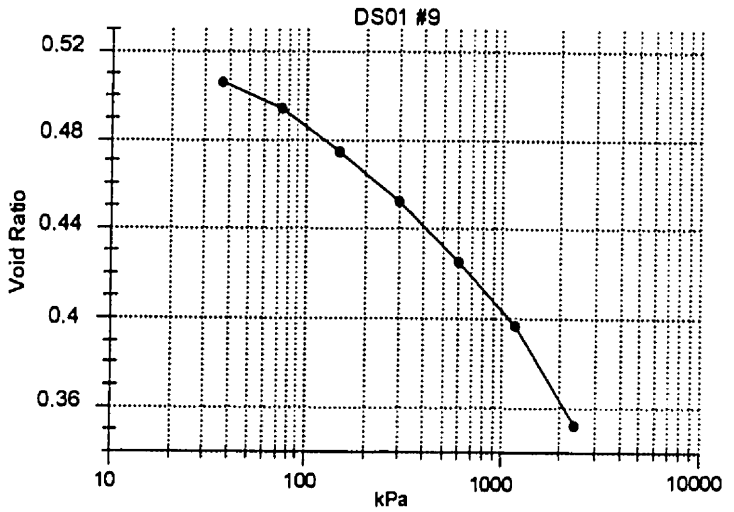
DS01 #9
0.52
0.48
0.44
0.4
0.36
Void Ratio
10
100
1000
10000
kPa

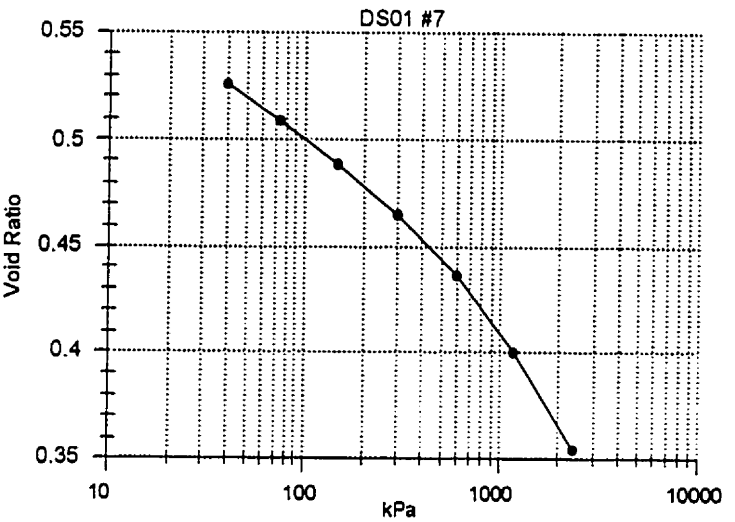
DS01 #7
0.55
0.5
0.45
0.4
0.35
Void Ratio
10
100
1000
10000
kPa

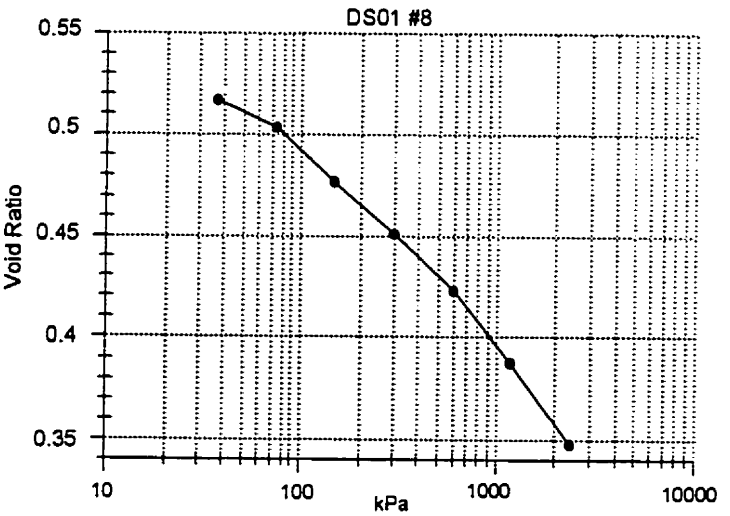
DS01 #8
0.55
0.5
0.45
0.4
0.35
Void Ratio
10
100
1000
10000
kPa

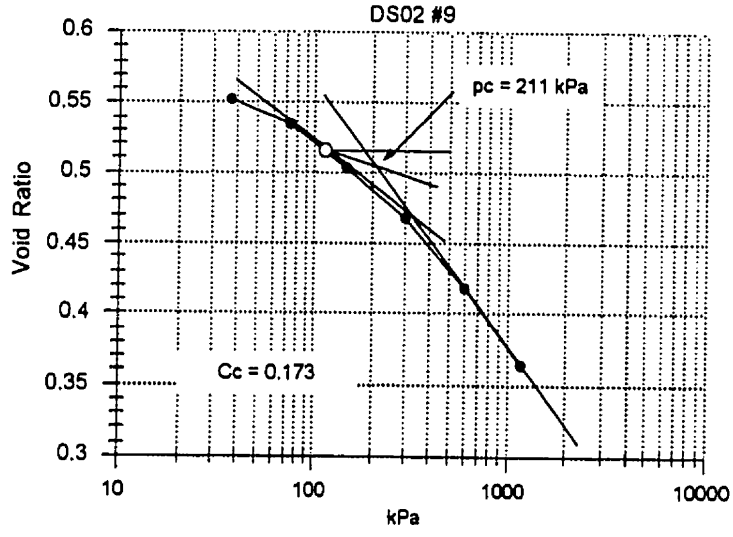
DS02 #9
pc = 211 kPa
Cc = 0.173
Void Ratio
0.6
0.55
0.5
0.45
0.4
0.35
0.3
10
100
1000
10000
kPa

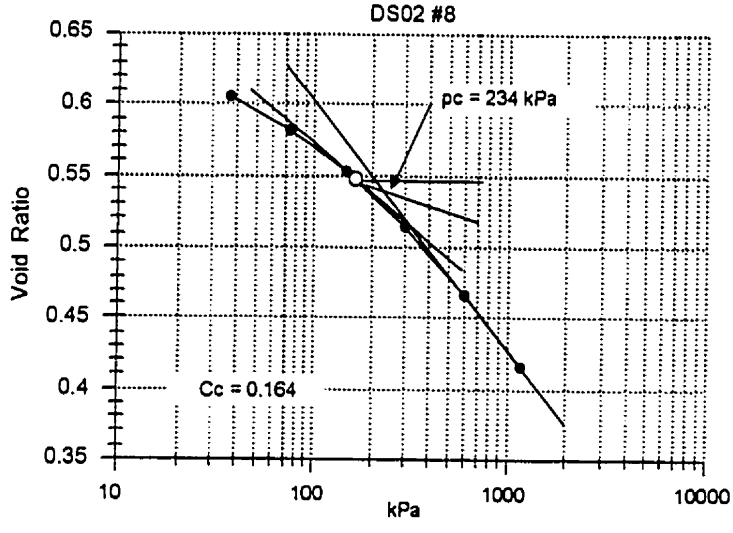
DS02 #8
pc = 234 kPa
Cc = 0.164
Void Ratio
0.65
0.6
0.55
0.5
0.45
0.4
0.35
10
100
1000
10000
kPa

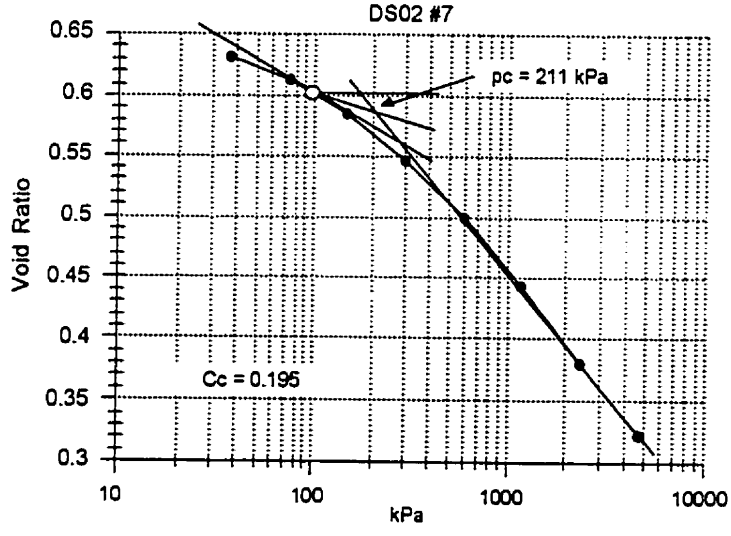
DS02 #7
pc = 211 kPa
Cc = 0.195
Void Ratio
0.65
0.6
0.55
0.5
0.45
0.4
0.35
0.3
10
100
1000
10000
kPa

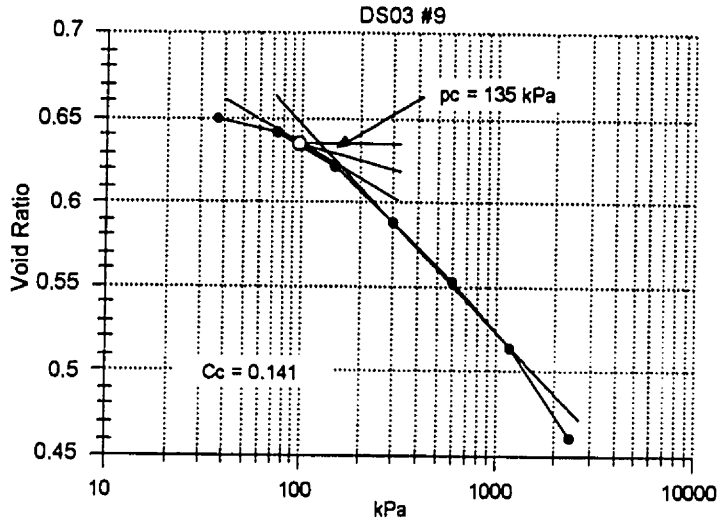
DS03 #9
0.7
0.65
0.6
0.55
0.5
0.45
Void Ratio
pc = 135 kPa
Cc = 0.141
10
100
1000
10000
kPa

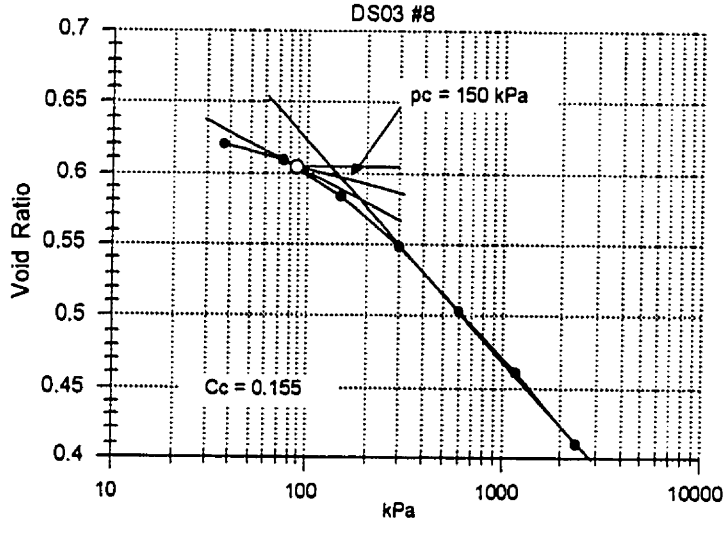
DS03 #8
0.7
0.65
0.6
0.55
0.5
0.45
0.4
Void Ratio
pc = 150 kPa
Cc = 0.155
10
100
1000
10000
kPa

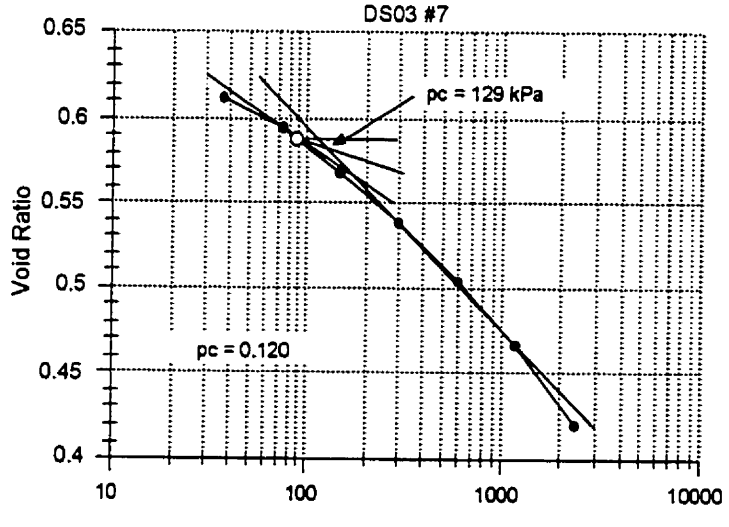
DS03 #7
0.65
0.6
0.55
0.5
0.45
0.4
Void Ratio
pc = 129 kPa
pc = 0.120
10
100
1000
10000

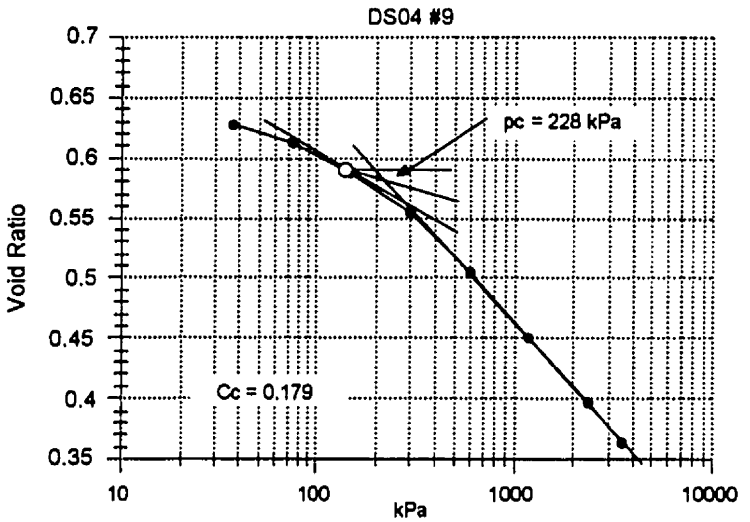
DS04 #9
Void Ratio
0.7
0.65
0.6
0.55
0.5
0.45
0.4
0.35
pc = 228 kPa
Cc = 0.179
10
100
1000
10000
kPa

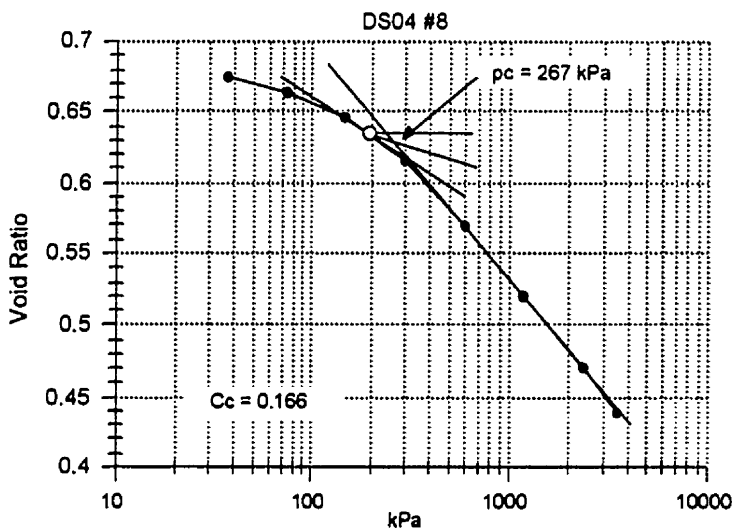
DS04 #8
Void Ratio
0.7
0.65
0.6
0.55
0.5
0.45
0.4
pc = 267 kPa
Cc = 0.166
10
100
1000
10000
kPa

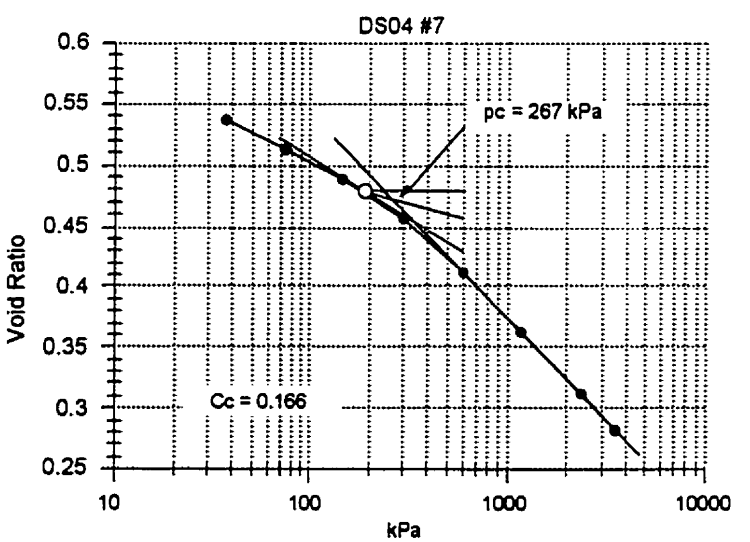
DS04 #7
Void Ratio
0.6
0.55
0.5
0.45
0.4
0.35
0.3
0.25
pc = 267 kPa
Cc = 0.166
10
100
1000
10000
kPa

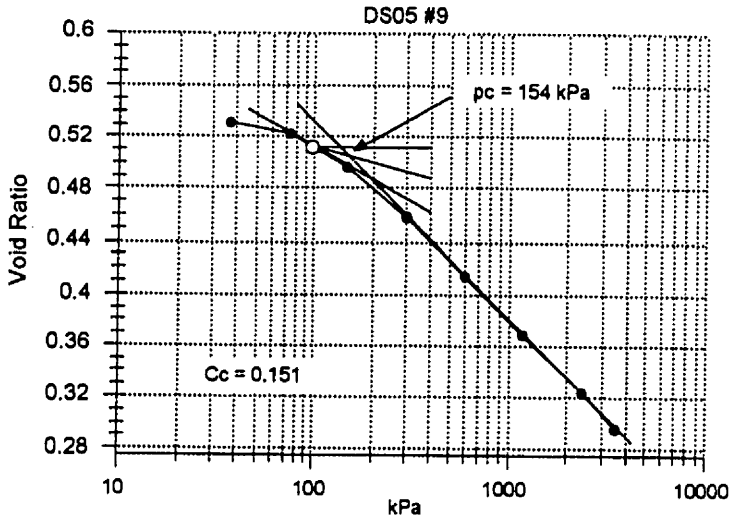
DS05 #9
pc = 154 kPa
Cc = 0.151
Void Ratio
0.6
0.56
0.52
0.48
0.44
0.4
0.36
0.32
0.28
10
100
1000
10000
kPa

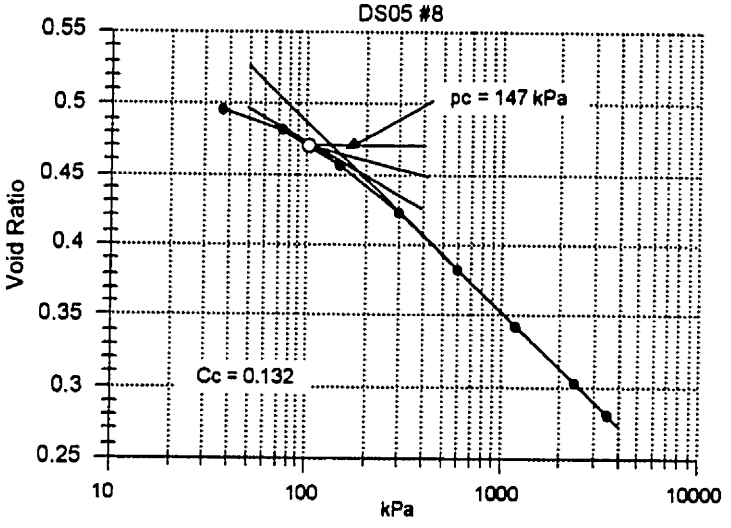
DS05 #8
pc = 147 kPa
Cc = 0.132
Void Ratio
0.55
0.5
0.45
0.4
0.35
0.3
0.25
10
100
1000
10000
kPa

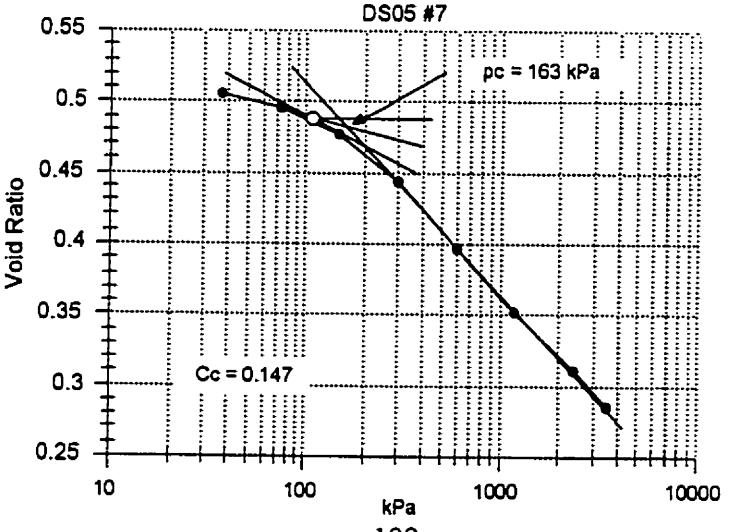
DS05 #7
pc = 163 kPa
Cc = 0.147
Void Ratio
0.55
0.5
0.45
0.4
0.35
0.3
0.25
10
100
1000
10000
kPa

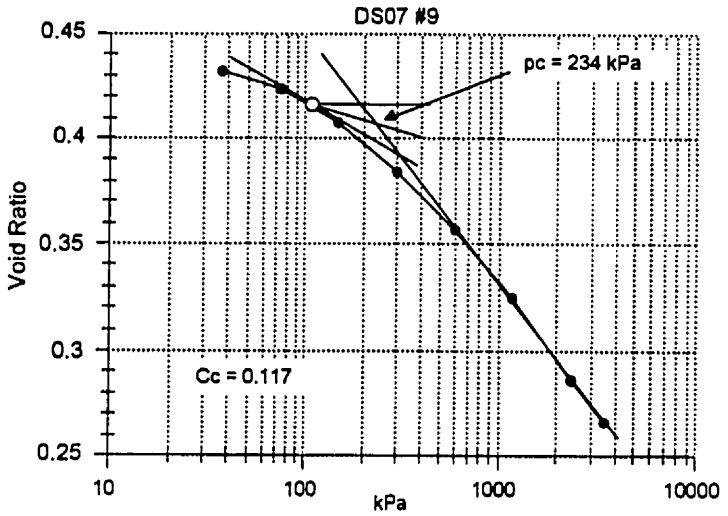
DS07 #9
pc = 234 kPa
Cc = 0.117
Void Ratio
0.45
0.4
0.35
0.3
0.25
10
100
1000
10000
kPa

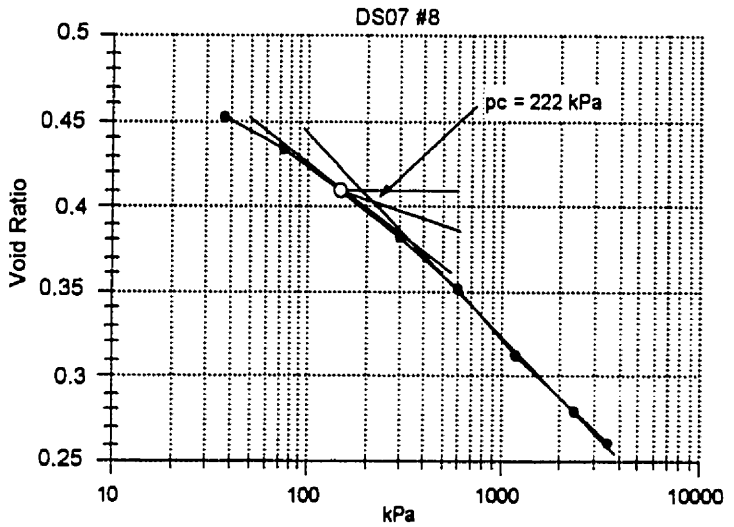
DS07 #8
pc = 222 kPa
Void Ratio
0.5
0.45
0.4
0.35
0.3
0.25
10
100
1000
10000
kPa

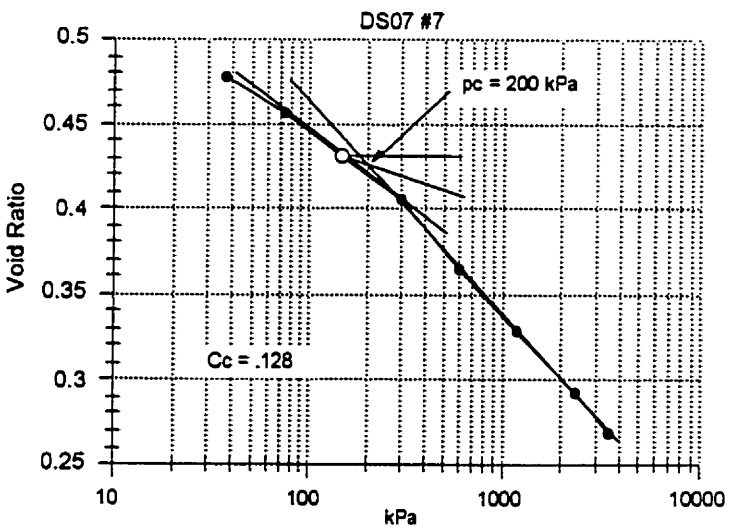
DS07 #7
pc = 200 kPa
Cc = .128
Void Ratio
0.5
0.45
0.4
0.35
0.3
0.25
10
100
1000
10000
kPa

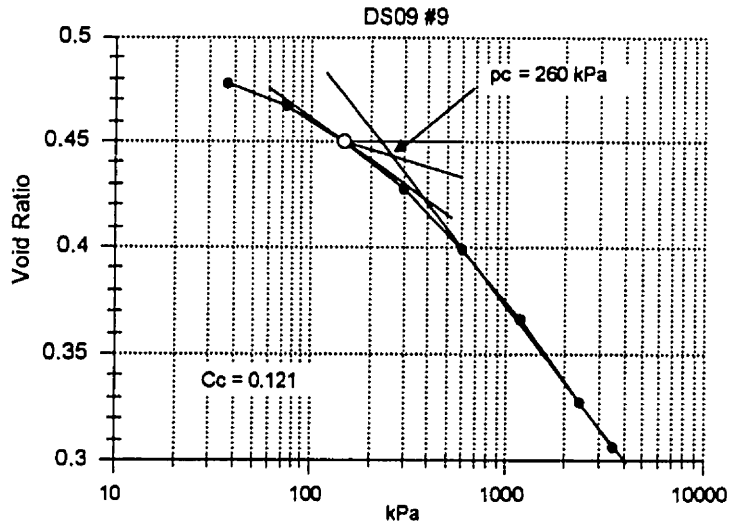
DS09 #9
pc = 260 kPa
Cc = 0.121
Void Ratio
0.5
0.45
0.4
0.35
0.3
10
100
1000
10000
kPa

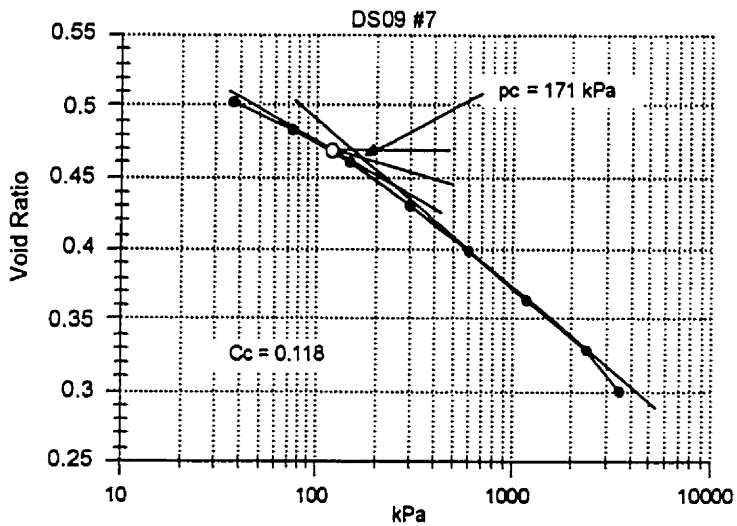
DS09 #7
pc = 171 kPa
Cc = 0.118
Void Ratio
0.55
0.5
0.45
0.4
0.35
0.3
0.25
10
100
1000
10000
kPa

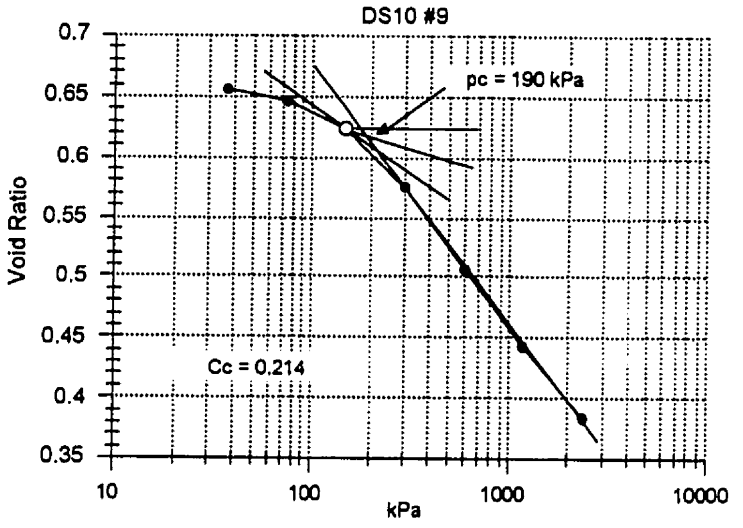
DS10 #9
pc = 190 kPa
Cc = 0.214
Void Ratio
0.7
0.65
0.6
0.55
0.5
0.45
0.4
0.35
10
100
1000
10000
kPa

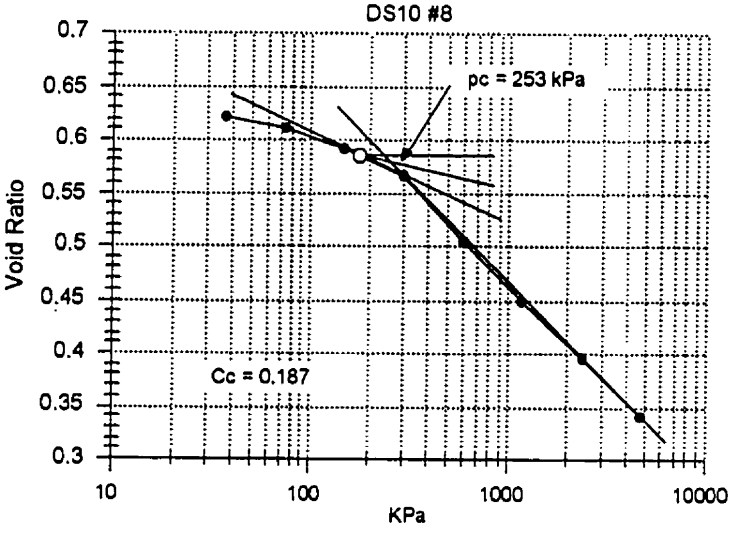
DS10 #8
pc = 253 kPa
Cc = 0.187
Void Ratio
0.7
0.65
0.6
0.55
0.5
0.45
0.4
0.35
0.3
10
100
1000
10000
KPa

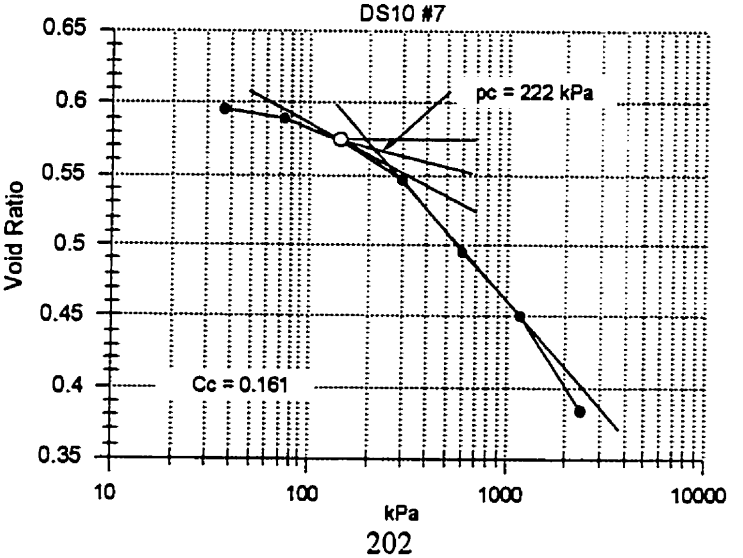
DS10 #7
pc = 222 kPa
Cc = 0.161
Void Ratio
0.65
0.6
0.55
0.5
0.45
0.4
0.35
10
100
1000
10000
kPa

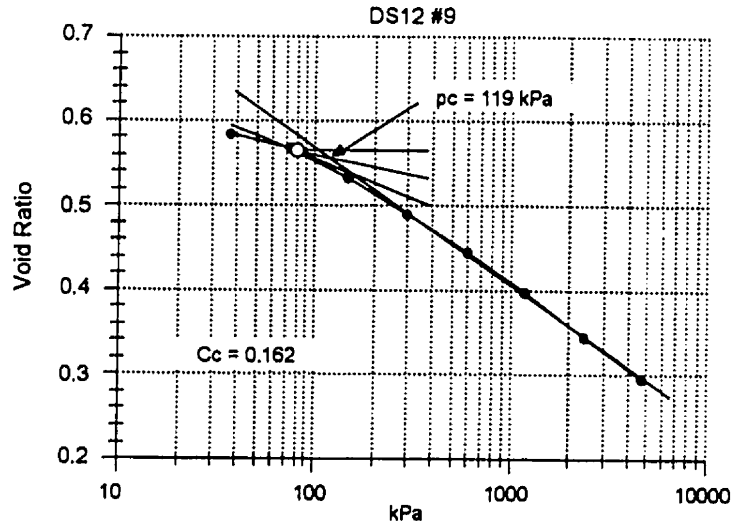
DS12 #9
pc = 119 kPa
Cc = 0.162
Void Ratio
kPa
0.7
0.6
0.5
0.4
0.3
0.2
10
100
1000
10000

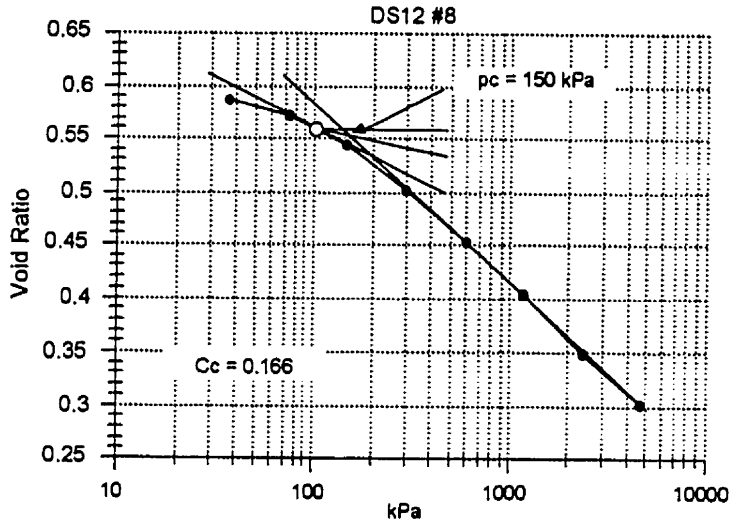
DS12 #8
pc = 150 kPa
Cc = 0.166
Void Ratio
kPa
0.65
0.6
0.55
0.5
0.45
0.4
0.35
0.3
0.25
10
100
1000
10000

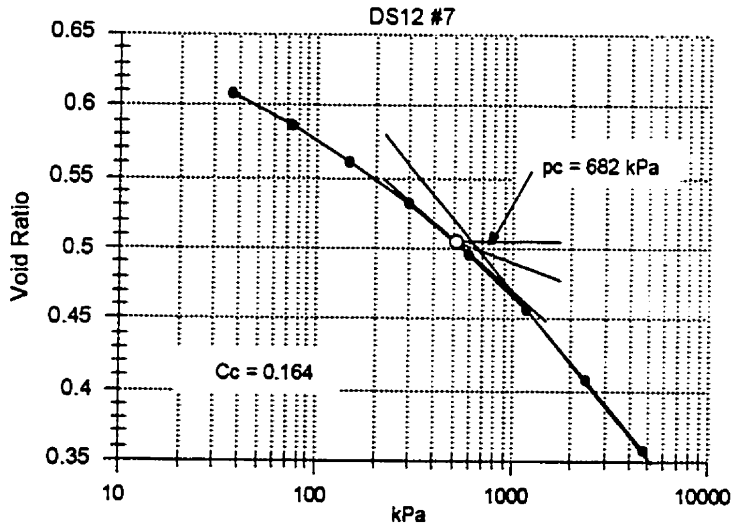
DS12 #7
pc = 682 kPa
Cc = 0.164
Void Ratio
kPa
0.65
0.6
0.55
0.5
0.45
0.4
0.35
10
100
1000
10000

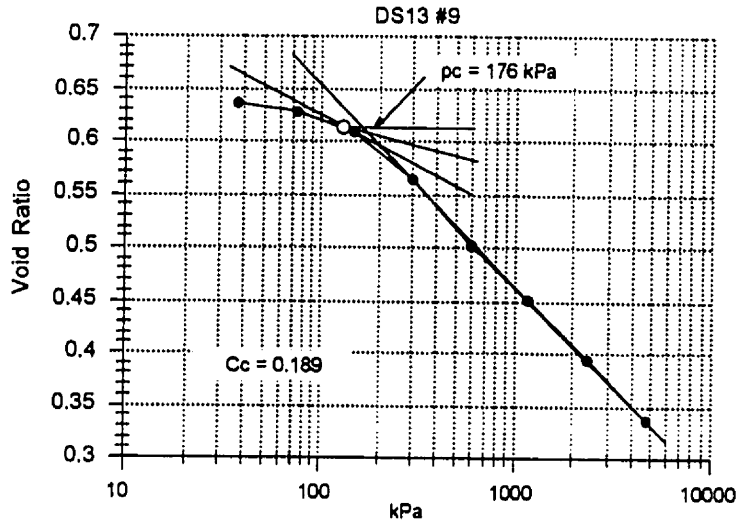
DS13 #9
pc = 176 kPa
Cc = 0.189
Void Ratio
0.7
0.65
0.6
0.55
0.5
0.45
0.4
0.35
0.3
10
100
1000
10000
kPa

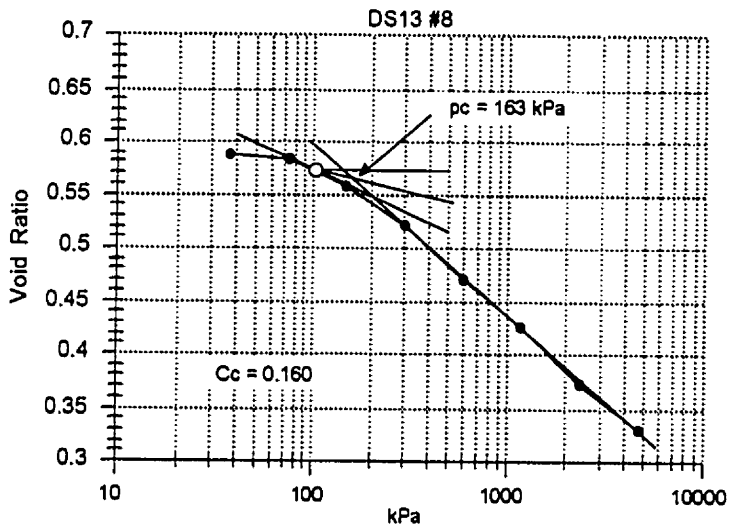
DS13 #8
pc = 163 kPa
Cc = 0.160
Void Ratio
0.7
0.65
0.6
0.55
0.5
0.45
0.4
0.35
0.3
10
100
1000
10000
kPa

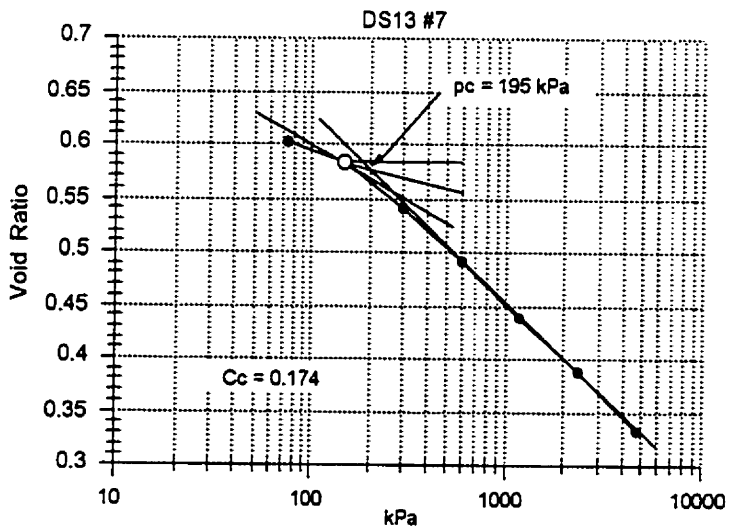
DS13 #7
pc = 195 kPa
Cc = 0.174
Void Ratio
0.7
0.65
0.6
0.55
0.5
0.45
0.4
0.35
0.3
10
100
1000
10000
kPa

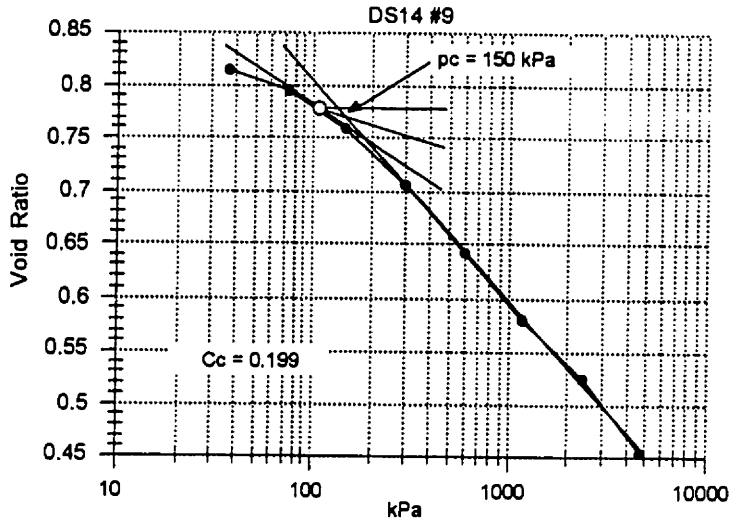
DS14 #9
pc = 150 kPa
Cc = 0.199
Void Ratio
kPa
0.85
0.8
0.75
0.7
0.65
0.6
0.55
0.5
0.45
10
100
1000
10000

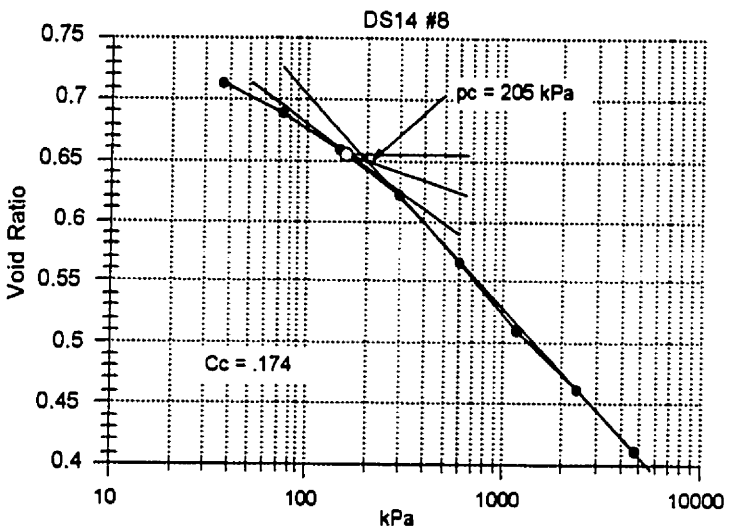
DS14 #8
pc = 205 kPa
Cc = .174
Void Ratio
kPa
0.75
0.7
0.65
0.6
0.55
0.5
0.45
0.4
10
100
1000
10000

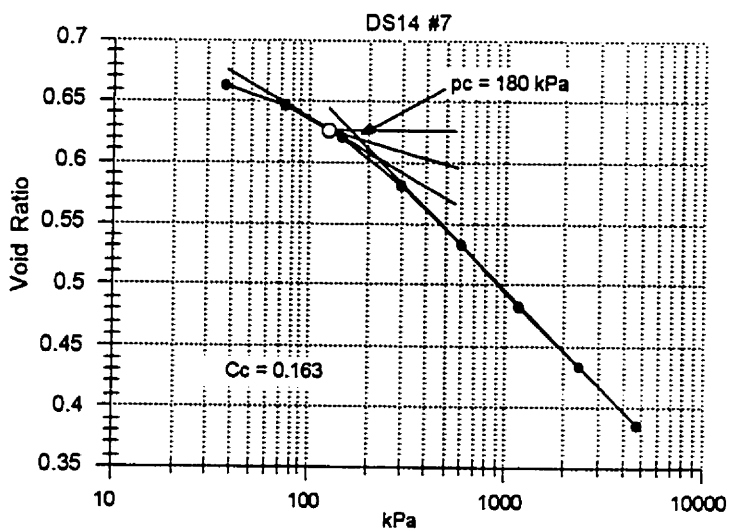
DS14 #7
pc = 180 kPa
Cc = 0.163
Void Ratio
kPa
0.7
0.65
0.6
0.55
0.5
0.45
0.4
0.35
10
100
1000
10000

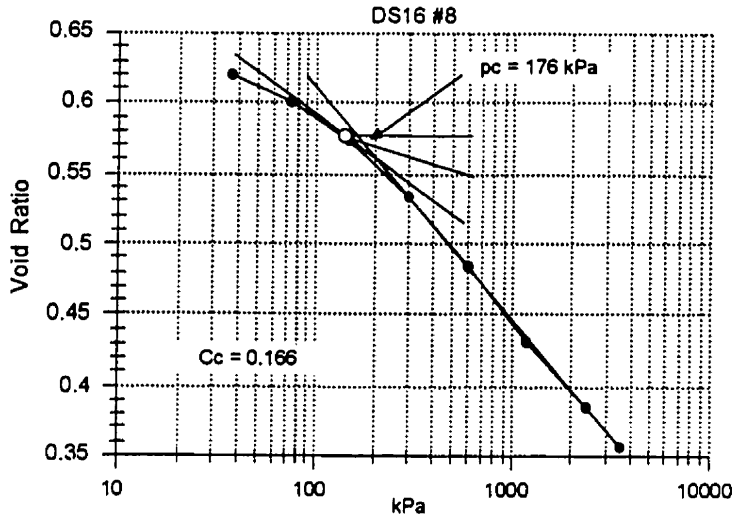
DS16 #8
pc = 176 kPa
Cc = 0.166
Void Ratio
0.65
0.6
0.55
0.5
0.45
0.4
0.35
10
100
1000
10000
kPa

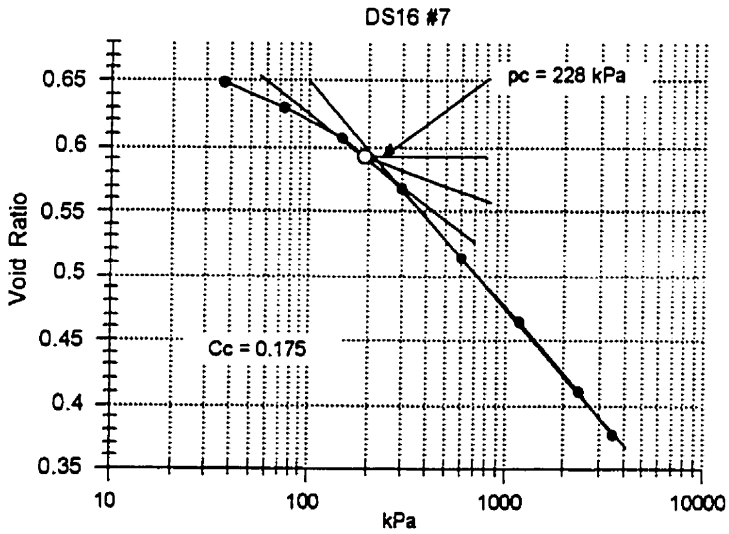
DS16 #7
pc = 228 kPa
Cc = 0.175
Void Ratio
0.65
0.6
0.55
0.5
0.45
0.4
0.35
10
100
1000
10000
kPa

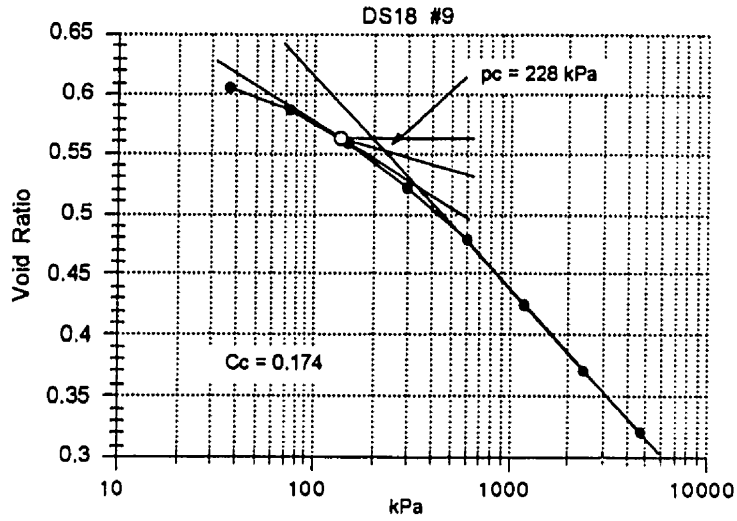
DS18 #9
pc = 228 kPa
Cc = 0.174
Void Ratio
0.65
0.6
0.55
0.5
0.45
0.4
0.35
0.3
10
100
1000
10000
kPa

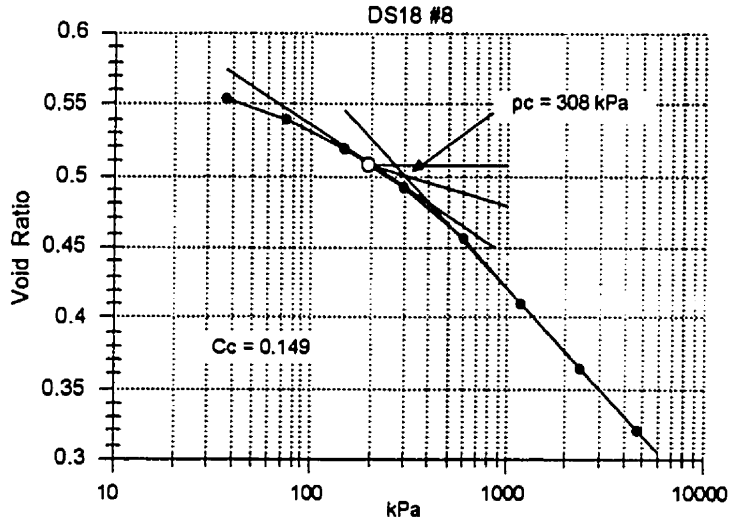
DS18 #8
pc = 308 kPa
Cc = 0.149
Void Ratio
0.6
0.55
0.5
0.45
0.4
0.35
0.3
10
100
1000
10000
kPa

Appendix IV

Diamicton Grain Size Data

HYDROMETER AND SIEVE ANALYSES										
Sample #:	DS01		Date:	26/09/96						
Hydrometer = 152H			Sample mass = 50.00 gm			Clast specific gravity = 2.65				
time	e-time (T) min	hydrom. reading	control reading	temp C	R	K	L (cm)	d (mm)	phi	P %
15 secs	0.25	35	3.0	21.6	32.0	0.0134	11.1	0.089289	3.485	64
30 secs	0.5	33	3.0	21.6	30.0	0.0134	11.4	0.063984	3.966	60
1 min	1	31.5	3.0	21.6	28.5	0.0134	11.6	0.045639	4.454	57
2 min	2	29	3.0	21.6	26.0	0.0134	12	0.032823	4.929	52
5 min	5	27	3.0	21.6	24.0	0.0134	12.4	0.021102	5.566	48
10 min	10	25.5	3.0	21.6	22.5	0.0134	12.6	0.015041	6.055	45
15 min	15	24.5	3.0	21.6	21.5	0.0134	12.8	0.012378	6.336	43
30 min	30	23	2.5	21.6	20.5	0.0134	12.95	0.008804	6.828	41
60 min	60	22	2.5	21.6	19.5	0.0134	13.15	0.006273	7.317	39
90 min	90	21	3.0	21.7	18.0	0.0134	13.3	0.005151	7.601	36
120 min	120	20.5	3.0	21.7	17.5	0.0134	13.4	0.004478	7.803	35
4 hrs	240	19.5	3.0	21.7	16.5	0.0134	13.6	0.00319	8.292	33
8 hrs	480	18.5	3.0	21.4	15.5	0.0134	13.75	0.002268	8.784	31
24 hrs	1440	16.5	3.0	21.7	13.5	0.0134	14.1	0.001326	9.559	27
Wt of sample on #230 sieve = 19.0 g										
Sieve #	Samp/siev	Sieve wt	Sample wt	Wt %	Cum wt%	P %	phi			
18	417.7	416.9	0.8	1.6	1.6	98.4	0			
35	390.3	388.4	1.9	3.8	5.4	94.6	1			
60	362.9	357.6	5.3	10.6	16.0	84.0	2			
120	344.7	338.4	6.3	12.6	28.6	71.4	3			
230	343.4	338.8	4.6	9.2	37.8	62.2	4			
pan	371.9	371.6	0.3	0.6	38.4	61.6	5			
Total			19.2							

HYDROMETER AND SIEVE ANALYSES										
Sample #:	**DS02**		**Date:**	**26/09/96**						
Hydrometer = 152H			Sample mass = 50.00 gm			Clast specific gravity = 2.65				
time	**e-time (T)**	**hydrom.**	**control**	**temp**	**R**	**K**	**L**	**d**	**phi**	**P %**
	min	**reading**	**reading**	**C**			**(cm)**	**(mm)**		
15 secs	0.25	36	3.0	21.6	33.0	0.0134	10.9	0.088481	3.498	66
30 secs	0.5	34.5	3.0	21.6	31.5	0.0134	11.15	0.063279	3.982	63
1 min	1	32	3.0	21.6	29.0	0.0134	11.5	0.045442	4.46	58
2 min	2	30	3.0	21.6	27.0	0.0134	11.9	0.032686	4.935	54
5 min	5	28	3.0	21.6	25.0	0.0134	12.2	0.020931	5.578	50
10 min	10	27	3.0	21.6	24.0	0.0134	12.4	0.014922	6.066	48
15 min	15	26	3.0	21.6	23.0	0.0134	12.5	0.012232	6.353	46
30 min	30	25	2.5	21.6	22.5	0.0134	12.6	0.008684	6.847	45
60 min	60	23.5	2.5	21.6	21.0	0.0134	12.9	0.006213	7.33	42
90 min	90	23	3.0	21.7	20.0	0.0134	13	0.005093	7.617	40
120 min	120	22.5	3.0	21.7	19.5	0.0134	13.15	0.004436	7.817	39
4 hrs	240	21.5	3.0	21.7	18.5	0.0134	13.3	0.003154	8.308	37
8 hrs	480	20.5	3.0	21.4	17.5	0.0134	13.4	0.002239	8.803	35
24 hrs	1440	18.5	3.0	21.7	15.5	0.0134	13.75	0.001309	9.577	31
Wt of sample on #230 sieve = 17.2 g										
Sieve #	**Samp/siev**	**Sieve wt**	**Sample wt**	**Wt %**	**Cum wt%**	**P %**	**phi**			
18	417.6	416.9	0.7	1.4	1.4	98.6	0			
35	390.1	388.4	1.7	3.4	4.8	95.2	1			
60	362.1	357.6	4.5	9.0	13.8	86.2	2			
120	344.4	338.4	6.0	12.0	25.8	74.2	3			
230	342.9	338.8	4.1	8.2	34.0	66.0	4			
pan	371.7	371.7	0.0	0.0	34.0	66.0	5			
Total			17							

HYDROMETER AND SIEVE ANALYSES										
Sample #:	DS03		Date:	26/09/96						
Hydrometer = 152H			Sample mass = 50.00 gm			Clast specific gravity = 2.65				
time	e-time (T)	hydrom.	control	temp	R	K	L	d	phi	P %
	min	reading	reading	C			(cm)	(mm)		
15 secs	0.25	37.5	3.0	21.5	34.5	0.0134	10.65	0.08746	3.515	69
30 secs	0.5	35.5	3.0	21.5	32.5	0.0134	11	0.062852	3.992	65
1 min	1	33.5	3.0	21.5	30.5	0.0134	11.3	0.045045	4.472	61
2 min	2	31.5	3.0	21.5	28.5	0.0134	11.6	0.032271	4.954	57
5 min	5	29	3.0	21.5	26.0	0.0134	12	0.020759	5.59	52
10 min	10	28.5	3.0	21.5	25.5	0.0134	12.1	0.01474	6.084	51
15 min	15	27.5	3.0	21.6	24.5	0.0134	12.3	0.012134	6.365	49
30 min	30	26	2.5	21.6	23.5	0.0134	12.45	0.008632	6.856	47
60 min	60	25	2.5	21.6	22.5	0.0134	12.6	0.006141	7.347	45
90 min	90	23.5	3.0	21.7	20.5	0.0134	12.95	0.005083	7.62	41
120 min	120	23	3.0	21.7	20.0	0.0134	13	0.00441	7.825	40
4 hrs	240	22	3.0	21.7	19.0	0.0134	13.3	0.003154	8.308	38
8 hrs	480	21	3.0	21.4	18.0	0.0134	13.3	0.002231	8.808	36
24 hrs	1440	19	3.0	21.7	16.0	0.0134	13.7	0.001307	9.579	32
Wt of sample on #230 sieve = 16.6 g										
Sieve #	Samp/siev	Sieve wt	Sample wt	Wt %	Cum wt%	P %	phi			
18	417.7	416.9	0.8	1.6	1.6	98.4	0			
35	390.1	388.4	1.7	3.4	5.0	95.0	1			
60	361.7	357.6	4.1	8.2	13.2	86.8	2			
120	343.7	338.4	5.3	10.6	23.8	76.2	3			
230	343.1	338.7	4.4	8.8	32.6	67.4	4			
pan	371.8	371.6	0.2	0.4	33.0	67.0	5			
Total			16.5							

HYDROMETER AND SIEVE ANALYSES										
Sample #:	DS04		Date:	26/09/96						
Hydrometer = 152H			Sample mass = 50.00 gm			Clast specific gravity = 2.65				
time	e-time (T) min	hydrom. reading	control reading	temp C	R	K	L (cm)	d (mm)	phi	P %
15 secs	0.25	36	3.0	21.5	33.0	0.0134	10.9	0.088481	3.498	66
30 secs	0.5	33	3.0	21.5	30.0	0.0134	11.4	0.063984	3.966	60
1 min	1	31	3.0	21.5	28.0	0.0134	11.7	0.045835	4.447	56
2 min	2	29	3.0	21.5	26.0	0.0134	12	0.032823	4.929	52
5 min	5	27	3.0	21.5	24.0	0.0134	12.4	0.021102	5.566	48
10 min	10	26	3.0	21.5	23.0	0.0134	12.5	0.014982	6.061	46
15 min	15	25	3.0	21.6	22.0	0.0134	12.7	0.01233	6.342	44
30 min	30	24	2.5	21.6	21.5	0.0134	12.8	0.008753	6.836	43
60 min	60	22.5	2.5	21.6	20.0	0.0134	13	0.006237	7.325	40
90 min	90	22	3.0	21.7	19.0	0.0134	13.3	0.005151	7.601	38
120 min	120	21	3.0	21.7	18.0	0.0134	13.3	0.004461	7.808	36
4 hrs	240	20.5	3.0	21.7	17.5	0.0134	13.4	0.003166	8.303	35
8 hrs	480	19	3.0	21.4	16.0	0.0134	13.7	0.002264	8.787	32
24 hrs	1440	17.5	3.0	21.7	14.5	0.0134	13.9	0.001317	9.569	29
Wt of sample on #230 sieve = 17.5 g										
Sieve #	Samp/siev	Sieve wt	Sample wt	Wt %	Cum wt%	P %	phi			
18	417.5	416.9	0.6	1.2	1.2	98.8	0			
35	389.8	388.3	1.5	3.0	4.2	95.8	1			
60	361.6	357.6	4.0	8.0	12.2	87.8	2			
120	343.7	338.4	5.3	10.6	22.8	77.2	3			
230	344.5	338.8	5.7	11.4	34.2	65.8	4			
pan	372.0	371.7	0.3	0.6	34.8	65.2	5			
Total			17.4							

HYDROMETER AND SIEVE ANALYSES										
Sample #:	**DS05**		**Date:**	**26/09/96**						
Hydrometer = 152H			Sample mass = 50.00 gm			Clast specific gravity = 2.65				
time	**e-time (T)**	**hydrom.**	**control**	**temp**	**R**	**K**	**L**	**d**	**phi**	**P %**
	min	**reading**	**reading**	**C**			**(cm)**	**(mm)**		
15 secs	0.25	34	3.0	21.5	31.0	0.0134	11.2	0.08969	3.479	62
30 secs	0.5	31	3.0	21.5	28.0	0.0134	11.7	0.064821	3.947	56
1 min	1	28.5	3.0	21.5	25.5	0.0134	12.1	0.046612	4.423	51
2 min	2	26	3.0	21.5	23.0	0.0134	12.5	0.0335	4.9	46
5 min	5	23.5	3.0	21.5	20.5	0.0134	12.95	0.021565	5.535	41
10 min	10	23	3.0	21.6	20.0	0.0134	13	0.015278	6.032	40
15 min	15	22	3.0	21.6	19.0	0.0134	13.3	0.012618	6.308	38
30 min	30	21	2.5	21.6	18.5	0.0134	13.3	0.008922	6.808	37
60 min	60	20	2.5	21.6	17.5	0.0134	13.4	0.006333	7.303	35
90 min	90	19	3.0	21.7	16.0	0.0134	13.7	0.005228	7.579	32
120 min	120	18.5	3.0	21.7	15.5	0.0134	13.75	0.004536	7.784	31
4 hrs	240	17.5	3.0	21.7	14.5	0.0134	13.9	0.003225	8.277	29
8 hrs	480	17	3.0	21.4	14.0	0.0134	14	0.002288	8.771	28
24 hrs	1440	15	3.0	21.7	12.0	0.0134	14.3	0.001335	9.549	24
Wt of sample on #230 sieve = 21.0 g										
Sieve #	**Samp/siev**	**Sieve wt**	**Sample wt**	**Wt %**	**Cum wt%**	**P %**	**phi**			
18	417.7	416.9	0.8	1.6	1.6	98.4	0			
35	390.2	388.4	1.8	3.6	5.2	94.8	1			
60	362.7	357.6	5.1	10.2	15.4	84.6	2			
120	345.3	338.4	6.9	13.8	29.2	70.8	3			
230	344.9	338.8	6.1	12.2	41.4	58.6	4			
pan	372.0	371.7	0.3	0.6	42.0	58.0	5			
Total			21.0							

HYDROMETER AND SIEVE ANALYSES										
Sample #:	DS07		Date:	26/09/96						
Hydrometer = 152H			Sample mass = 50.00 gm			Clast specific gravity = 2.65				
time	e-time (T) min	hydrom. reading	control reading	temp C	R	K	L (cm)	d (mm)	phi	P %
15 secs	0.25	25.5	3.0	21.5	22.5	0.0134	12.6	0.095131	3.394	45
30 secs	0.5	23.0	3.0	21.5	20.0	0.0134	13	0.068327	3.871	40
1 min	1	21.0	3.0	21.5	18.0	0.0134	13.3	0.048869	4.355	36
2 min	2	19.0	3.0	21.5	16.0	0.0134	13.7	0.035071	4.834	32
5 min	5	17.0	3.0	21.5	14.0	0.0134	14	0.022422	5.479	28
10 min	10	16.5	2.5	21.6	14.0	0.0134	14	0.015855	5.979	28
15 min	15	16.0	2.5	21.6	13.5	0.0134	14.1	0.012992	6.266	27
30 min	30	15.5	2.5	21.6	13.0	0.0134	14.2	0.009219	6.761	26
60 min	60	14.5	3.0	21.7	11.5	0.0134	14.4	0.006565	7.251	23
90 min	90	14.0	3.0	21.7	11.0	0.0134	14.5	0.005379	7.539	22
120 min	120	13.5	3.0	21.7	10.5	0.0134	14.6	0.004674	7.741	21
4 hrs	240	13.0	3.0	21.7	10.0	0.0134	14.7	0.003316	8.236	20
8 hrs	470	12.5	3.0	21.4	9.5	0.0134	14.75	0.002374	8.719	19
24 hrs	1440	11.0	3.0	21.7	8.0	0.0134	15	0.001368	9.514	16
Wt of sample on #230 sieve = 28.5 g										
Sieve #	Samp/siev	Sieve wt	Sample wt	Wt %	Cum wt%	P %	phi			
18	418.0	416.9	1.1	2.2	2.2	97.8	0			
35	392.3	388.4	3.9	7.8	10.0	90.0	1			
60	366.9	357.6	9.3	18.6	28.6	71.4	2			
120	346.4	338.4	8.0	16.0	44.6	55.4	3			
230	344.6	338.7	5.9	11.8	56.4	43.6	4			
pan	371.9	371.6	0.3	0.6	57.0	43.0	5			
Total			28.5							

HYDROMETER AND SIEVE ANALYSES

Sample #:	**DS08**		**Date:**	**26/09/96**						
Hydrometer = 152H			Sample mass = 50.00 gm			Clast specific gravity = 2.65				
time	**e-time (T)**	**hydrom.**	**control**	**temp**	**R**	**K**	**L**	**d**	**phi**	**P %**
	min	**reading**	**reading**	**C**			**(cm)**	**(mm)**		
15 secs	0.25	27	3.0	21.5	24.0	0.0134	12.4	0.094373	3.405	48
30 secs	0.5	24	3.0	21.5	21.0	0.0134	12.9	0.068064	3.877	42
1 min	1	22	3.0	21.5	19.0	0.0134	13.3	0.048869	4.355	38
2 min	2	20	3.0	21.5	17.0	0.0134	13.5	0.034814	4.844	34
5 min	5	18	3.0	21.5	15.0	0.0134	14	0.022422	5.479	30
10 min	10	17	2.5	21.6	14.5	0.0134	13.9	0.015798	5.984	29
15 min	15	16.5	2.5	21.6	14.0	0.0134	14	0.012946	6.271	28
30 min	30	15.5	2.5	21.6	13.0	0.0134	14.2	0.009219	6.761	26
60 min	60	14.5	3.0	21.7	11.5	0.0134	14.4	0.006565	7.251	23
90 min	90	14	3.0	21.7	11.0	0.0134	14.5	0.005379	7.539	22
120 min	120	13.5	3.0	21.7	10.5	0.0134	14.6	0.004674	7.741	21
4 hrs	240	12.5	3.0	21.7	9.5	0.0134	14.75	0.003322	8.234	19
8 hrs	470	12	3.0	21.4	9.0	0.0134	14.8	0.002378	8.716	18
24 hrs	1440	11	3.0	21.7	8.0	0.0134	15	0.001368	9.514	16

Wt of sample on #230 sieve = 27.6 g

Sieve #	**Samp/siev**	**Sieve wt**	**Sample wt**	**Wt %**	**Cum wt%**	**P %**	**phi**
18	418.2	416.9	1.3	2.6	2.6	97.4	0
35	391.6	388.4	3.2	6.4	9.0	91.0	1
60	365.4	357.6	7.8	15.6	24.6	75.4	2
120	347.1	338.4	8.7	17.4	42.0	58.0	3
230	344.9	338.8	6.1	12.2	54.2	45.8	4
pan	371.8	371.6	0.2	0.4	54.6	45.4	5
Total			27.3				

HYDROMETER AND SIEVE ANALYSES										
Sample #:	DS09		Date:	26/09/96						
Hydrometer = 152H			Sample mass = 50.00 gm			Clast specific gravity = 2.65				
time	e-time (T) min	hydrom. reading	control reading	temp C	R	K	L (cm)	d (mm)	phi	P %
15 secs	0.25	33.5	3.0	21.5	30.5	0.0134	11.3	0.090089	3.472	61
30 secs	0.5	31	3.0	21.5	28.0	0.0134	11.7	0.064821	3.947	56
1 min	1	29	3.0	21.5	26.0	0.0134	12	0.046419	4.429	52
2 min	2	27.5	3.0	21.5	24.5	0.0134	12.3	0.033231	4.911	49
5 min	5	25	3.0	21.5	22.0	0.0134	12.7	0.021356	5.549	44
10 min	10	24	2.5	21.6	21.5	0.0134	12.8	0.01516	6.044	43
15 min	15	23	2.5	21.6	20.5	0.0134	12.95	0.012451	6.328	41
30 min	30	22	2.5	21.6	19.5	0.0134	13.15	0.008872	6.817	39
60 min	60	20.5	3.0	21.7	17.5	0.0134	13.4	0.006333	7.303	35
90 min	90	20	3.0	21.7	17.0	0.0134	13.5	0.00519	7.59	34
120 min	120	19	3.0	21.7	16.0	0.0134	13.7	0.004528	7.787	32
4 hrs	240	18.5	3.0	21.7	15.5	0.0134	13.75	0.003207	8.284	31
8 hrs	470	17.5	3.0	21.4	14.5	0.0134	13.9	0.002304	8.761	29
24 hrs	1440	16	3.0	21.7	13.0	0.0134	14.2	0.001331	9.554	26
Wt of sample on #230 sieve =		21.3								
Sieve #	Samp/siev	Sieve wt	Sample wt	Wt %	Cum wt%	P %	phi			
18	417.9	416.9	1.0	2.0	1.8	98.2	0			
35	390.6	388.3	2.3	4.6	6.4	93.6	1			
60	362.9	357.6	5.3	10.6	17.0	83.0	2			
120	344.9	338.4	6.5	13.0	30.0	70.0	3			
230	344.4	338.8	5.6	11.2	41.2	58.8	4			
pan	371.8	371.6	0.2	0.4	41.6	58.4	5			
Total			20.9							

HYDROMETER AND SIEVE ANALYSES

Sample #: **DS10** **Date:** **26/09/96**

Hydrometer = 152H Sample mass = 50.00 gm Clast specific gravity = 2.65

time	e-time (T) min	hydrom. reading	control reading	temp C	R	K	L (cm)	d (mm)	phi	P %
15 secs	0.25	39	3.0	21.5	36.0	0.0134	10.4	0.086427	3.532	72
30 secs	0.5	36.5	3.0	21.5	33.5	0.0134	10.8	0.062278	4.005	67
1 min	1	35	3.0	21.5	32.0	0.0134	11.1	0.044644	4.485	64
2 min	2	33	3.0	21.5	30.0	0.0134	11.4	0.031992	4.966	60
5 min	5	31	3.0	21.5	28.0	0.0134	11.7	0.020498	5.608	56
10 min	10	30.5	2.5	21.6	28.0	0.0134	11.7	0.014494	6.108	56
15 min	15	30	2.5	21.6	27.5	0.0134	11.8	0.011885	6.395	55
30 min	30	28.5	2.5	21.6	26.0	0.0134	12	0.008475	6.883	52
60 min	60	27	3.0	21.7	24.0	0.0134	12.4	0.006092	7.359	48
90 min	90	26.5	3.0	21.7	23.5	0.0134	12.45	0.004984	7.649	47
120 min	120	26	3.0	21.7	23.0	0.0134	12.5	0.004325	7.853	46
4 hrs	240	24.5	3.0	21.7	21.5	0.0134	12.8	0.003095	8.336	43
8 hrs	470	24	3.0	21.4	21.0	0.0134	12.9	0.00222	8.815	42
24 hrs	1440	21.5	3.0	21.7	18.5	0.0134	13.3	0.001288	9.601	37

Wt of sample on #230 sieve = 13.5 g

Sieve #	Samp/siev	Sieve wt	Sample wt	Wt %	Cum wt%	P %	phi
18	417.2	416.9	0.3	0.6	0.6	99.4	0
35	389.3	388.3	1.0	2.0	2.6	97.4	1
60	360.8	357.6	3.2	6.4	9.0	91.0	2
120	342.8	338.4	4.4	8.8	17.8	82.2	3
230	343.0	338.8	4.2	8.4	26.2	73.8	4
pan	371.9	371.7	0.2	0.4	26.6	73.4	5
Total			13.3				

HYDROMETER AND SIEVE ANALYSES										
Sample #:	**DS11**		**Date:**	**26/09/96**						
Hydrometer = 152H			Sample mass = 50.00 gm			Clast specific gravity = 2.65				
time	**e-time (T)**	**hydrom.**	**control**	**temp**	**R**	**K**	**L**	**d**	**phi**	**P %**
	min	**reading**	**reading**	**C**			**(cm)**	**(mm)**		
15 secs	0.25	33.5	3.0	21.5	30.5	0.0134	11.3	0.090089	3.472	61
30 secs	0.5	30.5	3.0	21.5	27.5	0.0134	11.8	0.065097	3.941	55
1 min	1	29	3.0	21.5	26.0	0.0134	12	0.046419	4.429	52
2 min	2	27	3.0	21.5	24.0	0.0134	12.4	0.033366	4.905	48
5 min	5	25.5	3.0	21.5	22.5	0.0134	12.6	0.021272	5.555	45
10 min	10	24.5	2.5	21.6	22.0	0.0134	12.7	0.015101	6.049	44
15 min	15	24	2.5	21.6	21.5	0.0134	12.8	0.012378	6.336	43
30 min	30	22.5	2.5	21.6	20.0	0.0134	13	0.008821	6.825	40
60 min	60	21	3.0	21.7	18.0	0.0134	13.3	0.006309	7.308	36
90 min	90	20.5	3.0	21.7	17.5	0.0134	13.4	0.005171	7.595	35
120 min	120	20	3.0	21.7	17.0	0.0134	13.5	0.004494	7.798	34
4 hrs	240	19	3.0	21.7	16.0	0.0134	13.7	0.003202	8.287	32
8 hrs	470	18.5	3.0	21.4	15.5	0.0134	13.75	0.002292	8.769	31
24 hrs	1440	17	3.0	21.7	14.0	0.0134	14	0.001321	9.564	28
Wt of sample on #230 sieve = 20.2 g										
Sieve #	**Samp/siev**	**Sieve wt**	**Sample wt**	**Wt %**	**Cum wt%**	**P %**	**phi**			
18	417.5	416.9	0.6	1.2	1.2	98.8	0			
35	390.2	388.3	1.9	3.8	5.0	95.0	1			
60	363.1	357.6	5.5	11.0	16.0	84.0	2			
120	345.0	338.4	6.6	13.2	29.2	70.8	3			
230	344.1	338.7	5.4	10.8	40.0	60.0	4			
pan	371.9	371.6	0.3	0.6	40.6	59.4	5			
Total			20.3							

HYDROMETER AND SIEVE ANALYSES

Sample #:	**DS12**		**Date:**	**26/09/96**						
Hydrometer = 152H			Sample mass = 50.00 gm			Clast specific gravity = 2.65				
time	**e-time (T)**	**hydrom.**	**control**	**temp**	**R**	**K**	**L**	**d**	**phi**	**P %**
	min	**reading**	**reading**	**C**			**(cm)**	**(mm)**		
15 secs	0.25	36.5	3.0	21.5	33.5	0.0134	10.8	0.088074	3.505	67
30 secs	0.5	34.0	3.0	21.5	31.0	0.0134	11.2	0.06342	3.979	62
1 min	1	32.5	3.0	21.5	29.5	0.0134	11.45	0.045343	4.463	59
2 min	2	30.0	3.0	21.5	27.0	0.0134	11.9	0.032686	4.935	54
5 min	5	28.5	3.0	21.5	25.5	0.0134	12.1	0.020846	5.584	51
10 min	10	27.5	3.5	21.4	24.0	0.0134	12.4	0.014922	6.066	48
15 min	15	27.0	3.5	21.4	23.5	0.0134	12.45	0.012208	6.356	47
30 min	30	25.5	3.0	21.5	22.5	0.0134	12.6	0.008684	6.847	45
60 min	60	24.0	3.0	21.6	21.0	0.0134	12.9	0.006213	7.33	42
90 min	90	23.5	3.0	21.6	20.5	0.0134	12.95	0.005083	7.62	41
120 min	120	22.5	3.0	21.6	19.5	0.0134	13.15	0.004436	7.817	39
4 hrs	240	22.0	3.0	21.7	19.0	0.0134	13.3	0.003154	8.308	38
8 hrs	524	21.0	3.0	21.4	18.0	0.0134	13.3	0.002135	8.872	36
24 hrs	1440	19.0	3.0	21.7	16.0	0.0134	13.7	0.001307	9.579	32
Wt of sample on #230 sieve = 16.2 g										
Sieve #	**Samp/siev**	**Sieve wt**	**Sample wt**	**Wt %**	**Cum wt%**	**P %**	**phi**			
18	417.2	416.9	0.3	0.6	0.6	99.4	0			
35	389.4	388.3	1.1	2.2	2.8	97.2	1			
60	360.9	357.6	3.3	6.6	9.4	90.6	2			
120	343.8	338.3	5.5	11.0	20.4	79.6	3			
230	344.5	338.8	5.7	11.4	31.8	68.2	4			
pan	371.9	371.7	0.2	0.4	32.2	67.8	5			
Total			16.1							

HYDROMETER AND SIEVE ANALYSES

Sample #:	**DS13**		**Date:**	**26/09/96**						
Hydrometer = 152H			Sample mass = 50.00 gm			Clast specific gravity = 2.65				
time	**e-time (T)**	**hydrom.**	**control**	**temp**	**R**	**K**	**L**	**d**	**phi**	**P %**
	min	**reading**	**reading**	**C**			**(cm)**	**(mm)**		
15 secs	0.25	36.5	3.0	21.5	33.5	0.0134	10.8	0.088074	3.505	67
30 secs	0.5	34.0	3.0	21.5	31.0	0.0134	11.2	0.06342	3.979	62
1 min	1	32.5	3.0	21.5	29.5	0.0134	11.45	0.045343	4.463	59
2 min	2	30.0	3.0	21.5	27.0	0.0134	11.9	0.032686	4.935	54
5 min	5	27.5	3.0	21.5	24.5	0.0134	12.3	0.021017	5.572	49
10 min	10	27.0	3.5	21.4	23.5	0.0134	12.45	0.014952	6.064	47
15 min	15	26.0	3.5	21.4	22.5	0.0134	12.6	0.012281	6.347	45
30 min	30	24.0	3.0	21.5	21.0	0.0134	12.9	0.008787	6.83	42
60 min	60	22.0	3.0	21.6	19.0	0.0134	13.3	0.006309	7.308	38
90 min	90	21.0	3.0	21.6	18.0	0.0134	13.3	0.005151	7.601	36
120 min	120	20.0	3.0	21.6	17.0	0.0134	13.5	0.004494	7.798	34
4 hrs	240	19.0	3.0	21.7	16.0	0.0134	13.7	0.003202	8.287	32
8 hrs	524	18.0	3.0	21.4	15.0	0.0134	13.8	0.002175	8.845	30
24 hrs	1440	16.5	3.0	21.7	13.5	0.0134	14.1	0.001326	9.559	27

Wt of sample on #230 sieve = 16.2 g

Sieve #	**Samp/siev**	**Sieve wt**	**Sample wt**	**Wt %**	**Cum wt%**	**P %**	**phi**
18	417.4	417.0	0.4	0.8	0.8	99.2	0
35	389.8	388.4	1.4	2.8	3.6	96.4	1
60	361.6	357.6	4.0	8.0	11.6	88.4	2
120	343.6	338.4	5.2	10.4	22.0	78.0	3
230	343.8	338.8	5.0	10.0	32.0	68.0	4
pan	371.8	371.7	0.1	0.2	32.2	67.8	5
Total			16.1				

HYDROMETER AND SIEVE ANALYSES										
Sample #:	DS14		Date:	26/09/96						
Hydrometer = 152H			Sample mass = 50.00 gm			Clast specific gravity = 2.65				
time	e-time (T)	hydrom.	control	temp	R	K	L	d	phi	P %
	min	reading	reading	C			(cm)	(mm)		
15 secs	0.25	40.0	3.0	21.5	37.0	0.0134	10.2	0.085592	3.546	74
30 secs	0.5	37.0	3.0	21.5	34.0	0.0134	10.7	0.061989	4.012	68
1 min	1	35.0	3.0	21.5	32.0	0.0134	11.1	0.044644	4.485	64
2 min	2	33.5	3.0	21.5	30.5	0.0134	11.3	0.031851	4.972	61
5 min	5	31.0	3.0	21.5	28.0	0.0134	11.7	0.020498	5.608	56
10 min	10	31.0	3.5	21.4	27.5	0.0134	11.8	0.014556	6.102	55
15 min	15	30.0	3.5	21.4	26.5	0.0134	11.95	0.01196	6.386	53
30 min	30	29.0	3.0	21.5	26.0	0.0134	12	0.008475	6.883	52
60 min	60	27.0	3.0	21.6	24.0	0.0134	12.4	0.006092	7.359	48
90 min	90	26.0	3.0	21.6	23.0	0.0134	12.5	0.004994	7.646	46
120 min	120	25.0	3.0	21.6	22.0	0.0134	12.7	0.004359	7.842	44
4 hrs	240	24.5	3.0	21.7	21.5	0.0134	12.8	0.003095	8.336	43
8 hrs	524	23.0	3.0	21.4	20.0	0.0134	13	0.002111	8.888	40
24 hrs	1440	21.0	3.0	21.7	18.0	0.0134	13.3	0.001288	9.601	36
Wt of sample on #230 sieve = 13.5 g										
Sieve #	Samp/siev	Sieve wt	Sample wt	Wt %	Cum wt%	P %	phi			
18	417.3	416.9	0.4	0.8	0.8	99.2	0			
35	389.5	388.3	1.2	2.4	3.2	96.8	1			
60	360.8	357.6	3.2	6.4	9.6	90.4	2			
120	342.6	338.4	4.2	8.4	18.0	82.0	3			
230	343.3	338.8	4.5	9.0	27.0	73.0	4			
pan	371.9	371.7	0.2	0.4	27.4	72.6	5			
Total			13.7							

HYDROMETER AND SIEVE ANALYSES

Sample #:	**DS16**		**Date:**	**26/09/96**						
Hydrometer = 152H			Sample mass = 50.00 gm			Clast specific gravity = 2.65				
time	**e-time (T)**	**hydrom.**	**control**	**temp**	**R**	**K**	**L**	**d**	**phi**	**P %**
	min	**reading**	**reading**	**C**			**(cm)**	**(mm)**		
15 secs	0.25	39.5	3.0	21.5	36.5	0.0134	10.3	0.086011	3.539	73
30 secs	0.5	35.5	3.0	21.5	32.5	0.0134	11	0.062852	3.992	65
1 min	1	33.0	3.0	21.5	30.0	0.0134	11.4	0.045244	4.466	60
2 min	2	31.0	3.0	21.5	28.0	0.0134	11.7	0.03241	4.947	56
5 min	5	28.0	3.0	21.5	25.0	0.0134	12.2	0.020931	5.578	50
10 min	10	28.0	3.5	21.4	24.5	0.0134	12.3	0.014861	6.072	49
15 min	15	27.5	3.5	21.4	24.0	0.0134	12.4	0.012183	6.359	48
30 min	30	26.0	3.0	21.5	23.0	0.0134	12.5	0.00865	6.853	46
60 min	60	24.0	3.0	21.6	21.0	0.0134	12.9	0.006213	7.33	42
90 min	90	23.5	3.0	21.6	20.5	0.0134	12.95	0.005083	7.62	41
120 min	120	23.0	3.0	21.6	20.0	0.0134	13	0.00441	7.825	40
4 hrs	240	22.0	3.0	21.7	19.0	0.0134	13.3	0.003154	8.308	38
8 hrs	524	20.0	3.0	21.4	17.0	0.0134	13.5	0.002151	8.861	34
24 hrs	1440	19.0	3.0	21.7	16.0	0.0134	13.7	0.001307	9.579	32

Wt of sample on #230 sieve = 15.5 g

Sieve #	**Samp/siev**	**Sieve wt**	**Sample wt**	**Wt %**	**Cum wt%**	**P %**	**phi**
18	417.4	416.9	0.5	1.0	1.0	99.0	0
35	389.5	388.4	1.1	2.2	3.2	96.8	1
60	360.2	357.4	2.8	5.6	8.8	91.2	2
120	341.8	338.4	3.4	6.8	15.6	84.4	3
230	346.2	338.8	7.4	14.8	30.4	69.6	4
pan	372.2	371.7	0.5	1.0	31.4	68.6	5
Total			15.7				

HYDROMETER AND SIEVE ANALYSES										
Sample #:	DS18		Date:	26/09/96						
Hydrometer = 152H			Sample mass = 50.00 gm			Clast specific gravity = 2.65				
time	e-time (T)	hydrom.	control	temp	R	K	L	d	phi	P %
	min	reading	reading	C			(cm)	(mm)		
15 secs	0.25	35.0	3.0	21.5	32.0	0.0134	11.1	0.089289	3.485	64
30 secs	0.5	30.5	3.0	21.5	27.5	0.0134	11.8	0.065097	3.941	55
1 min	1	28.0	3.0	21.5	25.0	0.0134	12.2	0.046804	4.417	50
2 min	2	25.5	3.0	21.5	22.5	0.0134	12.6	0.033634	4.894	45
5 min	5	23.0	3.0	21.5	20.0	0.0134	13	0.021607	5.532	40
10 min	10	22.5	3.0	21.6	19.5	0.0134	13.15	0.015366	6.024	39
15 min	15	21.5	3.0	21.6	18.5	0.0134	13.3	0.012618	6.308	37
30 min	30	20.0	3.0	21.6	17.0	0.0134	13.5	0.008989	6.798	34
60 min	60	19.0	3.0	21.6	16.0	0.0134	13.7	0.006403	7.287	32
90 min	90	18.0	3.0	21.6	15.0	0.0134	13.8	0.005247	7.574	30
120 min	120	17.5	3.0	21.6	14.5	0.0134	13.9	0.004561	7.777	29
4 hrs	240	16.0	3.0	21.7	13.0	0.0134	14.2	0.003259	8.261	26
8 hrs	493	15.5	3.0	21.4	12.5	0.0134	14.25	0.002278	8.778	25
24 hrs	1440	14.0	3.0	21.7	11.0	0.0134	14.5	0.001345	9.539	22
Wt of sample on #230 sieve = 20.4 g										
Sieve #	Samp/siev	Sieve wt	Sample wt	Wt %	Cum wt%	P %	phi			
18	417.7	416.9	0.8	1.6	1.6	98.4	0			
35	390.0	388.4	1.6	3.2	4.8	95.2	1			
60	362.3	357.6	4.7	9.4	14.2	85.8	2			
120	344.7	338.4	6.3	12.6	26.8	73.2	3			
230	345.4	338.8	6.6	13.2	40.0	60.0	4			
pan	372.0	371.7	0.3	0.6	40.6	59.4	5			
Total			20.3							

Appendix V

Control Well Logs

Key to identification of lithologies in control logs

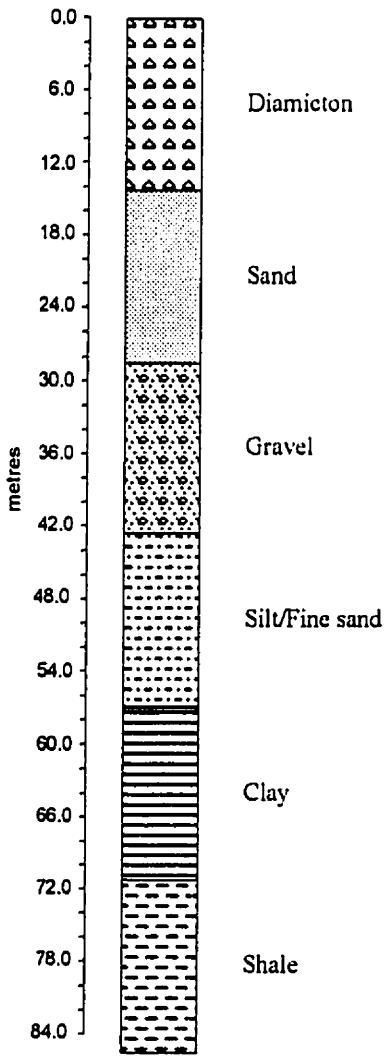

Control Log for DS01

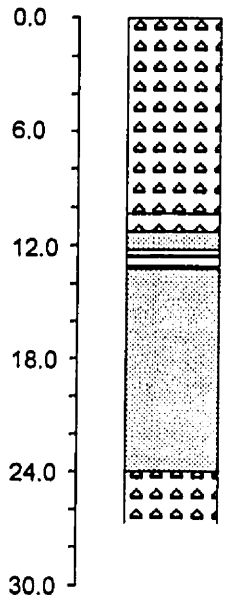

Alberta Environment Water Well report 192584

Location: NE Sec. 5, Twp. 60, Rg. 11, W of 4 M.
400 m N of sampled site.

Source: Alberta Environment.

Average Preconsolidation value: not obtained

Control Log for DS02

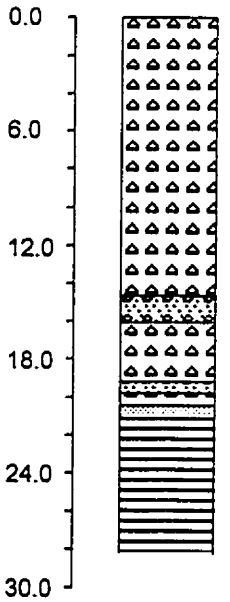

Alberta Environment Water Well report 191494

Location: NE Sec. 14, Twp. 50, Rg. 10, W of 4 M.
500 m WNW of sampled site.

Source: Alberta Environment.

Average Preconsolidation value: 234 kPa

Control Log for DS03 and DS14

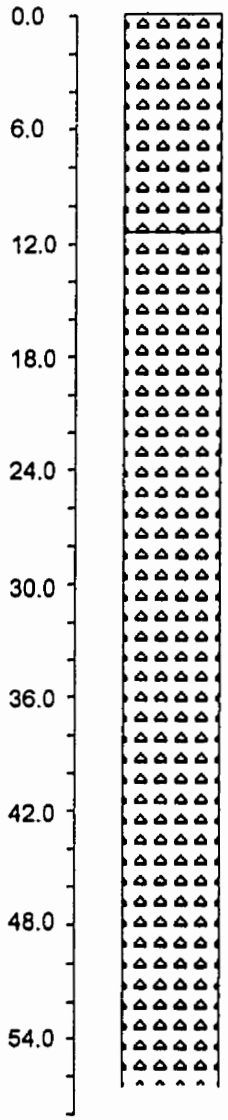

Alberta Geological Survey testhole 77 SR 10

Location: NE of LSD 1, Sec. 33, Twp. 58, Rg. 9, W of 4 M. 125 m E of sampled site.

Source: Andriashek, 1985.

Average Preconsolidation value: 138 kPa (DS03)
178 kPa (DS14)

Control Log for DS04

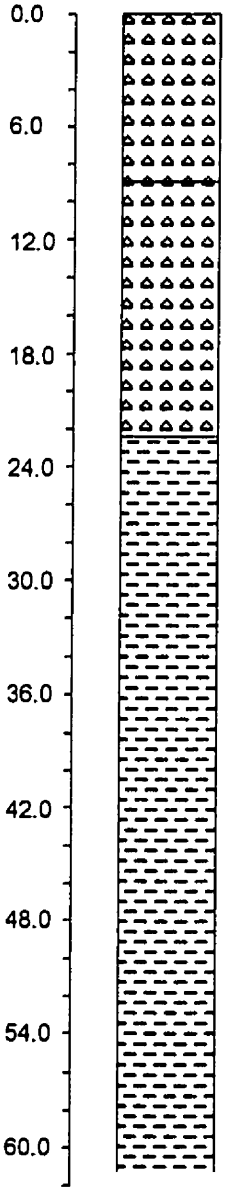

Alberta Environment Borehole

Location: NW Sec. 36, Twp. 47, Rg. 1, W of 4 M.
175 m N of sampled site.

Source: Mougeot, 1991.

Average Preconsolidation value: 260 kPa

Control Log for DS05

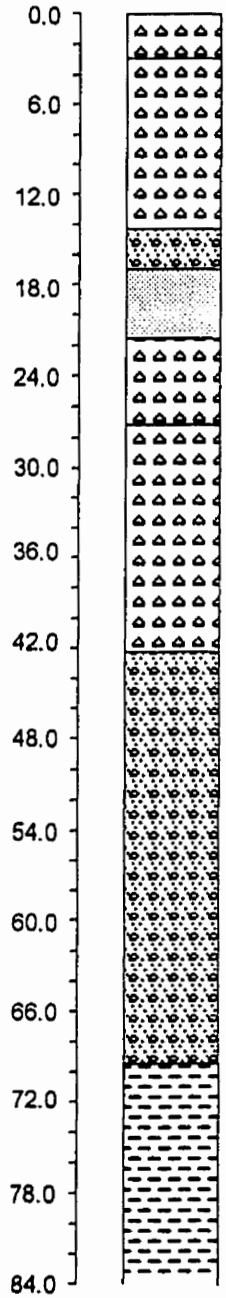

Alberta Environment Borehole

Location: SE Sec. 8, Twp. 50, Rg. 1, W of 4 M.
250 m WSW of sampled site

Source: Mougeot, 1991.

Average Preconsolidation value: 155 kPa

Control Log for DS07

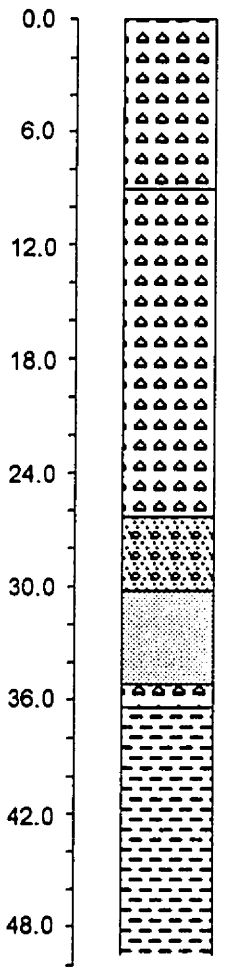

Alberta Environment Borehole

Location: NW Sec. 36, Twp. 47, Rg. 1, W of 4 M.
175 m N of sampled site.

Source: Mougeot, 1991.

Average Preconsolidation value: 219 kPa

Control Log for DS08 and DS09

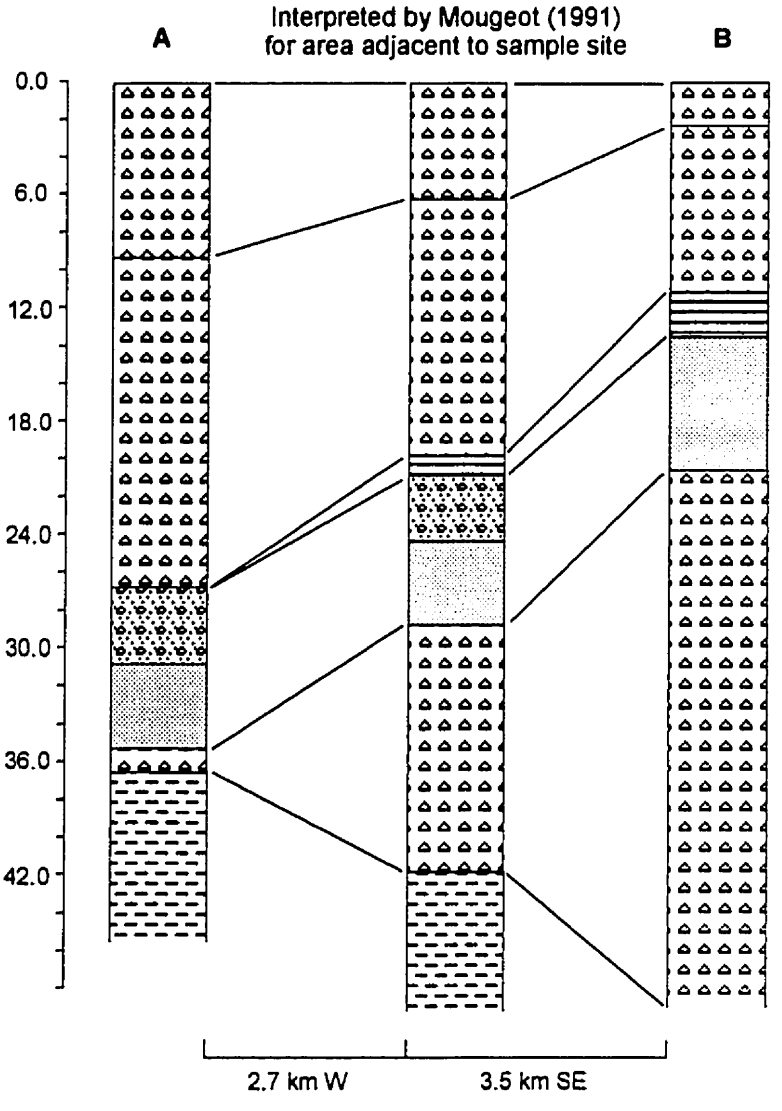

Alberta Environment Boreholes

A: Location: LSD. 14, Sec. 23, Twp. 57, Rg. 7, W of 4 M.
2.7 km W of sampled site.

B: Location: LSD. 13, Sec. 32, Twp. 57, Rg. 7, W of 4 M.
3.5 km SE of sampled site.

Source: Mougeot, 1991.

Average Preconsolidation value: 260 kPa

Control Log for DS10

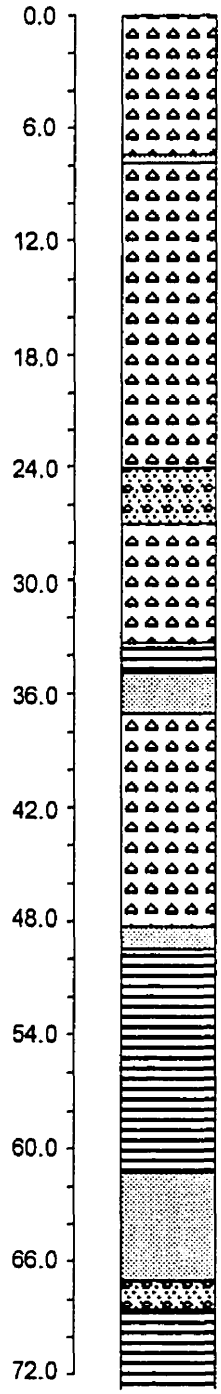

Alberta Environment Water Well Report 160263

Location: LSD. 9, Sec. 18, Twp. 65, Rg. 12, W of 4 M.
200 m N of sampled site.

Source: Alberta Environment.

Average Preconsolidation value: 222 kPa

Control Log for DS11

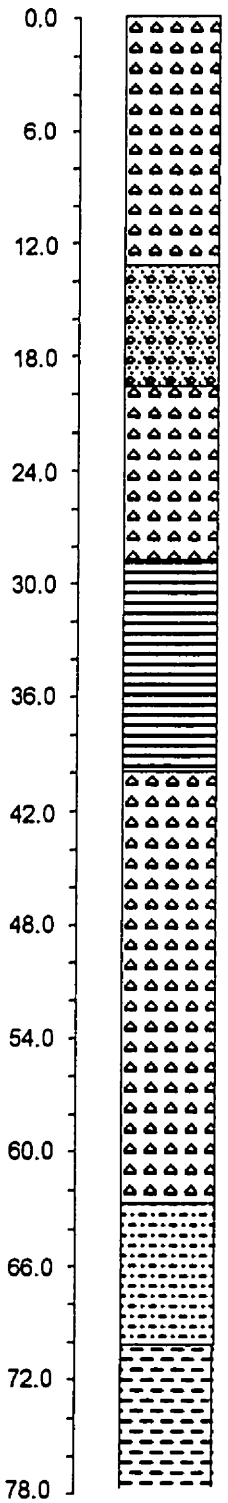

Alberta Environment Borehole

Location: NE Sec. 34, Twp. 64, Rg. 13, W of 4 M.
250 m N of sampled site.

Source: Andirashek, 1985.

Average Preconsolidation value: not obtained

Control Log for DS12

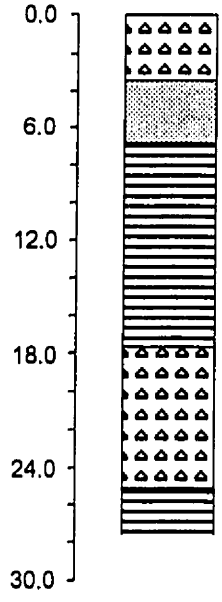

Alberta Environment Borehole

Location: LSD. 8, Sec. 16, Twp. 64, Rg. 12, W of 4 M.
550 m N of sampled site.

Source: Andriashek, 1985.

Average Preconsolidation value: 137 kPa

Control Log for DS13

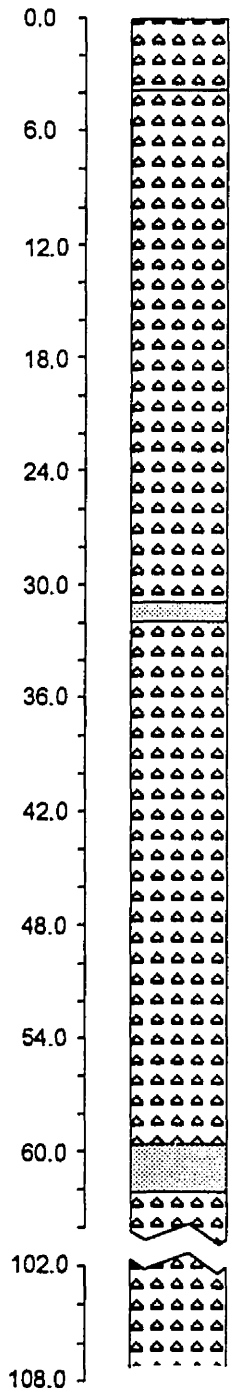

Alberta Environment Water Well report 154635

Location: NW, Sec. 07, Twp. 60, Rg. 9, W of 4 M.
400 m SE of sample site.

Source: Alberta Environment

Average Preconsolidation value: 178 kPa

Control Log for DS16

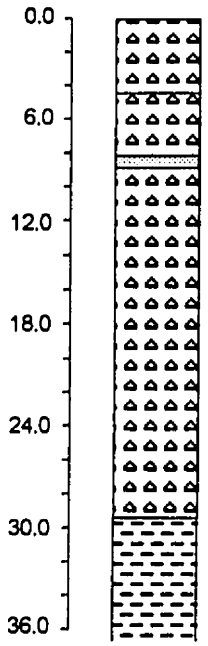

Alberta Environment Water Well report 155119

Location: LSD. 9, Sec. 25, Twp. 52, Rg. 3, W of 4 M.
50 m S of sampled site.

Source: Alberta Environment.

Average Preconsolidation value: 202 kPa

Control Log for DS18

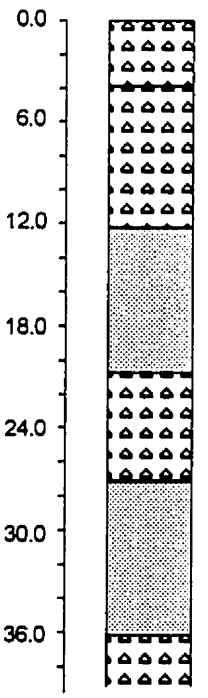

Alberta Environment Water Well report 167109

Location: LSD. 13, Sec. 36, Twp. 52, Rg. 4, W of 4 M.
80 m E of sampled site.

Source: Alberta Environment.

Average Preconsolidation value: 268 kPa

IMAGE EVALUATION
TEST TARGET (QA-3)

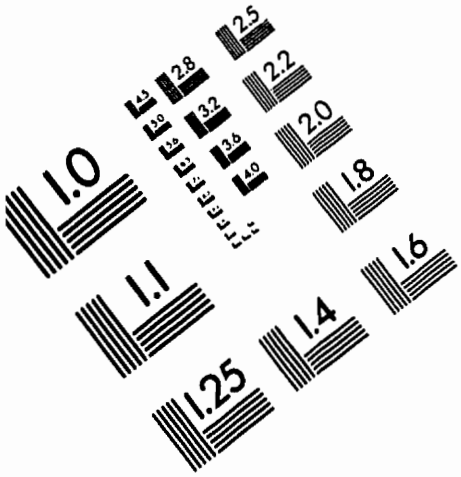

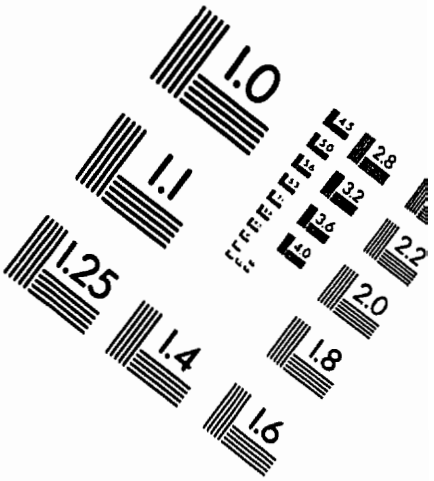

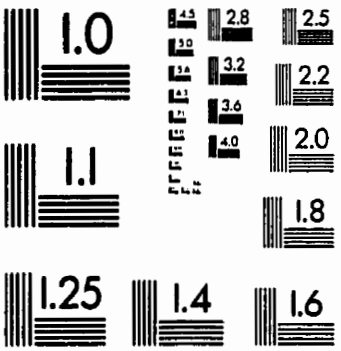

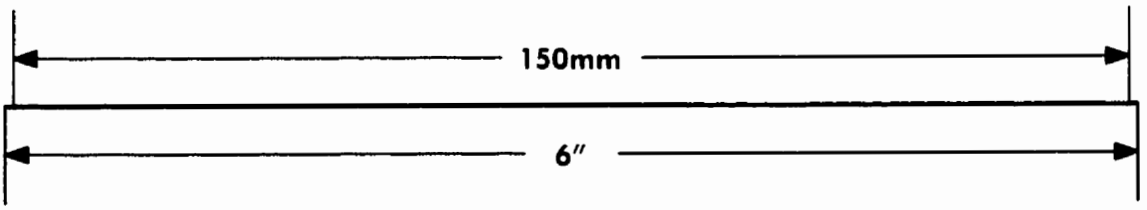

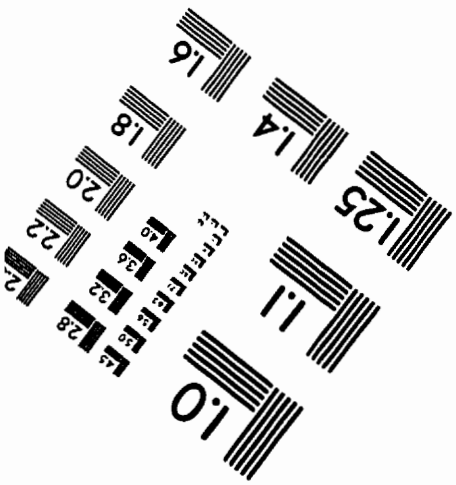

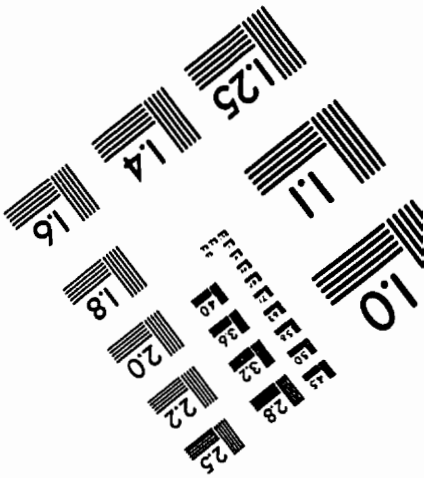

APPLIED IMAGE, Inc
1653 East Main Street
Rochester, NY 14609 USA
Phone: 716/482-0300
Fax: 716/288-5989